SINGLE DOMAIN ANTIBODIES IN TISSUE ENGINEERING

Emilie Dooms Rodrigues

SINGLE DOMAIN ANTIBODIES IN TISSUE ENGINEERING

Emilie Dooms Rodrigues

2014

Members of the Graduation Committee:

Chairman:	Prof. Dr. ir. J. W. M. Hilgenkamp	University of Twente
Promoters:	Prof. Dr. H. B. J. Karperien	University of Twente
	Prof. Dr. C. A. van Blitterswijk	University of Twente
Co-promoter:	Dr. M. El Khattabi	QVQ B.V., Utrecht
Members:	Prof. Dr. ir. P. Jonkheijm	University of Twente
	Prof. Dr. J. de Boer	University of Twente
	Prof. Dr. S. Muyldermans	Vrije Universiteit Brussel, Belgium
	Prof. Dr. C. T. Verrips	QVQ B.V., Utrecht
	Prof. Dr. D. W. Grijpma	University of Twente
	Prof. Dr. C. W. G. M. Löwik	Leiden University Medical Center

SINGLE DOMAIN ANTIBODIES IN TISSUE ENGINEERING

Emilie Dooms Rodrigues

PhD Thesis, University of Twente, Enschede, The Netherlands

ISBN: 978-90-365-3735-3

The research described in this thesis was performed at the Departments of Developmental BioEngineering and Tissue Regeneration of the University of Twente, Enschede, The Netherlands and at QVQ B.V., Utrecht, The Netherlands. The research described in this thesis was performed at the Departments of Developmental BioEngineering and Tissue Regeneration of the University of Twente, Enschede, The Netherlands and at QVQ B.V., Utrecht, The Netherlands.

Cover design by Manuel Dooms Rodrigues.

SINGLE DOMAIN ANTIBODIES IN TISSUE ENGINEERING

DISSERTATION

to obtain
the degree of doctor at the University of Twente,
on the authority of the rector magnificus
Prof. dr. H. Brinksma
on account of the decision of the graduation committee,
to be publicly defended
on Thursday, September 4th 2014, at 14.45 hours

By

Emilie Dooms Rodrigues

born on 31st May, 1983
at Woluwe-Saint-Lambert, Belgium

Promoters:

Prof. Dr. H. B. J. Karperien
Prof. Dr. C. A. van Blitterswijk

Co-promoter:

Dr. M. El Khattabi

ISBN: 978-90-365-3735-3

À Papa et Maman
À Lelel

À Tantine et Andre

e Tiago

Acknowledgements

Acknowledgements

I would like to express my gratitude to Prof. Dr. Marcel Karperien and Prof. Dr. Clemens van Blitterswijk for giving me the opportunity to conduct my PhD research in the departments of Developmental BioEngineering and Tissue Regeneration. Moreover I would like to thank Prof. Dr. Theo Verrips, Dr. Mohamed El Khattabi, Prof. Dr. Pascal Jonkheijm, Prof. Dr. Jan de Boer, Prof. Dr. Serge Muyldermans, Prof. Dr. Dirk Grijpma and Prof. Dr. Clemens Löwik for being part of the graduation committee.
Thank you to my colleagues, friends and family.

I am lucky.

Emilie Rodrigues

Summary

Summary

The aim of this thesis is to demonstrate the potential of VHH in tissue engineering applications, with a focus on bone and cartilage tissue regeneration. After a general introduction to this thesis in chapter 1, the selection of VHH targeting growth factors is described in chapter 2. VHH were selected to target growth factors relevant in skeletal tissue engineering and VHH were found to modulate BMP activity with high affinity. Chapter 3 describes the immobilization of VHH and its potential to reversibly immobilize BMP6 to a surface. The strategy consisted in the combination of orthogonal supramolecular interactions for the immobilization of the polyhistidine-tagged VHH at a surface and its subsequent ability to bind and release BMP6. The system was able to deliver BMP6 and improved osteogenic activity of MSC-like cells. In chapter 4, two strategies are presented for the incorporation of VHH in biomaterials. One approach consisted in the incorporation of VHH in electrospun fibers of poly(ethylene oxide). In this procedure the VHH were homogeneously distributed in the fibers. The VHH remained biologically active after the electrospinning process and were able to potentiate osteogenic differentiation. In the second approach, VHH were incorporated in an *in situ* gelating dextran-based hydrogel. Retention and controlled release of VHH was shown. Chapter 5 presents another approach for directional VHH immobilization on biomaterial surface. Based on genetic engineering, VHH were engineered with a unpaired cysteine at the C-terminus capable of directional grafting to poly(trimethylene carbonate). VHH were able to capture and release BMP6 whilst BMP6 remained functional for cell differentiation. In chapter 6, a VHH targeting bone mimicking ceramic hydroxyapatite (HA) was selected and tested *in vivo* in mouse for bone binding capacities. Fluorescently labelled VHH successfully showed specific accumulation in the skeleton. Chapter 7 presents a bivalent VHH with dual specificity towards BMP7 and HA. The bivalent VHH permits a non-covalent functionalization of biomaterials with growth factors. Chapter 8 presents a set of VHH targeting DKK1, a key molecule in degenerative and inflammatory joint disease. VHH were incorporated in injectable thermo reversible hydrogels resulting in a controlled release of VHH over time. In chapter 9, different strategies were explored to select VHH targeting osteoarthritic or healthy cartilage. One approach consisted in the use of a non-immunized phage library targeting macroscopically looking arthritic and healthy human cartilage. The second approach consisted of engineering a VHH with a peptide sequence, previously identified, targeting collagen type II. The peptide sequence was inserted in the complementary determining region 3 of the VHH. Unfortunately, neither of these approaches resulted in in the selection of VHH with the desired effect. Finally, chapter 10 discusses the results obtained in this thesis and gives an outlook on the potential applications of VHH in tissue engineering.

Table of Contents

Chapter 1
General Introduction

General Introduction

The art of tissue engineering

Tissue engineering is a multidisciplinary field aimed at developing solutions for repair, and/or regeneration of tissues. The main tunable ingredients in tissue engineering are (1) scaffolds, which are mostly used for mechanical support, (2) biomolecules (growth factors) responsible for orchestrated cell stimulation and (3) cells. This cocktail of variables presents a platform for the tissue engineer to develop tailor made treatment strategies [1-3].

Scaffolds function to replace or augment various structures and tissues in the body and provide mechanical support. The scaffolds are designed to create an optimal microenvironment for tissue formation or regeneration by mimicking the extracellular matrix (ECM) [2]. The ECM is a structured three-dimensional network consisting of a mixture of structural and functional molecules (proteins and polysaccharides) specific for each type of tissue. Beyond the physical support, the ECM functions as a reservoir of bioactive molecules such as growth factors and growth factors antagonists. These biomolecules provide a tailored control over biological signals in the surroundings. The dynamic activation of biological processes by arrays of growth factors and the inhibition of their activity by their respective antagonist, in combination with biological cues in extracellular matrix proteins, eventually determines the cellular response such as differentiation, maturation, proliferation, migration and new tissue formation. Therefore, a smart selection of the biomaterial to generate the scaffold and an adequate set of growth factors are paramount for a suitable scaffold performance [4, 5].

The first generation of biomaterials was selected based on their biocompatibility and tolerance by the body [2]. However, scaffolds of these biomaterials do not actively support tissue formation due to the lack of biological cues. Therefore, biomaterials with added functionalities are being developed. Micro patterning of several polymers with different wettability showed to have an influence on protein adsorption and a subsequent effect on cell morphology and guidance [6, 7]. High-throughput biological screening has been developed in order to better understand the importance of cell-surface topography interactions and their effect on cellular responses [8]. Nanostructured materials have also shown to influence interactions at the cell-material interface [9, 10]. Whilst physical and mechanical properties of biomaterials such as porosity, charge, topography and chemical composition can influence cell behavior, the incorporation of biomolecules can also trigger specific signaling pathways [2].

Biomaterial functionalization

Current strategies used for smart scaffold biofabrication involve the incorporation of biomolecules (peptides, growth factors or genetically modified growth factors) in biomaterials and their delivery. Such biomolecules are of interest to apply as modulating tools having a direct effect on cell and tissue faith. The incorporation of biomolecules in biomaterials has been approached by non-covalent coupling or covalent coupling [11].

Non-covalent immobilization of biomolecules can be achieved either by physical entrapment, adsorption or ionic interaction while covalent coupling can be established via functional groups present or introduced in the biomaterial and/ or biomolecule [11].
Biomaterials have been coated with peptides or proteins to improve cell adhesion. For example coating with integrin-binding RGD peptides or heparin-binding peptides showing an enhanced cell adhesion on various biomaterials [12-14]. There are other cell recognition motifs besides RGD sequences that can act as secondary binding moieties such as present in proteins like fibronectin, collagen and laminin [12]. In an alternative strategy biomaterials can be coated with growth factors and peptides that stimulate cell differentiation. This can be achieved, for instance, by coating of the biomaterial surface with the collagen-mimetic peptide GFOGER [15] or by the incorporation of bone morphogenetic proteins in biomaterials formulations [16, 17]. Both strategies improved osteoblast differentiation.
The use of proteins over peptides bears some disadvantages. Proteins must be produced, isolated and purified from organisms, which might elicit undesirable immune responses; proteins are not stable for extended period of time and are exposed to proteolytic degradation [12, 18]. In addition, recombinant proteins may trigger immunological responses. BMP7 has been incorporated in collagen granules and tested in clinical studies where 10% of patients developed antibodies against the recombinant human BMP7 [19]. Furthermore, protein immobilization by covalent coupling to surfaces is generally not very well controlled. Several strategies for immobilization of growth factors employ a random coupling of the protein to the surface leading to non-homogeneous coverage of the surface and in reduced efficiency of the growth factor due to inaccessible and/ or damaged bioactive sites [20]. For example, the coupling might be achieved via the bioactive site thereby inactivating the growth factor. Finally, genetically modified proteins, which are more laborious to produce, might trigger unknown side effects and need additional testing to obtain FDA approval for clinical applications.
As mentioned, ECM proteins, growth factors and biofunctional peptide sequences have been introduced in biomaterials (hydrogels, polymers, ceramics) in the attempt to obtain cellular functionality and tissue morphogenesis. Most of the strategies require the incorporation of exogenous growth factors, which apart from its expense, might as well need to be genetically modified.
Exploratory research for systems capable of capturing, modulating and concentrating endogenous growth factors are needed for a more efficient cell response.

Translational research
In our industrialized world, where physical and chemical separation processes are well known and established, it is possible to capture individual compounds from a complex mixture by, for instance, affinity chromatography. Affinity chromatography is a separation method based on reversible interaction between a protein and a ligand coupled to a matrix. This technique offers a high selectivity and specificity for the molecule of interest. In this thesis we translated and adapted this well working process to tissue

engineering applications, i.e. by utilizing special binding molecules such as antibodies coupled to a matrix (biomaterial) we would be able to capture specific endogenous biomolecules from the surrounding of the implant in a reversible fashion. In this way we might be able to produce a reservoir of biomolecules relevant to modulate and enhance new tissue formation/ regeneration.

Conventional antibodies have long been exploited for interactions with molecules to modulate their biological effect. Conventional antibodies are complex molecules consisting of four interconnected protein chains. The large size and complexity dictate a number of limitations for the application of such antibodies. Furthermore, production costs are high arguing against its wide spread application [21]. Large efforts have been made for the development of smaller antibodies. Alternatively, the use of naturally or synthetically derived antigen binding fragments (Fabs), single chain variable fragments (scFv) or heavy chain only antibodies (HcAb) revealed suboptimal activities due to their low affinity and limited stability [22].

Most of the problems discussed above concerning conventional antibodies can be overcome by the use of special antibodies.

VHH technology

The *Camelidae* family expresses a special class of antibodies that are devoid of light chains [23]. These antibodies are called heavy chain only antibodies, which are formed by two protein chains (Figure 1). The antigen-binding domain of such single chain antibody is called variable heavy chain of the heavy chain only antibody (VHH) [23, 24]. VHH are uniquely small antibody fragments (~15 kDa) capable of binding specifically and with high affinity epitopes in the antigen [21]. They are simple and easy to clone and subsequently to genetically modify since they consist of one single gene. They can be recombinantly produced in bacteria and yeast [21, 25, 26].

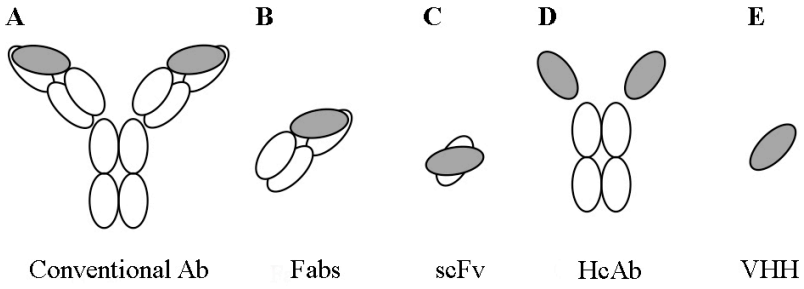

Figure 1. Schematic structure of antibodies. (A) Structure of conventional monoclonal antibody (mAb) IgG, (B) antibody fragments (Fabs), (C) single chain variable fragment (scFv), (D) heavy chain only antibody (HcAb), (E) variable heavy chain of the heavy chain only antibody (VHH). The heavy variable domains are represented in grey. Adapted from [33, 40].

Moreover, VHH are highly soluble and refold easily upon heat-denaturation [27, 28]. In addition, genetic modifications in the VHH sequence may allow for increased yield productions [29] and increased solubility [30]. The structure of the VHH allows for a multitude of genetic modifications and combinations (Figure 2). VHH possess genetic and structural features that make them highly suitable for widespread application in therapy, diagnostic screening and research [21, 31, 32].

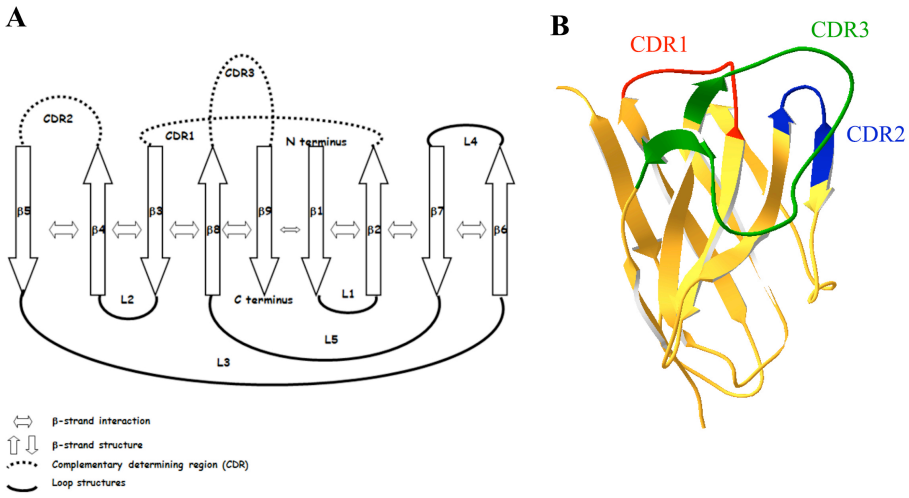

Figure 2. Schematic representation of a VHH and its regions and interactions. VHH is organized in 9 anti-parallel beta-strands connected with loops. Three of these loops form the complementary determining regions (CDR1, CDR2 and CDR3). Loops 1, 2, 3 and 5 are located away from the CDRs and theoretically do not interfere with binding of the VHH to its antigen. Adapted from [29, 41]. (B) Cartoon of VHH G7 with CDR1, CDR2 and CDR3 highlighted in red, blue and green respectively [42-44].

Moreover, VHH versatility permits them to improve several therapeutic applications such as treatment of cancer [25, 33, 34] and HIV-1 [35, 36] with reduced immunogenic responses due to their close homology with human antibody fragments. VHH can be used in tissue engineering to functionalize biomaterials. VHH can be explored as building blocks capable to bridge the gap between biology and materials. The integration of VHH in biomaterials is a potent tool to tailor cell attachment, growth, differentiation and migration and consequently increase successful tissue regeneration, reconstruction and replacement of lost and worn out tissues. VHH can play an important role as carrier of growth factors to establish or maintain a local reservoir of biologically active growth factors. Furthermore, VHH/ growth factor interactions might be important to stabilize the growth factors and present them to their receptors.

Active immunization of dromedaries is most often used to isolate VHH with affinities in the lower nanomolar or even picomolar range for the antigen [21]. Phage display technology allow for the specific selection of VHH through a number of biopanning

rounds (Figure 3) [37]. The mRNA from blood, lymph nodes or spleen lymphocytes of (non) immunized llamas is isolated and converted into cDNA. The V domain of the heavy chain immunoglobulin reservoir is amplified by PCR. The pool of VHH genes is then inserted into a phage-display plasmid. Phagemid libraries are obtained. Fusion proteins are displayed on the tip of gIIIp of the phage. Rounds of panning allow for the isolation of single phages containing the genetic information of the VHH.
The combination of phage display technology and VHH offers promising possibilities to target biomolecules and biomaterials relevant in tissue engineering applications.

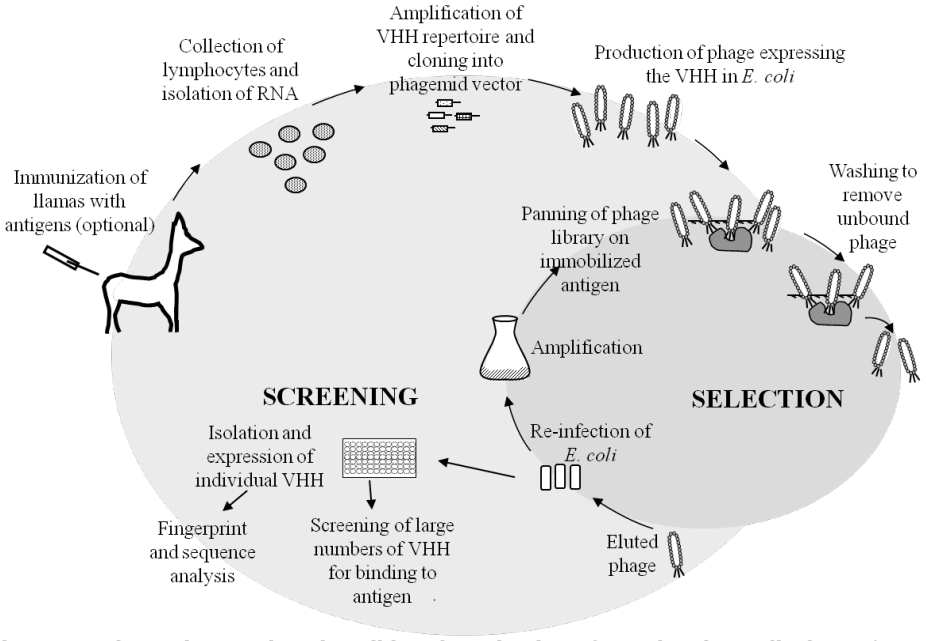

Figure 3. Schematic overview describing the selection of VHH by phage display. Schematic overview of the strategy for isolation of VHH targeting the antigen after immunization (optional) of llama. Adapted from [45].

Future perspectives

VHH are promising tools in tissue engineering. VHH are an alternative for the use of direct immobilization of exogenous growth factors on surfaces or in bulk materials. With the aid of VHH, endogenous growth factors can be rescued, concentrated and modulated at the site defect. VHH present a novel non-covalent and reversible strategy for the immobilization of growth factors in biomaterials. The versatility of the VHH, in combination with phage display, allow for a selection of a multitude of VHH binding to growth factor and biomaterials. VHH targeting growth factors can be engineered for non-covalent or covalent immobilization on surfaces. In addition, VHH can be engineered in order to obtain bivalent VHH with hetero specificity where two VHH binding units target different epitopes, for example growth factor and biomaterial. These VHH are capable of

modulating and orchestrate a biological cascade of events. Bivalent VHH binding different epitopes in the same target molecule can also be engineered to increase avidity, which might result in higher affinity towards the antigen. Polyvalent VHH can further be engineered for multiple combinations (Figure 4). VHH can be employed as carriers for imaging agents relevant for therapies and diagnostics (theragnostics) [33]. VHH can be engineered with functional groups for a directional coupling of fluorophores. VHH can be employed as a core for genetic modifications and grafting of peptide sequences in the complementary domains involved in the epitope binding recognition [24]. Peptide sequences can also be coupled to functional groups genetically incorporated at the C-terminus of the VHH. In bivalent or polyvalent VHH, cleavable linkers between the VHH units might be envisaged in order to trigger coordinated cell responses. VHH can be selected for binding to complex 3D systems such as tissues [38, 39].

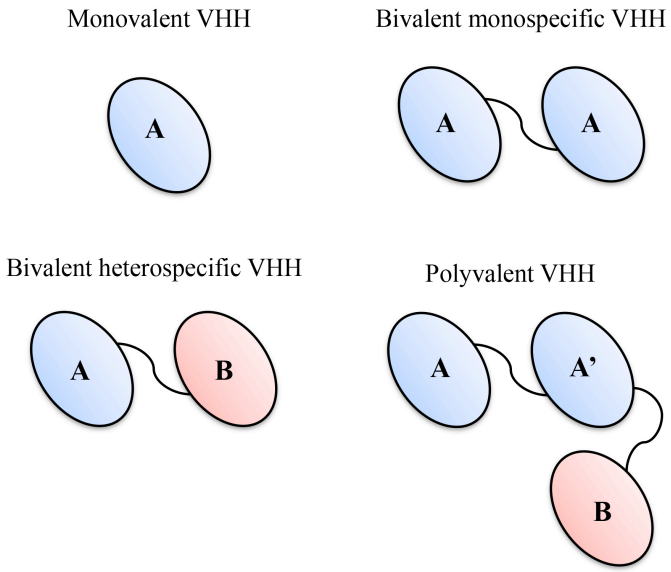

Figure 4. Schematic illustration of engineered VHH. Monovalent VHH (A) can be engineered in a monospecific bivalent VHH (A-A) or heterospecific bivalent VHH (A-B) binding two different epitopes. In addition, polyvalent VHH can be engineered (A-A'-B) with multiple binding targets.

The use of VHH in biomaterials functionalization does not require genetic modifications in growth factors and ideally do not require exogenous growth factors. VHH can be used theoretically for the functionalization of a wide range of biomaterials (ceramics, polymers, hydrogels). They might be integrated in a variety of techniques that are used for processing of these biomaterials into scaffolds like electrospinning, solvent casting, bioplotter, phase separation, etc.. The biomaterials could be functionalized with VHH either by direct anchoring through covalent coupling, or indirect via non-covalent interactions like adsorption or antibody – antigen interactions.

Taken together, VHH present a novel strategy for a functionalization of biomaterials by capturing relevant biomolecules for tissue regeneration from the vicinity of its implantation creating a microenvironment favorable for a coordinated tissue formation. VHH are novel binding molecules in tissue regeneration with great potential to improve patient care and quality of life.

Thesis Outline

The aim of this thesis is to demonstrate the potential of VHH in tissue engineering applications, with a focus on bone and cartilage tissue regeneration and develop novel functionalized biomaterials with relevant biological responses.
Chapter 1 gives a general introduction on the background in tissue engineering, biomaterial functionalization and VHH technology.
Chapter 2 presents the selection of VHH targeting growth factors bone morphogenetic protein (BMP) BMP6 and BMP7 with high affinity, which are highly relevant in skeletal tissue engineering. Biological differentiation assays reveals VHH modulation activity on BMP6 and BMP7. It further explores the physiological response of explanted metatarsals to BMP stimulation and the role of VHH in modulating BMPs effect on cartilage hypertrophy.
Chapter 3 demonstrates the potential of VHH as a carrier system for reversible growth factor immobilization on a surface in a proof-of-concept study. A combination of orthogonal supramolecular interactions is employed for the directed and homogeneous immobilization of polyhistidine-tagged VHH targeting BMP6. The system was further tested and acknowledged for the delivery of BMP6 to cells and improved osteogenic activity.
Chapter 4 presents two strategies for the incorporation of VHH in two types of biomaterials. First, VHH were incorporated in electrospun fibers of poly(ethylene oxide) (PEO). Homogenous distribution of the VHH in the electrospun fibers was shown. In addition, it was shown that the VHH remained biologically active and thus can withstand the forces and high voltage electrical fields used to obtain the fibers. In the second approach, VHH were incorporated in an *in situ* gelating dextran-based hydrogel. Retention of the VHH in the hydrogel and its controlled release over time was shown. We tested the hypothesis that inclusion of an N-linked glycosylation site in the VHH C-terminus followed by production in yeast would yield a glycosylated, and thus larger VHH and that this would increase the retention time of the VHH in the hydrogel.
Chapter 5 presents a genetically engineered VHH capable of directional grafting to poly(trimethylene carbonate) (PTMC) surfaces whilst its biological activity towards growth factors remained functional for cell differentiation. An unpaired cysteine was introduced at the C-terminus of the VHH and covalently coupled to uncrosslinked methacrylate conjugated PTMC by Michel type reaction. The release of BMP6 from

VHH was measured and the biological activity of the coupled VHH was assessed in an osteoblast differentiation assay.

Chapter 6 presents a VHH targeting bone-mimicking ceramic hydroxyapatite (HA) with binding capacities to bone. For *in vivo* evaluation VHH were site-directed conjugated to the near infrared fluorophore IRDye800CW. The potential of this VHH as a targeting agent to bone was confirmed by its injection in mice and its specific accumulation in the skeleton.

Chapter 7 presents a non-covalent strategy for binding of growth factors to biomaterial surfaces by means of an engineered bivalent VHH with dual specificity targeting HA and the growth factor (BMP7). The bivalent remained multifunctional.

Chapter 8 presents a set of VHH selected for targeting DKK1, a key molecule in degenerative and inflammatory joint disease, capable of modulating Wnt/ BMP signaling. VHH targeting DKK1 were further incorporated in an injectable thermo reversible hydrogel. Incorporation in this hydrogel resulted in controlled release of the VHH over a period of a few weeks. *Chapter 9* presents strategies developed for the selection of VHH in 3D systems such as cartilage tissue. Two strategies were explored to select VHH that can bind to osteoarthritic or healthy cartilage. A non-immunized phage library of the llama was used for isolation of VHH with specific affinity for macroscopically looking healthy human cartilage isolated *post-mortem* or arthritic cartilage derived from an arthroplasty. Another approach consisted of engineering a VHH by inserting in its complementary determining region 3 (CDR3) a previously identified peptide sequence targeting collagen type II.

Chapter 10 contains the general discussion, main conclusions of this thesis and recommendations for the future use of VHH in tissue engineering.

References

1. Tayalia, P. and D.J. Mooney, *Controlled Growth Factor Delivery for Tissue Engineering.* Advanced Materials, 2009. **21**(32-33): p. 3269-3285.
2. Lee, E.J., F.K. Kasper, and A.G. Mikos, *Biomaterials for tissue engineering.* Annals of biomedical engineering, 2014. **42**(2): p. 323-37.
3. Langer, R. and J.P. Vacanti, *Tissue engineering.* Science, 1993. **260**(5110): p. 920-6.
4. Sakiyama-Elbert, S.E. and J.A. Hubbell, *Functional biomaterials: Design of novel biomaterials.* Annual Review of Materials Research, 2001. **31**: p. 183-201.
5. Liu, X.Y., P.K. Chu, and C.X. Ding, *Surface nano-functionalization of biomaterials.* Materials Science & Engineering R-Reports, 2010. **70**(3-6): p. 275-302.
6. Papenburg, B.J., et al., *One-step fabrication of porous micropatterned scaffolds to control cell behavior.* Biomaterials, 2007. **28**(11): p. 1998-2009.
7. Papenburg, B.J., et al., *Insights into the role of material surface topography and wettability on cell-material interactions.* Soft Matter, 2010. **6**(18): p. 4377-4388.
8. Unadkat, H.V., et al., *High-throughput biological screening of cell-surface topography interactions.* Tissue Engineering Part A, 2008. **14**(5): p. 858-858.
9. Koegler, P., et al., *The influence of nanostructured materials on biointerfacial interactions.* Advanced Drug Delivery Reviews, 2012. **64**(15): p. 1820-1839.
10. Kriparamanan, R., et al., *Nanotopography: Cellular responses to nanostructured materials.* Journal of Nanoscience and Nanotechnology, 2006. **6**(7): p. 1905-1919.
11. Luginbuehl, V., et al., *Localized delivery of growth factors for bone repair.* European journal of pharmaceutics and biopharmaceutics : official journal of Arbeitsgemeinschaft fur Pharmazeutische Verfahrenstechnik e.V, 2004. **58**(2): p. 197-208.
12. Hersel, U., C. Dahmen, and H. Kessler, *RGD modified polymers: biomaterials for stimulated cell adhesion and beyond.* Biomaterials, 2003. **24**(24): p. 4385-415.
13. Glass, J.R., et al., *Characterization of a hyaluronic acid-Arg-Gly-Asp peptide cell attachment matrix.* Biomaterials, 1996. **17**(11): p. 1101-1108.
14. Lebaron, R.G. and K.A. Athanasiou, *Extracellular matrix cell adhesion peptides: Functional applications in orthopedic materials.* Tissue Engineering, 2000. **6**(2): p. 85-103.
15. Wojtowicz, A.M., et al., *Coating of biomaterial scaffolds with the collagen-mimetic peptide GFOGER for bone defect repair.* Biomaterials, 2010. **31**(9): p. 2574-2582.
16. Karageorgiou, V., et al., *Bone morphogenetic protein-2 decorated silk fibroin films induce osteogenic differentiation of human bone marrow stromal cells.* Journal of Biomedical Materials Research Part A, 2004. **71A**(3): p. 528-537.
17. Barradas, A.M., et al., *Osteoinductive biomaterials: current knowledge of properties, experimental models and biological mechanisms.* European cells & materials, 2011. **21**: p. 407-29; discussion 429.
18. Cai, L., C.B. Dinh, and S.C. Heilshorn, *One-pot Synthesis of Elastin-like Polypeptide Hydrogels with Grafted VEGF-Mimetic Peptides.* Biomaterials science, 2014. **2**(5): p. 757-765.
19. Friedlaender, G.E., *OP-1 clinical studies.* Journal of Bone and Joint Surgery-American Volume, 2001. **83A**: p. S160-S161.
20. Kuhl, P.R. and L.G. GriffithCima, *Tethered epidermal growth factor as a paradigm for growth factor-induced stimulation from the solid phase.* Nature Medicine, 1996. **2**(9): p. 1022-1027.
21. Harmsen, M.M. and H.J. De Haard, *Properties, production, and applications of camelid single-domain antibody fragments.* Appl Microbiol Biotechnol, 2007. **77**(1): p. 13-22.
22. Bell, A., et al., *Differential tumor-targeting abilities of three single-domain antibody formats.* Cancer Letters, 2010. **289**(1): p. 81-90.
23. Muyldermans, S., et al., *Camelid immunoglobulins and nanobody technology.* Vet Immunol Immunopathol, 2009. **128**(1-3): p. 178-83.

24. Muyldermans, S., *Single domain camel antibodies: current status.* J Biotechnol, 2001. **74**(4): p. 277-302.
25. Muyldermans, S., *Nanobodies: natural single-domain antibodies.* Annual review of biochemistry, 2013. **82**: p. 775-97.
26. Smolarek, D., O. Bertrand, and M. Czerwinski, *Variable fragments of heavy chain antibodies (VHHs): a new magic bullet molecule of medicine?* Postepy Higieny I Medycyny Doswiadczalnej, 2012. **66**: p. 348-358.
27. Dolk, E., et al., *Induced refolding of a temperature denatured llama heavy-chain antibody fragment by its antigen.* Proteins, 2005. **59**(3): p. 555-64.
28. van der Linden, R.H., et al., *Comparison of physical chemical properties of llama VHH antibody fragments and mouse monoclonal antibodies.* Biochimica et biophysica acta, 1999. **1431**(1): p. 37-46.
29. Gorlani, A., et al., *Antibody engineering reveals the important role of J segments in the production efficiency of llama single-domain antibodies in Saccharomyces cerevisiae.* Protein engineering, design & selection : PEDS, 2012. **25**(1): p. 39-46.
30. Hamerscasterman, C., et al., *Naturally-Occurring Antibodies Devoid of Light-Chains.* Nature, 1993. **363**(6428): p. 446-448.
31. Wesolowski, J., et al., *Single domain antibodies: promising experimental and therapeutic tools in infection and immunity.* Med Microbiol Immunol, 2009. **198**(3): p. 157-74.
32. Hassanzadeh-Ghassabeh, G., et al., *Nanobodies and their potential applications.* Nanomedicine, 2013. **8**(6): p. 1013-26.
33. Oliveira, S., et al., *Targeting tumors with nanobodies for cancer imaging and therapy.* Journal of controlled release : official journal of the Controlled Release Society, 2013.
34. Cortez-Retamozo, V., et al., *Efficient cancer therapy with a nanobody-based conjugate.* Cancer Research, 2004. **64**(8): p. 2853-2857.
35. Strokappe, N., et al., *Llama Antibody Fragments Recognizing Various Epitopes of the CD4bs Neutralize a Broad Range of HIV-1 Subtypes A, B and C.* Plos One, 2012. **7**(3).
36. McCoy, L.E., et al., *Potent and broad neutralization of HIV-1 by a llama antibody elicited by immunization.* Journal of Experimental Medicine, 2012. **209**(6): p. 1091-1103.
37. Smith, G.P. and V.A. Petrenko, *Phage Display.* Chem Rev, 1997. **97**(2): p. 391-410.
38. Cheung, C.S., J.C. Lui, and J. Baron, *Identification of chondrocyte-binding peptides by phage display.* Journal of orthopaedic research : official publication of the Orthopaedic Research Society, 2013. **31**(7): p. 1053-8.
39. Hughes, C., et al., *Human single chain fragment variable (scFv) that specifically targets arthritic cartilage.* Arthritis Rheum, 2010.
40. Coppieters, K., et al., *Formatted anti-tumor necrosis factor alpha VHH proteins derived from camelids show superior potency and targeting to inflamed joints in a murine model of collagen-induced arthritis.* Arthritis and Rheumatism, 2006. **54**(6): p. 1856-1866.
41. Strokappe, N., et al., *Llama antibody fragments recognizing various epitopes of the CD4bs neutralize a broad range of HIV-1 subtypes A, B and C.* PloS one, 2012. **7**(3): p. e33298.
42. Roy, A., A. Kucukural, and Y. Zhang, *I-TASSER: a unified platform for automated protein structure and function prediction.* Nature protocols, 2010. **5**(4): p. 725-38.
43. Zhang, Y., *I-TASSER server for protein 3D structure prediction.* BMC bioinformatics, 2008. **9**: p. 40.
44. Roy, A., J. Yang, and Y. Zhang, *COFACTOR: an accurate comparative algorithm for structure-based protein function annotation.* Nucleic acids research, 2012. **40**(Web Server issue): p. W471-7.
45. Forsman, A., et al., *Llama antibody fragments with cross-subtype human immunodeficiency virus type 1 (HIV-1)-neutralizing properties and high affinity for HIV-1 gp120.* J Virol, 2008. **82**(24): p. 12069-81.

Chapter 2

Modulation of BMP6 and BMP7 activity by means of VHH

Emilie Dooms Rodrigues[1], Mohamed El Khattabi[2], Jeroen Leijten[1], Ellie B. M. Landman[1], Sabrina Oliveira[3], Clemens van Blitterswijk[4], Theo Verrips[2], Marcel Karperien[1]

[1] Department of Developmental BioEngineering, MIRA Institute for Biomedical Technology and Technical Medicine, Faculty of Science and Technology, University of Twente, Enschede, The Netherlands;
[2] QVQ BV, Utrecht, The Netherlands;
[3] Division Cell Biology, Department of Biology, Science Faculty, Utrecht University, Utrecht, The Netherlands;
[4] Department of Tissue Regeneration, MIRA Institute for Biomedical Technology and Technical Medicine, Faculty of Science and Technology, University of Twente, Enschede, The Netherlands.

Abstract

Bone morphogenetic proteins (BMPs) are of high relevance to many skeletal tissue engineering approaches. Although BMP family members are relatively homologous, they have distinct biological effects. Specific control over the activity of the distinct BMP family members may lead to the generation of improved tissue engineering approaches. Such control can be exerted by antibodies, which are able to capture, concentrate, inhibit or enhance the activity of specific BMPs.
In this study, we present the selection of highly specific single domain antibody fragments of heavy chain antibodies of *Camelidae* (VHH) directed against BMP6 and BMP7. VHH were found to selectively bind the BMPs. The dissociation constants ranged between 1 nM and 0.6 μM. Moreover, the VHH demonstrated to possess inhibitory or stimulatory activities toward the cognate BMP. Monovalent VHH were found to potentiate the effect of BMP6 and BMP7 in cell culture and to steer hypertrophic differentiation of cartilage in metatarsals explants. Moreover, bivalent VHH directed against BMP6 was found to be more efficient as compared to monovalent VHH. Together, our results indicate that VHH are a powerful tool in controlling growth factors and their activity, in amongst others, tissue engineering applications.

Keywords: BMP, Affinity, Bioactivity, VHH, Differentiation

Introduction

Tissue engineering is a revolutionary discipline that promises novel clinical solutions for amongst others bone and cartilage disorders [1]. Traditionally, tissue engineering is based on cell-seeded scaffolds that are stimulated with growth factors. As such, control over the used growth factors is a major determinant of the clinical outcome of tissue-engineered implants. In recent years, much effort has been dedicated to the development of smart bioactive scaffolds with controlled growth factor delivery [2]. Current strategies for bone and cartilage regeneration rely mostly on key growth factors such as bone morphogenetic proteins (BMPs) [1, 3], which belong to a subgroup of the transforming growth factor-β (TGF-β) superfamily [4]. Their role in bone and cartilage regeneration has been established. Accordingly, BMPs have been proven to induce bone and cartilage formation [3, 5, 6], and are already applied clinically [3]. The short half-life and instability of BMPs require the administration of supra-physiological dosages to induce tissue repair [5]. Besides the potential carcinogenic side effects of supraphysiological doses of BMPs [7] in combination with uncontrolled effects at distant sites, the use of exogenous BMPs for bone regeneration is currently under reconsideration [8]. To circumvent these disadvantages, solutions are being designed to sequester endogenously produced BMPs locally / *in situ* and to promote a sustained reversible bioactive release.

Antibodies can play an essential role as carriers of growth factors, due to their capacity to bind tightly and specifically to their targets. When coupled to a biomaterial, antibodies can be loaded with exogenous growth factors or capture locally produced growth factors to create a reservoir of biologically active factors, thereby controlling cell differentiation at the biomaterial implant site.

Antibody- growth factor interactions are capable of stabilizing growth factors and presenting them to their receptors to catalyze downstream signaling pathways. Moreover, antibodies are capable to act as agonists or antagonists of growth factors thereby interfering with the signaling pathways. Conventional antibodies are large size molecules consisting of four protein chains. The large size and the complex association between the different chains dictate a number of limitations for the application of such antibodies. Moreover, production costs of these antibodies is high arguing against its wide spread application [9]. *Camelidae* express a special class of heavy chain antibodies that are devoid of light chains, which are consequently formed by two protein chains. The antigen binding domain of such single chain antibody is called variable heavy chain of the heavy chain only antibody (VHH) [10]. VHH are uniquely small antibody fragments capable of binding selectively and with high affinity to a specific epitope [9]. They are easy to clone (one single gene) and well expressed in bacteria and yeast [9, 11-13]. Moreover, VHH are highly soluble and show the ability to refold after denaturation [14, 15]. VHH possess genetic and structural features that make them highly suitable for widespread application in therapy, diagnostic screening and research [9, 16, 17]. Moreover, VHH versatility permits them to improve upon several therapeutic applications such as cancer therapeutics [11, 18, 19] and human immunodeficiency virus (HIV)-1 [20, 21]. The use

of VHH in tissue engineering is yet to be explored. The integration of such VHH in biomaterials is a potent tool to influence cell attachment, growth, differentiation and migration and consequently increase successful tissue regeneration.
BMPs functionally support various processes [22]. BMPs can be found in different cell types and can be expressed in several differentiation states resulting in distinct performances. Typical members of the BMP family are BMP6 and BMP7, the latter is also known as Osteogenic protein-1 (OP-1) which has demonstrated the ability to repair bone and cartilage [3, 23]. Hypertrophy is the terminal stage in endochondral ossification, which prepares the chondrocyte for apoptosis and the cartilage to be turned over into bone [24]. BMP6 and BMP7 both stimulate chondrogenesis, but only BMP6 induces hypertrophy [25, 26] whilst BMP7 inhibits it [27]. Moreover, BMP6 is expressed in hypertrophic chondrocytes, whereas BMP7 is expressed in proliferating chondrocytes that are primed for hypertrophic differentiation [26]. The ability to steer (non-) hypertrophic differentiation during chondrogenesis is expected to have great value in tissue engineering approaches aiming at articular cartilage reconstruction or bone regeneration.
In the present work we have explored the possibility of using VHH for tissue engineering solutions. Specifically, we have studied the ability of VHH to act as agonist or antagonist to BMP6 and BMP7 to control cell differentiation. We report that VHH can specifically target BMP family members and affect their downstream signal transduction. This identifies VHH as promising candidates to orchestrate the differential expression of BMPs. Next to the flexibility, low cost production and ability to couple to biomaterials, VHH may therefore provide a promising tool for the spatiotemporal control of signaling events, and may constitute a platform for instructive functionalization of biomaterials.

Materials and methods

Llama immunization and VHH phage library construction
All immunizations were approved by the Utrecht University ethical committee for animal experimentation. Two llamas were immunized with recombinant human BMP6 (R&D systems, #507-BP/CF) and with recombinant human BMP7 (R&D systems, #354-BP/CF). The antigens were mixed with the adjuvant Stimune (CEDI Diagnostics, Lelystad, The Netherlands) and injected intramuscularly at days 0, 14, 28 and 35. At day 44, peripheral blood lymphocytes (PBLs) were isolated for RNA extraction and library construction. The VHH phage display libraries were generated as previously described [20, 28, 29] and transferred to *Escherichia coli* strain TG1 [*supE hsd_5 thi* (*lac-proAB*) F(*traD36 proAB_ lacI*q *lacZ_M15*)] by electroporation.

Selection of VHH targeting growth factors
Phage display [30] was used to select phages binding to BMP6 or BMP7 using the VHH phage display libraries described above. The phages were selected via the panning

method by coating a MaxiSorp plate (Nunc, Thermo Scientific) overnight at 4 ºC with decreasing concentrations of BMP6 and BMP7 (5 μg, 2 μg and 0.2 μg) in phosphate buffered saline (PBS, Gibco). Phages (approximately 10^{10} colony forming units (cfu)), were incubated for 2 hours at room temperature with the wells coated with BMP and blocked with 4% Marvel (dried skimmed milk, Premier International Foods) in PBS. After thorough washing, phages binding to BMP6 or BMP7 were eluted by incubating in 100 mM triethylamine (TEA) for 15 minutes at room temperature. Eluted phages were immediately neutralized by the addition of 1M Tris-HCl, pH 7.5. DNA information of the selected phages was rescued by infection of *E. coli* TG1 strain and subsequent selection on agar plates for ampicillin resistance. To obtain recombinant bacteriophages expressing the VHH as fusion proteins with the bacteriophage gene III product for the second round of selection, rescued TG1 *E. coli* were grown to logarithmic phase and then infected with helper phage VCSM13 (Stratagene, La Jolla, CA, USA) [31]. The phages were used in the second panning round of selection, on wells coated with BMP6 and BMP7 as described above. Selected phages from single colonies from the second round of selection were sequenced (Macrogen). The VHH clones selected were named C2, G7 and H1.

VHH plasmids, production and purification

E. coli strains TG1 or DH5α were used for the maintenance of the plasmids and expression of proteins. DNA information of the selected VHH was subcloned into a plasmid containing C-terminus Myc and His tags (pMEK219). For the production of the VHH, *E. coli* with plasmid pMEK219 with the subcloned VHH, was grown in Luria Broth (LB) or 2x yeast extract and tryptone (YT) medium supplemented with 2% (w/v) glucose and antibiotic, ampicillin 100 μg/ ml. VHH expression was induced by the addition of 1 mM isopropyl β-D-1-thiogalactopyranoside **(**IPTG) and cultivation at 37^{o}C for 4 hours, while shaking [32, 33]. VHH proteins were purified from the periplasmic fraction via the C-terminus his-tag by cobalt affinity chromatography (TALON His-Tag Purification Resin, ClonTech). Purified VHH were analyzed by means of sodium dodecyl sulfate polyacrylamide gel electrophoresis (SDS-PAGE) and Coomassie staining. The final VHH concentration was determined from the UV absorption at 280 nm (NanoDrop 1000 Spectrophotometer, Thermo Scientific) and the theoretical mass extinction coefficient.

VHH binding specificity

Binding specificity of the purified VHH to BMP6 and BMP7 was tested in an enzyme-linked immunosorbent assay (ELISA) binding assay. MaxiSorp plate wells were coated overnight at 4^{o}C with BMP6 or BMP7 (30 nM) in PBS. After blocking of the wells with 4% Marvel in PBS, a concentration range of VHH (ranging from 0 to 7 μM) in 2% Marvel were incubated for 2 hours in the coated and blocked wells. The wells were washed with PBS Tween (PBS containing 0.5% (v/v) Tween-20, PBST) and PBS. Bound VHH were detected by incubation with a rabbit anti-VHH serum (K976) and a donkey

anti-rabbit antibody coupled to a peroxidase. The amount of HRP was developed by the addition of Tetramethylbenzidine (TMB, 1-Step Ultra TMB-ELISA, Thermo Scientific). The reactions were stopped by the addition of H_2SO_4 and measured at 450 nm (Micro Plate Reader).

VHH biological activity

Mouse KS483-4C3 pre-osteoblast cell line was used as a model for osteogenic differentiation [34]. Cells were cultured in α-MEM (Gibco) supplemented with 10% fetal bovine serum (FBS; Cambrex), 100 U/ml penicillin (Gibco) and 100 μg/ml streptomycin (Gibco) and were incubated at 37 ºC in humidified atmosphere and 5% CO_2. To perform differentiation assays, cells were seeded at a density of 10 000 cells/cm^2 (day 0). Upon reaching confluence (day 4) cells were cultured for 3 days with ascorbic acid (50 μg/ml; Sigma Aldrich) and stimulated with BMP6 (100 ng/ml; R&D Systems) or BMP7 (300 ng/ml; R&D Systems) in the presence or absence of VHH C2, G7 or H1 (1 μg/ ml). At day 7, cells were washed with PBS and lysed with CDPStar lysis buffer (Roche). To evaluate alkaline phosphatase (ALP) activity, cell lysate was added to CDPStar reagent (Roche) and luminescence was measured using Vector Microplate Luminometer (Promega). The luminescence units were corrected for DNA content. DNA concentration was determined via proliferation assay according to manufacturer's protocol (CyQuant Cell Proliferation Assay Kit; Invitrogen).

Construction of monospecific bivalent VHH H1-H1 recognizing growth factors

The generation of polymeric constructs was performed as previously described [35]. Briefly, bivalent construct connected by a flexible sequence (GS-linker) represented by a repeat of the pentapeptide 'Gly-Gly-Gly-Gly-Ser' (Gly_4/ Ser linker) was generated by PCR. Separate PCR reactions were performed for each VHH subunit (N-terminus and C-terminus) using different sets of primers encompassing different parts of the linker and restriction sites: *BamH*I at the 3' and *Sfi*I at the 5'for the N-terminus VHH subunit, and *BamH*I at the 5' and *Bst*EII at the 3'for the C-terminus VHH subunit. The different subunits were cloned into the expression vector pMEK222 containing C-terminus FLAG and His6 tags. The monospecific bivalent VHH (H1-H1) was produced in *E. coli* after IPTG induction and purified with Talon as described above.

Biological activity of homospecific bivalent versus monovalent VHH

C2C12 cells were used as a model for osteogenic differentiation. Cells were cultured in Dulbecco's Modified Eagles Medium (DMEM; Gibco) supplemented with 10% fetal bovine serum (FBS; Cambrex), 100 U/ml penicillin (Gibco) and 100 μg/ml streptomycin (Gibco) and were incubated at 37 ºC in humidified atmosphere and 5% CO_2. To assess the differentiation of C2C12, cells were seeded with at a density of 10 000 cells/cm^2 (day 0). Upon reaching confluence (day 4) cells were cultured for 3 days with ascorbic acid (50 μg/ml; Sigma Aldrich) and stimulated with BMP6 (100 ng/ ml; R&D Systems) and in the presence or absence of VHH H1 or H1-H1 in a concentration range of 0 to

100 nM. At day 7, cells were washed with PBS and lysed with CDPStar lysis buffer (Roche). To evaluate ALP activity, cell lysate was added to CDPStar reagent (Roche) and luminescence was measured using Vector Microplate Luminometer (Promega). The luminescence units were corrected for DNA content. DNA concentration was determined via proliferation assay according to manufacturer's protocol (CyQuant Cell Proliferation Assay Kit; Invitrogen).

Mouse fetal metatarsals culture

All mouse experiments were approved by the Utrecht University ethical committee for animal experimentation. Mouse fetal metatarsals were isolated from FVB mouse embryos (time-paired, Harlan) at day 17.5 of gestation [36]. After isolation, metatarsals were individually cultured in 24-well plates in 200 μl per well of α-MEM, supplemented with 10% FBS, 100 U/ml penicillin, 100 mg/ml streptomycin and 1% Glutamax (Invitrogen) for 48 hours. After this equilibration period, metatarsals were cultured in the presence of BMP6 (100 ng/ml; R&D Systems) in the presence or absence of VHH H1 or H1-H1 (0.5 μg/ml) up to 7 days for histological and morphometric analysis. The medium was not changed during the culture period.

Histological and morphometric analysis of metatarsals

For histological examination, specimens were fixed in 10% buffered formalin and dehydrated through baths of progressively higher concentrations of ethanol before embedding in paraffin. Five micrometer longitudinal sections were cut using a rotary microtome (HM355S Microm International). Paraffin sections were deparaffinized in xylene and rehydrated through incubations in progressively decreasing concentrations of ethanol solutions. Sections were stained for glycosaminoglycans using 0.5% Alcian Blue for 30 minutes and counterstained with 1% Nuclear Fast Red in 5% aluminum sulfate for 5 minutes.

The total area of the metatarsals cross sections was determined using image analysis software (ImageJ).

Statistical Analysis

Statistical analyses were performed using GraphPad Prism version 5.00 for Windows, GraphPad Software (San Diego, California). Analyses were based on one-way ANOVA and a Tukey's Post-hoc test ($p < 0.05$) among all samples or between samples and controls. In the case where only differences between sample and control were to be assessed a t-test was used to determine statistical differences ($p < 0.05$).

Results

VHH targeting BMP6 and/or BMP7

To investigate the possibility of using VHH for tissue engineering solutions, VHH were selected from phage display libraries constructed from RNA isolated from PBLs of llamas immunized with BMP6 and BMP7 [37]. After two selection rounds, a clear enrichment was found on the antigen coated wells compared to empty wells. Several clones were selected for further screening using binding to either BMP6, BMP7 or to both BMP6 and BMP7. From two master plates of 190 VHH clones, the selection of individual clones was sized down by grouping on basis of restriction patterns and ELISA binding assay (data not shown). In supplementary data (Figure S1A) the sequences of a complete set of the selected VHH families can be found. In Figure S1B the biological effects of these VHH are shown displaying a wide variety of activities (inhibiting (VHH: C2, F2, F11, H1, H9) or potentiating (VHH: G1, G7) BMP activity) and selectivity for either BMP6 (VHH: G1, H1) or BMP7 (VHH: F2, F11, G7, H9) or both (VHH: C2). Of this list, three clones were selected for further characterization based on binding specificity. These clones were VHH C2, G7 and H1, representing binders of both BMP6 and BMP7, BMP7 or BMP6, respectively. As expected, the amino acid sequences of the three VHH clones were found to be distinct and to belong to different families of VHH (Figure 1A).

The genes of the three VHH were subcloned into expression plasmids and produced and purified as indicated in Materials and Methods. Purity of the VHH was assessed by SDS-PAGE and Coomassie staining (Figure 1B). The clear bands observed of ca. 16 kDa correspond to the monovalent VHH and are in agreement with values found in literature [16, 38].

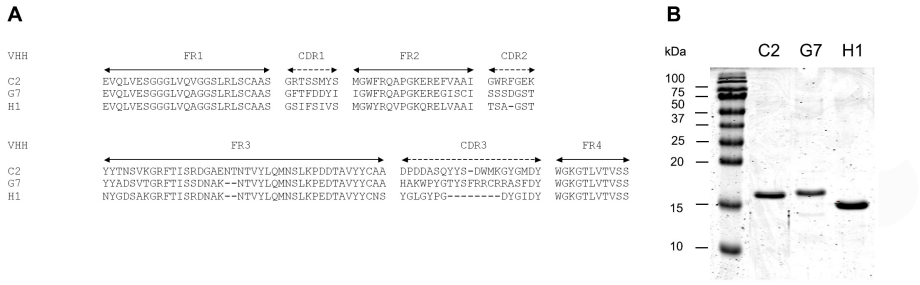

Figure 1. Characterization of VHH targeting BMPs. (A) Alignment of the amino acid sequence of VHH C2, G7 and H1 targeting both BMP6 and BMP7, BMP7 and BMP6, respectively. Frame works (FR) and complementary determining regions (CDR) of the VHH are indicated according to Chothia [39]. (B) Purified VHH C2, G7 and H1 were sized-separated by a 15% SDS-PAGE and stained with Coomassie Brilliant Blue. Molecular weight markers (in kDa) are indicated at the left.

Selected VHH bind BMP6 and/or BMP7

To confirm the specific binding of VHH to BMP6 and/or BMP7, binding studies were performed using ELISA measurements. To determine the affinity between VHH and BMP a titration series of VHH over a range of 0.7 nM to 7 μM was performed while BMP coating was kept constant at 30 nM throughout the series. When binding of VHH to BMP6 and/or BMP7 occurred a change in signal was measured (Figure 2).

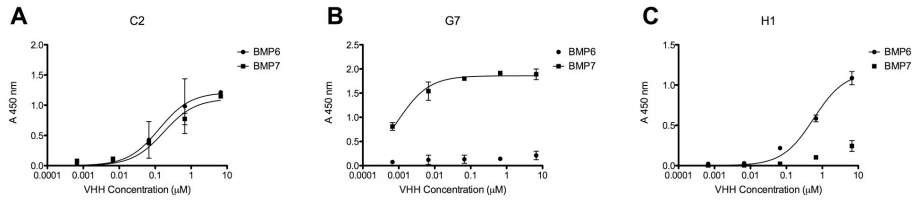

Figure 2. Dose-response binding of the selected VHH to BMP6 and BMP7. Binding of the VHH C2 (A), G7 (B) and H1 (C) to BMP6 and BMP7 was determined by solid phase ELISA. Nunc Maxisorp wells coated with BMP6 or BMP7 (30 nM) or PBS (negative control) were incubated with the indicated VHH concentrations and bound VHH were detected with a rabbit anti-VHH serum and a Donkey anti-rabbit antibody coupled to a peroxidase. Colorimetric conversion of *O*-phenyldiamine (OPD) in the presence of H_2O_2 was measured at 450 nm (A 450 nm). Data represent the mean +/- SD of 2 independent experiments.

The data indicated that VHH C2 binds to both BMP6 and BMP7 with similar affinities (~0.1 μM) (Table 1). VHH G7 binds exclusively to BMP7 with an exceptionally high affinity of 0.9 nM (Table 1). Finally, VHH H1 binds to BMP6 only (Figure 2) with an affinity of ~0.6 μM (Table 1). The K_d deducted from fitting of experimental ELISA data to specific binding models are in agreement with values found in literature for VHH [11, 40]. The three selected VHH did not show any binding to BMP2 and BMP4 (data not shown).

Table 1. Dissociation constant, K_d, of the indicated VHH calculated by fitting the ELISA data generated in Figure 2 to a one-site binding model. N.A., not applicable.

	K_d	
VHH	**BMP6**	**BMP7**
C2	$1.3x10^{-7}$ M	$1.7x10^{-7}$ M
G7	N.A.	$9.5x10^{-10}$ M
H1	$5.7x10^{-7}$ M	N.A.

The selected VHH are bioactive

To evaluate the potential of the selected VHH for application in tissue engineering strategies, their ability to inhibit or enhance activity of BMPs in an osteoblast differentiation experiment was tested. KS483-4C3 murine pre-osteoblast cells were

cultured in standard osteogenic conditions in the presence or absence of BMPs supplemented with VHH. In KS483-4C3 cells, ALP activity was induced in the presence of BMP6 and BMP7 by 2.9 and 4.2 fold, respectively (Figure 3A). In the presence of VHH C2, ALP activity induced by either BMP6 or BMP7 was inhibited to approximately 50% (Figure 3B). Interestingly, in the presence of VHH G7, ALP activity induced by BMP7 was further potentiated to approximately 230%, whereas no significant effect on ALP activity induced by BMP6 was measured (Figure 3B). In the presence of VHH H1, ALP activity induced by BMP6 was inhibited to approximately 30%. The inhibition of ALP activity by VHH H1 induced by BMP7 was not significant (Figure 3B). For the function of the complete set of the selected VHH see Figure S1B (supplementary information).

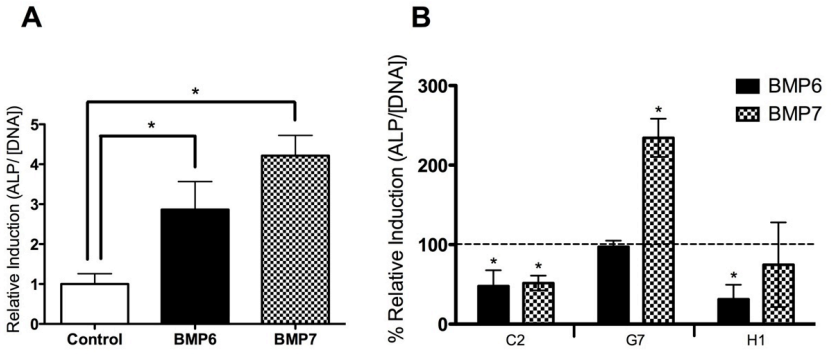

Figure 3. Effect of VHH on BMP signal transduction. (A) Effect of BMP6 and BMP7 on ALP production in the murine cell line KS483-4C3. The ALP activity was normalized for the total DNA content of KS483-4C3 cells after 7 days of culture, and expressed as relative induction with respect to non-treated cells. Data is expressed as the mean of 3 independent experiments +/- SD (B) Biological effect of VHH in the presence of BMP6 or BMP7 on cell differentiation. KS483-4C3 cells were stimulated with BMP6 or BMP7 in the presence of VHH clones (C2, G7 and H1). The ALP activity is normalized by the total DNA content of KS483 cells after 7 days of culture, measured and expressed relative to control cultures treated with either BMP6 or BMP7 in the absence of VHH. Values are expressed as % change relative to control, which was set at 100%. * $p < 0.05$. The experiment was repeated three-times and means of the values were represented in the graph and standard deviations (error bars) are indicated. * $p < 0.05$.

Bivalent VHH increased biological activity

We then investigated whether the effectiveness of the BMP modulating VHH could be further improved by engineering the monovalent VHH into a bivalent VHH.

A bivalent variant of the VHH H1 (VHH H1-H1) was engineered as described in Materials and Methods. The resulting bivalent VHH H1-H1 (schematically illustrated in Figure 4A) was produced in *E. coli*. The molecular size of the bivalent VHH was as expected approximately double the size of the monovalent VHH H1, and only minor degradation occurred as evidenced by minute amounts of lower molecular weight bands (Figure 4B). Moreover, genetic modification of the VHH from a monovalent to bivalent

variant did not suffer from steric hindrance as predicted by I-TASSER (Figure 4C) [41-43]. To determine whether VHH H1-H1 increased the potency of VHH H1 in inhibiting ALP activity induced by BMP6, an osteogenic differentiation assay was performed. In C2C12 cells, the ALP activity was strongly induced by the addition of BMP6 by 13 fold (Figure 5A). In the presence of BMP6 and VHH H1 at 1 nM, ALP activity was decreased with 12%, whereas an equimolar amount of VHH H1-H1 significantly decreased ALP activity with 49% (Figure 5B). This indicated that bivalency synergistically enhanced the effect of the VHH H1. At 10 and 100 nM VHH concentration, the enhancing effect of bivalency was not observed as both monovalent and bivalent VHH H1 inhibited BMP6-induced ALP by more than 80% (Figure 5B).

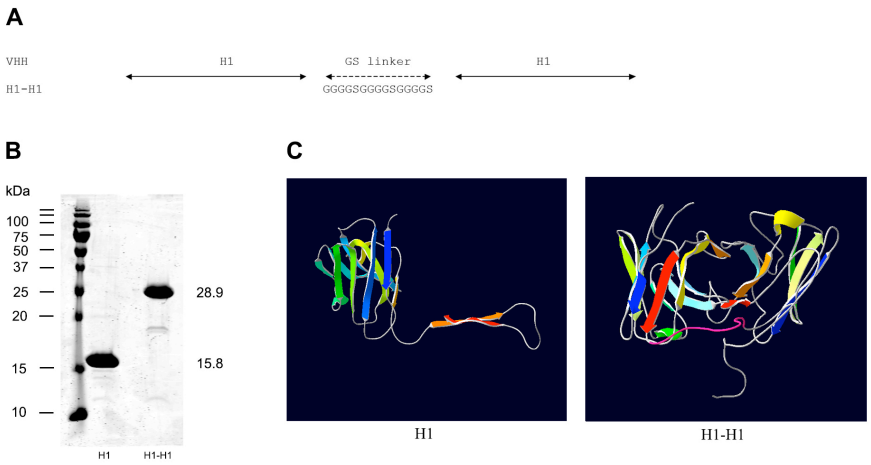

Figure 4. Characterization of bivalent VHH H1. (A) Schematic representation of amino acid sequence of genetically engineered VHH H1-H1. (B) Purified VHH H1 and H1-H1 were sized-separated by a 15% SDS-PAGE and stained with Coomassie Brilliant Blue. Molecular weight markers (in kDa) are indicated at the left. Calculated molecular weights of the monovalent H1 and bivalent H1 are indicated at the right. (C) Predicted 3D protein models of the generated VHH monovalent H1 (left) where the protein chain is represented by ribbons and colored with rainbow spectrum from N-terminus (blue) to C-terminus (red) and bivalent H1-H1 (right) where the GS linker is highlighted pink.

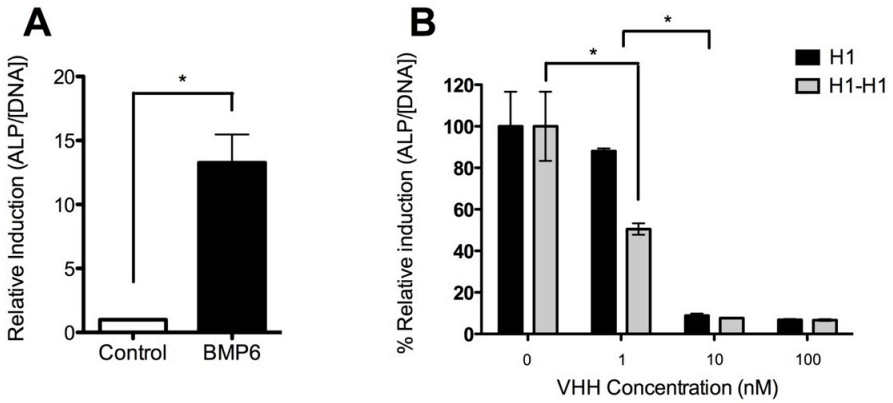

Figure 5. Effect of bivalent VHH (H1-H1) on ALP expression by BMP6. (A) Effect of BMP6 on production of ALP by C2C12 cells. The ALP activity was normalized to the total DNA content of C2C12 cells after 7 days of culture, and expressed as relative induction with respect to non-treated cells. Data are expressed as the mean of 3 experiments +/- SD. (B) Amount of ALP produced by C2C12 cells in the presence of BMP6 and the indicated monovalent and bivalent VHH H1 concentrations, relative to the amount of ALP produced by the same cells in the presence of BMP6 (set as 100%). The ALP activity was normalized to the total DNA content of C2C12 cells after 7 days of culture, and expressed as relative induction with respect to control (cells treated with BMP6). The experiment was repeated three times and expressed as mean +/- SD. * $p < 0.05$.

Metatarsals respond to BMP6 stimulation and VHH treatment

Fetal metatarsals were incubated with BMP6 in the presence or absence of monovalent or bivalent VHH H1 to assess VHH's influence on induced cartilage growth and tissue differentiation. Macroscopic examination of explanted metatarsals cultured up to 7 days with BMP6 revealed a significant growth in length, and a marked increase in volume of the metatarsals (Figure 6A and 6B). The monovalent VHH H1 significantly reduced the effect of BMP6. However, the metatarsal volume was still larger than metatarsals incubated in the absence of BMP6 (Figure 6A and 6B). In agreement with cell culture experiments an equimolar concentration of bivalent VHH H1 reduced the volume and area of the metatarsals treated with BMP6 even further (Figure 6A and 6B). Bivalent VHH H1 was more effective than monovalent VHH H1 in preserving the original shape of the metatarsals and obstructing the effect of BMP6 on metatarsals. The primary ossification site did not show any significant changes. Histological analysis revealed that treatment with BMP6 potently induced hypertrophic differentiation and longitudinal growth in mouse fetal metatarsals (Figure 6C). Treatment of metatarsals with BMP6 and monovalent VHH H1 showed a marked reduction in hypertrophy of the cells. The reduction was further pronounced in metatarsals treated with BMP6 and bivalent VHH H1. Cell volume/area of this last treatment was undistinguishable from the sections of the non-treated metatarsals (Figure 6C).

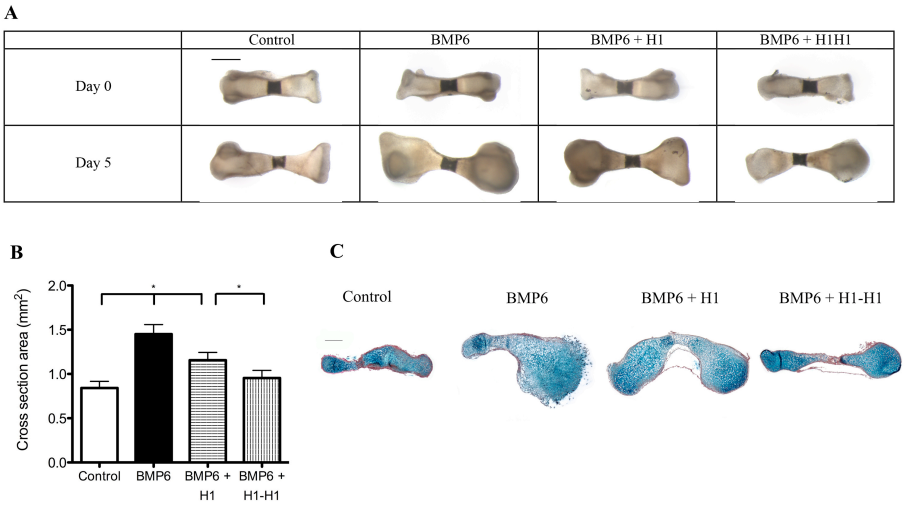

Figure 6. Effect of monovalent and bivalent VHH H1 on growth and differentiation of mouse metatarsals induced by BMP6. (A) Microphotographs of representative metatarsals at different time points and different treatments. Scale bar represents 500 μm. A representative metatarsal out of 5 replicates is shown. (B) Average metatarsals cross-section areas in (mm^2) calculated using image analysis by ImageJ. Treatment of metatarsals is indicated on the X-axis. Data represents the mean of five independent experiments +/- SD. * $p < 0.05$. (C) Histological analysis of metatarsals explants treated as indicated. The metatarsals were stained with Alcian Blue and Nuclear fast red. A representative example out of 5 replicates is shown. Scale bar represents 250 μm.

Discussion

In this study we have generated, isolated and characterized VHH that can act as targeting agents for BMP6 and/or BMP7. We demonstrated that the selected VHH can specifically bind to BMP6, BMP7 or both BMP6 and BMP7. Next to specificity in binding, we showed that the VHH also displayed relevant biological activity. Both BMP inhibiting and potentiating VHH were selected. Here we have demonstrated that the use of an immunized library of VHH, together with specific selection techniques, allows for efficient identification of these functionalized antibodies even when llamas are co-immunized with structurally related antigens such as BMP6 and BMP7.

VHH can be very specific and versatile with high binding constant values as shown for VHH G7. Dissociation constants can be used as a preliminary tool for drug design. In tissue engineering it is of upmost importance to design a scaffold/implant with spatiotemporal release of growth factors that matches the natural tissue regeneration pattern and remodeling phases [44]. The meticulous control over the release of different growth factors might allow a cost-effective, robust and predictable tissue engineering performance. VHH can be a versatile tool to accomplish spatio-temporally controlled release. Unlike growth factors that are highly susceptible for manipulation such as formulation of these factors in a drug depot or coupling to a biomaterial, VHH are far less sensitive and do not lose biological activity upon heating and treatment with a variety of organic solvents [9, 15].

Different antibodies and thus different VHH can bind to different epitopes. VHH C2 has a similar K_d for BMP6 and BMP7 and acts as an antagonist for both BMP6 and BMP7. Nevertheless, it is unclear whether the binding site of VHH C2 is the same for BMP6 and BMP7. VHH binding to the different epitopes can explain the effects of increase, decrease or no-effect on BMP activity. The steric hindrance to access the different epitopes is also a factor that explains the biological activity of the VHH.

Surprisingly, VHH G7 potentiated the biological activity of BMP7 in induction of ALP. Various possibilities can explain the potentiating effect of a VHH. For example, the conjugation of VHH G7 with BMP7 may induce a conformational change in BMP7 facilitating the binding to its receptor [45]. Furthermore, it is known that the activity of BMP7 is potently inhibited by the presence of antagonists such as Noggin, Chordin and Gremlin [3]. It is conceivable that VHH G7 interferes with this antagonistic activity by preventing their binding and thus counter acting this antagonist mediated inactivation of BMP7 [46]. More detailed follow-up studies are warranted to explain this potentiation phenomenon.

The effectiveness of the desired control over BMPs via VHH could be further improved by engineering a bivalent construct. Indeed this is shown in our study with bivalent VHH (H1-H1) as it further reduced ALP activity in *in vitro* biological assays. Particularly at low concentrations, the bivalent VHH appears more effective than an equimolar concentration of monovalent VHH.

The control over growth factors is important for the regulation of tissue formation. In this study, we have shown that BMP6 induced tissue growth in explanted metatarsals cultured *ex vivo* in accordance with literature [47]. Co-treatment with VHH inhibited this effect compared with control. In particular, bivalent VHH (H1-H1) was even more efficient than its monovalent form (H1). These results are in accordance with the findings obtained in cell culture experiments confirming the efficacy of mono VHH and increased efficiency of bivalent VHH.
VHH can further be employed to enhance tissue engineering strategies. For example, VHH could be used for the modification of biomaterials to enhance their biological instructive properties through coupling to biomaterial surfaces. In this way, VHH could act as concentrators of endogenous and/or exogenous growth factors creating a depot function at the biomaterial cell surface for sustained release. This system does not require genetic or chemical modifications of growth factors, as no covalent coupling between growth factor and biomaterials is required. Alternatively, it is possible to engineer polyvalent VHH targeting distinct growth factors. As such, it is possible to present cells with distinct growth factors simultaneously, which might provide additional control over cell behavior. Furthermore, VHH can stabilize growth factors by its interactions. VHH can also be used as imaging tools when associated with fluorophores or other imaging agents [18] and help clarify the mechanism behind the signal transduction of growth factor receptors [48].

Conclusion

In this study we have isolated VHH that specifically interact with BMP6 and BMP7. They either inhibit BMP activity or, in case of VHH G7, potentiate the effect of BMP7. This allows for unprecedented control over growth factors signaling in tissue engineering applications by incorporating these VHH in tissue engineering strategies, for example by conjugation to biomaterials.
The versatile properties of the VHH render this novel antibody platform very valuable in the field of tissue engineering based research where several disease mechanisms are in need of agonists and antagonists. Furthermore, polyvalent bioactive molecules offer the possibility for more effective therapeutics.

Acknowledgements

This work was supported by project P2.02 OAControl of the research program of the BioMedical Materials Institute, co-funded by the Dutch Ministry of Economic Affairs, Agriculture and Innovation.
The authors acknowledge long-term program support of the Dutch Arthritis Association to MK.

Supplementary information

A

VHH	FR1	CDR1	FR2	CDR2
C2	EVQLVESGGGLVQVGGSLRLSCAAS	GRTSSMYS	MGWFRQAPGKEREFVAAI	GWRFGEK
F2	EVQLVESGGGFVQAGGSLRLSCAAS	GSIFSINA	MGWYRQAPGKQRELVAAI	T-SGGST
F11	EVQLVESGGGLVQAGGSLRLSCAAS	GRTFSGYV	AGWFRQAPGKEREFVAAS	S-WSGIT
G1	EVQLVESGGGLVQAGGSLRLSCAAS	RRISGIYA	MGWYRQSPGKERELVAAI	T-TSDHT
G7	EVQLVESGGGLVQAGGSLRLSCAAS	GFTFDDYI	IGWFRQAPGKEREGISCI	SSSDGST
H1	EVQLVESGGGLVQAGGSLRLSCAAS	GSIFSIVS	MGWYRQVPGKQRELVAAI	TSA-GST
H9	EVQLVESGGGLVQAGGSLRLSCAAS	GSAFSINA	MGWYRQGPGKQRTLVARI	T-SGGST

VHH	FR3	CDR3	FR4
C2	YYTNSVKGRFTISRDGAENTNTVYLQMNSLKPDDTAVYYCAA	DPDDASQYYS-DWMKGYGMDY	WGKGTLVTVSS
F2	NYADSVKGRFTISRDNAK--NTLYLQMNSLKPEDTAVYYCSA	VTILLTS-----GGWGSGNDY	WGQGTQVTVSS
F11	YYGDSVKGRFTISRDNAK--NTVYLQMNSLKPEDTAVYYCGA	GKGYYKD--------YRGYDY	WGQGTQVTVSS
G1	NYADFVKGRFTISRDKVN--NTVYLEMNTLKPEDTAVYYCKQ	S------------AWG-RNDY	WGQGTRVTVSS
G7	YYADSVTGRFTISSDNAK--NTVYLQMNSLKPEDTAVYYCAA	HAKWPYGTYSFRRCRRASFDY	WGKGTLVTVSS
H1	NYGDSAKGRFTISRDNAK--NTVYLQMNSLKPEDTAVYYCNS	YGLGYPG--------DYGIDY	WGKGTLVTVSS
H9	NYADSVKGRFTISRDNAK--NTVYLQMNSLKPEDTAVYYCYA	VHSKLST-----TGWGTIGDY	WGQGTQVTVSS

B

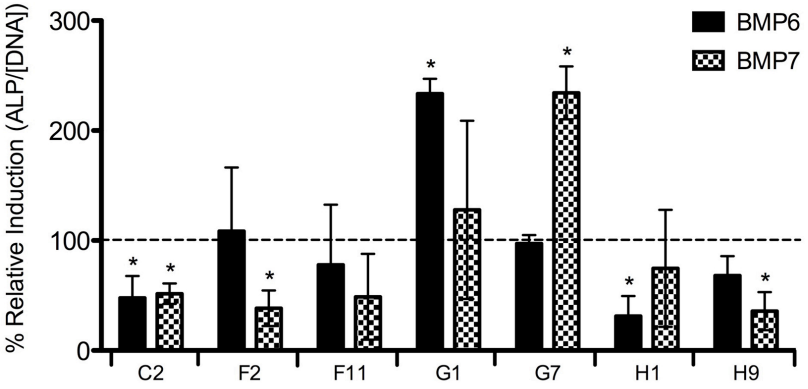

Figure S1. Complete set of VHH selected targeting BMP6 and/or BMP7. (A) Amino acid sequences alignment of VHH selected targeting BMP6 and/or BMP7. (B) Biological effect of VHH in the presence of BMP6 or BMP7 on cell differentiation. KS483 cells were stimulated with (100 ng/ml) BMP6 or (300 ng/ml) BMP7 in the presence of (1 µg/ml) VHH clones (C2, F2, F11, G1, G7, H1 and H9). The ALP activity is normalized by the total DNA content of KS483 cells after 7 days of culture, measured and expressed relative to control cultures treated with either BMP6 or BMP7 in the absence of VHH. Values are expressed as % change relative to control, which was set at 100%. * $p < 0.05$.

References

1. Reddi, A.H., *Morphogenesis and tissue engineering of bone and cartilage: inductive signals, stem cells, and biomimetic biomaterials.* Tissue engineering, 2000. **6**(4): p. 351-9.
2. Lee, K., E.A. Silva, and D.J. Mooney, *Growth factor delivery-based tissue engineering: general approaches and a review of recent developments.* Journal of the Royal Society, Interface / the Royal Society, 2011. **8**(55): p. 153-70.
3. Bessa, P.C., M. Casal, and R.L. Reis, *Bone morphogenetic proteins in tissue engineering: the road from the laboratory to the clinic, part I (basic concepts).* Journal of tissue engineering and regenerative medicine, 2008. **2**(1): p. 1-13.
4. Namatollahi, L., et al., *[A novel human bone morphogenetic protein-7 variant with an enriched heparin-binding site].* Molekuliarnaia biologiia, 2013. **47**(3): p. 453-60.
5. Bessa, P.C., M. Casal, and R.L. Reis, *Bone morphogenetic proteins in tissue engineering: the road from laboratory to clinic, part II (BMP delivery).* Journal of tissue engineering and regenerative medicine, 2008. **2**(2-3): p. 81-96.
6. Ducy, P. and G. Karsenty, *The family of bone morphogenetic proteins.* Kidney International, 2000. **57**(6): p. 2207-2214.
7. Kim, M. and S. Choe, *BMPs and their clinical potentials.* Bmb Reports, 2011. **44**(10): p. 619-634.
8. Jeon, O., et al., *Long-term delivery enhances in vivo osteogenic efficacy of bone morphogenetic protein-2 compared to short-term delivery.* Biochemical and biophysical research communications, 2008. **369**(2): p. 774-80.
9. Harmsen, M.M. and H.J. De Haard, *Properties, production, and applications of camelid single-domain antibody fragments.* Appl Microbiol Biotechnol, 2007. **77**(1): p. 13-22.
10. Muyldermans, S., *Single domain camel antibodies: current status.* J Biotechnol, 2001. **74**(4): p. 277-302.
11. Muyldermans, S., *Nanobodies: natural single-domain antibodies.* Annual review of biochemistry, 2013. **82**: p. 775-97.
12. Smolarek, D., O. Bertrand, and M. Czerwinski, *Variable fragments of heavy chain antibodies (VHHs): a new magic bullet molecule of medicine?* Postepy Higieny I Medycyny Doswiadczalnej, 2012. **66**: p. 348-358.
13. van de Laar, T., et al., *Increased heterologous protein production by Saccharomyces cerevisiae growing on ethanol as sole carbon source.* Biotechnol Bioeng, 2007. **96**(3): p. 483-94.
14. Dolk, E., et al., *Induced refolding of a temperature denatured llama heavy-chain antibody fragment by its antigen.* Proteins, 2005. **59**(3): p. 555-64.
15. van der Linden, R.H., et al., *Comparison of physical chemical properties of llama VHH antibody fragments and mouse monoclonal antibodies.* Biochimica et biophysica acta, 1999. **1431**(1): p. 37-46.
16. Wesolowski, J., et al., *Single domain antibodies: promising experimental and therapeutic tools in infection and immunity.* Med Microbiol Immunol, 2009. **198**(3): p. 157-74.
17. Hassanzadeh-Ghassabeh, G., et al., *Nanobodies and their potential applications.* Nanomedicine, 2013. **8**(6): p. 1013-26.
18. Oliveira, S., et al., *Targeting tumors with nanobodies for cancer imaging and therapy.* Journal of controlled release : official journal of the Controlled Release Society, 2013.
19. Cortez-Retamozo, V., et al., *Efficient cancer therapy with a nanobody-based conjugate.* Cancer Research, 2004. **64**(8): p. 2853-2857.
20. Strokappe, N., et al., *Llama Antibody Fragments Recognizing Various Epitopes of the CD4bs Neutralize a Broad Range of HIV-1 Subtypes A, B and C.* Plos One, 2012. **7**(3).
21. McCoy, L.E., et al., *Potent and broad neutralization of HIV-1 by a llama antibody elicited by immunization.* Journal of Experimental Medicine, 2012. **209**(6): p. 1091-1103.
22. Bragdon, B., et al., *Bone morphogenetic proteins: a critical review.* Cellular signalling, 2011. **23**(4): p. 609-20.

23. Chubinskaya, S., M. Hurtig, and D.C. Rueger, *OP-1/BMP-7 in cartilage repair.* International orthopaedics, 2007. **31**(6): p. 773-81.
24. Minina, E., et al., *Interaction of FGF, lhh/Pthlh, and BMP signaling integrates chondrocyte proliferation and hypertrophic differentiation.* Developmental Cell, 2002. **3**(3): p. 439-449.
25. Grimsrud, C.D., et al., *BMP-6 is an autocrine stimulator of chondrocyte differentiation.* Journal of Bone and Mineral Research, 1999. **14**(4): p. 475-482.
26. Kronenberg, H.M., *Developmental regulation of the growth plate.* Nature, 2003. **423**(6937): p. 332-336.
27. Caron, M.M., et al., *Hypertrophic differentiation during chondrogenic differentiation of progenitor cells is stimulated by BMP-2 but suppressed by BMP-7.* Osteoarthritis and cartilage / OARS, Osteoarthritis Research Society, 2013. **21**(4): p. 604-13.
28. Frenken, L.G., et al., *Isolation of antigen specific llama VHH antibody fragments and their high level secretion by Saccharomyces cerevisiae.* J Biotechnol, 2000. **78**(1): p. 11-21.
29. Roovers, R.C., et al., *Efficient inhibition of EGFR signaling and of tumour growth by antagonistic anti-EFGR Nanobodies.* Cancer Immunol Immunother, 2007. **56**(3): p. 303-317.
30. Hamerscasterman, C., et al., *Naturally-Occurring Antibodies Devoid of Light-Chains.* Nature, 1993. **363**(6428): p. 446-448.
31. El Khattabi, M., et al., *Llama single-chain antibody that blocks lipopolysaccharide binding and signaling: Prospects for therapeutic applications.* Clinical and Vaccine Immunology, 2006. **13**(10): p. 1079-1086.
32. Saerens, D., et al., *Single domain antibodies derived from dromedary lymph node and peripheral blood lymphocytes sensing conformational variants of prostate-specific antigen.* J Biol Chem, 2004. **279**(50): p. 51965-72.
33. Roovers, R.C., et al., *High-affinity recombinant phage antibodies to the pan-carcinoma marker epithelial glycoprotein-2 for tumour targeting.* Br J Cancer, 1998. **78**(11): p. 1407-16.
34. van der Horst, G., et al., *Downregulation of Wnt signaling by increased expression of Dickkopf-1 and -2 is a prerequisite for late-stage osteoblast differentiation of KS483 cells.* J Bone Miner Res, 2005. **20**(10): p. 1867-77.
35. Conrath, K.E., et al., *Camel single-domain antibodies as modular building units in bispecific and bivalent antibody constructs.* Journal of Biological Chemistry, 2001. **276**(10): p. 7346-7350.
36. Haaijman, A., et al., *Inhibition of terminal chondrocyte differentiation by bone morphogenetic protein 7 (OP-1) in vitro depends on the periarticular region but is independent of parathyroid hormone-related peptide.* Bone, 1999. **25**(4): p. 397-404.
37. Hoogenboom, H.R., et al., *Antibody phage display technology and its applications.* Immunotechnology, 1998. **4**(1): p. 1-20.
38. de Marco, A., *Biotechnological applications of recombinant single-domain antibody fragments.* Microbial cell factories, 2011. **10**: p. 44.
39. Chothia, C., et al., *Conformations of immunoglobulin hypervariable regions.* Nature, 1989. **342**(6252): p. 877-83.
40. Hulsik, D.L., et al., *A gp41 MPER-specific Llama VHH Requires a Hydrophobic CDR3 for Neutralization but not for Antigen Recognition.* Plos Pathogens, 2013. **9**(3).
41. Zhang, Y., *I-TASSER server for protein 3D structure prediction.* BMC bioinformatics, 2008. **9**: p. 40.
42. Roy, A., A. Kucukural, and Y. Zhang, *I-TASSER: a unified platform for automated protein structure and function prediction.* Nature protocols, 2010. **5**(4): p. 725-38.
43. Roy, A., J. Yang, and Y. Zhang, *COFACTOR: an accurate comparative algorithm for structure-based protein function annotation.* Nucleic acids research, 2012. **40**(Web Server issue): p. W471-7.

44. Lowery, J.W. and M.P. de Caestecker, *BMP signaling in vascular development and disease.* Cytokine & Growth Factor Reviews, 2010. **21**(4): p. 287-298.
45. Strange, P.G., *Agonist binding, agonist affinity and agonist efficacy at G protein-coupled receptors.* British journal of pharmacology, 2008. **153**(7): p. 1353-63.
46. Groppe, J., et al., *Structural basis of BMP signalling inhibition by the cystine knot protein Noggin.* Nature, 2002. **420**(6916): p. 636-42.
47. Kugimiya, F., et al., *Involvement of endogenous bone morphogenetic protein (BMP)2 and BMP6 in bone formation.* Journal of Biological Chemistry, 2005. **280**(42): p. 35704-35712.
48. Heukers, R., et al., *Endocytosis of EGFR requires its kinase activity and N-terminal transmembrane dimerization motif.* Journal of cell science, 2013. **126**(Pt 21): p. 4900-12.

Chapter 3

A Supramolecular Host-Guest Carrier System for Growth Factors Employing VHH Fragments

Jordi Cabanas-Danés[1], Emilie Dooms Rodrigues[2], Ellie B. M. Landman[2], Jasper van Weerd[1,2], Clemens van Blitterswijk[3], Theo Verrips[4], Jurriaan Huskens[1], Marcel Karperien[2], Pascal Jonkheijm[1]

[1] Molecular Nanofabrication Group, MESA+ Institute for Nanotechnology, Faculty of Science and Technology, University of Twente P.O. Box 217, 7500 AE, Enschede, Netherlands;

[2] Departments of Developmental Bioengineering and [3] Tissue Regeneration, MIRA Institute for Biomedical Technology and Technical Medicine, Faculty of Science and Technology, University of Twente P.O. Box 217, 7500 AE, Enschede, Netherlands;

[4] Cellular Architecture and Dynamics, Department of Biology, Faculty of Science, Utrecht University, Padualaan 8, 3584 CH, Utrecht, Netherlands.

Abstract

A supramolecular strategy is presented for the assembly of growth factors employing His_6-tagged single domain antibodies (VHH). A combination of orthogonal supramolecular interactions of β-cyclodextrin (βCD)-adamantyl (Ad) host-guest and N-nitrilotriacetic acid (NTA)-histidine (His) interactions was employed to generate reversible and homogeneous layers of growth factors. A single domain antibody VHH fragment was identified to bind to the human bone morphogenetic protein-6 (hBMP6) growth factor and could be recombinantly expressed in E. coli. The VHH fragment was equipped with a C-terminal hexahistidine (His_6) tether to facilitate the assembly on βCD surfaces using a linker that contains an Ad group to bind to the βCD receptors and an NTA moiety to interact with the His_6-tag upon co-complexation of Ni^{2+} ions. After exploring the thermodynamic and kinetic stability of the VHH assemblies on βCD surfaces using a variety of experimental techniques including microcontact printing (μCP), surface plasmon resonance (SPR), microscale thermophoresis (MST) and theoretical models for determining the thermodynamic behavior of the system, hBMP6 was assembled onto the VHH-functionalized surfaces. After analyzing the immobilized hBMP6 using immunostaining, the biological activity of hBMP6 was demonstrated in cell differentiation experiments. Early osteogenic differentiation was analyzed in terms of alkaline phosphatase (ALP) activity of KS483-4C3 mouse progenitor cells and the results indicated that the reversibly immobilized growth factors were functionally delivered to the cells. In conclusion, the supramolecular strategy used here offers the necessary affinity, reversibility and temporal control to promote biological function of the growth factors that were delivered by this strategy.

Keywords: Supramolecular chemistry, Delivery, Self-Assembly, Growth Factor, Immobilization

Introduction

Growth factors are considered major therapeutic agents that profoundly affect cell function [1-6]. However, direct bolus delivery or systemic administration of growth factors are of limited clinical use as excessive dosing is required to detect a measurable effect, which potentially could lead to off-target effects [7]. Correct localization and balance of growth factors can be regulated by their encapsulation in carrier systems such as hydrogels, scaffolds or layer-by-layer systems, which generally sustain the spatial availability of growth factors facilitated by their diffusion into tissue [8-21]. An elegant strategy recently reported by Maynard *et al.* relied on the stabilization of basic fibroblast growth factors by covalent conjugation with a heparin-mimicking polymer [22]. Here we report the supramolecular capture of growth factors by using single monomeric variable antibody fragments engineered from heavy chain antibodies found in camelids (VHH fragments). Several therapeutic applications employing VHH in cancer, infectious and immune diseases have recently been reviewed [23-25]. Unique characteristics of VHH fragments such as their small size (12-20 kDa), elevated stability in aqueous and even in organic solvents and higher temperatures and reproducible recombinant production make them promising candidates to explore for activating surfaces in tissue regeneration. In addition, selection of VHH binders to growth factors can be conveniently done by means of phage display. VHH are amenable for genetic engineering allowing the site-specific introduction of reactive groups through which they can be site-specifically immobilized to surfaces yielding homogeneously oriented layers of VHH fragments under physiological conditions following supramolecular strategies [26, 27].

Supramolecular strategies, as opposed to covalent attachment, yield reversibility providing a means to release growth factors and prompt a biological function directly influenced by the desorption. Hence the delivery can be controlled by valency and dissociation rate constants. Although supramolecular chemistry has been successfully used to create biomimetic systems [28-37], up to now, reports that show the potentialities of supramolecular growth factor delivery systems predominantly employ peptide fragments to allow for binding of growth factors to supramolecular assemblies. For example, Stupp *et al.* have bound transforming growth factor β-1 (TGF-β) to oligopeptides that were displayed on the surface of self-assembled nanotubular systems [38]. Such supramolecular carrier systems promoted chondrogenic differentiation of human mesenchymal stem cells [38]. Up to now promising reports exist on the use of supramolecular host-guest systems, such as cyclodextrin and cucurbituril hosts, for the delivery of transcription factors [39], for the release of peptides and proteins [40-42] and to modulate cell adhesion [43-46], however, yet no reports exist for their application as growth factor carrier systems [11, 28-30, 47].

We here present a supramolecular strategy to deliver growth factors on β-cyclodextrin (βCD) surfaces using VHH as an intermediate. The method requires simple assembly steps in physiological conditions and offers the possibility to fine-tune affinities and dissociation rate constants by molecular design. We demonstrate the feasibility of our

approach using human bone morphogenetic protein 6 (hBMP-6) as a model growth factor that is not recombinantly available and therefore cannot be expressed with His-tags to allow for direct non-covalent immobilization. hBMP-6 belongs to the TGF-β superfamily and is known to play significant roles in cartilage and bone morphogenesis and repair and is already used as a therapeutic protein for inducing bone growth [48-50].

Scheme 1. Schemetically Presented Is The Assembly Of hBMP-6 On Supramolecular βCD Host Surfaces. The Self-Assembly Follows Either A Step-wise (Three Steps) Or One-Pot Procedure. See Text For Details. Chemical Structures Of The Building Blocks Are Given At The Bottom.

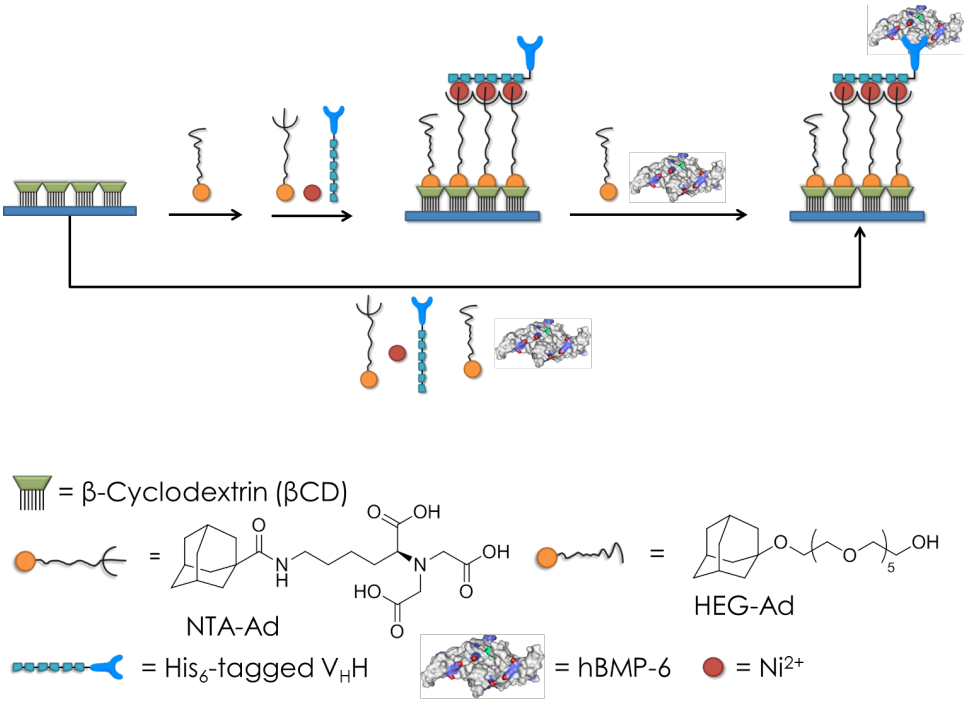

Results and Discussion

Design and Characterization of VHH Construct

VHH clones that bind to hBMP-6 were selected following a phage display approach (see Supporting information for details). Affinity selection (biopanning) was carried out on hBMP-6 coated plates (0.2-5 µg/well), which were incubated with the phage VHH immune library that was constructed after immunization of llamas. After the second round, the relative binding strength of selected phage VHH clones were assessed against each other using an enzyme-linked immunosorbent assay (ELISA) (See Supporting Figure S1a). Subsequently, the strongest binding VHH clone was sub-cloned in an

expression vector with a C-terminal His-tag and recombinantly produced in E. Coli hosts. After purification using affinity chromatography, a single band at 16 kDa was detected by sodium dodecylsulfate-polyacrylamide gel electrophoresis (SDS-PAGE) (See Supporting Figure S1b) in agreement with related VHH binders described in literature [22-25].

The interaction of the purified VHH construct with hBMP-6 was confirmed using microscale thermophoresis (MST) and ELISA measurements. To determine the affinity between VHH and hBMP-6 in solution, MST was used. A titration series of hBMP-6 over a range of 0.04 nM to 0.7 µM was performed while fluorescently labeled VHH was kept constant at 20 nM throughout the series. Upon binding of hBMP-6, a change in thermophoretic signal was observed as shown in Figure 1a. Subsequent fitting of the data to a 1:1 binding model yielded a dissociation constant K_d of 7.4 (± 0.4) x 10^{-8} M and therefore $K_a = 1/K_d = 1.4 \times 10^7$ M^{-1}. These values are comparable to the ones found in literature for VHH interactions with different binding partners [22-25, 51-53]. The obtained affinity was compared with affinity studies carried out in an ELISA assay format. To the hBMP-6 coated microtiter plates, a series of VHH solutions in the range of 0-3.3 µM was added and assayed by ELISA (Figure 1b). After fitting the experimental data to a Langmuir model, a K_a of 1.9 (± 0.2) x 10^6 M^{-1} was estimated, which is one order of magnitude lower than the affinity measured by MST, which is a known effect when comparing solution assays with array formats [26, 27].

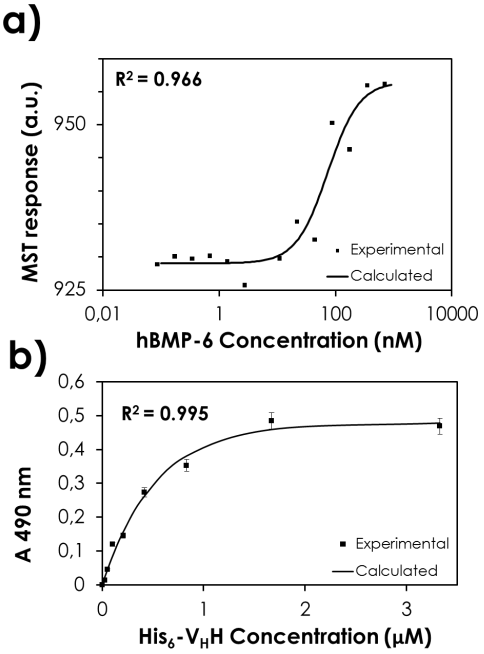

Figure 1. VHH binding to hBMP-6 analyzed a) in solution by microscale thermophoresis (MST) and b) on microtiter plates by ELISA (duplicate read-out).

Surface Assembly Analysis

With these VHH constructs with high affinity towards hBMP-6 in hand, we sought to employ the C-terminal His_6-tag on the recombinantly produced VHH for the assembly onto supramolecular βCD host surfaces through specific interaction with adamantyl (Ad) guest functionalized nitrilotri(acetic acid) (NTA) linkers [54-56]. To fabricate this supramolecular carrier system a step-wise assembly process (Scheme 1) was adopted using the (NTA)-Ni(II)-His_6-tag interaction and orthogonal linkers consisting of three steps, i.e. (1) pre-incubation of the βCD surface with an ethylene glycol based mono-adamantyl linker (HEG-Ad) for minimizing the non-specific protein adsorption, (2) a solution of NTA-monoadamantyl linker (NTA-Ad) and VHH in the presence of Ni(II) ions while maintaining the same concentration of HEG-Ad and (3) a solution of hBMP-6 was used [39-40]. Alternatively, after assembling HEG-Ad, a one-pot assembly step with all components was performed (Scheme 1). The assembly was performed at a physiological pH of 7.4, which ensures complexation of Ni(II) ions to the majority of the NTA moieties [50].

Supramolecular βCD host monolayers on gold were placed in an SPR flow cell [40]. After the baseline became stable while flowing PBS buffer, a solution of HEG-Ad (0.1 mM in PBS) was flown for 10 min until a stable signal was observed (Figure 2a, triangles). Successively, a solution of 0.5 μM VHH•Ni(II)•NTA-Ad (in a ratio of 1:5:5) in the presence of 0.1 mM HEG-Ad was injected and flown continuously (0.1 mL min^{-1}) (Figure 2a, squares). The observed increase in the SPR signal reached thermodynamic equilibrium after 10 min (Figure 2a, spheres)). This observation indicates that VHH•(Ni(II)•NTA-Ad)$_x$ (x=1-3) species have replaced monovalent HEG-Ad confirming that higher valent adamantyl VHH•(Ni(II)•NTA-Ad)$_x$ (x>1) were preferentially interacting with the supramolecular βCD host surface as determined by the effective concentration (C_{eff}). To demonstrate the reversibility of the assembly of VHH, a solution containing 10 mM of competing ligand EDTA and 10 mM of βCD in PBS were added to the flow cell while monitoring the SPR response (Figure 2a, spheres). Although a sudden initial increase in the SPR intensity was observed due to the large change in refractive index when using a concentrated solution of EDTA and βCD, the baseline was totally restored upon rinsing the system with PBS for 5 min (Figure 2a, arrows). This result indicates the complete disassembly of the molecules from the βCD surface. To assess the thermodynamic stability of the VHH constructs at the βCD surface, a titration series of VHH•Ni(II)•NTA-Ad (1:5:5) in the range of 0.5-20 μM was performed while recording the change in the SPR resonant angle. Between each titration step a disassembly cycle was performed to restore the βCD surface as described above. Upon addition of HEG-Ad, which represents the first step of the assembly of each titration step, a constant increase in SPR intensity was observed (Figure 2a). The second step of the assembly was marked by a gradual increase in the change of the SPR resonant angle saturating above 20 μM of VHH (Figures 2a and 2b).

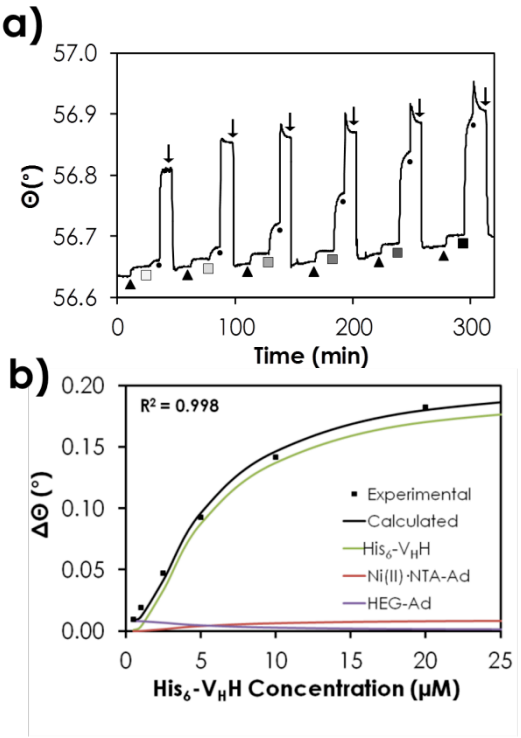

Figure 2. A) SPR data of a titration series of VHH·Ni(II)·NTA-Ad (1:5:5) to βCD plates in the presence of 0.1 mM HEG-Ad. Symbols indicate switching of the buffer to: 0.1 mM HEG-Ad (▲), increasing concentrations of VHH·Ni(II)·NTA-Ad (1:5:5; □-■) in the presence of 0.1 mM HEG-Ad, 10 mM βCD/EDTA in PBS (●) and PBS (↓). B) Experimental change of SPR resonant angle (ΔΘ at thermodynamic equilibrium; black markers) versus VHH concentration fitted to the theoretical model (See Supporting Information). The contribution of the assembly of the different molecules to the signal is given.

The SPR data were satisfactorily fitted to a thermodynamic model that accounts for all species possibly bound to the βCD surface (Figure 2b, see Supporting Information for details). The model shows that at low concentrations of VHH (< 1 μM), the major contribution to the (still low) SPR signal originates from the assembly of monovalent HEG-Ad, while above 2 μM of VHH, when the coverage becomes appreciable, the major contribution to the rise in SPR signal originates from trivalent VHH•(Ni(II)•NTA Ad)$_3$ species (70%) as expected [55]. This indicates that the trivalent complex is the main species contributing to the coverage at the whole range of concentrations until surface saturation (See Figure 2b and Supporting Figure S2b). Fixing the values of the intrinsic binding constants $K_{i,HEG}$ = 2.6 x 10^4 M^{-1} and $K_{i,NTA}$ = 1.2 x 10^4 M^{-1} as found in literature [51], an association constant K_1 of 6.3 x 10^4 M^{-1}, which represents the first interaction of Ni(II)•NTA-Ad to the His$_6$-tag, and a value for C_{eff} of 0.02 M were found to fit the experimentally observed changes in SPR resonant angle (Figure 2b). From these values, the second (K_2) and third (K_3) association constants of the consecutive bonding of His$_2$-

units to Ni(II)•NTA-Ad were calculated to be 1.5 x 10^4 M^{-1} and 1.95 x 10^3 M^{-1} in agreement with values found in literature [50, 57]. The overall binding constant for the trivalent complex on the βCD surface ([VHH] = 2 μM and [Ni(II)•NTA-Ad] = 10 μM) was calculated to be in the order of 10^6 M^{-1} in agreement with literature [58] and for the divalent complex in the order of 10^5 M^{-1}. In both cases, the multivalent interactions lead to highly stable assemblies bound to the surface while still reversible.

Release of VHH Fragments

To visualize the release of the VHH carrier system fluorescence microscopy was used. To this end, VHH was first fluorescently labeled with a Cy3-dye following standard procedures (see Supporting Information). Cy3-VHH was used for patterning employing the well-established microcontact printing (μCP) method with a polydimethylsiloxane (PDMS) stamp [40, 59]. Such stamps were inked for 2 min with a mixture of 1 μM Cy3-VHH:Ni(II):NTA-Ad (1:5:5) in PBS buffer. After inking, the stamp was blown dry and put into conformal contact with a supramolecular host glass surface for 5 min. After removing the stamp, the slides were directly imaged. As a reference, the same experiment was performed in which the PDMS stamp was inked with a 1 μM solution of VHH without Ni(II):NTA-Ad added. In both cases, uniform dot patterns of 50 μm diameter and spaced by 10 μm were clearly visible with an excellent contrast with the background as imaged using fluorescence microscopy (See Figure 3a and Supporting Figure S3). After extensive rinsing for 30 min with PBS, the patterns disappeared in the case of the reference experiment, which lacked the supramolecular NTA-Ad linker, whereas clear patterns remained visible in the case when NTA-Ad was co-printed (See Supporting Figure S3). These results indicate that the interactions between VHH and the surface are governed by specific NTA·Ni(II)·His_6-tag interactions as envisioned. Subsequently, after washing the patterns of the supramolecular VHH carrier system with a solution containing 10 mM of βCD and EDTA the patterns disappeared (see Supporting Figure S3), which is characteristic of reversible supramolecular interactions between the protein and the surface. The observations made by fluorescence microscopy suggest that homogeneous layers of oriented VHH are fabricated as a result of specific and reversible supramolecular interactions, in agreement with the SPR studies.

To acquire more information about the release of the VHH fragments from the supramolecular VHH carrier system under in vitro conditions, a series of substrates patterned with Cy3-VHH·Ni(II)·NTA-Ad were immersed in cell culture medium and four frames were recorded with a 0.2 sec exposure time using an inverted fluorescence microscope (Figure 3a-d). When plotting the decay of the fluorescence intensity versus time (Figure 3e), after 7 days around 80% of the fluorescence of the Cy3-VHH disappeared from the βCD host surfaces. When the data were fitted with first-order kinetics a dissociation rate constant of k_d = ~10^{-6} s^{-1} was found, which compares favorably to an example in literature of immobilizing His_6-tagged proteins on covalently modified NTA-surfaces [60].

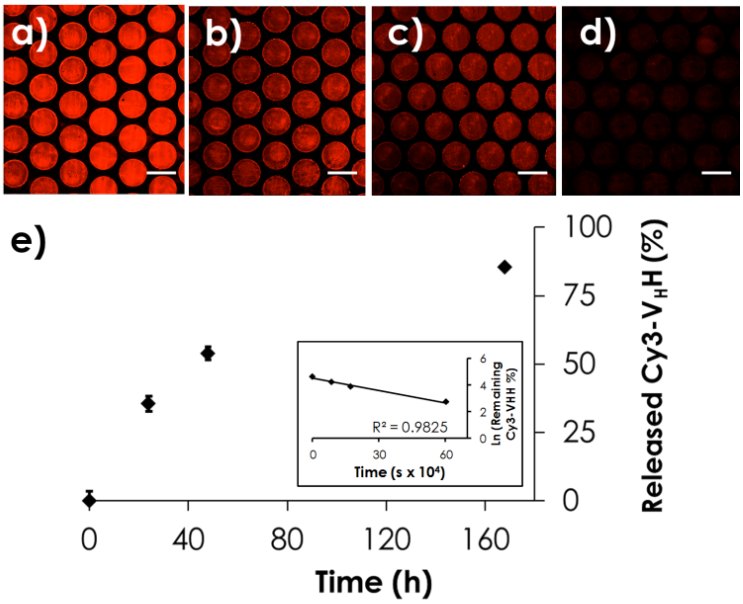

Figure 3. a) Fluorescence microscopy image of Cy3-VHH patterned by μCP on βCD glass slides recorded immediately after printing and washing. Frames recorded with 0.2 sec exposure time after immersion for b) 24 h, c) 48 h and d) 168 h in cell culture medium. Scale bars indicate 100 μm. e) Release of Cy3-VHH is plotted relative to the initial fluorescence intensity versus time. Inset shows the linear fitting of the corresponding logarithmic values.

Growth Factor Assembly

The ability to extend the release of VHH beyond days provides an interesting opportunity to apply our supramolecular carrier system for the delivery of growth factors to cells. To investigate whether the VHH carrier system can be loaded with hBMP-6 growth factors, patterns of dots of VHH were fabricated on glass slides as described above and subsequently incubated with a solution containing hBMP-6 (0.7 μM) for 1 h, according to the step-wise approach (Scheme 1). After sequential coupling for 1 h of a primary antibody (Ab) specific to hBMP-6 and a FITC-labeled secondary Ab, the slides were imaged using fluorescence microscopy (Figure 4c). The recorded images show clearly that the fluorescently labeled antibody was selectively immobilized on the printed VHH patterns. When surfaces were blocked with BSA in addition to HEG-Ad prior to incubating the slides with hBMP-6 and antibodies, the signal-to-noise was enhanced. When the immunoassay was carried out on the VHH patterns in the absence of hBMP-6 no fluorescent patterns were observed (Figure 4b). Similar results were obtained when the one-pot procedure was followed. When hBMP-6 loaded surfaces were immersed in cell culture medium, inspection of the surfaces using fluorescence microscopy showed that the disappearance of the growth factor and VHH fragments occurred in the same time window as compared to the VHH only system. SPR studies were also performed in

the case of following the one-pot assembly scheme. After recording a baseline by continuously flowing a solution of 0.1 mM HEG-Ad, the flow was switched to a solution of hBMP-6 in the presence of different concentrations of VHH (and Ni(II)·NTA-Ad) while monitoring the SPR intensity (Figure 4a). When a 50 nM solution of hBMP-6 was used in the presence of a 2 µM solution of VHH, an increase in the SPR resonant angle was observed when compared to the case when a 2 µM solution of VHH·Ni(II)·NTA-Ad was flown without hBMP-6 (Figure 4a, short dashed versus dotted line). A similar observation was made when using a 210 nM solution of hBMP-6 in the presence of a 5 µM solution of VHH (Figure 4a, long dashed versus dot-dashed line). When a solution containing only hBMP-6 was flown, no increase in the SPR intensity was observed, indicating that non-specific interactions between hBMP-6 and the background surface are insignificant (Figure, 4a, straight line). These results confirm that hBMP-6 can specifically be loaded onto the VHH carrier system, in agreement with MST and ELISA studies, while in addition hBMP-6 can be immuno-stained on the VHH carrier system, presumably indicating that the active conformation of the growth factor is maintained.

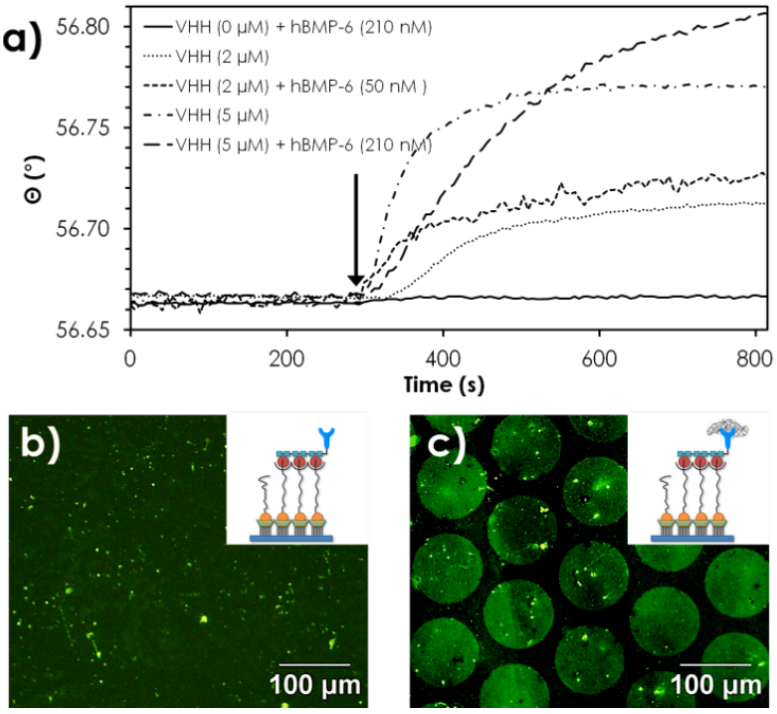

Figure 4. a) SPR sensograms of flowing VHH·Ni(II)·NTA-Ad with/without hBMP-6 as indicated in the legend over a βCD slide. The solutions were pre-mixed for at least 30 min before injection (arrow) in the presence of 0.1 mM of HEG-Ad. Fluorescence microscopy images after immunostaining the patterned (dots of 100 µm in diameter and spaced by 20 µm) supramolecular VHH carrier systems b) unloaded and c) loaded with hBMP-6. Insets show a scheme representing each assembly.

Cell response

To explore the bioactivity of the supramolecularly loaded hBMP-6 surfaces, the induction of alkaline phosphatase (ALP) was measured as early marker of osteogenic differentiation of KS483 mouse progenitor cells [61]. After cell culturing on hBMP-6 functionalized surfaces for 7 days a Live/Dead assay showed negligible cytotoxicity (Figure 5c). From a series of hBMP-6 functionalized surfaces and controls, the ALP activity was measured and normalized to the DNA content. Data is expressed as relative induction in comparison to bare glass substrates (Figure 5a) or to a layer of immobilized VHH (Figure 5b). When hBMP-6 was loaded onto the VHH carrier system in a step-by-step assembly process, the ALP activity was 6-fold higher in comparison to the case when VHH functionalized surfaces were used that lacked hBMP-6 (Figure 5a). In contrast, ALP activity was enhanced at best 2-fold when soluble hBMP-6 was simply adsorbed to surfaces that lack the VHH carrier system or glass only. No induction of ALP activity was observed for the VHH carrier system without hBMP-6. These results confirm that presenting hBMP-6 through VHH functionalized surfaces show the best differentiation response as assessed by measuring ALP activity after 7 days of differentiation [61, 62]. This increase in differentiation response could be attributed to the activity of hBMP-6 only. When hBMP-6 was partly denatured at 95 °C after loading the VHH carrier system, the ALP activity was significantly decreased. An ELISA experiment was performed to determine the amount of surface loaded hBMP-6 on the VHH carrier system, which was prepared following the step-by-step procedure. The released amount of hBMP-6 after 7 days was determined to be 142 ± 17 ng. This result may give reason to the higher ALP activity observed for hBMP-6 loaded surfaces when compared with reference experiments on glass and on substrates functionalized with VHH in which 100 ng of hBMP-6 was added to the cell culture medium. However, when cells were seeded on hBMP-6 loaded surfaces that were prepared following the one-pot assembly procedure using a solution of 100 ng of hBMP-6 and 0.5 μM VHH·Ni(II)·NTA-Ad (1:5:5), a 6-fold relative induction of the ALP production was observed with respect to the case when hBMP-6 was left out of the assembly solution to give VHH-only surfaces (Figure 5b). These results show that irrespective of the assembly procedure, biologically relevant amounts of hBMP-6 can be functionally delivered to cells through the supramolecular VHH carrier system.

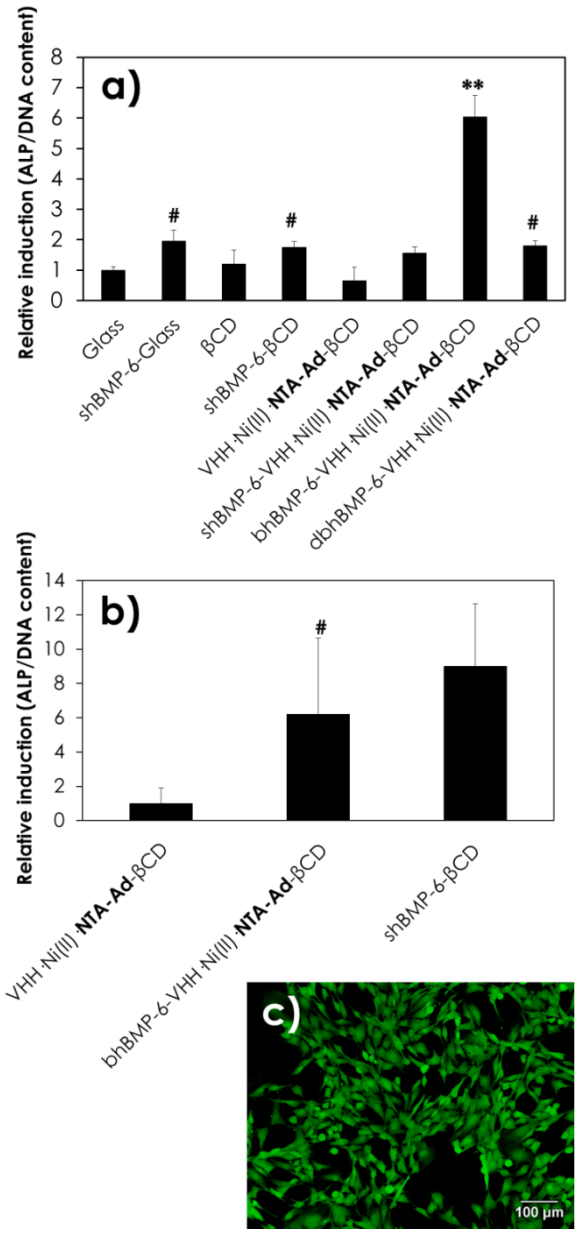

Figure 5. ALP activity normalized by the total DNA content of KS483 cells after 7 days of culture, expressed as relative induction with respect to a) a glass control following a step-by-step assembly procedure or to b) a supramolecular VHH carrier system following a one-pot assembly procedure. Notation: 's' in shBMP-6 represents soluble growth factor supplemented to the cell medium; 'b' in bhBMP-6 represents growth factor bound to the carrier system; 'db' in dbhBMP-6 represents growth factor denatured at high temperature upon loading. # $p < 0.05$ compared to VHH·Ni(II)·NTA-Ad, ## $p<0.01$ compared to VHH·Ni(II)·NTA-Ad and ** $p<0.01$ compared to all cases. c) Live-dead assay showing KS483 cells seeded on supramolecular VHH carrier system loaded with hBMP-6.

Conclusion

We demonstrated that employing VHH fragments gives access to capturing growth factors with high affinities while their recombinant production is convenient and gives entry to modification through genetic engineering. While VHH fragments resemble human antibodies, immune response is presumably negligible as opposed to other peptide systems [23-25]. Our results show that irrespective of the assembly procedure, biologically relevant amounts of hBMP-6 can be functionally loaded onto the supramolecular VHH carrier system and successively delivered to cells. We show that growth factors can be sequestered to the VHH carrier system indicating that locally excreted growth factors can possibly be bound to the surface assisted by VHH. Introduction of supramolecular coupling strategies offers additional opportunities to modulate release profiles through variation of binding strengths [40] and dissociation rates or combination of supramolecular with covalent strategies [63]. Using oriented VHH fragments on surfaces to carry growth factors provides a novel opportunity to incorporate growth factors in various systems such as hydrogels or scaffolds [45] and we believe that this will open new ways to develop instructed biomaterials.

Acknowledgement

Work by J.C-D., E.D.R. and E.B.M.L. was funded by Project P2.02 OAcontrol of the research program of the BioMedical Materials Institute, co-funded by the Dutch Ministry of Economic Affairs. Work by J.v.W was funded by Nanonext NL (06C.11). The work by P.J. was funded by a starting grant from the European Research Council (no 259183 Sumoman).

Supporting information

Experimental Section

Materials and Synthesis

Commercial grade reagents were purchased from Sigma-Aldrich and were used without further purification unless otherwise stated. Recombinant human BMP-6 (hBMP-6) was purchased from R&D Systems. High-purity water (Millipore, R = 18.2 MΩ) was used. ^{1}H-NMR spectra were recorded on a Varian Unity INOVA (300 MHz) spectrometer. Electrospray Ionization (positive mode) high resolution mass spectra were recorded on a WATERS LCT mass spectrometer.

Hexa(ethylene glycol) mono(adamantyl ether) (HEG-Ad) was synthetized according to literature [S1]. Mono(adamantyl) L-lysine-nitrilotri(acetic acid) NTA-Ad was synthetized according to literature [S1, S2]. βCD surfaces were prepared according to literature on gold [S3] and on glass [S4].

Llama immunization, VHH phage library construction and VHH selection

A VHH phage display library was generated from the immunization of 2 llamas. Llamas were immunized with hBMP-6. hBMP-6 was mixed with the adjuvant Stimune (CEDI Diagnostics, Lelystad, The Netherlands) and injected intramuscularly at days 0, 14, 28 and 35. The VHH phage display library was generated as previously described [S5, S6]. After immunization, total RNA was extracted from peripheral blood lymphocytes, converted into complementary DNA and cloned in a phage-display plasmid. Phage display was used to select phages binding to hBMP-6 using an immunized llama VHH phage display library. The phages were selected via the panning method by coating, overnight at 4 °C, a MaxiSorp plate (Nunc, Thermo Scientific) with decreasing concentrations of hBMP-6 (5 µg, 2 µg and 0.2 µg) in phosphate buffered saline (PBS, Gibco). Phage VHH immune library (approximately 10^{10} colony forming units (cfu)), was incubated for 2 h at room temperature to the wells blocked with 4% Marvel (dried skimmed milk, Premier International Foods) in PBS. After thorough washing, the phage VHH clones binding to the coating were eluted by incubating 100 mM Et_3N for 15 min at room temperature and immediately neutralized by the addition of 1M Tris-HCl pH 7.5. DNA information of the selected phages was rescued by infection of Escherichia coli (*E. coli*) TG1 strain and subsequent selection on agar plates for ampicillin resistance. To obtain recombinant bacteriophages expressing the VHH as fusion proteins with the bacteriophage gene III product, transformed TG1 *E. coli* were grown to logarithmic phase and then infected with helper phage VCSM13 (Stratagene, La Jolla, CA, USA). The phage particles were produced overnight in medium containing ampicillin and kanamycin. The phages were precipitated with polyethylene glycol (PEG) and used in the second panning round of selection on wells coated with hBMP-6 as described above.

Selected phages from single colonies from the second round of selection were sequenced (Macrogen).

VHH plasmids, production and purification

E. coli strain TG1 and/or DH5α was used for the maintenance of the plasmids, infection by the phages and expression of proteins. DNA information of the individually selected and isolated VHH were sub-cloned into a plasmid containing C-terminal Myc and His tags. *E. coli* TG1 and/ or DH5α was grown in Luria Broth (LB) or Yeast extract and tryptone (YT) medium containing 2% (w/v) glucose and antibiotic, ampicillin 100 µg/ml. VHH were produced from *E. Coli* TG1 by isopropyl β-D-1-thiogalactopyranoside (IPTG) lac promoter induction at 37 °C for 4 hours under non static conditions. VHH proteins were produced in *E. coli* TG1 and purified from the periplasmic fraction via the C-terminal his-tag by cobalt affinity chromatography (TALON His-Tag Purification Resin, ClonTech). Release from the column was induced by 200 µM imidazole solution in PBS and eluents were dialyzed against PBS for two days at 4 °C to remove imidazole. Purified VHH were analyzed by means of SDS polyacrylamide gel electrophoresis (SDS-PAGE). The final VHH concentration was determined from the UV absorption at 280 nm (NanoDrop 1000 Spectrophotometer, Thermo Scientific) and the theoretical molar extinction coefficient. VHH was labeled with a fluorescent dye using the Amersham Cy3 mono-reactive dye pack (GE Healthcare Europe GmbH, Germany) according to the manufacturer's protocol and purified via dialysis against PBS overnight to a ratio of 4 dyes/ protein.

Phage and VHH ELISA for binder selection

Either the supernatant (as a source of phages) or the periplasmatic fractions resulting from the VHH productions were directly incubated (1h at room temperature) in ELISA plates coated with hBMP-6. Bound VHH were detected upon 1h incubation at room temperature with a rabbit anti-VHH (α-K212, self-produced) (1/5000) and a 1h incubation at room temperature with a secondary donkey anti-rabbit antibody coupled to a peroxidase (DARPO) (1/10000) second antibody. H_2O_2 and ortho-phenylenediamine (OPD) were used at a ratio 1/1000 as substrates for the peroxidase reaction. Plates were measured with a Bio-Rad model 550 plate reader. Absorbance of OPD was measured at 490 nm after the reaction was stopped by adding 1M H_2SO_4.

hBMP-6 ELISA

Cell culture medium was collected after 7 days and the amount of hBMP-6 was quantified by an ELISA assay according to the manufacturer's instructions (Duo Set ELISA development kit, R&D systems).

PDMS preparation and µCP experiments

Silicon wafer-based masters with etched structures were prepared by UV photolithography. The master's surface was fluorinated using 1H,1H,2H,2H-

perfluorododecyltrichlorosilane (PFDTS). Poly(dimethylsiloxane) (PDMS) (Dow Corning) stamps were fabricated by curing the degassed mixture (10:1 elastomer, curing agent) of the components of SYLGARD® 184 silicone elastomer kit on the surface of the master at 60 °C overnight. PDMS stamps were first oxidized in an oxygen-plasma reactor (Plasma-Prep II plasma etcher, SPI supplies, USA) at an oxygen pressure of 1.0 bar, a vacuum pressure of 160 mbar and a current of 40 mA for 20 sec. The stamps were then stored in water. Prior to use, the stamps were dried with a flow of dry N_2 and then incubated with 100 µL of a 1 µM solution of Cy3-VHH:Ni(II):NTA-Ad (1:5:5) for 2 min. After removing the excess of the inking solution, the dried stamps were brought into conformal contact with the βCD functionalized surfaces for 5 min. Afterwards the substrates were visualized with fluorescence microscopy or washed as described in the main text. For all experiments, $NiCl_2$ was used as Ni(II) source and Cy3-VHH:Ni(II):NTA-Ad were pre-incubated together for 30 min to maximize complexation and in addition, ratio of 1:5:5 was used, which offers two extra Ni(II) ions and NTA-Ad than the three required to saturate the His_6-tag. The quantification of protein bound to the substrates at different time points was performed via the fluorescence intensity quantification of protein arrays by using the particle counting routine of the free software ImageJ. For the immobilization of the N-(lissamine-rhodamine B)-labeled divalent adamantyl guest, the same concentrations and printing times were used. For the immobilization of hBMP-6, VHH(H1):Ni(II):NTA-Ad (1:5:5) was printed as described above. Subsequently, the background was blocked with a 0.1 mM BSA solution in PBS buffer via 1 h incubation at room temperature. The substrates were then rinsed 3 times with PBS buffer including 1 mM Tween-20 during 10 min on the orbital shaker and finally rinsed with PBS buffer. The substrates were incubated with a solution of 700 nM hBMP-6 in PBS buffer containing 1% BSA for 1h at room temperature and rinsed as previously described.

hBMP-6 immunostaining

Following protein immobilization via µCP in the desired patterns, substrates were incubated with PBS containing 1% BSA for 1 h and washed again three times as described above to block the background against non-specific protein interactions. The hBMP-6 protein patterns were then incubated with 100 µL of a solution of 5 µg/mL of monoclonal anti-BMP-6 antibody produced in mouse (mouse IgG2B isotype, clone 74219.11) in PBS buffer including 1% BSA. After 1 h, the substrates were washed three times 10 min with PBS buffer including 1 mM Tween-20, rinsed with water and dried with a flow of dry N_2. Finally, 100 µL of a solution (20 µg/mL) of anti-mouse IgG (whole molecule, subclasses G1, Gg2a, G2b, and G3)-FITC produced in goat in PBS buffer including 1% BSA was used to incubate the samples for 1 h. The substrates were then washed again three times 10 min with PBS buffer including 1 mM Tween 20, rinsed with water and dried with a flow of dry N_2 and used for fluorescence microscopy imaging.

Cell culture

Prior to cell seeding, the substrates were sterilized with 70% ethanol and subsequently washed twice with PBS to remove any excess of ethanol. The mouse pre-osteoblast cell line KS483-4C3 was used as a model for osteogenic differentiation. Cells were plated at a density of 5000 cells/cm^2 and cultured in Minimal Essential Medium (MEM) alpha supplemented with 10% fetal bovine serum (FBS) and 100 U penicillin/streptomycin (Gibco) and 1% (v/v) Penicillin-Streptomycin solution (with 10,000 units penicillin and 10 mg streptomycin/mL, Sigma-Aldrich). Live/Dead assay (LIVE/DEAD® Viability/Cytotoxicity Kit, for mammalian cells, Molecular Probes®) was performed according to the protocol from the provider.

ALP quantification

For osteogenic differentiation, 0.2 mM ascorbic acid was added to the medium together with 100 ng/mL hBMP-6 delivered in a soluble form or a comparable concentration delivered via the substrate. After seven days of culturing KS483-4C3 cells, the cells were lysed in 200 µL lysis buffer (0.1 M K_2HPO_4 + 0.1 M KH_2PO_4 + 0.1% Triton X100, pH 7.8). ALP was detected and quantified using the CDP-star® Chemiluminescent Substrate (Sigma Aldrich). ALP production was corrected for DNA content, which was measured using the CyQuant Cell Proliferation assay (Invitrogen). Experiments were repeated at least three times. Error bars represent standard errors, and statistical analysis was performed using the one-way analysis of variance test (ANOVA) to evaluate the statistical differences and a Tukey's Post Hoc test (# $p < 0.05$ compared to VHH·Ni(II)·NTA-Ad, ## $p < 0.01$ compared to VHH·Ni(II)·**NTA-Ad** and ** $p < 0.01$ compared to all cases *$p < 0.05$ or ** $p < 0.005$).

Fluorescence Microscopy

Fluorescence microscopy images were recorded using an Olympus inverted microscope IX71 equipped with a mercury burner U-RFL-T as light source and a digital Olympus DR70 camera for image acquisition using the following Olympus filter cubes: 510 nm $\leq \lambda_{ex} \leq$ 550 nm for red emission ($\lambda_{em} \geq$ 580 nm) and 460 nm $\leq \lambda_{ex} \leq$ 490 nm for green emission ($\lambda_{em} \geq$ 520 nm). All fluorescence microscopy images were acquired in air.

SPR

SPR experiments were performed using an RT2005 surface plasmon spectrometer (Resonant Technologies GmbH, Germany) in Kretschmann configuration using a mechanically modulated HeNe-laser (λ = 632.8 nm). Refractive index matching oil (Cargille; series B; $n_D^{25\,°C} = 1.7000 \pm 0.0002$) between glass substrate and prism (Schott, LaSFN9) was used and a teflon flow cell (100 µL) of 0.9 cm in diameter was mounted on top of the gold layer on the surface of the glass substrate. The prism, sample and flow cell were mounted on a double goniometer with an electronic control unit to precisely set the angle position, the light was detected using a photodiode. A syringe pump (Aladdin WPI ltd, US) was used to flow the different solutions into the cell via Tygon R3607 tubes

(0.76 mm diameter) at a flow rate of 0.1 mL/min. All measurements were performed by tracking the SPR resonance angle while using a temperature controller, which was set to 21 °C.

MST

Microscale Thermophoresis (MST) measurements were performed using a Monolith NT115 (NanoTemper Technologies GmbH, Germany). A solution of 60 µM of VHH was labeled with a fluorescent dye (NT-647, NT-532 or NT-488) using Monolith NT™ Protein Labeling Kit (amine reactive) with the subsequent removal of excess dye within 45 min. The non-labeled titrant (hBMP-6) was diluted with PBS buffer in a dilution series with the highest concentration of 700 nM. 10 µL of the different dilutions were mixed with 10 µL of the fluorescent molecule. Mixed samples were loaded into glass capillaries and the MST analysis was performed.

Supplementary figures

a)

Antigen	[V_HH] (µg/well)	V_HH Clone 1	2	3	4	none
hBMP-6	2	0.116	0.111	0.533	0.103	0.064
	0.2	0.072	0.090	0.162	0.083	0.077
	0.02	0.069	0.077	0.093	0.072	0.076
	0	0.070	0.074	0.103	0.078	0.091
none	2	0.117	0.119	0.119	0.132	0.142

b)

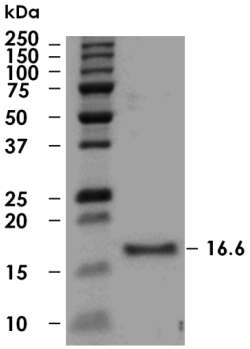

Figure S1. Table a) Selection of VHH clones that bind hBMP-6 via an ELISA (absorbance values at 490 nm). b) SDS-PAGE of the purified VHH.

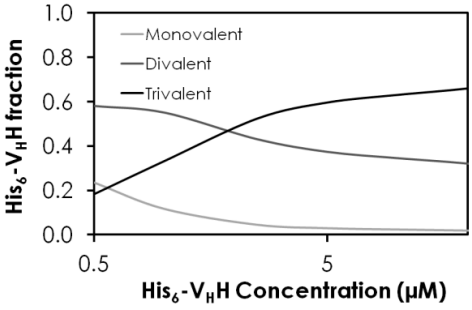

Figure S2. Speciation model corresponding to the possible valencies for the VHH·Ni(II)·NTA-Ad complex at the surface.

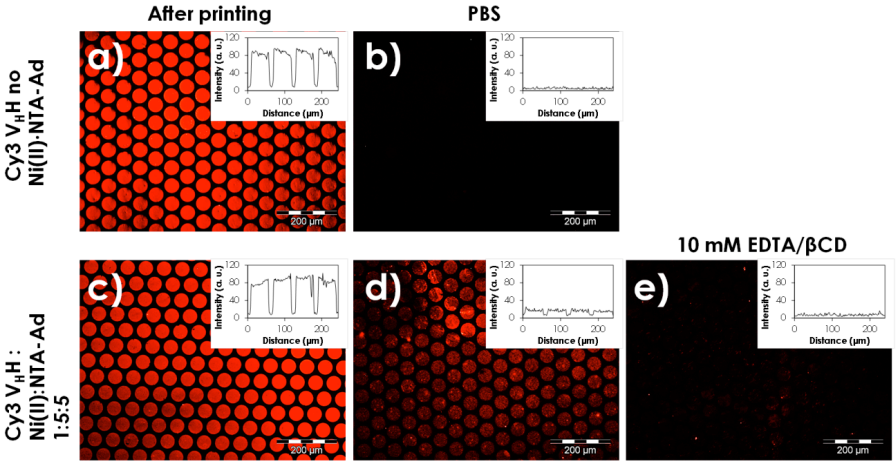

Figure S3. Fluorescence microscopy images of Cy3-VHH patterned by μCP on a βCD surface in the absence (top) or presence (bottom) of Ni(II)·NTA-Ad, a, c) directly after printing, b, d) after rinsing with PBS for 30 min) and e) after rinsing with a 10 mM solution of both βCD and EDTA. Insets show fluorescence intensity profiles of the patterns. Exposure time: 500 ms.

Thermodynamic model for fitting SPR titration data

The orthogonal interactions of NTA-Ad with both the βCD surface, in a monovalent fashion, as well as with His_6-tagged VHH in the presence of Ni(II), in a multivalent fashion, lead to the coexistence of multiple species with different valencies. In addition, the use of HEG-Ad to suppress unspecific protein adsorption yields competitive binding to surface-bound βCD. Scheme S1 represents all possible equilibria between all species in our system.

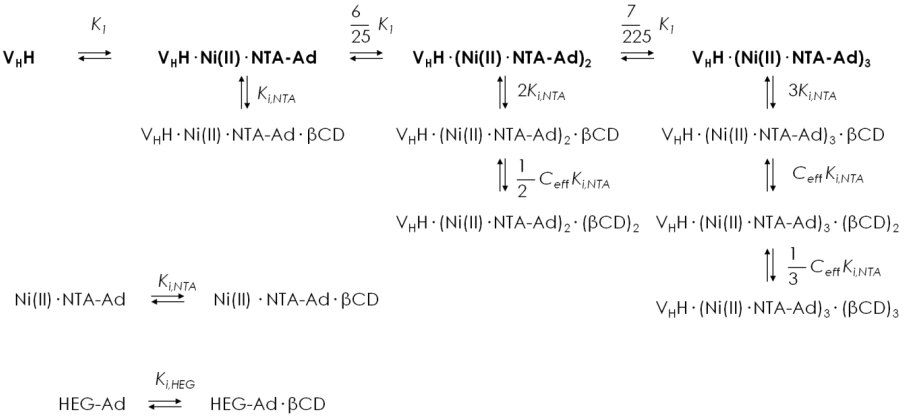

Scheme S1. Equilibria for all species participating in the immobilization of VHH at a βCD surface (above), for the binding of Ni(II)·NTA-Ad to a βCD surface (middle) and for the competitive binding of HEG-Ad to βCD (below). Complexation steps given in bold of Ni(II)·NTA-Ad to VHH take place in solution. K_1 is the equilibrium constant for the interaction between a His_2 unit of His_6-tagged VHH to Ni(II)·NTA-Ad, $K_{i,NTA}$ and $K_{i,HEG}$ are the intrinsic binding constants for the interaction between βCD and the Ad moieties of NTA-Ad or HEG-Ad respectively. For subsequent bindings to the βCD surface the binding will be affected by the effective concentration parameter (C_{eff}).

To fit our SPR data the following assumptions were made for the current system under study using prior knowledge of Ludden et al [S7].

i) At the working pH of 7.4 all NTA-Ad is complexed to Ni(II) [S7].

ii) Statistical factors relate the binding constants K_2 and K_3 with K_1 following the binding scheme of NTA-Ad with histidines in the presence of Ni(II) taking into account that the initial binding of Ni((II)·NTA-Ad to His_6-tag is 5 times as likely than to a His_2 unit (Scheme S2a) [S7]. Therefore,

$$K_1 = 5\,K_{i,His_2 \cdot Ni(II)} \tag{1}$$

From five possible cases in which VHH is bound to a single Ni(II)·NTA-Ad, two of them offer three His_2 units free for interacting and three of them only two. Moreover, the dissociation of His_2 from VHH·(Ni(II)·NTA-Ad)$_2$ is twice as likely when compared to the dissociation of His_2 from VHH·Ni(II)·NTA-Ad (Scheme S2b). Therefore,

$$K_2 = \frac{\left(3 \cdot \frac{2}{5} + 2 \cdot \frac{3}{5}\right)}{2} K_{i,His_2 \cdot Ni(II)} = \frac{6}{25} K_1 \tag{2}$$

From two VHH·Ni(II)·NTA-Ad cases offering three His_2 free for interacting with a second Ni(II)·NTA-Ad unit, only two of the His_2 allow binding to a third His_2 unit (Scheme S2b), whereas from three VHH·Ni(II)·NTA-Ad cases offering two His_2 free for interacting with a second Ni(II)·NTA-Ad unit, only in one case, both of the His_2 units allow binding to a third His_2 unit, whereas in the other two cases, binding to a third His_2 unit is not possible (Scheme S2b). In addition, upon binding VHH to three His_2, the dissociation is three times as likely when compared to case of the dissociation of His_2 from VHH·Ni(II)·NTA-Ad. Therefore,

$$K_3 = \frac{\frac{2}{5}\frac{2}{3}\frac{1}{5}}{3} K_{i,His_2\cdot Ni(II)} = \frac{7}{225} K_1 \qquad (3)$$

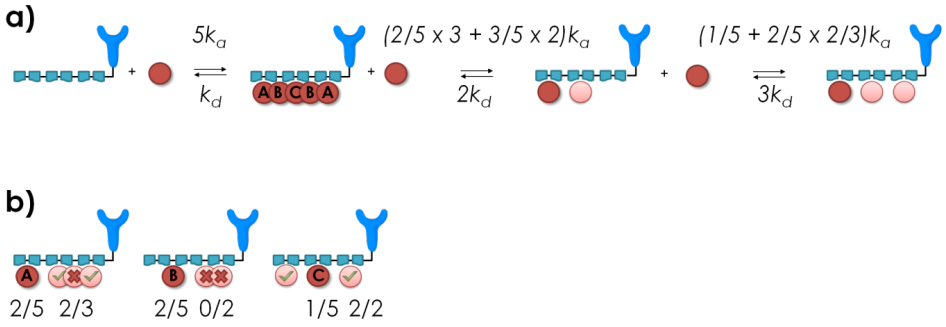

Scheme S2. Equilibria for the complexation of pairs of neighboring histidines from the His_6-tagged VHH to Ni(II)·NTA-Ad in solution (a) and origin of the statistical factors associated to subsequent bindings (b). Dots represent Ni(II)·NTA-Ad units for the first (solid red) and second (faint red) bindings. Capital letters in the dots indicate positions of equal statistics. Check marks and crosses indicate whether a third His_2 unit is available or not, resp., for the binding of an additional Ni(II)·NTA-Ad unit.

With these assumptions in mind, the following mass balances were constructed. Because the SPR experiments were performed in a flow system, the concentrations of solution species (in volume concentrations) are independent of the adsorption processes and are thus given by equations 4-6.

$$[VHH]_{tot} = [VHH]_{free} + [VHH\cdot Ni(II)\cdot NTA\text{-}Ad] + [VHH\cdot(Ni(II)\cdot NTA\text{-}Ad)_2] + [VHH\cdot(Ni(II)\cdot NTA\text{-}Ad)_3] \qquad (4)$$

$$[Ni(II)\cdot NTA\text{-}Ad]_{tot} = [Ni(II)\cdot NTA\text{-}Ad]_{free} + [VHH\cdot Ni(II)\cdot NTA] + 2[VHH\cdot(Ni(II)\cdot NTA\text{-}Ad)_2] + 3[VHH\cdot(Ni(II)\cdot NTA\text{-}Ad)_3] \qquad (5)$$

$$[HEG\text{-}Ad]_{tot} = [HEG\text{-}Ad]_{free} \qquad (6)$$

All surface species are formed by adsorption of solution species, and their concentrations (expressed in surface concentrations or relative coverage) are related to the coverage of βCD sites as given in equation 7.

$$[\beta CD]_{tot} = [\beta CD]_{free} + [VHH \cdot Ni(II) \cdot NTA\text{-}Ad \cdot \beta CD] + [VHH \cdot (Ni(II) \cdot NTA\text{-}Ad)_2 \cdot \beta CD] + [VHH \cdot (Ni(II) \cdot NTA\text{-}Ad)_3 \cdot \beta CD] + 2([VHH \cdot (Ni(II) \cdot NTA\text{-}Ad)_2 \cdot (\beta CD)_2] + [VHH \cdot (Ni(II) \cdot NTA\text{-}Ad)_3 \cdot (\beta CD)_2]) + 3[VHH \cdot (Ni(II) \cdot NTA\text{-}Ad)_3 \cdot (\beta CD)_3] + [Ni(II) \cdot NTA\text{-}Ad \cdot \beta CD] + [HEG\text{-}Ad \cdot \beta CD] \quad (7)$$

The binding constant for the complexation of the first His_2 unit of the VHH to the Ni(II)·NTA-Ad can be described as:

$$K_1 = \frac{[V_H H \cdot Ni(II) \cdot NTA - Ad]}{[V_H H] \cdot [Ni(II) \cdot NTA - Ad]} = 5 K_{i,His_2 \cdot Ni(II)} \quad (8)$$

Relating the binding of subsequent histidine pairs according to the statistical factors presented in Scheme S2, the binding constants for divalent and trivalent NTA-Ad species with the surface are:

$$K = \frac{[V_H H \cdot (Ni(II) \cdot NTA - Ad)_2 \cdot \beta CD]}{[V_H H \cdot (Ni(II) \cdot NTA - Ad)_2] \cdot [\beta CD]} = 2 K_{i,NTA} \quad (9)$$

$$K = \frac{[V_H H \cdot (Ni(II) \cdot NTA - Ad)_3 \cdot \beta CD]}{[V_H H \cdot (Ni(II) \cdot NTA - Ad)_3] \cdot [\beta CD]} = 3 K_{i,NTA} \quad (10)$$

Subsequent bindings are regulated by the effective concentration (C_{eff}), which incorporates characteristics such as the linker length and lattice parameter in the probing volume, giving the following binding constants:

$$K = \frac{[V_H H \cdot (Ni(II) \cdot NTA - Ad)_2 \cdot (\beta CD)_2]}{[V_H H \cdot (Ni(II) \cdot NTA - Ad)_2 \cdot \beta CD] \cdot [\beta CD]} = \frac{1}{2} C_{eff} K_{i,NTA} \quad (11)$$

$$K = \frac{[V_H H \cdot (Ni(II) \cdot NTA - Ad)_3 \cdot (\beta CD)_2]}{[V_H H \cdot (Ni(II) \cdot NTA - Ad)_3 \cdot \beta CD] \cdot [\beta CD]} = C_{eff} K_{i,NTA} \quad (12)$$

$$K = \frac{\left[V_H H \cdot \left(Ni(II) \cdot NTA - Ad\right)_3 \cdot \left(\beta CD\right)_3\right]}{\left[V_H H \cdot \left(Ni(II) \cdot NTA - Ad\right)_3 \cdot \left(\beta CD\right)_2\right] \cdot \left[\beta CD\right]} = \frac{1}{3} C_{eff} K_{i,NTA} \tag{13}$$

Substituting the equilibrium constant equations (8-13) into the mass balances (equations 4-7) (not shown) yields a set of numerically solvable equations with [VHH], [βCD], [Ni(II)·NTA-Ad] and [HEG-Ad] as variables. These equations, were solved in two steps, for the solution and surface species separately, by using a Simplex algorithm in a spreadsheet approach [S8]. By fixing the values of the intrinsic binding constants for the monovalent interactions with the βCD surface ($K_{i,NTA}$ = $1.2 \cdot 10^4$ M^{-1}), which are reported in literature for our system components [S1], and [Ni(II)·NTA-Ad] = 10 μM, the values for K_1 and C_{eff} were iteratively optimized to fit the theoretical SPR resonant angle change $\Delta\theta_{max}$ with the experimentally observed SPR data, assuming a contribution of all surface binding units (i.e. VHH·$(Ni(II)\cdot NTA\text{-}Ad)_x$ (x=1-3) and HEG-Ad) to the SPR signal. This yielded K_1 = $6.3 \cdot 10^4$ M^{-1} (K_2 = $1.50 \cdot 10^4$ M^{-1} and K_3 = $1.95 \cdot 10^3$ M^{-1}), C_{eff} = 0.02 M. Finally, the overall stability constant for VHH·$(Ni(II)\cdot NTA\text{-}Ad)_3$·$(\beta CD)_3$ was calculated using:

$$K = \left(K_{i,NTA}\right)^3 K_1 K_2 K_3 C_{eff}{}^2 \cdot \left[Ni(II) \cdot NTA - Ad\right]^3 \tag{14}$$

The value for C_{eff} in this case was smaller as compared to values used in literature (0.1 M) for optimizing the binding constant of maltose binding proteins (MBP) to βCD surfaces [S7]. This discrepancy was attributed to the difference in size and shape of VHH in comparison to MBP. While VHH (Mw = 16 kD, prolate spheroid, 4.4 x 2.8 nm) [S9] occupies less than three βCD cavities, MBP (Mw = 41 kDa, cubic, 3 x 4 x 6.5 nm) [S7] exceeds three βCD cavities. Even though both proteins have a single His_6-tag, the larger protein size of MBP can sterically reduce the probing volume for the (intramolecular) binding of the second and third adamantyl moieties in the case of MBP and at the same time shield the βCD cavities available within this probing volume from interactions of neighboring His-tagged proteins, while VHH, being a smaller protein, allows other protein units to interact with neighboring hosts at the molecular printboard while simultaneously causing a larger probing volume.

Thermodynamic model for fitting ELISA titration data

In a similar manner as described above, a simplified model to describe the interaction between non-immobilized VHH and hBMP-6 was used assuming a 1:1 interaction between the two components. The signal was related directly to the complex formation without accounting for possible interferences from the multiple steps of the ELISA procedure. Scheme S3 represents the equilibrium between all species, their binding constant, the simplified mass balances and the theoretical relationship between the

absorbance at 490 nm and the total concentration of VHH which was assumed to be exponential. In this case, optimized K_{VHH} and $A_{490,max}$ in a least-squares routine for the best fitting.

$$[V_HH] + [hBMP\text{-}6] \underset{}{\overset{K_{V_HH}}{\rightleftharpoons}} [V_HH \cdot hBMP\text{-}6]$$

$$K_{V_HH} = \frac{[V_HH \cdot hBMP-6]}{[V_HH] \cdot [hBMP-6]} \tag{15}$$

$$[VHH]_{tot} = [VHH] + [VHH \cdot hBMP\text{-}6] = [VHH] \cdot (1 + K_{VHH}[hBMP\text{-}6]) \tag{16}$$

$$[hBMP\text{-}6]_{tot} = [hBMP\text{-}6] + [VHH \cdot hBMP\text{-}6] = [hBMP\text{-}6] \cdot (1 + K_{VHH}[VHH]) \tag{17}$$

$$A_{490} = A_{490,max} \cdot \left(1 - e^{\left(-K_{V_HH}[VHH]_{tot}\right)}\right) \quad A_{490} = A_{490,max} \cdot \left(1 - e^{\left(-K_{VHH}[VHH]_{tot}\right)}\right) \tag{18}$$

Scheme S3. Equilibrium of the binding of the VHH to hBMP, simplified mass balances and exponential theoretical relationship between the absorbance at 490 nm and the total VHH concentration.

Supplementary References

[S1] M. J. W. Ludden, A. Mulder, R. Tampé, D. N. Reinhoudt, J. Huskens, *Angew. Chem. Int. Ed.* **2007**, *46*, 4104.

[S2] S. Lata, J. Piehler, *Nat. Protoc.* **2006**, *1*, 2104.

[S3] M. W. J. Beulen, J. Bügler, B. Lammerink, F. A. J. Geurts, E. M. E. F. Biemond, K. G. C. van Leerdam, F. C. J. M. van Veggel, J. F. J. Engbersen, D. N. Reinhoudt, *Langmuir* **1998**, *14*, 6424.

[S4] S. Onclin, A. Mulder, J. Huskens, B. J. Ravoo, D. N. Reinhoudt, *Langmuir* **2004**, *20*, 5460.

[S5] S. Muyldermans, *Rev. Mol. Biotechnol.* **2001**, *74*, 277

[S6] G. P. Smith, V. A. Petrenko, *Chem. Rev.* **1997**, *97*, 391.

References

1. Boden, S. D.; Kang, J.; Sandhu, H.; Heller, J. G., *Spine* **2002**, *27*, 2662.
2. Takeshita, S.; Zheng, L. P.; Brogi, E.; Kearney, M.; Pu, L. Q.; Bunting, S.; Ferrara, N.; Symes, J. F.; Isner, J. M. *J. Clin. Invest.* **1994**, *93*, 662.
3. Takeshita, S.; Pu, L. Q.; Stein, L. A.; Sniderman, A. D.; Bunting, S.; Ferrara, N.; Isner, J. M.; Jeffrey, M.; Symes, J. F. *Circulation* **1994**, *90*, 228.
4. Baumgartner, I.; Pieczek, A.; Manor, O.; Blair, R.; Kearney, M.; Walsh, K.; Isner, J. M. *Circulation* **1998**, *97*, 1114.
5. Hendel, R. C.; Henry, T. D.; Rocha-Singh, K.; Isner, J. M.; Kereiakes, D. J.; Giordano, F. J.; Simons, M.; Bonow, R. O. *Circulation* **2000**, *101*, 118.
6. Lee, C. H.; Cook, J. L.; Mendelson, A.; Moioli, E. K.; Yao, H.; Mao, J. J. *The Lancet* **2010**, *376*, 440.
7. Yancopoulos, G.D.; Davis, S.; Gale, N.W.; Rudge, J.S.; Wiegand, S.J.; Holash, J. *Nature* **2000**, *407*, 242.
8. Boontheekul, T.; Mooney, D.J. *Curr. Opin. Biotechnol.* **2003**, *14*, 559.
9. Patterson, J.; Martino, M.M.; Hubbell, J.A. *Materials Today* **2010**, *13*, 14.
10. Boudou, T. ; Crouzier, T. ; Ren, K. ; Blin, G. ; Picart, C. *Adv. Mater.* **2010**, *22*, 441.
11. Cabanas-Danés, J.; Huskens, J.; Jonkheijm, P. *J. Mater. Chem. B* **2014**, *2*, 2381.
12. Murray, J. ; Brown, L. ; Langer, R. *Cancer Drug Delivery* **1984**, *1*, 119.
13. Edelman, E. R. ; Mathiowitz, E. ; Langer, R. ; Klagsbrun, M. *Biomaterials* **1991**, *12*, 619.
14. Gombotz, W. R. ; Pettit, D. K. *Bioconjugate Chem.* **1995**, *6*, 332.
15. Mahoney, M. J.; Saltzman, W. M. *Proc. Natl. Acad. Sci. U. S. A.* **1999**, *96*, 4536.
16. Lee, K. Y. ; Peters, M. C.; Anderson, K. W.; Mooney, D. J. *Nature* **2000**, *408*, 998.
17. Richardson, T. P.; Peters, M. C.; Ennett, A. B.; Mooney, D. J. *Nat. Biotechnol.* **2001**, *19*, 1029.
18. Crouzier, T.; Fourel, L.; Boudou, T.; Albigès-Rizo, C.; Picart, C. *Adv. Mater.* **2011**, *23*, H111.
19. Crouzier, T.; Ren, K.; Nicolas, K.; Roy, C.; Picart, C. *Small* **2009**, *5*, 598.
20. Bastings, M. M. C.; Koudstaal, S.; Kieltyka, R. E.; Nakano, Y.; Pape, A. C. H.; Feyen, D. A. M.; van Slochteren, F. J.; Doevendans, P. A.; Sluijter, J. P. G.; Meijer, E. W.; Chamuleau, S. A. J.; Dankers, P. Y. W. Adv. Healthcare Mater. **2013**, *3*, 70.
21. Wylie, R. G.; Ahsan, S.; Aizawa, Y.; Maxwell, K. L.; Morshead, C. M.; Shoichet, M. S. *Nat. Mater.* **2011**, *10*, 799.
22. Nguyen, T. H.; Kim, S.-H.; Decker, C. G.; Wong, D. Y.; Loo, J. A.; Maynard, H. D. *Nat. Chem.* **2013**, *5*, 221.
23. Wesolowski, J.; Alzogaray, V.; Reyelt, J.; Unger, M.; Juarez, K.; Urrutia, M.; Cauerhff, A.; Danquah, W.; Rissiek, B.; Scheuplein, F.; Schwarz, N.; Adriouch, S.; Boyer, O.; Seman, M.; Licea, A.; Serreze, D.; Goldbaum, F.; Haag, F.; Koch-Nolte, F. *Med. Microbiol. Immunol.* **2009**, *198*, 157.
24. Huang, L.; Muyldermans, S.; Saerens, D. *Expert Rev. Mol. Diagn.* **2010**, *10*, 777.
25. de Marco, A. *Microb. Cell Fact.* **2011**, *10*, 44.
26. Wong, L. S.; Khan, F.; Micklefield, J. *Chem. Rev.* **2009**, *109*, 4025.
27. Jonkheijm, P.; Weinrich, D.; Schroeder, H.; Niemeyer, C.M.; Waldmann, H. *Angew. Chem. Int. Ed.* **2008**, *47*, 9618.
28. Aida, T.; Meijer, E. W.; Stupp, S. I. *Science* **2012**, *335*, 813.
29. Mager, M. D.; LaPointe, V.; Stevens, M. M. *Nat. Chem.* **2011**, *3*, 582.
30. Rybtschinski, B. *ACS Nano* **2011**, *5*, 6791.
31. H. W. Jun, V. Yuwono, S. E. Paramonov, J. D. Hartgerink, *Adv. Mater.* **2005**, *17*, 2612.
32. Nallur, S. K. M.; Voskuhl, J.; Bultema, J. B.; Boekema, E. J.; Ravoo, B. J. *Angew. Chem. Int. Ed.* **2011**, *50*, 9747.
33. Lee, D.-W.; Park, K. M.; Banerjee, M.; Ha, S. H.; Lee, T.; Suh, K.; Paul, S.; Jung, H.; Kim, J.; Selvapalam, N.; Ryu, S. H.; Kim, K. *Nat. Chem.* **2011**, *3*, 154.
34. Kim, C.; Agasti, S. S.; Zhu, Z.; Isaacs, L.; Rotello, V. M., *Nat. Chem.* **2010**, *2*, 962.

35. Meyer, R.; Niemeyer, C.M. *Small*, **2011**, *7*, 3211.
36. Dankers, P. Y. W.; Harmsen, M. C.; Brouwer, L. A.; Luyn, M. J. A.; Meijer, E. W. *Nat. Mater.* **2005**, *4*, 568.
37. Krogman, K. C.; Lowery, J. L.; Zacharia, N. S.; Rutledge, G. C.; Hammond, P. T. *Nat. Mater.* **2009**, *8*, 512.
38. Shah, R. N.; Shah, N. A.; Del Rosario Lim, M. M.; Hsieh, C.; Nuber, G.; Stupp, S. I. *Proc. Natl. Acad. Sci. U. S. A.* **2010**, *107*, 3293.
39. Liu, Y.; Wang, H.; Kamei, K. I.; Yan, M.; Chen, K.-J.; Yuan, Q.; Shi, L.; Lu, Y.; Tseng, H.-R. *Angew. Chem. Int. Ed.* **2011**, *50*, 3058.
40. Yang, L.; Gómez-Casado, A.; Young, J. F.; Nguyen, N. D.; Cabanas-Danés, J.; Huskens, J.; Brunsveld, L.; Jonkheijm, P. *J. Am. Chem. Soc.* **2012**, *134*, 19199.
41. González-Campo, A.; Brasch, M.; Uhlenheuer, D.; Gómez-Casado, A.; Yang, L.; Brunsveld, L.; Huskens, J.; Jonkheijm, P. *Langmuir* **2012**, *28*, 16364.
42. Tian, F.; Cziferszky, M.; Jiao, D.; Wahlström, K.; Geng, J.; Scherman, O. A. *Langmuir* **2011**, *27*, 1387.
43. An, Q.; Brinkmann, J.; Huskens, J.; Krabbenborg, S.; de Boer, J.; Jonkheijm, P. *Angew. Chem. Int. Ed.* **2012**, *51*, 12233.
44. Neirynck, P.; Brinkmann, J.; An, Q.; van der Schaft, D.; Gustav Milroy, L.; Jonkheijm, P.; Brunsveld, L. *Chem. Commun.* **2013**, *49*, 3679.
45. Boekhoven, J.; Rubert Pérez, C. M.; Sur, S.; Worthy, A.; Stupp, S. I. *Angew. Chem. Int. Ed.* **2014**, *52*, 12077.
46. Park, K. M.; Yang, J.-A.; Jung, H.; Yeom, J.; Park, J. S.; Park, K.-H.; Hoffman, A. S.; Hahn, S. K.; Kim, K. *ACS Nano* **2012**, *6*, 2960.
47. Brinkmann, J.; Cavatorta, E.; Sankaran, S.; Schmidt, B.; van Weerd, J.; Jonkheijm, P. *Chem. Soc. Rev.* **2014**, DOI: 10.1039/C4CS00034J.
48. Vukicevic, S.; Grgurevic, L. *Cytokine Growth Factor Rev.* **2009**, *20*, 441.
49. Li, R. H.; Wozney, J. M. *Trends in Biotechnol.* **2001**, *19*, 255.
50. Kemmis, C. M.; Vahdati, A.; Weiss, H. E.; Wagner, D. R. *Biochem. Biophys. Res. Commun.* **2010**, *401*, 20.
51. van der Linden, R. H. J.; Frenken, L. G. J.; de Geus, B.; Harmsen, M. M.; Ruuls, R. C.; Stok, W.; de Ron, L.; Wilson, S.; Davis, P.; Verrips, C. T. *Biochim. Biophys. Acta, Protein Struct. Mol. Enzymol.* **1999**, *1431*, 37.
52. Spinelli, S.; Frenken, L. G. J.; Hermans, P.; Verrips, T.; Brown, K.; Tegoni, M.; Cambillau, C. *Biochemistry* **2000**, *39*, 1217.
53. De Genst, E.; Silence, K.; Decanniere, K.; Conrath, K.; Loris, R.; Kinne, J. r.; Muyldermans, S.; Wyns, L. *Proc. Natl. Acad. Sci. U.S.A.* **2006**, *103*, 4586.
54. González-Campo, A.; Eker, B.; Gardeniers, H.J.G.E.; Huskens, J.; Jonkheijm, P. *Small* **2012**, *8*, 3531.
55. Ludden, M. J. W.; Mulder, A.; Schulze, K.; Subramaniam, V.; Tampé, R.; Huskens, J. *Chem. Eur. J.* **2008**, *14*, 2044
56. Ludden, M. J. W.; Mulder, A.; Tampé, R.; Reinhoudt, D. N.; Huskens, J. *Angew. Chem. Int. Ed.* **2007**, *46*, 4104.
57. Lata, S.; Reichel, A.; Brock, R.; Tampé, R.; Piehler, J. *J. Am. Chem. Soc.* **2005**, *127*, 10205.
58. De, M.; Rana, S.; Rotello, V. M. *Macromol. Biosci.* **2009**, *9*, 174.
59. Voskuhl, J.; Brinkmann, J.; Jonkheijm, P. *Curr. Opin. Chem. Biol.* **2014**, *18*, 1-7.
60. Nakamura, I.; Makino, A.; Ohmae, M.; Kimura, S. *Macromol. Biosci.* **2010**, *10*, 1265.
61. van der Horst, G.; van der Werf, S. M.; Farih-Sips, H.; van Bezooijen, R. L.; Löwik, C. W.G. M.; Karperien, M. *J. Bone Min. Res.* **2005**, *20*, 1867.
62. Tsai, M.-T.; Li, W.-J.; Tuan, R. S.; Chang, W. H. *J. Orthop. Res.* **2009**, *27*, 1169.
63. Wasserberg, D.; Nicosia, C.; Tromp, E. E.; Subramaniam, V.; Huskens, J.; Jonkheijm, P. *J. Am. Chem. Soc.* **2013**, *135*, 3104.

Chapter 4

Incorporation of single domain antibodies in biomaterials for skeletal tissue regeneration

Adapted from:
Electrospinning single domain antibodies for skeletal tissue regeneration

Emilie Dooms Rodrigues[1], Maqsood Ahmed[2], Mohamed El Khattabi[3], Jan de Boer[2], Clemens van Blitterswijk[2], Theo Verrips[3], Lorenzo Moroni[2] and Marcel Karperien[1]

[1] Department of Developmental BioEngineering, MIRA Institute for Biomedical Technology and Technical Medicine, Faculty of Science and Technology, University of Twente, Enschede, The Netherlands;
[2] Department of Tissue Regeneration, MIRA Institute for Biomedical Technology and Technical Medicine, Faculty of Science and Technology, University of Twente, Enschede, The Netherlands;
[3] QVQ BV, Utrecht, The Netherlands.

Abstract

Through the selective functionalization of scaffolds, targeted biological responses can be triggered. The aim of this work is to study the possibility to incorporate novel proteins in biomaterials without losing their biological activity and obtain bioactive biomaterials suitable for skeletal tissue engineering. Non-conventional antibodies, single domain antibody fragments (VHH), have been selected to inhibit or potentiate bone morphogenetic proteins (BMPs), which are relevant in bone and cartilage regeneration. These uniquely small antibodies are capable of high affinity binding of antigens with high selectively. They are highly soluble, stable and easy to manipulate genetically. VHH were incorporated in Poly(ethylene oxide) (PEO) electrospun fiber membranes. VHH-PEO fiber membranes were produced by electrospinning an aqueous solution of polymer and purified VHH under ambient conditions. The biological activity of the VHH dissolved from the PEO fibers was assessed by alkaline phosphatase (ALP) activity on C2C12 myoblasts cells. The VHH G7, targeting BMP7, still potentiated the ALP activity as reported in previous studies. In addition, VHH G7 and a genetically engineered version, where a N-linked glycosylation site was introduced, were incorporated in dextran-tyramine (dex-TA) hydrogels. The VHH were released from the hydrogel in a sustained manner.
These one step non-denaturing processes of biomaterial functionalization have potential applications in tissue engineering.

Keywords: Biomaterials, Functionalization, Electrospinning, Hydrogel, VHH, BMP7

Introduction

Bone and cartilage tissue regeneration require the fusion of a smart biomaterial, key growth factors and cells. The optimization of these features leads to the development of new materials and techniques. Bone morphogenetic proteins (BMPs) are key molecules in skeletal tissue regeneration. Targeting of these proteins permits the manipulation of molecular pathways and cellular responses relevant in skeletal formation. BMP7, also known as osteogenic protein 1 (OP-1), has a specific role in bone and cartilage morphogenesis and kidney formation [1-3]. In addition, BMP7 has confirmed osteogenic differentiation potential in animal models and is in clinical use [4]. So far, the common capture and immobilization of growth factors has been done through the use of conventional antibodies [5]. Conventional antibodies are large and complex molecules, which dictate a number of limitations for their applications [6]. Single domain antibodies of heavy chain antibodies of *Camelidae* (VHH), however, have significant advantages over conventional antibodies. VHH are unique small molecules (circa 15 kDa) capable of binding specifically to a target, are easy to clone as they consist of a single gene, highly soluble and stable, and have close homology with human antibody fragments. VHH are effective in targeting growth factors efficiently without compromising their biological activity. Previously we have isolated VHH targeting BMP7 by phage display. VHH clone G7 was able to bind to BMP7 with high affinity and was able to enhance its osteogenic differentiation effect (chapter 2 of this thesis). VHH can also be used as molecules to attract endogenous BMPs and create a local concentration of growth factors when they are bound to a biomaterial surface. VHH are a potential tool to create a reservoir of molecules that are spatially controlled and released which can enhance bone and cartilage regeneration with minimal related treatment costs. Furthermore, the versatility of the VHH permits genetic modifications and expression in yeast strains. This combination allows for the manipulation of VHH molecular weight by the introduction of a N-glycosylation site, which in a yeast strain with engineered glycosylation machinery is able to produce glycosylated proteins [6-8]. In addition, production of VHH in yeast enables the expression of VHH at high levels [6]. Another advantage is that glycosylation sites can be advantageously used to bind a VHH to a biomaterial through chemical crosslinking or can be used as an anchor of VHH in a dense polymer network such as present in hydrogels.

Biodegradable scaffolds have been employed as a template for tissue regeneration. First generation scaffolds were designed principally to be bioinert and merely provide a physical support for cell growth. More recently, bioactive scaffolds have been designed to influence cell behavior via a range of distinct mechanisms. The potential to functionalize scaffolds with bioactive agents, which can induce the appropriate biological response in a spatially and temporally controlled manner, is a promising strategy for engineering the cellular niche.

The selection of biomaterials is intrinsically related with its final application as much as the techniques utilized for its fabrication/ construction.

Electrospinning has been proposed as a promising technology for the fabrication of polymeric bioactive scaffolds relevant in skeletal tissue engineering. The resultant micro- and nano-fibrous meshes, with a high surface area and tunable porosity, are analogous to the fibrous structure of the native extracellular matrix (ECM) [9]. Electrospun scaffolds have previously been shown to be an effective drug delivery device, where the rate of drug release can be fine-tuned with the careful manipulation of the electrospinning parameters and thus fiber morphology [9-11].
Alternatively, injectable hydrogels are three-dimensional networks that mimic the dynamic microenvironment for cells in soft tissue [12]. Recently, enzymatic crosslinking of hydrogels have been introduced to formulate injectable hydrogels such as dextran-tyramine (dex-TA) conjugates [13, 14]. The crosslinking is catalyzed by horseradish peroxidase (HRP) in combination with hydrogen peroxide (H_2O_2).
In this study, the potential application of VHH in functionalizing biomaterials was evaluated. In particular, VHH were incorporated into polymeric formulation for electrospinning and in dex-TA hydrogels. The biological activity of the VHH in electrospun fibers and the VHH release profile from hydrogels were assessed.
The incorporation of VHH is a novelty in the biomaterials and tissue engineering field opening the doors for new developments in tissue regeneration.

Materials and methods

VHH selection, production and characterization
The selection of VHH targeting BMP7, VHH production and characterization can be found elsewhere (chapter 2 of this thesis). In brief, VHH targeting BMP7 were selected by phage display from a library derived of a llama immunized with BMP6 and BMP7. Two rounds of bio panning selection were performed on wells coated with BMP7. VHH G7 was selected to specifically bind to BMP7. VHH G7 dissociation constant (Kd) was ~1 nM. Its osteogenic differentiation potential was assessed using the C2C12 mouse myoblast cell line and the KS483-4C3 preosteoblast cell line.

VHH labeling with fluorescent dye
To visualize the VHH distribution on the electrospun fibrous membranes, VHH G7 was randomly labeled with an amine reactive Alexa Fluor 488 carboxylic acid, succinomidyl ester (Invitrogen) fluorescent dye. The VHH solution was concentrated using concentration columns (AMICON ULTRA 0.5 columns, Merck Millipore), and a protein concentration of 10 mg/ml was reached. A buffer exchange procedure was performed to dissolve VHH in 0.2 M sodium bicarbonate buffer (pH 8.3) using ZEBA spin desalting columns (7K MWCO, 0.5 ml, Thermo scientific, United States). A 10-fold excess of 10 mg/ml amine-reactive dye was added, reaction was left shaking for two hours at room temperature. To separate the conjugate from unreacted labeling reagent, dialyses against PBS was performed using ZEBA columns. Absorbance at 280 nm and 650 nm were

measured by UV-VIS in a Nanodrop-1000 Spectrophotometer. From these measurements the protein concentration and degree of labeling (DOL) were calculated.

Fabrication of electrospun fibers

For electrospinning, a 5% (w/v) solution of polyethylene oxide (PEO) was prepared in distilled H_2O. Before use, the solution was left to stir for a minimum period of 12 hours at room temperature or until completely dissolved. Then, a syringe containing the described solution was pumped at a controlled flow rate (0.5 ml/hour) using a syringe pump (KDS 100, KD Scientific). Polytetrafluoroethylene (PTFE) tubing was used to connect the syringe tip (diameter = 0.8 mm) and the electrospinning nozzle to which a high voltage was applied (Gamma High Voltage Research Inc., FL, USA). The electrospun fibers were collected on an aluminium collector after electrospinning 2 ml of the polymer solution. A working distance (distance from the collector to the spinneret) of 20 cm and a voltage of 20 kV were used. The temperature during spinning was 25°C and the humidity varied between 30% and 35%. Following the addition of VHH to the aqueous polymer solution, the same electrospinning parameters were used. A total volume of 600 ml of VHH with a concentration of 0.85 mg/ml was added to the polymer formulation. Discs with a diameter of 15.6 mm were punched out of the aluminium collector for surface characterization and cell culture experiments.

Environmental scanning electron microscopy

Prior to imaging electrospun fibers, samples were gold sputtered (Cressington 108 auto, 'cool' sputter coater, 60 seconds at 40 uA) and subsequently analyzed with ESEM (Philips Electron Optics, XL30 ESEM FEG).

Fluorescent imaging

Electrospun membranes were imaged using a BD Pathway (BD Biosciences) fluorescent microscope. Distribution of the VHH was identified using a fluorescently tagged VHH incorporated into the fibers. Control samples with no VHH were used to ensure that no autofluorescence from the scaffold was present.

Electrospun fibers characterization

Fiber diameter was determined from scanning electron microscopy (SEM) (XL 30 ESEM-FEG, Philips/FEI) images. A minimum of 3 images per sample were taken and a minimum of 10 fibers were measured per image to determine fiber diameters using an in-house macro developed for Image J (National Institutes of Health, Bethesda, MD, USA).

Biological activity of VHH

To assess the biological activity of VHH G7 before and after incorporation in electrospun fiber membranes, a biological system was set up with C2C12 used as a model for osteogenic differentiation [15]. C2C12 cells were cultured in Dulbecco's Modified Eagles Medium (DMEM; Gibco) supplemented with 10% fetal bovine serum (FBS;

Cambrex), 100 U/ml penicillin (Gibco) and 100 μg/ml streptomycin (Gibco) and were incubated at 37 ºC in humidified atmosphere and 5% CO_2. C2C12 cells were seeded on the water soluble electrospun meshes discs at a cell density of 10 000 cells/ cm^2 and cultured for 7 days with ascorbic acid (50 μg/ml; Sigma Aldrich) in the presence or absence of BMP7 (100 ng/ml; R&D Systems) with or without VHH G7 (1 μg/ml) under standard conditions. At day 7, cells were washed with PBS and lysed with CDPStar lysis buffer (Roche). To evaluate alkaline phosphatase activity (ALP), cell lysate was added to CDPStar reagent (Roche) and luminescence was measured using Victor Microplate Luminometer (Promega). The luminescence units were corrected for DNA content. DNA concentration was determined via a proliferation assay according to the manufacturer's protocol (CyQuant Cell Proliferation Assay Kit; Invitrogen).
The biological activity of VHH after undergoing the electrospinning process was similarly assessed. Electrospun fibrous membranes discs of 15.6 mm diameter with or without VHH G7 were solubilized with 200 μl/well of medium Dulbecco's Modified Eagles Medium (DMEM; Gibco) supplemented with 10% fetal bovine serum (FBS; Cambrex), 100 U/ml penicillin (Gibco) and 100 μg/ml streptomycin (Gibco). The supernatant was added to C2C12 cells, cultured and ALP activity was evaluated as described above.

Genetic modification of VHH G7
VHH G7 was genetically modified in order to introduce a N-linked glycosylation site in Loop 4 at K76, away from the complementary determining regions (CDRs). VHH G7 with the substitution K76N was modeled using the online program I-TASSER for protein folding [16-18]. The N-linked glycosylation site was introduced using site directed mutagenesis. Forward and reverse primers were designed to substitute the lysine at position 76 into an asparagine to obtain a N-linked glycosylation site (NXT/S). The primers FwNNT (5' GACAACGCCAACAACACGGTGTATCTGC-3') and RevNNT (5'CACCGTGTTGTTGGCGTTGTCACTGGAG-3') were used to introduce the mutation by overlap extension using the forward (PG705) and reverse (AFS03) primers of the plasmid pUR4585 as follows: PCR fragments generated with the primers FwNNT + AFS03 and RevNNT + PG705. After purification of the PCR fragments, they were used as template for a PCR using the primers PG705 and AFS03. The generated fragment was digested with the restriction enzymes *Pst*I and *Eco*91I and cloned into the plasmid pUR4585 production of Glyco-VHH G7 in yeast strain VW K18 GAL1. In pUR4585, VHH expression is under the control of the GAL7 promoter and is induced by addition of galactose to the medium. The same VHH fragment was also cloned into the expression plasmid pMEK219 containing a C-terminus myc and His6 tags for VHH production in bacteria.

VHH production and purification in bacteria
E. coli strain TG1 was used for the maintenance of the plasmids and expression of proteins. For the production of the VHH G7 K76N in bacteria, *E. coli* containing the

plasmid with the mutated VHH, was grown in Luria Broth (LB) or 2x Yeast Tryptone (YT) medium, supplemented with 2% (w/v) glucose and ampicillin at 100 mg/ ml. VHH expression was induced by the addition of 1 mM isopropyl β-D-1-thiogalactopyranoside (IPTG) and cultivation at 37^{o}C for 4 hours, while shaking [19, 20]. VHH proteins were purified from the periplasmic fraction, prepared by freeze-thawing of the bacteria in PBS, via the C-terminus his-tag by cobalt affinity chromatography (TALON His-Tag Purification Resin, ClonTech). Purified VHH were analyzed by sodium dodecyl sulfate polyacrylamide gel electrophoresis (SDS-PAGE) and Coomassie staining. The final VHH concentration was determined from the UV absorption at 280 nm (NanoDrop 1000 Spectrophotometer, Thermo Scientific) and the theoretical mass extinction coefficient.

VHH production and purification in yeast

Saccharomyces Cerevisiae containing the plasmid with the VHH G7 K76N was at a first instance grown for 48 hours at 30^{o}C in selective medium composed of Yeast Nitrogen Base (YNB) without amino acids at a concentration of 6.7 g/l and glucose 20 g/l [21]. Subsequently the cultures were up scaled in expression medium composed of YP Broth (yeast extract and bactopeptone at a concentration of 10 g/l and 20 g/l, respectively), glucose 20 g/l and galactose 5 g/l at 30^{o}C. After 48 hours of growth the yeast cells were removed by centrifugation and the supernatant used to purify VHH with Ni^{2+} affinity chromatography by AKTA (GE Healthcare Life Sciences).

EndoH digestion

To confirm the presence of N-linked glycosylation, yeast produced VHH (Glyco-VHH) was incubated with increasing concentrations of Endoglycosidase H enzyme (Endo H, New England Biolabs), which degrades N-linked sugars with high specificity. The apparent molecular weight of the digested VHH was assessed by SDS-PAGE and Coomassie staining.

Function of the glyco-VHH G7

In order to assess if the introduction of a N-glycosylation site in Loop 4 interferes with binding of the VHH to BMP7, an ELISA assay was performed. MaxiSorp plate wells were coated overnight at 4^{o}C with BMP7 (1 µg/ml) in PBS. After blocking of the wells with 4% Marvel in PBS, a concentration range of VHH G7 K76N produced in E. coli or yeast (ranging from 0.1 to 10 µg/ml) in 2% Marvel were incubated for 2 hours in the coated and blocked wells. The wells were washed with PBS Tween (PBS containing 0.5% (v/v) Tween-20, PBST) and PBS. Bound VHH were detected by incubation with a rabbit anti-VHH serum (K976) and a donkey anti-rabbit antibody coupled to a peroxidase. The amount of HRP was developed by the addition of *O*-phenyldiamine (OPD) in the presence of hydrogen peroxidase (H_2O_2). The reactions were stopped by the addition of sulfuric acid (H_2SO_4) and measured at 490 nm (Micro Plate Reader).

Dextran-tyramine hydrogel formulation and VHH release profile

Unglycosylated and glycosylated VHH K76N were incorporated in hydrogel samples in order to assess their release profile.

Hydrogel samples (~60 µl) were prepared in vials by the addition of a mixture of H_2O_2 and horseradish peroxidase (HRP) to solutions of dextran-tyramine (dex-TA) hydrogels and VHH solution to obtain a 10% w/v hydrogel as previously described [22]. Dextran-tyramine conjugates with a molecular weight of dextran of 14 000 g/mol (dex14k) and a degree of substitution (DS) of tyramine groups (TA) of 10 was used. The DS is defined as the number of tyramide residues per 100 anhydroglycose rings of dextran. Dext-TA conjugates were prepared as reported previously [23]. To a VHH solution (50 µl, 0.2 µg/µl) or PBS, and 12.5 mg of lyophilized dex14k-TA DS10, a freshly prepared solution of 1% H_2O_2 (5 µl) and HRP (5 µl, 250 units/ml) in PBS were added. The contents were gently mixed. The gelation time was determined by the tilting method. Within one minute the formulation was in the gel state. On top of crosslinked gels, 60 µl of PBS was added. Two phases were visible. The samples were incubated at room temperature and the supernatant was rescued hourly over a time span of six hours and substituted with new PBS. The rescued supernatant samples were incubated in maxisorp plates and an ELISA was performed (as described above) to determine the VHH concentration released in the samples.

Statistical Analysis

Statistical analyses were performed using GraphPad Prism version 5.00 for Windows, GraphPad Software (San Diego, California). Analyses were based on one-way ANOVA and a Tukey's Post-hoc test ($p < 0.05$) among all samples or between samples and controls.

Results

VHH incorporated in electrospun fiber membranes

VHH were dissolved in an aqueous PEO solution and electrospun to create fibrous membranes. The incorporation of VHH did show evidence of beads formation on the fibers produced with VHH (Figure 1A and B). The distribution of the VHH through the fibers was verified via fluorescent microscopy. The VHH were randomly labelled by NHS chemistry with alexa fluor 488 fluorophore prior to incorporation into the fibers with a degree of labelling (DOL) of 1.030, suggesting that each VHH contained ~1 fluorophore. Following electrospinning, the fibers were then fluorescently imaged. The distribution of VHH throughout the electrospun fibers appeared to be homogenous (Figure 1C and D). The estimated concentration of VHH distributed on the fibrous membrane, considering a homogeneous distribution, was 4 µg/cm^2. Although the incorporation of VHH in electrospun fibers led to the formation of beads, there was no significant influence over electrospinning parameters, with no empirical changes in

electrospinning and fiber diameter remained consistent at 245 ± 64 nm for the VHH free fibers and 259 ± 67 nm for the PEO-VHH fibers (Figure 1 E and F).

The electrospun VHH are bioactive

The biological activity of the VHH was assessed before and after the electrospinning process. C2C12 cells were cultured in standard conditions in order to test their osteogenic differentiation by addition or not of BMP7 in presence or absence of VHH added in solution or from the dissolved electrospun fiber membranes.

In C2C12 cells, ALP activity was induced by the addition of BMP7 by 1.8 fold and in the presence of VHH G7, added in solution, the ALP activity was further potentiated to 2.4 fold when compared with the control (Figure 2A). The VHH on its own did not have any significant difference on ALP levels when compared with the control.

The VHH, which underwent the electrospinning process, were extracted from the PEO fibrous membrane after solubilization in cell culture medium. A liquid solution was obtained. The supernatant was added to C2C12 cells and ALP levels were measured. The ALP activity of C2C12 cells was induced by the addition of BMP7 by 70 fold and in the presence of VHH G7 and BMP7 the ALP activity was further enhanced to 480 fold when compared with the control (Figure 2B). The presence of the VHH from the dissolved fiber membrane, in the absence of BMP7, did not show any significant effect when compared with the control.

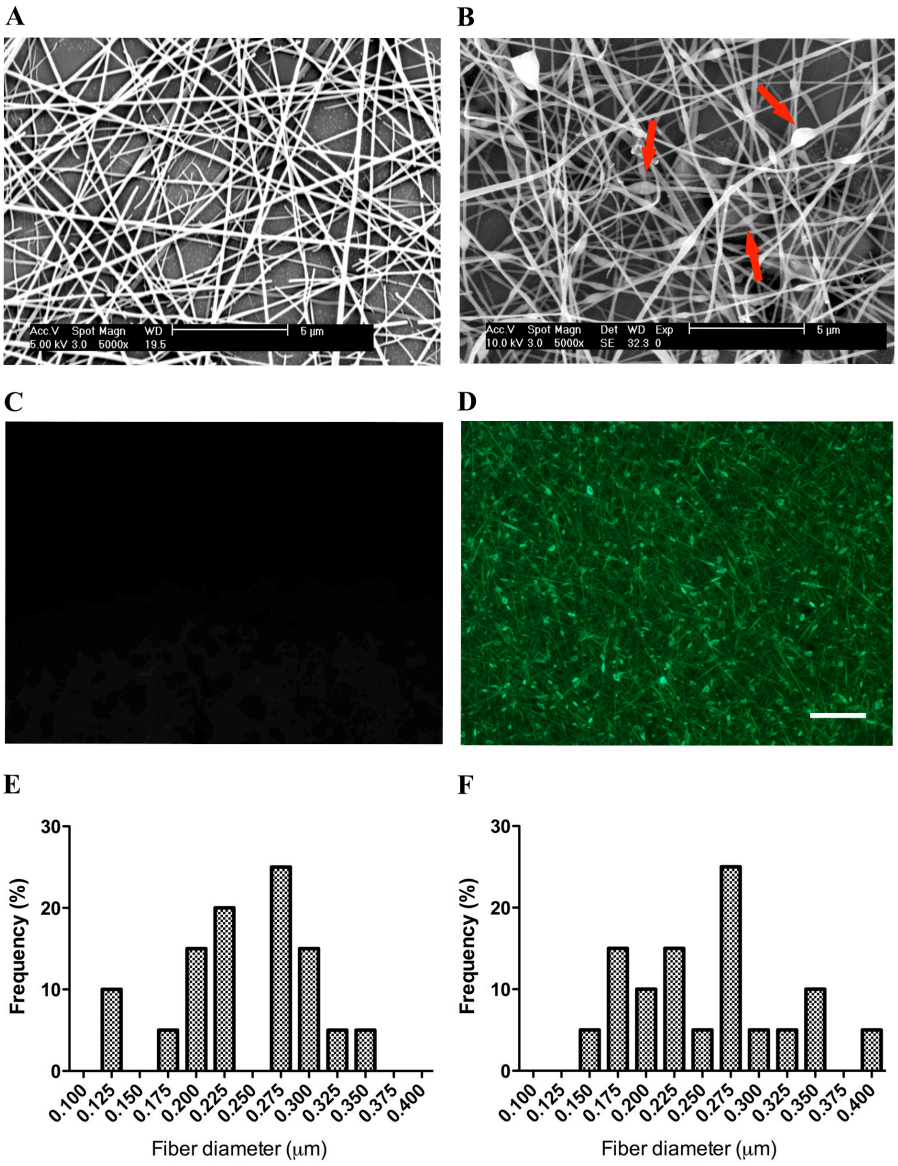

Figure 1. Electrospun fiber membranes characterization. (A and B) SEM images of electrospun fibers without and with VHH G7 (4 µg/cm^2), respectively. Beads are indicated with arrows. (C and D) Fluorescent images of electrospun fibers without or with fluorescently labeled VHH G7. Scale bar represents 20 µm. (E and F) Histogram fiber diameter distribution for electrospun fibers without and with VHH.

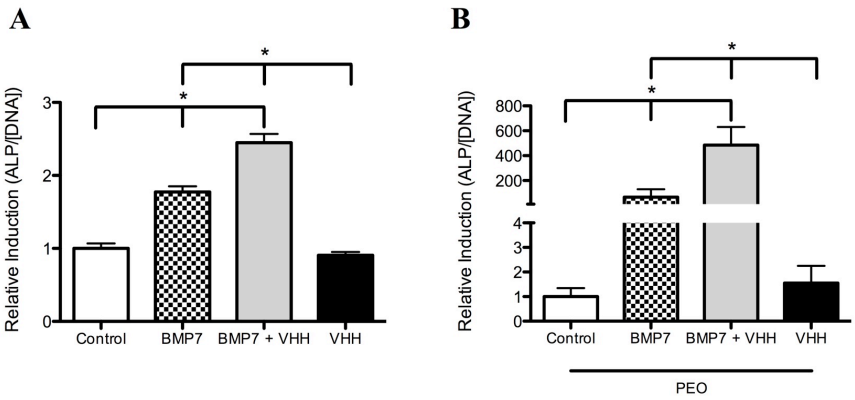

Figure 2. Biological activity of VHH in solution and from dissolved electrospun fibers. (A) C2C12 cells were cultured in standard osteogenic conditions in the presence or absence of BMP7 (100 ng/ml) and/or VHH (1 µg/ml). ALP activity was measured in C2C12 and normalized by the total DNA content of the wells, and expressed as relative induction compared to negative control as mean fold induction of 6 independent experiments +/- SD. * p< 0.05. (B) PEO-VHH and PEO-VHH-free electrospun fiber membranes were dissolved in cell culture medium and added to C2C12 cells in the absence or presence of BMP7 in standard osteogenic differentiation medium. ALP activity was measured and normalized by the total DNA content, and expressed as mean relative fold induction compared to negative control. * p< 0.05. (N=6).

Glyco-VHH characterization

To facilitate integration of VHH into materials made of polysaccharides such as dextran, a glycosylation site was introduced into VHH G7 directed against BMP7 using site directed mutagenesis (mutagenesis by overlap extension) (Figure 3A). The N-linked glycosylation site was introduced in loop 4 at the same side of the CDRs of the VHH as predicted by I-TASSER (Figure 3B) [16-18]. Modeling demonstrated no significant effect of the amino acid change on overall VHH structure.

Mutated VHH was expressed in yeast *S. cervesia* and was found to migrate at higher apparent molecular weight than the same sequence expressed in *E. coli* (Figure 3C, lane 1 and 2). The presence of glycosyl groups was confirmed by digestion with the enzyme EndoH, which degrades N-linked sugars with high specificity. By using increasing amounts of EndoH, more VHH was running at the position of the same VHH expressed in *E. coli*, which is unable to add glycosyl groups to proteins (Figure 3C, lanes 3-5), indicating that the increase in molecular weight was due to the addition of glycosyl groups which were effectively removed by EndoH.

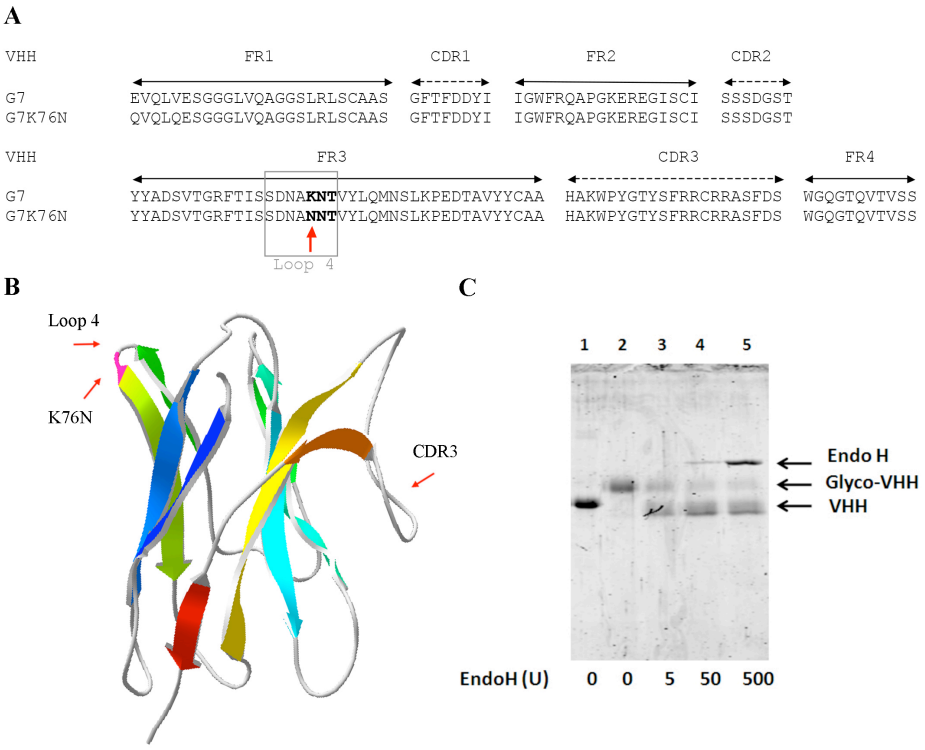

Figure 3. (A) Amino acid sequences alignment of VHH G7 and genetically modified G7K76N, where a N-linked glycosylation site was introduced in Loop 4 using site directed mutagenesis. Frame works (FR) and complementary determining regions (CDR) of the VHH are indicated according to Chothia [33]. (B) Schematic representations of modeled VHH G7. Protein chain is represented by ribbons and colored with rainbow spectrum from N-terminus (blue) to C-terminus (red). The mutation site is highlighted in pink at Loop 4. (C) SDS gel of VHH digestion with EndoH. lane 1 – VHH in bacteria, normal VHH, lane 2 – VHH produced in yeast with glycosyl group (higher MW), lane 3, 4 and 5 – digestion of glycosyl group (cleavage of group) by enzyme Endo H with different concentrations where the different bands show the different VHH forms.

Glycosylated VHH binds to BMP7

Unglycosylated and glycosylated VHH K76N were tested for binding to BMP7 in a solid phase ELISA. A titration series of VHH over a range of 0.1 to 10 µg/ml was performed while BMP7 coating was kept constant at 1 µg/ml throughout the series. When binding of VHH to BMP7 occurred a change in signal was measured (Figure 4). It was observed that unglycosylated and glycosylated VHH bind to BMP7 in a dose dependent manner. Both VHH display a similar binding curve. It was found that the mutation K76N and the attachment of N-linked glycosyl groups in yeast, did not affect the binding of VHH to BMP7.

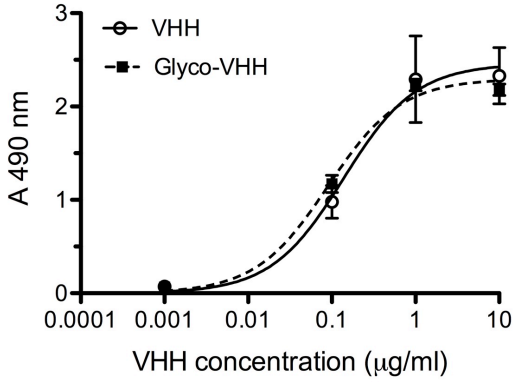

Figure 4. Dose-response binding of VHH and glyco-VHH to BMP7. Binding of the VHH G7K76N and glyco-VHH G7K76N to BMP7 was determined by solid phase ELISA. Nunc Maxisorp wells coated with BMP7 (30 nM) or PBS (negative control) were incubated with the indicated VHH concentrations and bound VHH were detected with a rabbit anti-VHH serum and a Donkey anti-rabbit antibody coupled to a peroxidase. Colorimetric conversion of *O*-phenyldiamine (OPD) in the presence of H_2O_2 was measured at 490 nm (A 490 nm). Data represent the mean +/- SD of 3 independent experiments.

VHH release profiles from dextran-tyramine conjugates

Enzymatic crosslinking of dextran-tyramine conjugates has been shown to be of relevance for *in situ* forming hydrogels [23]. Integration of the VHH into a dextran-tyramine gel was assayed by crosslinking the dextran-tyramine polymers using HRP and H_2O_2 in the presence of unglycosylated and glycosyalated VHH K76N as described [23]. The gelation times of dex-TA hydrogels was measured by the vial tilting method. The gelation time was shorter than one minute for both VHH.

To allow growth factors (BMP7) modulation over prolonged period of time, VHH diffusion in the hydrogel is greatly desired. The diffusion of VHH out of the hydrogel into the overlaid PBS solution was detected by ELISA using a polyclonal antibody against VHH (Figure 5). In the first three hours, more unglycosylated VHH was released from the hydrogel compared to the glycosylated VHH suggesting better entrapment of the glycosylated VHH in the hydrogel network. Both gels showed a sustained release throughout the time span of the experiment.

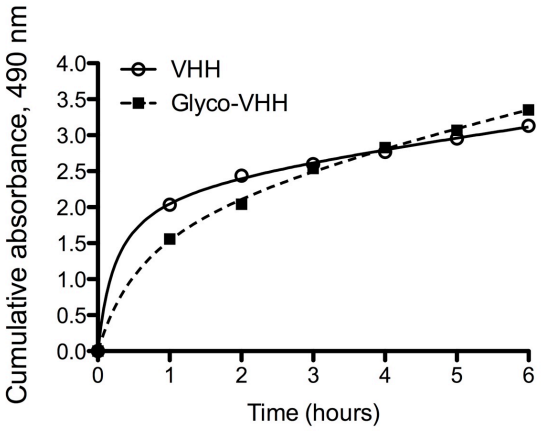

Figure 5. Release profile of VHH G7K76N and Glyco-VHH G7K76N from a dextran tyramide hydrogel. Cumulative release profile of dextran-tyramine conjugates loaded with unglycosylated (VHH) and glycosylated (Glyco-VHH) K76N as a function of time over six hours.

Discussion

The present work shows the incorporation of VHH in biomaterials. VHH-PEO fibrous membranes were produced by electrospinning a polymeric solution of purified VHH and the remaining biological activity of the VHH after the electrospinning process was assessed. Furthermore, VHH were genetically modified and incorporated in dex-TA hydrogels where its release profile was assessed.

As previously described (chapter 2 of this thesis) the VHH G7 targeting BMP7 were selected by phage display from an immunized llama phage display library. The VHH selected showed to be biologically active potentiating the osteogenic differentiation of C2C12 cells *in vitro* in the presence of BMP7.

Electrospinning is capable of producing fibrous membranes conducive for cell culture. An advantage of electrospinning is the small amounts of polymer required for electrospinning and therefore small amounts of VHH are required whilst the concentration is ensured. Here, we demonstrate the possible incorporation of bioactive molecules in a fibrous membrane. The incorporation of VHH, targeting growth factors, in electrospun fibers would permit the formation of a reservoir of endogenous growth factors *in situ*. The VHH were incorporated in a water-soluble polymeric formulation and underwent the electrospinning process. The incorporation of VHH in the polymeric solution provoked the emergence of beads in the fibrous networks still it did not significantly alter its properties. Beads on the fibers are often related to instabilities of the jet of polymer solution [24]. Principle contributing factors are solution viscosity, net charge density carried by the electrospinning jet and surface tension of the solution. As there were no significant differences in solution viscosity, it is likely that the doping of

the PEO solution with the VHH antibody increased the charge density of the polymer solution causing the minor beads observed on the fibers.

VHH were fluorescently labeled prior to incorporation in polymer solution and electrospinning process for visualization purposes. The VHH labeling was efficient. Fluorescence demonstrated homogenous distribution of the VHH in the electrospun fiber membrane.

Fibrous membranes were solubilized in order to extract the VHH in an active form and obtain an aqueous solution suitable for osteogenic assay experiments. The bioactivity of the VHH was clearly retained as demonstrated in an *in vitro* osteogenic differentiation assay. We showed that the VHH potentiated BMP7 induced ALP activity, which is an early marker for osteogenic differentiation in C2C12 cells. . As described elsewhere (chapter 2 of this thesis), VHH G7 is a super agonist to BMP7, which in combination with BMP7 potentiates its biological effect. After release of the VHH from the electrospun fibers by its dissolution in culture medium, the VHH was still able to potentiate BMP7 induced ALP expression [25]. Although the VHH underwent the electrospinning process, this unnatural environment did not perturb the biological activity of the protein. This effect could be due to the inherent capacity of VHH to refold very efficiently in its natural conformation upon denaturing when brought into physiological solvents. This ability make VHH withstand many weak organic solvents that normally perturb the biological activity of proteins or even relatively high temperatures [26]. Alternatively, due to its inherent stability, the electrospinning process and the incorporation in the PEO fibers may not have affected the 3D structure of the VHH. Our experimental set up does not allow us to distinguish between these two explanations. This allowed us to conclude that the VHH present in the fibrous membrane can withstand the electrospinning process without affecting their biological activity, i.e. correct refolding of the protein [26]. However, the stability of the VHH is also dependent on its amino acid sequence, which may affect refolding; therefore the efficiency of VHH with distinct frameworks might vary. Interestingly, VHH G7 codes for two additional cysteine residues, next to the canonical disulfide bond formed by the cysteine residues at positions 22 and 96. These two cuysteine residues are believed to form an extra disulfide bridge, which should insure an extra stability of the VHH (chapter 2 of this thesis). The proper selection of the solvent and the electrospinning conditions are of upmost importance as the unnatural conditions may eventually influence the biological activity of the VHH. Incorporation of VHH can be envisaged in non water-soluble polymer solutions in order to assess the stability of the VHH in other types of solvents [27] and the biological activity of the VHH into/onto the polymeric fibers. In non water-soluble membranes, the release profile of the VHH can be determined and the polymeric solution tuned in order to obtain the desired characteristics of release. Another possibility is the use of coaxial fibers where the proteins are incorporated in the core matrix to minimize the contact with more harsh solvents present in the shell [28-30]. It can be envisaged the use of several VHH targeting different growth factors for a more customized targeting and release [31].

Whilst the polymer solution can be tuned, engineering a VHH is also a possibility. If a VHH possesses a N-linked glycosylation site in its amino acid sequence and it is expressed in yeast, a N-linked glycosylated VHH can be produced [21]. VHH G7 was genetically modified to introduce a N-linked glycosylation site using site directed mutagenesis. The VHH was expressed in yeast wild type for building glycosylation at the N-glycosylation site [6-8]. Further advantages of the production in yeast are the increase in VHH production levels and the N-glycosylation site may increase the stability of the VHH [8]. The glyco-VHH produced revealed a higher molecular weight as expected due to the presence of a glycosyl group. The binding affinity of the modified VHH to BMP7 was not jeopardized by the existence of a glycosyl group, which is also in accordance with the predicted model with I-TASSER [16-18]. Alternatively, the introduction of a glycosylation site could be envisaged in loop 5, at the opposite side of the binding site and avoid potential steric hindrance.

Another advantage of glycosylated VHH is that the glycosyl group can be advantageously used to bind a VHH to an implant/biomaterial through chemical crosslinking with carbohydrates in the implant/ biomaterial or can be used as an anchor of VHH in a dense polymer network as observed in hydrogels. Hydrogels have been widely used for cartilage tissue regeneration. The use of injectable hydrogels is a strategy in cartilage regeneration as they guarantee local delivery of drugs in the knee joint and can improve therapy efficacy since no super physiological concentrations are required. Here, we incorporated glycosylated VHH in dex-TA hydrogels and evaluated its release in time. VHH and dex-TA were incubated with HRP and H_2O_2, which catalyzed a crosslinking reaction between the tyramine residues conjugated to dextran. The incorporation of VHH in the gel formulation did not show any significant change in gelation time, suggesting that the used VHH concentration still allowed for the crosslinking of the hydrogel network. The release profile of the VHH throughout the hydrogel was assessed by ELISA. Glycosylated VHH showed slight increased retention time when compared with the unglycosylated VHH, which is likely due to the increased size of the glycosylated VHH in which the glycosyl units may act as anchors [32]. The gelation condition of such Dex-TA conjugates also influence biological performance. It can be envisaged the incorporation of cells together with the VHH during the crosslinking reaction and obtain a biomaterial functionalized with growth factor binding VHH and cells for *in situ* gel formation. The effect on tissue formation in culture can then be determined. The system presented here allows for a protein friendly technology and tailor made release behavior.

The present results show 2D systems capable to evolve into 3D systems for sustained release of VHH and consequently growth factors from biomaterials. The function of VHH can be spread to several applications owed to their versatility. The combination of VHH targeting key molecules in tissue regeneration and the functionalization of biomaterials by these opens an avenue of opportunities in tissue engineering.

Conclusion

Electrospun fibers can be functionalized by the incorporation of novel proteins targeting growth factors, namely VHH, in the electrospinning polymer formulation prior to electrospinning process. The VHH can withstand electrospinning process, under mild conditions, and remain biologically active. Functionalized VHH-PEO fibers may be a suitable platform for growth factor concentration to build an *in situ* reservoir of endogenous BMPs. It is an one step process for the construction of a bioactive scaffold with significant versatility for tissue regeneration.
Furthermore, genetic modification of VHH such that they can be produced as glycosylated antibodies in yeast were incorporated in dex-TA conjugates by crosslinking with HRP and H_2O_2. Both unglycosylated and glycosylated VHH were successfully incorporated in dex-TA hydrogels. The glycosylated VHH showed a net higher sustained release most likely due to their larger size and the ability of the glycosyl groups to act as anchor. *In situ* hydrogel formation from dex-TA conjugates, supplemented with VHH have a potential for protein modulation and regenerative cartilage engineering.
The versatility of the VHH allows them to be engineered for incorporation in diverse biomaterials.

Acknowledgements

This work was supported by project P2.02 OAControl of the research program of the BioMedical Materials Institute, co-funded by the Dutch Ministry of Economic Affairs, Agriculture and Innovation.
The long-term program support of the Dutch Arthritis Association to MK is gratefully acknowledged.
The authors would like to acknowledge the financial support from PIDON program PID101020.

References

1. Bessa, P.C., M. Casal, and R.L. Reis, *Bone morphogenetic proteins in tissue engineering: the road from the laboratory to the clinic, part I (basic concepts).* Journal of tissue engineering and regenerative medicine, 2008. **2**(1): p. 1-13.
2. Wang, Q., et al., *The Osteogenic Study of Tissue Engineering Bone with BMP2 and BMP7 Gene-Modified Rat Adipose-Derived Stem Cell.* Journal of Biomedicine and Biotechnology, 2012.
3. Caron, M.M., et al., *Hypertrophic differentiation during chondrogenic differentiation of progenitor cells is stimulated by BMP-2 but suppressed by BMP-7.* Osteoarthritis and cartilage / OARS, Osteoarthritis Research Society, 2013. **21**(4): p. 604-13.
4. Pecina, M., L.R. Giltaij, and S. Vukicevic, *Orthopaedic applications of osteogenic protein-1 (BMP-7).* International Orthopaedics, 2001. **25**(4): p. 203-208.
5. Chames, P., et al., *Therapeutic antibodies: successes, limitations and hopes for the future.* British journal of pharmacology, 2009. **157**(2): p. 220-33.
6. Harmsen, M.M. and H.J. De Haard, *Properties, production, and applications of camelid single-domain antibody fragments.* Appl Microbiol Biotechnol, 2007. **77**(1): p. 13-22.
7. Hamilton, S.R., et al., *Humanization of yeast to produce complex terminally sialylated glycoproteins.* Science, 2006. **313**(5792): p. 1441-3.
8. Ueda, T., et al., *Stabilization of lysozyme by introducing N-glycosylation signal sequence.* Journal of Biochemistry, 1996. **119**(1): p. 157-161.
9. Pham, Q.P., U. Sharma, and A.G. Mikos, *Electrospinning of polymeric nanofibers for tissue engineering applications: A review.* Tissue Engineering, 2006. **12**(5): p. 1197-1211.
10. Nezarati, R.M., M.B. Eifert, and E. Cosgriff-Hernandez, *Effects of Humidity and Solution Viscosity on Electrospun Fiber Morphology.* Tissue Engineering Part C-Methods, 2013. **19**(10): p. 810-819.
11. Son, Y.J., W.J. Kim, and H.S. Yoo, *Therapeutic applications of electrospun nanofibers for drug delivery systems.* Archives of Pharmacal Research, 2014. **37**(1): p. 69-78.
12. Geckil, H., et al., *Engineering hydrogels as extracellular matrix mimics.* Nanomedicine, 2010. **5**(3): p. 469-484.
13. Jin, R., et al., *Enzymatically-crosslinked injectable hydrogels based on biomimetic dextran-hyaluronic acid conjugates for cartilage tissue engineering.* Biomaterials, 2010. **31**(11): p. 3103-13.
14. Lee, F., J.E. Chung, and M. Kurisawa, *An injectable enzymatically crosslinked hyaluronic acid-tyramine hydrogel system with independent tuning of mechanical strength and gelation rate.* Soft Matter, 2008. **4**(4): p. 880-887.
15. Ebisawa, T., et al., *Characterization of bone morphogenetic protein-6 signaling pathways in osteoblast differentiation.* J Cell Sci, 1999. **112 (Pt 20)**: p. 3519-27.
16. Zhang, Y., *I-TASSER server for protein 3D structure prediction.* BMC bioinformatics, 2008. **9**: p. 40.
17. Roy, A., A. Kucukural, and Y. Zhang, *I-TASSER: a unified platform for automated protein structure and function prediction.* Nature protocols, 2010. **5**(4): p. 725-38.
18. Roy, A., J. Yang, and Y. Zhang, *COFACTOR: an accurate comparative algorithm for structure-based protein function annotation.* Nucleic acids research, 2012. **40**(Web Server issue): p. W471-7.
19. Saerens, D., et al., *Single domain antibodies derived from dromedary lymph node and peripheral blood lymphocytes sensing conformational variants of prostate-specific antigen.* J Biol Chem, 2004. **279**(50): p. 51965-72.
20. Roovers, R.C., et al., *High-affinity recombinant phage antibodies to the pan-carcinoma marker epithelial glycoprotein-2 for tumour targeting.* Br J Cancer, 1998. **78**(11): p. 1407-16.

21. Frenken, L.G., et al., *Isolation of antigen specific llama VHH antibody fragments and their high level secretion by Saccharomyces cerevisiae.* J Biotechnol, 2000. **78**(1): p. 11-21.
22. Jin, R., et al., *Enzymatically Crosslinked Dextran-Tyramine Hydrogels as Injectable Scaffolds for Cartilage Tissue Engineering.* Tissue Engineering Part A, 2010. **16**(8): p. 2429-2440.
23. Jin, R., et al., *Enzyme-mediated fast in situ formation of hydrogels from dextran-tyramine conjugates.* Biomaterials, 2007. **28**(18): p. 2791-800.
24. Fong, H., I. Chun, and D.H. Reneker, *Beaded nanofibers formed during electrospinning.* Polymer, 1999. **40**(16): p. 4585-4592.
25. Cheng, H., et al., *Osteogenic Activity of the Fourteen Types of Human Bone Morphogenetic Proteins (BMPs).* The Journal of Bone & Joint Surgery, 2003. **85**(8): p. 1544-1552.
26. Dumoulin, M., et al., *Single-domain antibody fragments with high conformational stability.* Protein Science, 2002. **11**(3): p. 500-515.
27. Luo, C.J., M. Nangrejo, and M. Edirisinghe, *A novel method of selecting solvents for polymer electrospinning.* Polymer, 2010. **51**(7): p. 1654-1662.
28. Jia, X., et al., *Sustained release of VEGF by coaxial electrospun dextran/PLGA fibrous membranes in vascular tissue engineering.* Journal of biomaterials science. Polymer edition, 2011. **22**(13): p. 1811-27.
29. He, C.L., et al., *Coaxial electrospun poly(L-lactic acid) ultrafine fibers for sustained drug delivery.* Journal of Macromolecular Science Part B-Physics, 2006. **45**(4): p. 515-524.
30. Qu, H., S. Wei, and Z. Guo, *Coaxial electrospun nanostructures and their applications.* Journal of Materials Chemistry A, 2013. **1**(38): p. 11513-11528.
31. Su, Y. and X. Mo, *Dual drug release from coaxial electrospun nanofibers.* Journal of controlled release : official journal of the Controlled Release Society, 2011. **152 Suppl 1**: p. e82-4.
32. Gandhi, M., et al., *Mechanistic examination of protein release from polymer nanofibers.* Molecular pharmaceutics, 2009. **6**(2): p. 641-7.
33. Chothia, C., et al., *Conformations of immunoglobulin hypervariable regions.* Nature, 1989. **342**(6252): p. 877-83.

Chapter 5

Reversible growth factor immobilization on poly(trimethylene carbonate) (PTMC) using engineered VHH

Emilie Dooms Rodrigues[1], Sebastien Blanquer[2], Bas van Bochove[1], Marijke de Graaff[1], Mohamed El Khattabi[3], Clemens van Blitterswijk[4], Theo Verrips[3], Dirk Grijpma[2] and Marcel Karperien[1]

[1] Department of Developmental BioEngineering, MIRA Institute for Biomedical Technology and Technical Medicine, Faculty of Science and Technology, University of Twente, Enschede, The Netherlands;
[2] Department of Biomaterials Science and Technology, Faculty of Science and Technology, University of Twente, Enschede, The Netherlands;
[3] QVQ BV, Utrecht, The Netherlands;
[4] Department of Tissue Regeneration, MIRA Institute for Biomedical Technology and Technical Medicine, Faculty of Science and Technology, University of Twente, Enschede, The Netherlands.

Abstract

Autologous bone grafting, the golden standard in the repair of critical size bone defects still has its disadvantages, like scarcity of donor material and donor site morbidity. Engineered (bio) materials, consisting of a polymer scaffold combined with growth factors and cells, may prove to be a good substitute for donor bone grafts. The aim of this study was to create a functionalized polymer surface for capturing and concentrating the growth factor bone morphogenetic protein 6 (BMP6). The surface of UV-cross-linked methacrylate conjugated poly(trimethylene carbonate) (PTMC) was functionalized by grafting of engineered llama-derived antibody fragments (VHH) directed against BMP6. Covalent coupling was achieved by a Michael type reaction between an unpaired cysteine introduced at the C-terminal of the VHH and uncrosslinked methacrylate conjugated PTMC. VHH were found to cover 25% to 50% of the PTMC surface and were biologically active. They were able to bind BMP6, which in turn stimulated early osteogenic differentiation of C2C12 cells cultivated on functionalized PTMC, as revealed by an increase in alkaline phosphatase (ALP) production. In conclusion, in this study a novel indirect approach for the immobilization of growth factors on a scaffold surface is presented which optimally preserves growth factor bioactivity. This approach can be used for the generation of bioactive implantable bone substitute grafts.

Keywords: Crosslinking, PTMC, VHH, BMP6, Bioactive

Introduction

The regeneration of tissue is a complex process, which depends on physical and chemical interactions and reactions well synchronized in space and time [1]. Many tissue regeneration strategies rely on growth factor delivery systems. The dose, location and duration of growth factor delivery can be controlled by polymeric delivery systems, which can be incorporated in scaffold design [1, 2]. Bone morphogenetic proteins (BMPs) are members of the transforming growth factor-β (TGF-β) super family, and play an important role in tissue regeneration [3]. BMP6 is an example that is involved in cartilage and bone formation [3-5].

Functionalization of biomaterials with bioactive molecules, such as growth factors, is a strategy to obtain biomimetic materials. Growth factors are coupled to biomaterials either by physical adsorption or chemical immobilization [6-8]. Grafting of proteins to biomaterials surface can be achieved by several strategies. Michael addition was recently proposed as an efficient method for attaching biological active molecules to biomaterials, involving conjugation of thiol functional groups with (metha)acrylate groups [9-11]. Immobilization of growth factors onto surfaces is recognized to be more efficient than soluble growth factors [12, 13] and extend the half-life of the biomolecule and prevent its metabolism [14]. However, direct coupling of growth factors via linkers entails some limitations. For example, the binding of the linker to the growth factor is not targeted resulting in random presentation of the growth factors at the material surface. Furthermore, covalent coupling is often associated with significant loss of growth factor's bioactivity [6]. Here we propose an alternative strategy for growth factor immobilization at the biomaterial surface, which circumvents these drawbacks, i.e. the indirect coupling of a growth factor to the biomaterial surface via an intermediate engineered protein of which the coupling to the biomaterial surface is controlled. Antibodies can play an essential role as carriers of growth factors. However, conventional antibodies are complex molecules with limitations such as their large size and high production costs. Moreover, conventional antibodies are usually randomly immobilized onto surfaces resulting in their occasional inactivation. A reversible and directional immobilization of growth factors on a surface can be achieved by means of llama-derived antibody fragments (VHH). VHH are small antibodies capable of binding to an epitope with high specificity and affinity. They are easy to clone, engineer and produce. Furthermore, VHH are highly stable and soluble and, in contrast to conventional antibodies and growth factors, are heat stable and resistant to a variety of mild organic solvents [15, 16]. VHH can be engineered for directed immobilization to surfaces by introducing functional groups at the C-terminus. VHH have been selected to specifically bind to BMP6 (chapter 2 of this thesis) with different binding affinities, which is paramount for a tunable release of growth factors.

Poly(trimethylene carbonate) (PTMC) is a biomaterial widely used in bone tissue regeneration strategies for its physical, mechanical and chemical properties. PTMC is a rubbery and amorphous polymer. PTMC is biocompatible and its biodegradation is well

studied [17, 18]. PTMC can be functionalized by photo-sensitive groups, such as (metha)acrylate groups, in order to create a network under ultraviolet (UV) radiation [18]. The properties of the material can be tailored by using different average molecular weight of the polymers and/or crosslinking time. The remaining unreacted groups can be used afterwards to covalently graft biomolecules, such as VHH, by a Michael-type addition reaction [19].
In this work we present a novel approach to functionalize PTMC polymer with engineered VHH for directional and reversible tethering of BMP6 onto the surface. BMP6 can be subsequently released to trigger biological responses in neighboring cells. This technology has great potential and can be adapted for the immobilization of a wide variety of growth factors and other bioactive molecules.

Materials and methods

Synthesis of PTMC macromers
Three-armed poly(trimethylene carbonate) (PTMC) macromers were synthesized by ring opening polymerization of trimethylene carbonate (TMC) (0.49 mol, FORUSORB, China) using trimethylolpropane (TMP) (0.016 mol, Fluka – Sigma Aldrich, Germany) as an initiator and 0.02% stannous octoate (Sn(Oct)2, Sigma Aldrich) as a catalyst (Figure 1) [20, 21]. The reaction was performed under argon atmosphere at 130°C for three days. The molecular weight of the polymer was controlled by adjusting the TMP to TMC ratio [18].
The PTMC oligomers were functionalized with methacrylic anhydride (Sigma Aldrich) by dissolution in dichloromethane (DCM) (Biosolve) and addition of an excess of 2.5 equivalent of methacrylic anhydride (0.0735 mol) and triethylamine (TEA) (0.0735 mol) (Sigma Aldrich). In order to avoid premature crosslinking 0.1% hydroquinone (Sigma Aldrich) was used. The reaction was left stirring for 5-7 days at room temperature [21].
The macromers were purified by precipitation in cold methanol and subsequently dried under vacuum for several days.

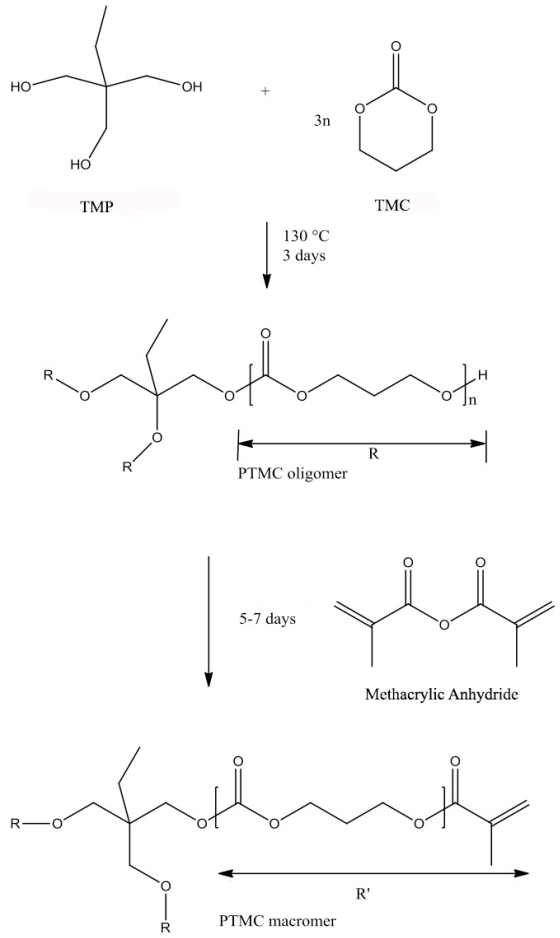

Figure 1. Synthesis of poly(trimethylene carbonate) (PTMC) macromers.

Preparation of PTMC network films

PTMC network films were prepared by solvent casting as described previously [22, 23]. PTMC macromers were mixed with 1% IGRACURE 2959 (CIBA) dissolved in 0.5 ml DCM. The mixture was casted on a silicon wafer, creating PTMC network films with a thickness of 300 μm. After drying the films under vacuum overnight, the films were crosslinked in a UV-crosslinker (I=3.8 mW/cm2) at 365 nm for 30 seconds (PTMC30) or 90 seconds (PTMC90) under a constant nitrogen flow. Discs with a diameter of 6 mm were punched out of the films for cell culture experiments and surface characterization.

^{1}H-NMR

Monomer conversions, molecular weights and degree of functionalization of the macromers were determined by ^{1}H-NMR spectroscopy (Varian Innova 300MHz, USA), using deuterated chloroform (CDCl3) as solvent (Merck Germany).

X-ray photoelectron spectroscopy

X-ray photoelectron spectroscopy (XPS) was performed to determine if and how much cysteine could bind to the PTMC surface. Measurements were performed on a Quantera SXM (scanning XPS microprobe) from Physical Electronics with an Al Kα monochromatic source at 1486.6 eV. Measurements were obtained at an auto Z-height of 24.65 mm and up, with the 100µ25W15keV X-ray beam at the standard beam-input and detector input angle of 45°. For this, Boc-Cys-OH (Sigma Aldrich) 5 mg/ml in milliQ water was grafted to PTMC surfaces that were cross-linked by UV radiation for 30s or 90s, for 2 hours at 37^{o}C in the dark. XPS of Boc-Cys-OH grafted surfaces were compared to equivalent none-grafted PTMC surfaces.

VHH characterization

VHH H1 targeting BMP6 was previously selected from an immunized llama repertoire by phage display as described elsewhere (chapter 2 of this thesis). DNA sequence of VHH H1 was cloned in the expression vector pMEK219 containing C-terminal Myc and His tag (VHH H1) and vector pQVQ61 containing a C-terminal cysteine, and FLAG and His tag (VHH H1-CYS). Both VHH proteins were produced in *E. coli* TG1 and purified from the periplasmic fraction via the C-terminal His-tag by cobalt affinity chromatography (TALON His-Tag Purification Resin, ClonTech). Purified VHH were analyzed by means of sodium dodecyl sulfate polyacrylamide gel electrophoresis (SDS-PAGE). The final VHH concentration was determined by UV absorption at 280 nm (NanoDrop 1000 Spectrophotometer, Thermo Scientific) and the theoretical mass extinction coefficient. VHH H1-CYS was modeled using the online program I-TASSER for protein modeling [24-26].

Grafting of VHH to PTMC films

To study the grafting of VHH to the uncrosslinked methacrylate groups in the PTMC network surface via Michael addition, VHH H1 and VHH H1-CYS were fluorescently labeled with Alexa Fluor 647 according to manufacturer's protocol (Life Technologies) before grafting to PTMC (Figure 2). With the assumption that on the PTMC surface there were enough reactive methacrylate groups available to cover the whole surface with VHH, it was calculated that 7.6×10^{-12} mol (~1.14×10^{-7} g) VHH (assuming a spheroid of 4.4 x 2.8 nm) were needed to cover a disc of 6 mm in diameter [27, 28]. VHH (0.2 µg) were added to PTMC networks discs in an excess of 2, relative to the amount of VHH that fit according to the calculation (7.6 pmol). VHH H1 and VHH H1-CYS were diluted in phosphate buffered saline (PBS, Dulbecco's PBS, PAA Laboratories, Austria) and a 50 µl droplet was added on the 6 mm diameter discs in a 96-wells plate. VHH were left

to react with PTMC surfaces for two hours at 37°C in the dark and thoroughly washed with PBS thereafter.

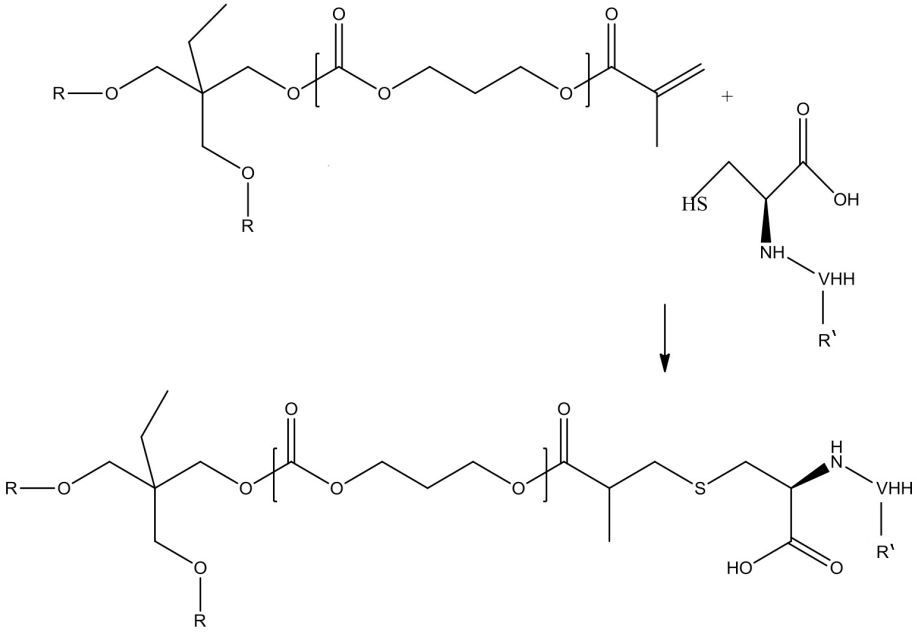

Figure 2. Michael addition of a VHH via C-terminal cysteine to functionalized PTMC. The thiol group from the VHH cysteine genetically introduced at the C-terminal of the VHH interacts with available methacrylate groups on the PTMC film.

Contact angle measurements

Contact angle measurements were performed to observe the effect of VHH grafting to PTMC surfaces on surface hydrophilicity. Measurements were performed using a DataPhysics OCA - Series device. Milli-Q droplets of 10 µl were put on the surface; subsequently the volume of the droplet was slowly increased to 30 µl and decreased again to 10 µl. Advancing and receding contact angle and droplet diameter were measured. Triplicates of samples crosslinked for 30s or 90s either non-grafted or grafted with VHH H1-CYS were measured.

BMP6 immobilization onto PTMC-VHH films

After grafting of VHH to PTMC films, a 2 µg/ml BMP6 (rhBMP6 R&D systems, catalog number 507-BP) in PBS solution, or 1% bovine serum albumin (BSA lyophilized powder, Sigma Aldrich) in PBS solution, was added in droplets of 50 µl to the 6 mm diameter discs, and allowed to bind for two hours at 37°C. Unbound BMP6 were washed off with PBS.

Detection of BMP6 on PTMC surfaces by immunofluorescence

Immunofluorescence was used to detect binding of BMP6 on VHH functionalized PTMC surfaces. PTMC90 discs of 6 mm diameter were placed into enzyme-linked immunosorbent assay (ELISA) plate wells (R&D systems). After blocking of the wells with 1% BSA in PBS, BMP6 (2 μg/ml) in 1% BSA was added to the wells and incubated for 1 hour. The wells were washed with PBS Tween (PBS containing 0.5% (v/v) Tween-20, PBST) and PBS. Bound BMP6 was detected by incubation with a mouse anti-BMP6 (4 μg/ml) and a fluorescent goat anti mouse (Alexa 488) (5μg/ml) antibody. Fluorescence was measured using VICTOR3 1420 Multilabel counter (Perkinelmer), CW filter F485, emission filter D520/10 M.

BMP6 release from PTMC surfaces

To determine the amount of BMP6 released in time from the VHH H1-CYS functionalized PTMC90 surface, an ELISA assay was performed using a human BMP6 ELISA kit (SIGMA-ALDRICH). Quantification of released BMP6 was performed according to manufacturer's protocol. Standard curve was made in duplicate using a concentration range of BMP6 from 0.262 - 1000 ng/ml (R&D Systems). PTMC90 discs functionalized with VHH H1-CYS and raw PTMC90 (non-functionalized with VHH) were incubated with BMP6. PBS was added to the wells to serve as a diffusion medium. The supernatant was collected at different time points for 7 days and added to the ELISA plate and incubated overnight at 4°C. After washing the wells with PBST, biotinylated human BMP6 detection antibody, HRP-Streptavidin solution and ELISA colorimetric TMB reagent were added with washing steps in between. Incubation times were respectively 1 hour, 45 and 30 minutes. Finally ELISA Stop Solution was added and absorbance was measured at 450 nm using Multiscan 60 (Thermo Scientific).

Biological activity of BMP6 on PTMC surfaces

To assess the biological activity of the BMP6 immobilized on the PTMC90 surfaces an osteogenic differentiation assay was used. C2C12 cells were cultured in DMEM (Dulbecco's modified eagle medium; Gibco) supplemented with 4.5 g/L glucose and L-glutamine, 10% (v/v) of fetal bovine serum (FBS) and 1% (v/v) penicillin-streptomycin under humidified conditions at 37°C and in an atmosphere of 5% CO2. Cells were seeded at 10 000 cells/cm^2 onto PTMC90 discs grafted with VHH H1-CYS and incubated with BMP6 (PTMC90-VHH+BMP6), and non-VHH conjugated PTMC90 discs incubated with (PTMC90+BMP6) or without BMP6 (PTMC90) and cultured for 4 days. Cells were washed with PBS and lysed with lysis buffer (10X diluted alkaline phosphatase activity (ALP) assay buffer with 0.1% Triton X-100) and frozen. To evaluate ALP activity, 6 mM p-nitrophenyl phosphate (PNPP) substrate solution was added to cell lysate and changes in absorbance over time were measured at 405 nm using TECAN Infinite M200 PRO microplate reader at room temperature. The absorbance was corrected for DNA content. DNA concentration was determined via proliferation assay according to manufacturer's protocol (CyQuant Cell Proliferation Assay Kit; Invitrogen).

Statistical analysis

Statistical analyses were performed using GraphPad Prism version 5.00 for Windows, GraphPad Software (San Diego, California). Analyses were based on one-way ANOVA and a Tukey's Post-hoc test among all samples or between samples and controls. $p < 0.05$ was considered as statistically significant.

Results

Synthesis and characterization of PTMC macromers

The first step of the synthesis of PTMC consists of a ring-opening polymerization of TMC, using TMP as initiator to obtain three armed oligomers and stannous octoate as catalyst. Monomer conversion was calculated using ^{1}H-NMR spectroscopy (89% – 99%) (Figure 3). The average molecular weight (Mn) was determined by ^{1}H-NMR and was around 3000 g/mol by comparing peak integrals of repeating CH2-groups from PTMC at 4.25 ppm and 2.06 ppm (Figure 3A, peaks a and b respectively) with peak integral of the CH3-group of TMP at 0.91 ppm (Figure 3A, peak g). PTMC oligomers were functionalized by methacrylic anhydride in the presence of TEA and hydroquinone. The methacrylate groups can be observed at 6.04 ppm (CH), 5.50 ppm (CH) and 1.88 ppm (CH3) (Figure 3B, peaks f, e and d respectively). The degree of functionalization was determined using the integral peak values of CH-groups at 6.04 ppm and/or 5.50 ppm (Figure 3B, peaks f and/or e) with peak integral of CH3-group of TMP at 0.91 ppm (Figure 3B, peak g) and could be calculated to be around 70 %. PTMC networks were obtained by solvent casting of a mixture of PTMC macromers with Irgacure 2959 as initiator in small amount of DCM. After drying, the films were crosslinked under ultraviolet (UV) light (365 nm) for 30 or 90 seconds resulting in PTMC30 and PTMC90, respectively.

Unreacted methacrylates remain available for Michael type addition reactions

We next determined whether unreacted methacrylate groups after photo curing of the PTMC films remain available for subsequent chemical modification, photocured PTMC films were first incubated with the amino acid cysteine (Boc-Cys-OH). To determine the efficiency of the cysteine grafting, an XPS measurement was performed. Successful Michael addition should result in the stable presence of sulfur elements on the PTMC surface. XPS measurements confirmed the presence of sulfur elements on PTMC surfaces incubated with Boc-Cys-OH (Figure 4). The percentage of sulfur elements found on PTMC crosslinked for 30 seconds (PTMC30) did not differ significantly from the percentage of sulfur elements on the surface of PTMC crosslinked for 90 seconds (PTMC90). Apparently, the increase in UV crosslinking time from PTMC30 and PTMC90 did not led to marked reduction in reactive methacrylate groups available at the surface of PTMC. On theoretical grounds, it is calculated that full coverage of the PTMC surface (100%) with cysteine results in the presence of 1 to 2% cysteine relative to

PTMC. However only 0.5% of sulfur elements were measured, which indicated that only 25 to 50% of cysteine could be grafted to the PTMC surface.

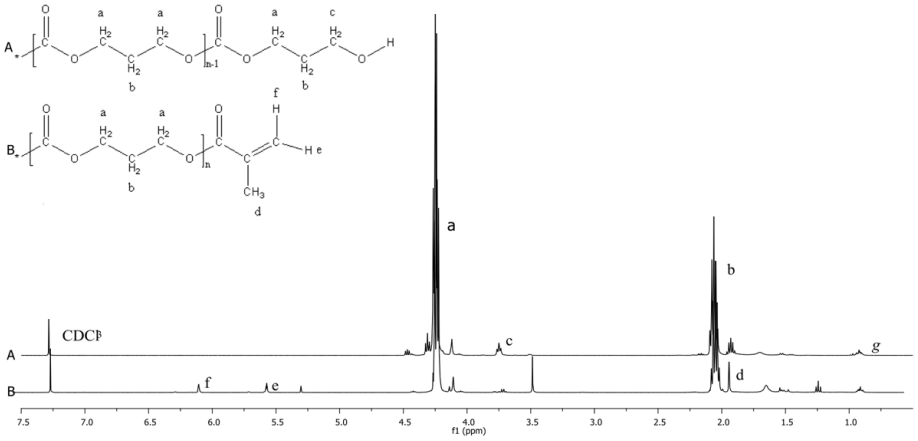

Figure 3. 1H-NMR spectra of PTMC oligomers (A) and macromers (B).

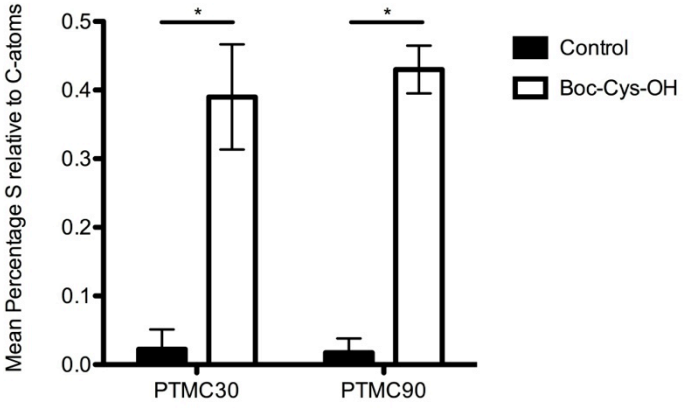

Figure 4. Cysteine grafted onto PTMC surfaces. Percentage of sulfur element relative to C-atoms on PTMC surfaces crosslinked for 30 and 90 seconds (PTMC30 and PTMC90 respectively) without external cysteine addition (Control) and grafted with Boc-Cys-OH molecules (Boc-Cys-OH), measured by XPS. Data represent the mean +/- SD of 4 independent experiments. *p< 0.05.

VHH modeling and cysteine accessibility for Michael reaction

In order to assess the accessibility of the cysteine introduced at the C-terminal of the VHH in a Michael-type addition reaction, modeling of the VHH H1-CYS was performed using the online program I-TASSER [24-26]. The predicted structure (Figure 5) showed an Ig fold with an elongated C-terminal, containing the cysteine residue with exposed SH-group. This predicted that the C-terminal cysteine was accessible for a Michael-type addition reaction.

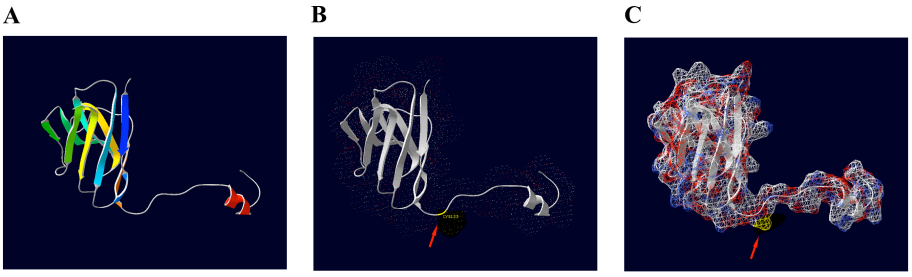

Figure 5. Structural model of VHH H1-CYS. (A) The protein chain is represented by ribbons and colored with rainbow spectrum from N-terminal (blue) to C-terminal (red). (B) Location of cysteine residue 123 (highlighted with red arrow) genetically incorporated at the C-terminal of the VHH for directed chemical reactions. (C) Surface prediction of VHH where sulfur surface is colored yellow.

VHH grafted to PTMC surfaces via C-terminal cysteine

To investigate if the grafting of VHH to PTMC surfaces occurs via the cysteine residue introduced at the C-*terminal*, VHH H1 and VHH H1-CYS were fluorescently labeled and left to react to PTMC surfaces. With the assumption that on the PTMC surface there were enough reactive methacrylate groups available to cover the whole surface with VHH, it was calculated that 7.6×10^{-12} mol (~1.14×10^{-7} g) VHH (assuming a spheroid of 4.4 x 2.8 nm) were needed to cover a disc of 6 mm in diameter [27, 28]. After reaction completion and washing unbound VHH, about 2-fold higher relative fluorescence was measured in the VHH H1-CYS condition compared to VHH H1, indicating that significantly more VHH H1-CYS was grafted to the PTMC surface than VHH H1 (Figure 6).

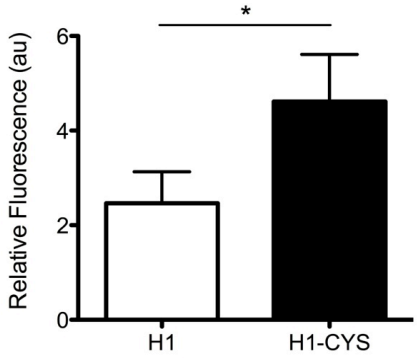

Figure 6. VHH binds to PTMC via cysteine at C-terminal. VHH H1 (devoid of cysteine at the C-terminal) and VHH H1-CYS (equipped with a cysteine at the C-terminal) fluorescently labeled with Alexa Fluor 488 were grafted onto PTMC surfaces via Michael reaction. Fluorescence is proportional to the amount of VHH grafted onto the PTMC surface. The fluorescence is expressed relative to control surface (PTMC90). Data represent the mean +/- SD of 15 independent experiments. *p < 0.05.

Contact angle of PTMC surfaces grafted with VHH

Water contact angle measurements were performed on PTMC surfaces grafted with VHH. VHH are hydrophilic proteins [29] and therefore the presence of VHH onto the PTMC surface is expected to alter the contact angle measurements. Advancing and receding contact angle measurements were performed for PTMC30 and PTMC90 grafted with or without VHH H1-CYS (Table 1). Both advancing and receding contact angle values were lower on surfaces grafted with VHH. This effect was measured both at PTMC30 and PTMC90. The contact angle measurements of PTMC30 grafted with VHH were lower than those of PTMC90. This is in agreement with the reported increase in contact angle measurements in relation to photo-crosslinking time [30]. Furthermore, hysteresis, which is the difference between the advancing and receding contact angle and a measurement for chemical heterogeneity or surface roughness [31], was found to increase on both PTMC surfaces when they were grafted with VHH. These findings indicated that the PTMC surface was grafted with VHH.

Table 1. Water contact angle measurements of PTMC surfaces crosslinked for 30 or 90 seconds with or without VHH H1-CYS grafted on the surface. * p< 0.05.

	Contact angle (°)		
Polymer surface	Advancing	Receding	Hysteresis [#]
PTMC 30	70,85 ± 1,12	33,90 ± 0,70	37.31
PTMC 30-VHH	68,61 ± 1,55	28,00 ± 1,79	49.31
PTMC 90*	87,77 ± 1,04	53,04 ± 0,69	35.84
PTMC 90-VHH*	81,97 ± 2,26	37,57 ± 1,53	49.12

[#] Difference between advancing and receding contact angle.

BMP6 binds to VHH grafted to PTMC90 surface

Immunofluorescence was performed to determine if BMP6 could bind to VHH grafted onto PTMC surfaces. The fluorescence measured in wells containing BMP6 on PTMC90 functionalized with VHH H1-CYS was higher compared to wells containing BMP6 on PTMC90 alone (Figure 7). This result demonstrated that the VHH remained functional after grafting at a PTMC90 surface. The fluorescence measured in wells with PTMC90 only and wells with BMP6 on PTMC90 showed the same value, indicating that the measured fluorescence was independent of the presence of BMP6 and represented non-specific association of the detecting antibodies with PTMC90. Surprisingly, nonspecific binding of the antibodies was markedly reduced in PTMC grafted with VHH, suggesting that covering of the PTMC surface with VHH blocked nonspecific binding sites.

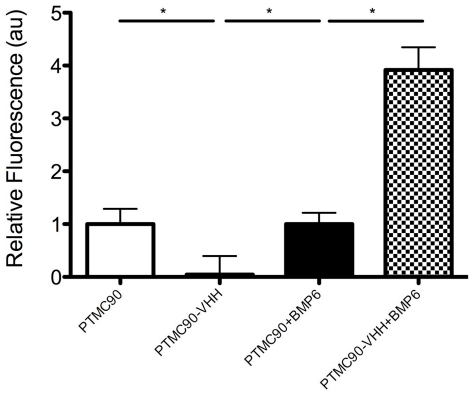

Figure 7. BMP6 binds to functionalized PTMC90 surface. Detection of BMP6 onto PTMC90 surfaces grafted with VHH by fluorescence. PTMC90 and PTMC90-VHH grafted films were incubated in wells in the presence or absence of BMP6. After several washes, bound BMP6 was detected with mouse anti-BMP6 and goat anti-mouse coupled to a fluorescent dye 488. The fluorescence is proportional to the amount of bound BMP6. The fluorescence is expressed relative to control surface (PTMC90). Fluorescence is expressed relative to control. Data represent the mean +/- SD of 3 independent experiments. * p< 0.05.

BMP6 release from PTMC90-VHH surfaces

To assess the release of BMP6 from PTMC90 surfaces functionalized with anti-BMP6 VHH H1-CYS, PTMC90-VHH discs pre-incubated with BMP6 were placed in PBS at 37°C for 7 days. The release of BMP6 was compared to discs of non-functionalized PTMC90 pre-incubated with the same amount of BMP6. The amount of BMP6 released from the surfaces was determined by an ELISA assay. Within the first 24 hours a burst release was observed, which was more pronounced for the non-functionalized PTMC surface (Figure 8). After this initial period, a linear release in time was observed until a plateau was reached after 7 days.

BMP6 released from VHH grafted surfaces appeared to have a more sustained release profile than the BMP6 released from non-functionalized surfaces and therefore a longer release of BMP6 was expected.

Total theoretical coverage of the surface with BMP6 would allow an amount of 360 ng/cm^2. The total amount of BMP6 released from the PTMC90-VHH surface was 54.4 ng/cm^2 (± 0.8) after 7 days while 66.1 ng/cm^2 (± 1.0) of BMP6 were released from the non-functionalized PTMC surface. Thus, it was estimated that 15% and 18% of BMP6 have been released from the surface PTMC90-VHH and PTMC90 respectively. A higher release of BMP6 was observed for the non-functionalized PTMC90 surface.

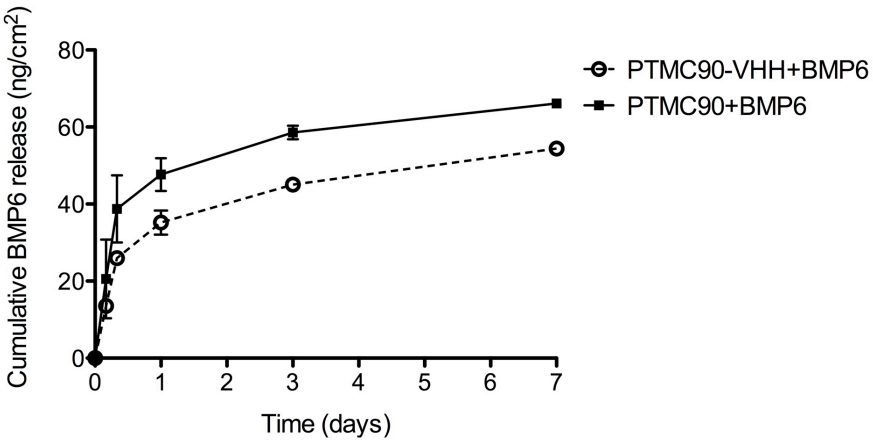

Figure 8. BMP6 release from PTMC90 surfaces. Quantification of BMP6 released from PTMC90-VHH+BMP6 (dashed line) or PTMC90+BMP6 (solid line) surfaces over a period of 7 days using an ELISA assay. Data represent the mean +/- SD of 3 independent experiments.

Bioactivity of immobilized BMP6

To evaluate the potential of concentrating BMP6 on a surface by means of VHH grafted to PTMC90 surfaces on differentiation of C2C12 cells, cells were cultured in osteogenic conditions for 4 days in the presence of BMP6 and PTMC90-VHH or PTMC90 discs. In C2C12 cells, ALP activity was induced by the presence of BMP6 by 8 fold and 17 fold

for PTMC90+BMP6 and PTMC90-VHH+BMP6 respectively (Figure 9). Since the same concentration of BMP6 was added to the wells in both systems, it can be concluded that anti-BMP6 VHH potentiated the bioactivity of BMP6 by at least 2-fold.

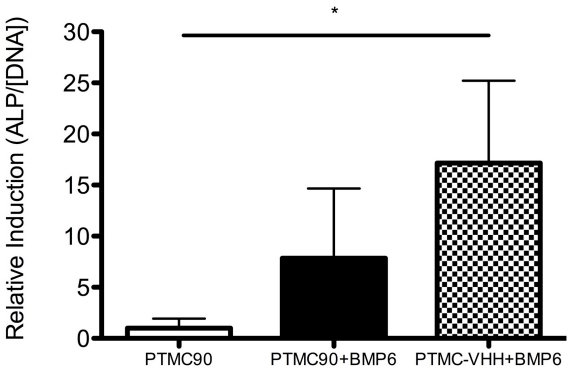

Figure 9. BMP6 concentrated on PTMC surface stimulates osteoblast differentiation. Assessment of biological activity of BMP6 in C2C12 cells. Addition of BMP6 on PTMC90 or PTMC90-VHH surfaces stimulated alkaline phosphatase (ALP) activity. Furthermore, the induction of ALP is further induced by BMP6 immobilized on functionalized PTMC surface. ALP activity is normalized by the total DNA content of C2C12 cells after 4 days of culture, and expressed as relative induction with respect to control (PTMC90). Data represent the mean +/- SD of 3 independent experiments. * $p < 0.05$.

Discussion

In this study a novel manner of presenting growth factors for tissue engineering is described using PTMC as a scaffolding material. We demonstrated that the synthesis of PTMC macromers functionalized with methacrylated end groups led successfully to a stable network after UV irradiation while free unsaturated bonds remained available for a subsequent Michael type addition reaction. The number of unsaturated methacrylate groups present on UV crosslinked PTMC can be modified by the time of UV-irradiation. The water contact angle of PTMC crosslinked for 30 seconds was significantly lower than the water contact angle of PTMC crosslinked for 90 seconds suggesting the presence of greater numbers of unsaturated methacrylated groups. However, to have a reproducible and reliable system it is essential that a proper PTMC network is created. For optimization of this system the minimal crosslink time and intensity of UV-light must be determined in order to obtain appropriate mechanical stability of the network while sufficient unsaturated bonds remain available for subsequent chemical reactions. Therefore, it was decided to continue experiments with PTMC discs that were crosslinked for 90 seconds.

Using the small molecule Boc-Cys-OH we next proved that the unsaturated bonds remained available for a Michael type addition reaction. Subsequently, VHH H1 was

engineered with an unpaired cysteine residue at the C-terminal. Modeling indicated that this cysteine was exposed and suitable for coupling *via* the thiol functional group. Importantly, the presence of this cysteine residue in the C-terminus of the VHH did not interfere with the structure of the Complementary Determining Regions of the VHH and was therefore not expected to alter with antigen binding. We demonstrated that modified VHH H1 with cysteine could be grafted to the PTMC surfaces. The grafting of VHH to PTMC surfaces was mainly achieved *via* the C-terminal cysteine of the VHH, however non-directed reactions with other functional groups such as hydroxyl or amine groups should not be discarded. In combination protein adsorption of PTMC, this explained the relative high background binding of VHH H1 lacking the C-terminal cysteine. Further effort should be devoted to determine the exact amount of VHH bound to PTMC surfaces and the nature of the bonds through which this is achieved.

The grafting efficiency of VHH onto PTMC surfaces depended on the methacrylate groups available on the surface and on the reaction conditions. The hydrophobicity of PTMC [32] did not facilitate the coupling of VHH and it can be hypothesized that the crosslinking takes place initially on the surface of the PTMC film and then in the core, thus the unsaturated free functions are embedded in the bulk of the material instead of accessible on the surface [33]. Through polymer mobility in the film, these unsaturated methacrylate groups may reposition to the surface. Michael-type reactions of thiols can take place in water at physiological temperature at near physiological pH [30, 34] and are reported to be rapid [11]. Therefore, in order to avoid any risk of denaturation of VHH, mild conditions were used for the grafting of VHH to the crosslinked PTMC surface. Interestingly, the results obtained in this research demonstrated the remarkable success of the grafting in PBS without any additive. The percentage of thiol groups, which are in the reactive ionized thiolate form, is determined by the pH. Therefore it is suggested that the Michael reaction should be performed in an alkaline environment to increase the amount of VHH grafted on the surface [11, 33]. Judged by analysis on a non-reducing SDS-PAGE of the VHH sample, less than 50% of the VHH was in a dimer form (not shown), leaving the remaining monomeric VHH ready to react with PTMC. More reactive SH groups from the VHH can be liberated using reducing agents, i.e. by pretreatment with tris (2-carboxyethyl) phosphine **(**TCEP) or dithiothreitol DTT prior to the Michael type addition reaction. However, reduction of internal disulfide bonds may prove detrimental to function and stability of the grafted VHH but VHH are well known for their efficient refolding in their native structure upon denaturation [35].

VHH grafted onto crosslinked PTMC surfaces were selected by phage display for specific binding to BMP6, which is a relevant molecule for skeletal tissue engineering. The oriented grafting of the VHH via the cysteine presents the VHH binding site to the outwards. Thus, the antigen binding site is not affected and is expected to be available to bind, capture and concentrate functional BMP6. The quantification of grafted VHH is crucial to determine the expected amount of BMP6 captured on the surface.

The release of BMP6 achieved from functionalized PTMC90 surfaces with VHH was sustained over the course of the experiment after an initial burst release. The cumulative

release of BMP6 was always lower in functionalized PTMC, compared to non-functionalized PTMC. Release of BMP6 from non-functionalized PTMC90 surface suggests that BMP6 can adsorb to PTMC surfaces non-specifically; without the need for a bridging VHH. Nevertheless, BMP6 captured on PTMC surfaces through the VHH was found to be at least 2-fold more active in stimulation of ALP, compared to BMP6 directly adsorbed to PTMC. More extended experiment should have been addressed in order to obtain later time points and the complete release profile of the BMP6.

Kinetics are crucial for the design of a controlled release of growth factors from a scaffold. In skeletal tissue regeneration different developmental phases are defined and therefore a time and space-restricted expression of growth factors is essential for successful tissue engineering [7]. The affinity of the VHH to growth factors is a feature to take into account while designing a VHH grafted scaffold. Low affinity of VHH to a growth factor will result in a faster release when compared with a VHH with high affinity for the same growth factor. The versatility of VHH allow for the selection of VHH with different affinities for a specific antigen. Additionally, VHH can be selected targeting different antigens. Therefore, an array of VHH targeting different growths factors, relevant in different phases of tissue repair, could be grafted on the surface of a biomaterial to orchestrate spatiotemporal release and further improve tissue repair.

BMP6 stimulation can be detected by ALP activity, an early marker for osteogenic differentiation. The BMP6 immobilized on the crosslinked PTMC surfaces grafted with VHH were still bioactive and cells responded to this *stimuli*. By coupling of a VHH directed against BMP6 to PTMC surface through the engineered cysteine residue at the C-terminal by Michael reaction, we could demonstrate that C2C12 differentiation directed by BMP6 was increased at least 2-fold when compared with PTMC without VHH. It can be hypothesized that BMP6 was stabilized in the presence of the VHH. The results presented here suggested that there was a concentration effect on cell differentiation. These results are in line with the findings reported elsewhere (chapter 3 of this thesis), where the supramolecular assembly of VHH, via a His-tag at the C-terminus of the VHH on a molecular printboard, lead to the functional delivery of BMP6 and bioresponsive osteogenic differentiation.

The immobilization of growth factors provides a different environment to cells compared to cells cultured in medium supplemented with soluble growth factors [12]. A step further is to translate the present platform into a 3D system. Indeed PTMC has been successfully used in rapid prototyping strategies to build complex 3D scaffolds [36]. Since the surface modification employed in this study is water based, it will be relatively easy to adapt the strategy developed for covalent crosslinking of VHH to 2D films to functionalization of 3D structures.

This novel approach presents an opportunity to manipulate cell signaling by controlling growth factor's spatiotemporal release indirectly.

Conclusions

In this research it has been shown that VHH are a potent tool to immobilize growth factors onto surfaces and deliver active growth factors to the environment in a sustained manner. The VHH were successfully grafted onto crosslinked PTCM surfaces by Michael addition. This novel approach can further be improved by the incorporation of multiple VHH targeting an assortment of growth factors relevant in tissue repair. The creation of a biocompatible, biodegradable and bioactive scaffold with orchestrated delivery of multi growth factors in space and time is a must for tissue regeneration.

References

1. Shin, H., S. Jo, and A.G. Mikos, *Biomimetic materials for tissue engineering.* Biomaterials, 2003. **24**(24): p. 4353-64.
2. Naderi, H., M.M. Matin, and A.R. Bahrami, *Review paper: Critical Issues in Tissue Engineering: Biomaterials, Cell Sources, Angiogenesis, and Drug Delivery Systems.* Journal of Biomaterials Applications, 2011. **26**(4): p. 383-417.
3. Bessa, P.C., M. Casal, and R.L. Reis, *Bone morphogenetic proteins in tissue engineering: the road from the laboratory to the clinic, part I (basic concepts).* Journal of tissue engineering and regenerative medicine, 2008. **2**(1): p. 1-13.
4. Grimsrud, C.D., et al., *BMP-6 is an autocrine stimulator of chondrocyte differentiation.* Journal of Bone and Mineral Research, 1999. **14**(4): p. 475-482.
5. Kronenberg, H.M., *Developmental regulation of the growth plate.* Nature, 2003. **423**(6937): p. 332-336.
6. Lee, K., E.A. Silva, and D.J. Mooney, *Growth factor delivery-based tissue engineering: general approaches and a review of recent developments.* Journal of the Royal Society, Interface / the Royal Society, 2011. **8**(55): p. 153-70.
7. Luginbuehl, V., et al., *Localized delivery of growth factors for bone repair.* European Journal of Pharmaceutics and Biopharmaceutics, 2004. **58**(2): p. 197-208.
8. Alberti, K., et al., *Functional immobilization of signaling proteins enables control of stem cell fate.* Nature Methods, 2008. **5**(7): p. 645-650.
9. Lutolf, M.P., et al., *Systematic modulation of Michael-type reactivity of thiols through the use of charged amino acids.* Bioconjugate Chemistry, 2001. **12**(6): p. 1051-1056.
10. Heggli, M., et al., *Michael-type addition as a tool for surface functionalization.* Bioconjugate Chemistry, 2003. **14**(5): p. 967-973.
11. Elbert, D.L. and J.A. Hubbell, *Conjugate addition reactions combined with free-radical cross-linking for the design of materials for tissue engineering.* Biomacromolecules, 2001. **2**(2): p. 430-441.
12. Ito, Y., *Covalently immobilized biosignal molecule materials for tissue engineering.* Soft Matter, 2007. **4**(1): p. 46-56.
13. Karageorgiou, V., et al., *Bone morphogenetic protein-2 decorated silk fibroin films induce osteogenic differentiation of human bone marrow stromal cells.* Journal of Biomedical Materials Research Part A, 2004. **71A**(3): p. 528-537.
14. Goddard, J.M. and J.H. Hotchkiss, *Polymer surface modification for the attachment of bioactive compounds.* Progress in Polymer Science, 2007. **32**(7): p. 698-725.
15. Dolk, E., et al., *Induced refolding of a temperature denatured llama heavy-chain antibody fragment by its antigen.* Proteins, 2005. **59**(3): p. 555-64.
16. van der Linden, R.H., et al., *Comparison of physical chemical properties of llama VHH antibody fragments and mouse monoclonal antibodies.* Biochimica et biophysica acta, 1999. **1431**(1): p. 37-46.
17. Zhang, Z., et al., *The in vivo and in vitro degradation behavior of poly(trimethylene carbonate).* Biomaterials, 2006. **27**(9): p. 1741-1748.
18. Schuller-Ravoor, S., *Advanced microstructures based on poly(trimethylene carbonate): Microfabrication & Stereolithography*, in *Polymer chemistry and biomaterials* 2011, University of Twente.
19. Masters, K.S., *Covalent Growth Factor Immobilization Strategies for Tissue Repair and Regeneration.* Macromolecular Bioscience, 2011. **11**(9): p. 1149-1163.

20. Song, Y., et al., *Flexible and elastic porous poly(trimethylene carbonate) structures for use in vascular tissue engineering.* Acta Biomaterialia, 2010. **6**(4): p. 1269-1277.
21. Schuller-Ravoo, S., J. Feijen, and D.W. Grijpma, *Flexible, elastic and tear-resistant networks prepared by photo-crosslinking poly(trimethylene carbonate) macromers.* Acta Biomaterialia, 2012. **8**(10): p. 3576-3585.
22. Yang, J.Y., et al., *Preparation and characterization of poly(L-lactide)-co-poly(trimethylene carbonate)/talc film.* International Journal of Biological Macromolecules, 2013. **62**: p. 411-417.
23. Papenburg, B.J., et al., *One-step fabrication of porous micropatterned scaffolds to control cell behavior.* Biomaterials, 2007. **28**(11): p. 1998-2009.
24. Zhang, Y., *I-TASSER server for protein 3D structure prediction.* BMC bioinformatics, 2008. **9**: p. 40.
25. Roy, A., A. Kucukural, and Y. Zhang, *I-TASSER: a unified platform for automated protein structure and function prediction.* Nature protocols, 2010. **5**(4): p. 725-38.
26. Roy, A., J. Yang, and Y. Zhang, *COFACTOR: an accurate comparative algorithm for structure-based protein function annotation.* Nucleic acids research, 2012. **40**(Web Server issue): p. W471-7.
27. Cabanas Danés, J., *Reversibly tethering growth factors to surfaces: guiding cell function at the cell-material interface*, 2013, Universiteit Twente.
28. Cortez-Retamozo, V., et al., *Efficient cancer therapy with a nanobody-based conjugate.* Cancer Research, 2004. **64**(8): p. 2853-2857.
29. Muyldermans, S., *Single domain camel antibodies: Current status.* Reviews in Molecular Biotechnology, 2001. **74**(4): p. 277-302.
30. Bat, E., et al., *Ultraviolet light crosslinking of poly(trimethylene carbonate) for elastomeric tissue engineering scaffolds.* Biomaterials, 2010. **31**(33): p. 8696-8705.
31. Berg, J.C., *An Introduction to Interfaces and Colloids*2010: World Scientific Publishing Company, Incorporated.
32. Wang, H., J.H. Dong, and K.Y. Qui, *Studies on properties and drug delivery systems of PTMC-b-PEG-b-PTMC block copolymers (vol A35, pg 811, 1998).* Journal of Macromolecular Science-Pure and Applied Chemistry, 1998. **A35**(10): p. 1761-1761.
33. Nilsson, K., et al., *Addition of thiol-containing ligands to a surface-active michael acceptor.* Macromolecules, 2007. **40**(4): p. 901-908.
34. Wang, R., et al., *Unprecedented access to functional biodegradable polymers and coatings.* Macromolecules, 2011. **44**(15): p. 6009-6016.
35. Harmsen, M.M. and H.J. De Haard, *Properties, production, and applications of camelid single-domain antibody fragments.* Appl Microbiol Biotechnol, 2007. **77**(1): p. 13-22.
36. Peltola, S.M., et al., *A review of rapid prototyping techniques for tissue engineering purposes.* Annals of medicine, 2008. **40**(4): p. 268-80.

Chapter 6

Targeting bone with a single domain antibody binding hydroxyapatite

Emilie Dooms Rodrigues[1], Sabrina Oliveira[2], Ivo Que[3], Mohamed El Khattabi[4], Jasper van Weerd[1,5], Ellie Landman[1], Clemens van Blitterswijk[6], Clemens W.G.M. Löwik[3], Theo Verrips[4], Alan Chan[3,7] and Marcel Karperien[1]

[1] Department of Developmental BioEngineering, MIRA Institute for Biomedical Technology and Technical Medicine, Faculty of Science and Technology, University of Twente, Enschede, The Netherlands;
[2] Division Cell Biology, Department of Biology, Science Faculty, Utrecht University, Utrecht, The Netherlands;
[3] Department of Radiology, Leiden University Medical Centre, The Netherlands;
[4] QVQ BV, Utrecht, The Netherlands;
[5] Molecular Nanofabrication Group, MESA$^+$ Institute for Nanotechnology, Faculty of Science and Technology, University of Twente P.O. Box 217, 7500 AE, Enschede, Netherlands;
[6] Department of Tissue Regeneration, MIRA Institute for Biomedical Technology and Technical Medicine, Faculty of Science and Technology, University of Twente, Enschede, The Netherlands;
[7] Percuros B.V., Enschede, The Netherlands.

Abstract

The aim of the present work is to isolate single domain antibodies (VHH), the smallest naturally derived antigen binding fragments, that specifically bind to hydroxyapatite (HA). VHH were selected for binding to HA by phage display. VHH clone MA10 was isolated which bound specific and with high affinity to HA (Kd ~120 nM). *Ex vivo*, MA10 bound specifically to the primary ossification center of cultured metatarsals isolated from 17-day-old embryos. For *in vivo* evaluation, VHH MA10 and the negative control VHH J3 were conjugated to the near infrared fluorophore IRDye800CW. The labelling did not affect binding of MA10 to HA. MA10-IR was injected intravenously in nude mice and specifically accumulated in the mineralized skeleton. MA10-IR was still detectable in the skeleton up to 20 days post-injection, whereas VHH J3-IR was cleared from bone tissues in the course of a few days. These results demonstrate the potential of VHH for bone targeting and imaging.

Keywords: Hydroxyapatite, Biomimetic, Bone, VHH, Imaging

Introduction

There is a need for an agent that can specifically target to bone either for imaging purposes or for localized drug delivery. Currently, very potent bone targeting agents are available, i.e. bisphosphonates, anti-resorptive agents, that are used for treatment of metabolic bone diseases are conjugated to technecium and used for skeletal imaging to monitor bone turnover [4, 5]. Bisphosphonates have also been used for drug targeting e.g. by conjugating to liposomes and drugs but so far with limited success [6]. Bisphosphonates predominantly accumulate at sites of high bone turnover which limits their even distribution throughout the skeleton [7]. Hence there is a need for new agents that efficiently and evenly target to bone.

Molecular imaging of antigens *in vitro* and *in vivo* commonly relies on the use of antibodies [8]. Antibodies or antibody fragments are widely applied in drug targeting strategies due to their high specificity for antigens. However, the use of conventional antibodies comprises drawbacks such as their complexity and large size rendering inherent limitations for applications as imaging probes [9]. Part of these problems can be circumvented by the use of the variable heavy chain of heavy chain only antibody (VHH), the smallest naturally derived antigen binding fragments. Due to their small size VHH can easily penetrate in tissue, are easy to clone and to modify genetically. They consist of a single gene, are highly stable and soluble, and have close homology with human antibody fragments [9]. VHH can be produced in yeast where no toxins are produced and production costs are low [10]. Furthermore, VHH have been reported as promising tools in imaging of tumors and monitoring the efficacy of therapy [11-13]. The versatility of the VHH allows for tailored engineering of the molecule. They can be conjugated with near-infrared fluorescent dyes and distribute and diffuse efficiently through solid tumours with high specificity. This results in high tumor uptake as optical molecular imaging tracers [13].

In bone tissue regeneration, calcium phosphates based biomaterials are widely used as bone graft substitutes, mostly because their chemical composition resembles the bone mineral phase [14]. Among calcium phosphates, hydroxyapatite (HA), a naturally occurring structure in bone mineral, is a biocompatible ceramic widely used as a scaffold in bone tissue engineering to substitute bone grafts [15, 16]. Peptide phage display has already been used for the selection of peptides targeting HA [17]. Therefore we reasoned that by selecting VHH targeting HA by means of phage display we would select putative binders for bone tissue. As such, we selected and identified potential probes for optical bone imaging and / or drug targeting.

In this study, we demonstrate that it is feasible to select VHH binding to hydroxyapatite with high affinity. VHH MA10 showed binding to HA in a dose dependent manner with an apparent affinity of ~120 nM. We further show that this VHH targeting HA, when conjugated to the near infrared fluorophore IRDye800CW (IR) could be used for the non-invasive imaging of the mineralized skeleton *ex vivo* and in a mouse model.

Materials and methods

Selection of VHH targeting HA

VHH binders towards HA were selected from a non-immunized llama VHH phage library (kindely provided by BAC BV). The construction of the non-immune library has been described before [18]. A two round selection was performed on HA plates. Pure HA plates measuring approximately 1.5 x 1.5 mm, and 0.1 mm thickness were supplied by Plasma Biotal Limited, UK (Figure 1A). Phages (approximately 10^{12} colony forming units (cfu)), were incubated for 2 hours at room temperature with 3 HA plates in wells of 96-wells microtiter plate. After thorough washing with phosphate buffered saline containing 0.05% Tween-20 (PBST), bound phages were eluted by incubation in 100 mM triethylamine (TEA) for 15 minutes at room temperature. Subsequently, eluted phages were immediately neutralized by the addition of 1M Tris-HCl, pH 7.5. DNA information of the selected phages was rescued by infection of *Escherichia coli* TG1 strain and subsequent selection on agar plates for ampicillin resistance. To obtain recombinant bacteriophages expressing the VHH as fusion proteins with the bacteriophage gene III product, transformed *E. coli* TG1 were grown to logarithmic phase and then infected with helper phage VCSM13 (Stratagene, La Jolla, CA, USA). The phage particles were precipitated with polyethylene glycol (PEG) and used in the second round of panning selection on pure HA plates as described above. Single clones from the second round of selection that showed binding to HA were sequenced (Macrogen). The selection yielded one VHH, named MA10, which displays good binding properties. This VHH was characterized further in this study.

Production and purification of the VHH

E. coli strain TG1 was used for the maintenance of the plasmids, infection by the phages and expression of proteins. The plasmid pUR8100 contained the DNA information of the individually selected VHH as well as a Myc and His tags at the C-terminal used for detection and purification.

E. coli TG1 was grown in Luria Broth (LB) or Yeast extract and tryptone (YT) medium containing 2% (w/v) glucose and ampicillin (100 µg/ml). VHH were expressed by *E. coli* TG1 after addition of 1 mM Isopropyl β-D-1-thiogalactopyranoside (IPTG). VHH were produced for 4 hours at 37^{o}C [19, 20]. VHH proteins were purified from the periplasmic fraction via the C-terminal His-tag by cobalt affinity chromatography (TALON His-Tag Purification Resin, ClonTech). Purified VHH were analyzed by sodium dodecyl sulfate polyacrylamide gel electrophoresis (SDS-PAGE). The final VHH concentration was determined by UV absorption at 280 nm (NanoDrop 1000 Spectrophotometer, Thermo Scientific) and the theoretical mass extinction coefficient. Theoretical mass extinction coefficients were calculated using Clone Manager 7 Software.

Binding specificity of VHH

Binding specificity of the purified VHH clone MA10 was tested in an enzyme-linked immunosorbent assay (ELISA) binding assay. 96-wells microtiter plate wells containing three pure HA plates (approximately 1.5 x 1.5 mm, and 0.1 mm thickness) were blocked with 2% BSA in PBS for two hours at room temperature to achieve blocking of non specific binding sites. Subsequently, wells were incubated with a serial dilution of VHH (ranging from 0 to 7 μM) in 1% BSA in PBS for two hours at room temperature. VHH 1B5 is an unrelated VHH targeting immunodeficiency virus type 1 (HIV-1) envelope proteins used as a negative control in this assay, which was a kind gift from Nika Strokkape (University of Utrecht, The Netherlands) [21]. The wells were washed with PBST and PBS. Bound VHH were detected by incubation with the mouse anti-myc antibody mAb 9E10 and a donkey anti-mouse antibody coupled to a peroxidase. The amount of HRP was developed by the addition of Tetramethylbenzidine (TMB, 1-Step Ultra TMB-ELISA, Thermo Scientific). The reactions were stopped by the addition of H_2SO_4 and measured at 450 nm (Micro Plate Reader). The dissociation constants (Kd) were obtained from subsequent fitting of experimental data to specific binding models.

Mouse fetal metatarsals culture

Animal experiments were approved by a local animal ethical committee. Mouse fetal metatarsals were isolated from FVB mouse embryos (time-paired, Harlan) at day 17.5 of gestation [22]. After isolation, metatarsals were individually cultured in wells of 24-well plates in 200 μl α-MEM, supplemented with 10% FBS, 100 U/ml penicillin, 100 mg/ml streptomycin and 1% Glutamax (Invitrogen) for 48 hours at 37 ºC in humidified atmosphere and 5% CO_2. After this equilibration period, metatarsals were incubated in the presence of VHH. To enable visualization, VHH MA10 and control VHH 1B5 were randomly labeled with Alexa Fluor 647 following the manufacturer's protocol (Invitrogen) resulting in VHH MA10-647 and 1B5-647.

MA10-647 or 1B5-647 (1 μg/ml) for 2 hours at 37 ºC in humidified atmosphere and 5% CO_2. After intensive wash with PBS the metatarsals were evaluated for fluorescence with BD Pathway (BD Biosciences) with an excitation filter at 628 ± 40 nm and emission filter at 692 ± 40 nm.

Binding of VHH-IR to HA

With the promising results of VHH MA10 binding to mineralized bone matrix, VHH MA10 and VHH J3, which was used as a non-HA binding control kindly provided by QVQ B.V. (Utrecht, the Netherlands) were selected for further tests in an *in vivo* mouse model. A direct labeling strategy was chosen to avoid interference with antigen-antibody interaction through site directed labeling of the C-terminus of the VHH. This was achieved through genetic introduction of an unpaired cysteine at the VHH's C-terminus (MA10-CYS), which could be conjugated to a maleimide containing IRDye 800 CW. VHH MA10-CYS was modeled using the online program I-TASSER for protein modeling [23-25]. The obtained VHH MA10-IR was tested for binding to HA to confirm

that the genetic modification and labeling did not interfere with the the function of the VHH. To avoid the presence of toxins, VHH were produced in the yeast *Sacchromyces cerivisiae*. Wells containing three pure HA plates (approximately 1.5 x 1.5 mm, and 0.1 mm thickness) were blocked with 2% BSA in PBS for two hours at room temperature to achieve blocking of non-specific binding sites. Subsequently, wells were incubated with a serial dilution of VHH MA10-IR and J3-IR (ranging from 10, 1 and 0.1 µg/ml) in 1% BSA in PBS for two hours in the dark at room temperature. The wells were washed with PBST and PBS. Bound VHH were detected with an Odyssey scanner (Licor Biosciences) using the 800 nm channel. The images were analyzed with the Odyssey Software v2.1.

Imaging of mineralized bones in mice

Balb C nu/nu mice (Charles River, France) were divided in two groups: one group was injected with VHH MA10-IR (35 or 70 µg/ 100 µl) and the other group was injected with the negative control VHH J3-IR (35 or 70 µg/ 100 µl). The dose of VHH to be injected was selected based on preliminary studies employing 140 and 230 µg/ 100 µl of VHH MA10-IR. The probes were injected intravenously through the tail vein. The PEARL Impulse imaging camera (Li-Cor. Lincoln, Nebraska) was used to image the mice. Mice were anesthetized with 2% of Isoflurane and imaged in ventral and dorsal positions at pre – and post-injection as well as at 1, 3, 24, 48, 72 hours and 7, 16 and 20 days post-injection. The results were analyzed with Pearl Impulse software 3.01. Mice were sacrificed with CO_2 at 20 days post-injection. Organs and skeleton were isolated and imaged.

Statistical Analysis

Statistical analyses were performed using GraphPad Prism version 5.00 for Windows, GraphPad Software (San Diego, California). Analyses were based on one-way ANOVA and a Tukey's Post-hoc test ($p< 0.05$) among all samples or between samples and controls. Error bars indicate standard deviation.

Results

Selection of VHH targeting HA

To investigate the possibility of targeting mineralized bone, VHH were selected from a non-immunized phage library. The selections were performed on HA plates contained in wells of a 96-wells microtiter plate (Figure 1A). A total of two rounds of selection were performed on HA plates to achieve an enrichment of phages binding to HA plates. Six single clones that showed binding to HA were selected during screening (not shown). After VHH expression and sequence determination, clone MA10 was selected for further characterization since this clone did not contain internal glycosylation sites, which could hamper production in yeast. VHH MA10 was purified from the periplasmic fraction of *E. coli* TG1 using TALON. The size and purity of the VHH were assessed by SDS-PAGE

where a single band was detected of ~16 kDa, which is in agreement with values found in literature [26, 27].

VHH MA10 was tested for specific binding to HA by ELISA. In parallel, an unrelated VHH, clone 1B5, was used as a negative control. To determine the affinity between the VHH and HA a titration series of VHH over a range of 0.7 nM up to 7 μM was performed on HA plates. When binding of VHH to HA occurred an increased signal was measured (Figure 1B). VHH MA10 showed binding to HA in a dose dependent manner with an apparent affinity of ~120 nM. The Kd deducted from fitting the experimental ELISA data to specific binding models are in agreement with values found in literature for VHH [28, 29]. Control VHH 1B5 did show approximatly 10% binding to HA at the highest VHH concentration. Overall, no relevant binding of non relevant VHH 1B5 to HA plates was observed.

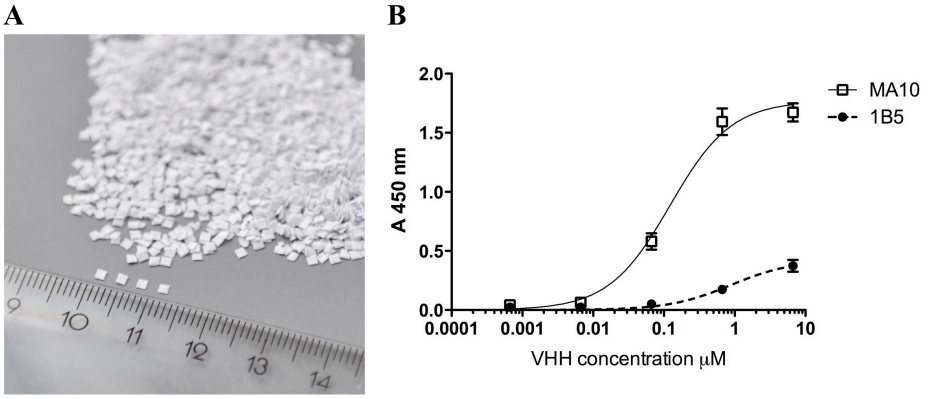

Figure 1. Solid phase ELISA of VHH to HA plates. (A) Photography of HA plates measuring approximately 1.5 x 1.5 mm, 0.1 mm thickness. (B) The indicated concentrations of VHH were incubated with wells containing three HA plates pre-incubated with 2 % BSA in PBS to achieve blocking of non-specific binding. After several washes, bound VHH were detected with a mouse anti-myc and a donkey anti-mouse antibody coupled to a peroxidase. The amount of converted HRP measured with TMB (Absorbance at 450 nm; A 450 nm) is proportional to the amount of bound VHH. VHH 1B5 is a non-relevant VHH used as a negative control. Data are expressed as the mean +/- standard deviation of at least 3 replicates.

MA10 targeting HA binds mineralized bone

We next tested whether MA10 could be used for visualizing mineralized bone using explanted mice fetal metatarsal. The metatarsals were incubated with VHH MA10-647 and the negative control VHH 1B5-647 or vehicle (Figure 2). For sake of detection both VHH were randomly labeled with Alexa fluor 647 nm fluorophore (describe in M&M). The degree of labeling obtained was 0.3 and 0.5 for VHH MA10-647 and 1B5-647, respectively. I.e. on average 30% and 50% of the VHH molecules were conjugated to the fluorophore. Fluorescent microscopy on the intact metatarsals revealed that VHH MA10-647 was specifically bound to the mineralized cartilaginous matrix of the primary center

of ossification. In addition binding was observed to the developing bone collar in which mineralized bone matrix is deposited (Figure 2). In contrast, VHH 1B5-647 binding to mineralized extracellular matrix was strongly reduced with exception of some non-specific fluorescence at the boundary of the mineralized and hypertrophic cartilage and with faint fluorescence in the bone collar. Interestingly, Alexa Fluor 647 did not display any significant auto fluorescence using an emission filter of 692 ± 40 nm.

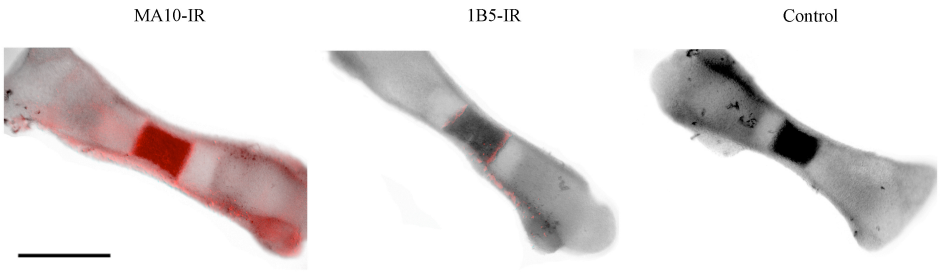

Figure 2. VHH-IR targeting mineralized extracellular matrix in metatarsals. Representative fluorescence image of mouse metatarsals incubated with fluorescently labeled VHH MA10-647 (1 µg/ml), control VHH 1B5-647 (1 µg/ml) or vehicle control. Metatarsals were incubated with VHH-647 and after extensive washing with PBS the metatarsals were evaluated for fluorescence (red) with BD Pathway with excitation filter at 628 ± 40 nm and emission filter at 692 ± 40 nm. Fluorescence was observed in the mineralized cartilaginous matrix of the primary ossification center and in the developing bone collar. Scale bar represents 0.25 mm. N=3.

Function of the directionally labeled VHH

VHH MA10 targeting HA and the non-binding VHH J3 were first engineered with an unpaired cysteine at the C-terminal allowing site-specific conjugation to the maleimide functionalized near-infrared fluorophore IRDye800CW. Modelling revealed that the unpaired cysteine at the C-terminal would not interfere with the antigen binding sites and should be available for conjugation (Figure 3). VHH MA10-IR and VHH J3-IR were obtained with a degree of labeling of 0.6 and 0.4, respectively, i. e. on average 60% and 40% of the VHH molecules were conjugated to the near-infrared fluorophore. In order to confirm that the genetic modification, the production in yeast and labeling did not alter the binding properties of the VHH a binding assay was performed. Fluorescently labelled VHH-IR were incubated with HA plates and fluorescence was measured after extensive washing (Figure 4A). VHH MA10-IR showed significantly higher fluorescence compared with VHH J3-IR at the same VHH concentration (Figure 4B). Fluorescence with J3-IR is likely explained by adsorption of the protein to hydroxyapatite, which has previously been reported.

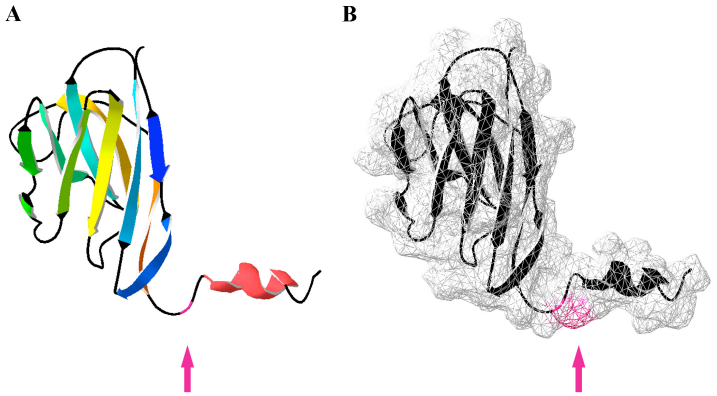

Figure 3. Structural model of VHH MA10-CYS. (A) The protein chain is represented by ribbons and colored with rainbow spectrum from N-terminus (blue) to C-terminus (red). The location of cysteine residue 120, genetically incorporated at the C-terminus of the VHH for directed chemical reactions, is highlighted in pink. (B) Surface prediction of VHH where sulfur surface is colored pink.

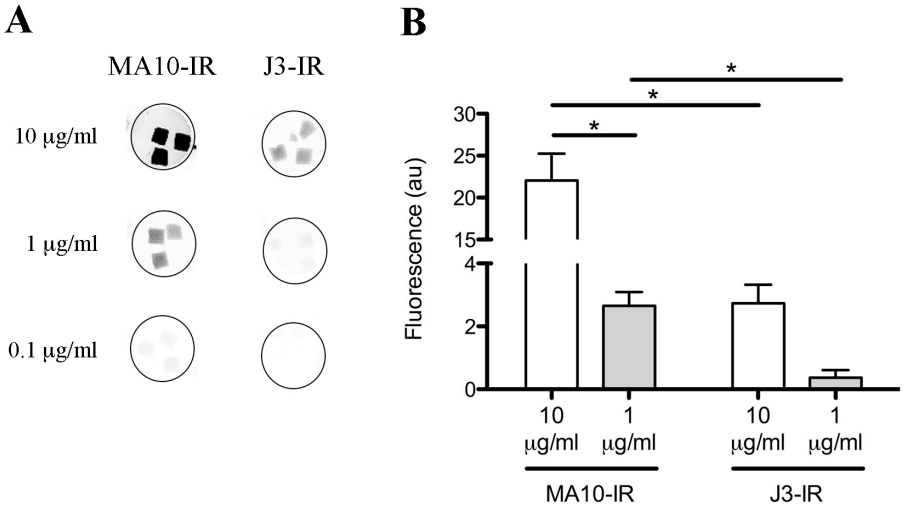

Figure 4. VHH-IR binding to HA plates. (A) Representative fluorescence image of wells containing 3 HA plates incubated with VHH MA10-IR or J3-IR at the indicated concentration. (B) Quantitative analysis of fluorescent signal measured with Odyssey. * $p<0.05$, N=6.

Infra-red labeled VHH MA10 binds to mineralized skeleton

To evaluate the potential of MA10-IR as a probe for optical imaging of bone tissue, nude mice were intravenously injected in the tail vein with MA10-IR and imaged at several time points post-injection (Figure 5A). Littermates were treated in the same way with the non-binding VHH J3-IR as negative control, and images of the two groups were compared. Images taken at early time points showed IR fluorescence throughout the complete body of the mouse in the case of MA10-IR (up to 7 days post-injection) and in the case of J3-IR (up to 3 days post-injection). At day 20 fluorescent label was still detectable in the skeleton of mice injected with MA10-IR in contrast to J3-IR injected mice and both groups were sacrificed. The skeleton and organs were isolated and imaged (Figure 5B). The dorsal and ventral images showed a clearly defined skeleton with high fluorescence measured for MA10-IR. Specific accumulation of MA10-IR occurred at mineralized bones. In contrast, no fluorescence was measured for the VHH J3-IR in the skeleton, which is in agreement with the results obtained in the *ex vivo* test (see Figure 2). For both VHH, liver, spleen and kidneys did show fluorescence after 20 days. Fluorescence is clearly visible at the kidneys for both groups. Obviously, J3-IR was much faster cleared from the body than MA10-IR suggesting that the targeting to the skeleton through binding to hydroxyapatite extents the retention time of the VHH in the body considerably for at least 20 days. Similar data were obtained when the VHH were injected at a dose of 35 µg/ 100 µl. Even at this lower dose, MA10-IR was still present in the skeleton after 20 days (Supplementary Figure S1). Remarkably, all skeletal elements were labelled with MA10-IR without evidence for regional hotspots, which could be indicative for sites with high bone turnover.

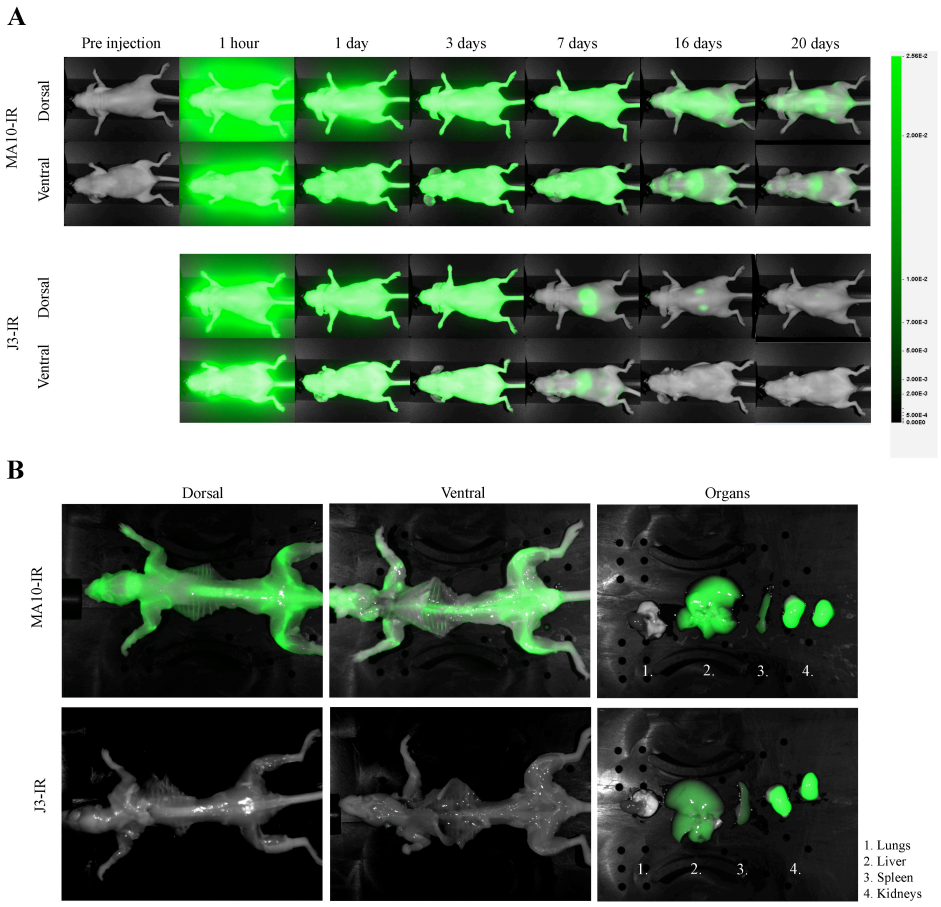

Figure 5. Fluorescence images over time of VHH MA10-IR (70 µg/ 100 µl injection sample) and negative control J3-IR (70 µg/ 100 µl injection sample) upon IV injection in Balb C nu/nu mice. (A) Live imaging. Dorsal and ventral images of the same mouse were obtained throughout a time period of 20 days after injection. (B) Postmortem imaging. At day 20, after the mice were sacrificed, the skeleton and organs were isolated and imaged. The VHH were injected IV in the tail vein.

Discussion

HA is a calcium phosphate biomaterial, extensively used as bone grafts substitutes mainly due to their chemical composition, which closely resembles natural bone mineral [14, 30]. We therefore selected this biomaterial for the isolation of VHH that could target mineralized bone.

Phage display is a well known and established technology which has already been utilized for the selection of peptides binding to HA [17]. In this study, we show for the first time, the selection of VHH targeting HA by means of phage display from a non-immunized library, which contains a myriad of VHH-phages with affinity towards a large

variety of epitopes. Despite the biocompatibility of HA, it was possible to identify a VHH (VHH MA10) binding with good affinity to this material. Our method has advantages over peptides, i.e. due to better presentation of the antigen binding site, higher affinities and specificities can be achieved. We here demonstrated the possibility to isolate VHH targeting non-peptide based anorganic structures.

The affinity of VHH is usually increased by immunization, suggesting that the sub-micromolar affinity selected from the non-immunized library may improve by immunization with HA [31]. Alternatively, a family-specific sub-library could be made as described elsewhere [32] for further selections, which may also result in binders with improved affinities.

Furthermore, we demonstrated that the selected VHH could be used for the targeting of mouse skeleton. Non-invasive imaging of bone tissue is a powerful tool with potential applications in bone tissue engineering, guided surgery, treatment of bone metastasis and treatment monitoring. Bone imaging can help clinicians in the identification and progression of bone diseases as well as the evaluation of therapy including grafted implants [3]. In this study, the VHH targeting HA (MA10) was conjugated to near IR fluorophore and appraised as a probe for optical imaging. The fluorophore was site-directed conjugated at an unpaired cysteine introduced at the C-terminal of the VHH, at the opposite site of the VHH binding site, reducing the possibilities of the labeling to affect the binding of the VHH to HA and mineralized bone. Indeed, *in vitro* studies showed that MA10-IR binding to HA was not hampered by steric hindrance caused by the conjugation. Modeling of the VHH also showed the C-terminal tail extended away from the antigen binding site and should be accessible for conjugation reactions. Furthermore, the production of VHH MA10 in yeast did not lead to differences in molecular weight, as no N-linked glycosylation site is present in the amino acid sequence of the VHH.

In vivo imaging was evaluated by injecting infra-red labeled VHH in nude mice. MA10-IR clearly showed specific binding to the mouse skeleton. To our knowledge, this is the first time a VHH was employed as a targeting molecule for mineralized bone. The small VHH size allowed for a rapid VHH distribution throughout the mouse body after one hour post-injection. Binding of VHH MA10-IR to mineralized bone, specifically delineated the mouse mineralized skeleton, and resulted in a long term retention of the VHH in the body. In contrast, VHH J3-IR was only present in some organs. These *in vivo* results show a clear distinction from absorption effect from binding effect. Only MA10-IR is retained in skeleton, while J3-IR is absorbed and quickly withdraws from skeleton. Spleen and kidneys represent the excretion routes for clearance of unbound molecules, however targeting of liver by MA10-IR and lungs by J3-IR was not easily explained. It is unknown if the fluorescence measured on the excretion is due to the conjugated VHH with the fluorophore or if it is a degradation product consisting of the fluorophore. More detailed follow-up studies are warranted to elucidate the differential VHH accumulation in the organs. In addition, if the stability of the complex conjugate VHH fluorophore is validated, the opportunity to monitor experiments for long period of time (at least 20

days) without significant loss in signal should be highlighted. Furthermore, the amount of VHH necessary to be injected for visualization of specific time points can be determined and tuned. Even at the lowest concentration tested in injections, the skeleton remained clearly visible up to 20 days post injection.
In the present work we demonstrated an improved performance of VHH for imaging purposes over the already existing bisphosphonates labeled with technecium. While the bisphosphonates partricularly are incorporated in sites in skeleton with high bone turnover [7], a more even distribution of the VHH over the whole skeleton was achieved. This makes the VHH a promising delivery vehicle for bone anabolic drugs to treat systemic bone disease like osteoporosis.
This non-invasive technology, by means of labeled VHH, can be employed for early detection of skeletal disorders and/or identify and delineate the diseases.
Besides imaging purposes, VHH could be used for drug targeting. For example by coating of liposomes, or conjugating of cytotoxic drugs for treatment of bone metastasis or by genetic engineering in which the VHH targeting bone is part of a multivalent antibody complex. The versatility of VHH allows for an endless combination.
We are now ready to identify the problem and afterwards engineer the VHH for targeting with therapeutic drugs.

Conclusion

With this study, we demonstrated the possibility to select VHH binding with high affinity to non-peptide epitopes present in HA. When conjugated to a near infrared probe, this VHH allowed the visualization of the mouse skeleton encouraging further developments for theragnostics tools paramount in treatment of skeletal diseases.

Acknowledgements

VHH 1B5 is a kind gift from Nika Strokappe. This work was supported by project P2.02 OAControl of the research program of the BioMedical Materials Institute, co-funded by the Dutch Ministry of Economic Affairs, Agriculture and Innovation. This research is supported by a long term program grant from the Dutch Arthritis Association provided to MK.

Supplementary information

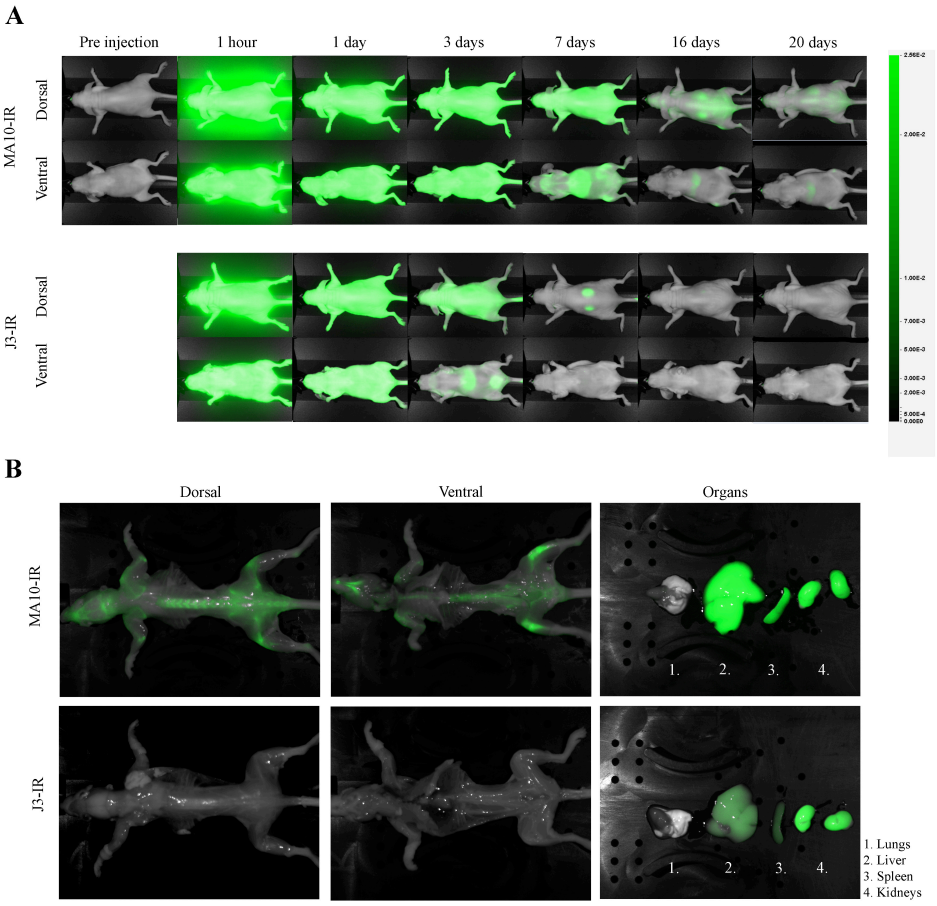

Figure S1. Fluorescence images over time of VHH MA10-IR (35 µg/ 100 µl injection sample) and negative control J3-IR (35 µg/ 100 µl injection sample) upon IV injection in Balb C nu/nu mice. (A) Live imaging. Dorsal and ventral images of the same mouse were obtained throughout a time period of 20 days after injection. (B) Postmortem imaging. At day 20, after the mice were sacrificed, the skeleton and organs were isolated and imaged. The VHH were injected IV in the tail vein.

References

1. Lavik, E. and R. Langer, *Tissue engineering: current state and perspectives.* Applied microbiology and biotechnology, 2004. **65**(1): p. 1-8.
2. Bose, S., M. Roy, and A. Bandyopadhyay, *Recent advances in bone tissue engineering scaffolds.* Trends in biotechnology, 2012. **30**(10): p. 546-54.
3. de Boer, J., C. van Blitterswijk, and C. Lowik, *Bioluminescent imaging: emerging technology for non-invasive imaging of bone tissue engineering.* Biomaterials, 2006. **27**(9): p. 1851-8.
4. Roelofs, A.J., et al., *Molecular mechanisms of action of bisphosphonates: Current status.* Clinical Cancer Research, 2006. **12**(20): p. 6222S-6230S.
5. Palma, E., et al., *Bisphosphonates as radionuclide carriers for imaging or systemic therapy.* Molecular Biosystems, 2011. **7**(11): p. 2950-2966.
6. Wang, G., M.E. Babadagli, and H. Uludag, *Bisphosphonate-derivatized liposomes to control drug release from collagen/hydroxyapatite scaffolds.* Molecular pharmaceutics, 2011. **8**(4): p. 1025-34.
7. Baron, R., S. Ferrari, and R.G.G. Russell, *Denosumab and bisphosphonates: Different mechanisms of action and effects.* Bone, 2011. **48**(4): p. 677-692.
8. Nicolaides, N.C., P.M. Sass, and L. Grasso, *Advances in targeted therapeutic agents.* Expert opinion on drug discovery, 2010. **5**(11): p. 1123-40.
9. Harmsen, M.M. and H.J. De Haard, *Properties, production, and applications of camelid single-domain antibody fragments.* Appl Microbiol Biotechnol, 2007. **77**(1): p. 13-22.
10. van der Vaart, J.M., *Expression of VHH antibody fragments in Saccharomyces cerevisiae.* Methods in molecular biology, 2002. **178**: p. 359-66.
11. Oliveira, S., et al., *Targeting tumors with nanobodies for cancer imaging and therapy.* Journal of controlled release : official journal of the Controlled Release Society, 2013.
12. Kijanka, M., et al., *Rapid optical imaging of human breast tumour xenografts using anti-HER2 VHHs site-directly conjugated to IRDye 800CW for image-guided surgery.* European Journal of Nuclear Medicine and Molecular Imaging, 2013. **40**(11): p. 1718-1729.
13. Oliveira, S., et al., *Rapid Visualization of Human Tumor Xenografts through Optical Imaging with a Near-infrared Fluorescent Anti-Epidermal Growth Factor Receptor Nanobody.* Molecular Imaging, 2012. **11**(1): p. 33-46.
14. Barradas, A.M., et al., *Osteoinductive biomaterials: current knowledge of properties, experimental models and biological mechanisms.* European cells & materials, 2011. **21**: p. 407-29; discussion 429.
15. Heise, U., J.F. Osborn, and F. Duwe, *Hydroxyapatite Ceramic as a Bone Substitute.* International Orthopaedics, 1990. **14**(3): p. 329-338.
16. Landi, E., et al., *Carbonated hydroxyapatite as bone substitute.* Journal of the European Ceramic Society, 2003. **23**(15): p. 2931-2937.
17. Roy, M.D., et al., *Identification of a Highly Specific Hydroxyapatite-binding Peptide using Phage Display.* Advanced Materials, 2008. **20**(10): p. 1830-1836.
18. Frenken, L.G., et al., *Isolation of antigen specific llama VHH antibody fragments and their high level secretion by Saccharomyces cerevisiae.* J Biotechnol, 2000. **78**(1): p. 11-21.
19. Saerens, D., et al., *Single domain antibodies derived from dromedary lymph node and peripheral blood lymphocytes sensing conformational variants of prostate-specific antigen.* J Biol Chem, 2004. **279**(50): p. 51965-72.
20. Roovers, R.C., et al., *High-affinity recombinant phage antibodies to the pan-carcinoma marker epithelial glycoprotein-2 for tumour targeting.* Br J Cancer, 1998. **78**(11): p. 1407-16.
21. Strokappe, N., et al., *Llama Antibody Fragments Recognizing Various Epitopes of the CD4bs Neutralize a Broad Range of HIV-1 Subtypes A, B and C.* Plos One, 2012. **7**(3).

22. Haaijman, A., et al., *Inhibition of terminal chondrocyte differentiation by bone morphogenetic protein 7 (OP-1) in vitro depends on the periarticular region but is independent of parathyroid hormone-related peptide.* Bone, 1999. **25**(4): p. 397-404.
23. Zhang, Y., *I-TASSER server for protein 3D structure prediction.* BMC bioinformatics, 2008. **9**: p. 40.
24. Roy, A., A. Kucukural, and Y. Zhang, *I-TASSER: a unified platform for automated protein structure and function prediction.* Nature protocols, 2010. **5**(4): p. 725-38.
25. Roy, A., J. Yang, and Y. Zhang, *COFACTOR: an accurate comparative algorithm for structure-based protein function annotation.* Nucleic acids research, 2012. **40**(Web Server issue): p. W471-7.
26. Wesolowski, J., et al., *Single domain antibodies: promising experimental and therapeutic tools in infection and immunity.* Med Microbiol Immunol, 2009. **198**(3): p. 157-74.
27. de Marco, A., *Biotechnological applications of recombinant single-domain antibody fragments.* Microbial cell factories, 2011. **10**: p. 44.
28. Hulsik, D.L., et al., *A gp41 MPER-specific Llama VHH Requires a Hydrophobic CDR3 for Neutralization but not for Antigen Recognition.* Plos Pathogens, 2013. **9**(3).
29. Muyldermans, S., *Nanobodies: natural single-domain antibodies.* Annual review of biochemistry, 2013. **82**: p. 775-97.
30. Zhou, H. and J. Lee, *Nanoscale hydroxyapatite particles for bone tissue engineering.* Acta biomaterialia, 2011. **7**(7): p. 2769-81.
31. Vanlandschoot, P., et al., *Nanobodies(R): new ammunition to battle viruses.* Antiviral Res, 2011. **92**(3): p. 389-407.
32. Koh, W.W.L., et al., *Generation of a Family-specific Phage Library of Llama Single Chain Antibody Fragments That Neutralize HIV-1.* Journal of Biological Chemistry, 2010. **285**(25): p. 19116-19124.

Chapter 7

Non-covalent functionalization of biomaterials through bivalent VHH

Emilie Dooms Rodrigues[1], Mohamed El Khattabi[2], Jasper van Weerd[1,3], Sabrina Oliveira[4], Clemens van Blitterswijk[5], Theo Verrips[2] and Marcel Karperien[1]

[1] Department of Developmental BioEngineering, MIRA Institute for Biomedical Technology and Technical Medicine, Faculty of Science and Technology, University of Twente, Enschede, The Netherlands;
[2] QVQ BV, Utrecht, The Netherlands;
[3]Molecular Nanofabrication Group, MESA$^+$ Institute for Nanotechnology, Faculty of Science and Technology, University of Twente P.O. Box 217, 7500 AE, Enschede, Netherlands;
[4] Division Cell Biology, Department of Biology, Science Faculty, Utrecht University, Utrecht, The Netherlands;
[5] Department of Tissue Regeneration, MIRA Institute for Biomedical Technology and Technical Medicine, Faculty of Science and Technology, University of Twente, Enschede, The Netherlands.

Abstract

Functionalization of biomaterial surfaces with growth factors such as bone morphogenetic proteins (BMPs) is a promising strategy to enhance tissue formation. While some success has been achieved by covalent binding of growth factors to biomaterial surfaces, this strategy results in modification of the growth factor, which may impact its biofunction. In this study we describe a non-covalent strategy for binding of growth factors to biomaterial surfaces by using engineered bivalent antibodies binding at one hand to the biomaterial surface and at the other hand to the respective growth factor. This strategy was tested by genetic fusion of previously identified VHH binding to hydroxyapatite and BMP7, respectively.

The bivalent VHH appeared to be biologically active as measured by its ability to enhance BMP7 osteogenic differentiation of C2C12 mouse myoblast cell line. Our study demonstrated that the bivalent VHH remained multifunctional and allowed for the retention of the binding activity in the two VHH units. This affinity platform can be further tuned to target different growth factors clinically relevant for bone tissue engineering.

Non-covalent sequestering of growth factors to biomaterial surfaces via engineering bivalent VHH is a promising strategy for biofunctionalization of scaffolds for tissue engineering without the need of growth factor modification.

Keywords: Hydroxyapatite, BMP7, bivalent VHH, scaffold functionalization

Introduction

Large bone defects remain a significant clinical issue. Existing therapies are based on the golden standard, auto and allografts, including all drawbacks associated [1].
Biomaterials are employed for the fabrication of scaffolds which are used as substitutes to restore, replace or regenerate tissue [2]. Scaffolds have an important role in tissue regeneration. Many strategies have emerged to improve scaffolds for tissue engineering, i.e. controlled release of growth factors by incorporating them in slow release materials or by adsorption to biomaterial surfaces [3]. Alternatively, growth factors can be attached to materials covalently by crosslinking or through linkers [4-6]. Disadvantage of this strategy is the chemical modification of the growth factor [7]. Since these strategies are based on random coupling, targeting accessible primary amines or carboxylic acid groups for binding of the linker, the chemical modification may damage bioactive functional groups and impact growth factor's activity resulting in loss of bioactivity [8]. The inherent problems with these strategies can be solved by using the unique properties of antibodies as an intermediate between surface and the growth factor. Antibodies bind to growth factors without chemical modifications, and based on affinity for growth factors the release of the growth factors from a surface can be tailored. Antibodies can be coupled to biomaterial surfaces through directed coupling based on supramolecular interactions (chapter 3 of this thesis), or through targeted coupling through genetically introduced amino acids, like cysteine in the C-terminal tail of the antibody (chapter 5 of this thesis) to avoid loss of function through coupling in a random approach. Alternatively, it seems feasible to isolate antibodies binding to epitopes in a biomaterial. When such antibodies are combined with antibodies targeting respective growth factors, the resulting bivalent antibodies can be used for non covalent coupling of growth factors to biomaterial surfaces in a dynamic way (Figure 1).
Bivalent antibodies can be generated by making use of conventional antibodies. However the complexity of these proteins and their large size are disadvantageous for tailored manipulation into bivalent antibodies and sets limitations to their production. In contrast, single domain antibodies (VHH), such as those found in the IgG repertoire of *Camelidae*, are uniquely small (~15kD) molecules derived from antibodies devoid of a light chain, which can be easily cloned and genetically modified, produced and purified [9].
Previous studies reported the selection of VHH targeting different growth factors such as tumor necrosis factor-alpha (TNF-α) [10], vascular endothelial growth factor (VEGF) [11] and Dickkopf-related protein 1 (DKK1) (chapter 8 of this thesis). Hence, VHH can be selected to specifically interact with growth factors, stabilize them and even manipulate positively or negatively their function. Previously we have isolated VHH with high specificity for BMP6 and BMP7. Among these, VHH G7 bound with high affinity to BMP7 and was able to potentiate its action in an osteogenic differentiation assay (manuscript in preparation, chapter 2 of this thesis).
In addition, we have previously shown that it is feasible to isolate VHH binding hydroxyapatite (HA) from a non-immunized phage display library (chapter 6 of this

thesis). HA is a biomimetic calcium phosphate frequently used as a bone graft substitute in bone tissue engineering [12-14].

In the present study we explored the possibility of making bivalent VHH by the genetic fusion of VHH G7, targeting BMP7, and VHH MA10 targeting HA. The resulting bivalent VHH G7MA10 retained its affinity for HA and BMP7. Our data shows the feasibility of using bivalent VHH targeting both growth factors and epitopes in a biomaterial surface as a novel strategy for biomaterial surface functionalization.

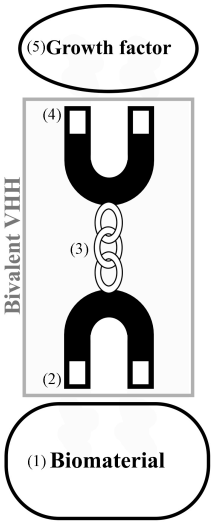

Figure 1. Schematic representation of the proposed system for the functionalization of biomaterials using bivalent VHH. The coating build up is summarized in a schematic overview. The bivalent VHH makes the bridge between the biomaterials (1) and the biology (5). The Bivalent VHH is composed of three elements: (2) a VHH targeting a biomaterial, (4) a VHH targeting a growth factor and (5) a linker with an optional cleavable sequence. In this study the bivalent VHH engineered targets HA as biomaterial and the growth factor BMP7.

Materials and methods

Selection of VHH targeting BMP7

The selection and characterization of VHH G7 targeting BMP7, is extensively described elsewhere (chapter 2 of this thesis). In brief, VHH were selected by phage display of a VHH-phage library generated from a llama immunized with BMP6 and BMP7. Two rounds of panning selection were performed on wells coated with BMP7. VHH G7 was selected to specifically bind to BMP7. VHH G7 had a dissociation constant of ~ 1 nM. In osteogenic differentiation assays this VHH potentiated the biological activity of BMP7.

Selection of a VHH targeting HA

The selection and characterization of VHH MA10 targeting HA, is extensively described elsewhere (chapter 6 of this thesis). In brief, VHH binders towards HA were selected from two non-immunized llama VHH phage libraries constructed from 9 llamas. A two round panning selection was performed on HA plates. VHH MA10 was selected to bind to HA. The calculated VHH MA10 dissociation constant was ~ 120 nM. In addition, VHH MA10 proved to bind to bone in *ex vivo* and *in vivo* mouse models.

VHH plasmids, production and purification

Escherichia coli strain TG1 was used for the maintenance of the plasmids, infection by the phages and expression of proteins. For detection purposes in following assays, two vectors with different tags were used in order to specifically detect the distinct VHH. Therefore, the DNA information of the individually selected and isolated VHH were subcloned into plasmid pMEK219 containing a C-terminus Myc and His tags and pMEK222 containing C-terminus FLAG and His tags.

E. coli TG1 was grown in Luria Broth (LB) or yeast extract and tryptone (YT) medium containing 2% (w/v) glucose and ampicillin at 100 µg/ml. VHH were produced from *E. Coli* TG1 by Isopropyl β-D-1-thiogalactopyranoside **(**IPTG) induction of the lac promoter at 37^{o}C for 4 hours under non static conditions [15, 16]. VHH proteins were produced in *E. coli* TG1 and purified from the periplasmic fraction via the C terminus His-tag by cobalt affinity chromatography (TALON His-Tag Purification Resin, ClonTech). Purified VHH were analyzed by means of sodium dodecyl sulfate polyacrylamide gel electrophoresis (SDS-PAGE). The final VHH concentration was determined from the UV absorption at 280 nm (NanoDrop 1000 Spectrophotometer, Thermo Scientific) and the theoretical mass extinction coefficient.

Construction of the bivalent VHH G7-MA10 recognizing BMP7 and HA

The bivalent G7-MA10 was constructed by genetic fusion of the cDNAs encoding VHH binding to BMP7, G7, and the VHH binding to HA, MA10 (Figure 2). PCR was used to amplify the VHH sequences. Different primers sets were designed to amplify the VHH G7, which will be located at the N-terminus and the VHH MA10, which will be placed at the C-terminus to generate a bivalent VHH (Table 1). The primers at the 3' of the N-terminus VHH and at the 5' of the C-terminus VHH encode a flexible sequence (GS-linker) represented by the pentapeptide 'Gly-Gly-Gly-Gly-Ser'. The primers contain a unique restriction site (*BamH*I). After PCR amplification, the generated fragments were digested with a unique N-terminal restriction site (*Sfi*I) and *BamH*I for the VHH located at the N-terminus, and with *BamH*I and a unique C-terminal restriction site (*BstE*II) for VHH located at the C-terminus. The fragments were ligated into the expression vector, pMEK222, which was digested with *Sfi*I and *BstE*II. The bivalent constructed was produced and purified as described above.

Table 1. List of sequences of primers used in the bivalent VHH construction.

Primer	Oligonucleotide sequence
M13Rev	GAGGTGCAATTGGTGGAGTCTGGG
Rev5GSBam	AGTAGGATCCGCCACCTCCTGAGGAGACCGTGACCTGGGTCCC
Fwd5GSBam	TCTTGGATCCGAGGTGCAGCTGGTGGAGTCTGGG
RevTVSS	TGAGGAGACGGTGACCTGGGTCCC

Competition of G7-MA10 with MA10 by ELISA

To show that the binding between the bivalent G7-MA10 and HA takes place via MA10 a competition assay was performed using an ELISA in two experimental designs. For detection purposes, two vectors with different tags were used.

1. Three plates of HA of homogeneous size (1.5 x 1.5 mm, and 0.1 mm thickness approximately) were incubated with 2% BSA in PBS to achieve blocking of non-specific binding sites. Subsequently, HA plates were incubated with an increasing concentration of the bivalent G7-MA10 produced from plasmid pMEK222((G7-MA10)-FLAG-His) (0 - 10 µg/ml). The competitor MA10 produced from plasmid pMEK219 (MA10-myc-His) was added in a constant concentration of 1 or 5 µg/sample in PBS and VHH were incubated for two hours at room temperature. The wells were washed with PBS Tween (PBS containing 0.5% (v/v) Tween-20, PBST) and PBS. Bound G7-MA10 was detected by incubation with a mouse anti-FLAG antibody and a donkey anti-mouse antibody coupled to a peroxidase. The amount of HRP was developed by the addition of OPD. The reactions were stopped by the addition of H_2SO_4 and measured at 490 nm (Micro Plate Reader).

2. Three plates of HA of homogeneous sizes (1.5 x 1.5 mm, and 0.1 mm thickness approximately) were incubated with 2% BSA in PBS to achieve blocking of non-specific binding sites. Subsequently, HA plates were incubated with a constant concentration of the bivalent G7-MA10 produced from plasmid pMEK222 ((G7-MA10)-FLAG-His) (1 µM). A concentration range of the competitor MA10 produced from plasmid pMEK219 (MA10-myc-His) was added (ranging from 0 to 25 µM) in PBS and VHH were incubated for two hours at room temperature. The wells were washed with PBST and PBS. Bound G7-MA10 was detected by incubation with a mouse anti-FLAG antibody and a donkey anti-mouse antibody coupled to a peroxidase. Bound MA10 was detected by incubation with a mouse anti-myc antibody (mAb 9E10) and a donkey anti-mouse antibody coupled to peroxidase. The amount of HRP was developed by the addition of Tetramethylbenzidine (TMB, 1-Step Ultra TMB-ELISA, Thermo Scientific). The reactions were stopped by the addition of H_2SO_4 and measured at 450 nm (Micro Plate Reader).

VHH biological activity

C2C12 mouse myoblast cells were used as a model for osteogenic differentiation. Previously we showed that VHH G7 targeting BMP7 was able to bind to BMP7 and enhanced its osteogenic potential when tested in C2C12 mouse myoblast cells (manuscript in preparation, chapter 4 of this thesis). We therefore tested if G7 moiety of the bivalent G7-MA10 was still able to enhance the osteogenic differentiation of BMP7. For this, cells were cultured in Dulbecco's Modified Eagles Medium (DMEM; Gibco) supplemented with 10% fetal bovine serum (FBS; Cambrex), 100 U/ml penicillin (Gibco) and 100 µg/ml streptomycin (Gibco) and were incubated at 37 ºC in humidified atmosphere and 5% CO_2. To assess the differentiation of C2C12, cells were seeded at a density of 10 000 cells/cm^2 (day 0) and cultured with ascorbic acid (50 µg/ml; Sigma Aldrich) and stimulated with a concentration range of BMP7 (ranging from 125 to 500 ng/ml) in the presence or absence of bivalent G7-MA10 at a constant concentration of 20 µg/ml. At day 7, cells were washed with PBS and lysed with CDPStar lysis buffer (Roche). To evaluate ALP activity, cell lysate was added to CDPStar reagent (Roche) and luminescence was measured using Vector Microplate Luminometer (Promega). The luminescence units were corrected for DNA content. DNA concentration was determined via a proliferation assay according to the manufacturer's protocol (CyQuant Cell Proliferation Assay Kit; Invitrogen).

Detection of BMP7 binding by G7-MA10

We further tested if the G7 moiety of the bivalent VHH was still able to bind to BMP7 after being immobilized onto HA plates. For this purpose, G7-MA10 was first immobilized on HA plates. Subsequently BMP7 was allowed to bind and bound BMP7 was detected by ELISA. Three plates of HA of homogeneous sizes (1.5 x 1.5 mm, and 0.1 mm thickness approximately) were incubated with 2% BSA in PBS for two hours at room temperature to achieve blocking of non-specific binding sites. Subsequently, HA plates were incubated with excess of the bivalent G7-MA10 (20 µg/ml) in order to saturate the surface. The wells were washed with PBST and a concentration range of BMP7 was added (ranging from 300 to 75 ng/ml) in PBS. Samples were incubated for two hours at room temperature. As control, HA plates were directly incubated with BMP7 with the same concentration range as specified before. The wells were washed with PBST and PBS. Bound BMP7 was detected by a mouse anti-human BMP7 biotinylated antibody (2 µg/ml) (R&D systems) and streptavidin coupled to peroxidase. The amount of HRP was developed by the addition of Tetramethylbenzidine (TMB, 1-Step Ultra TMB-ELISA, Thermo Scientific). The reactions were stopped by the addition of H_2SO_4 and measured at 450 nm (Micro Plate Reader).

Statistical Analysis

Statistical analyses were performed using GraphPad Prism version 5.00 for Windows, GraphPad Software (San Diego, California). Analyses were based on one-way ANOVA

and a Tukey's Post-hoc test ($p < 0.05$) among all samples or between samples and controls. Error bars indicate standard deviation.

Results

Construction of VHH bivalent

In order to explore the potential of VHH with dual specificity in functionalizing biomaterial surfaces, a bivalent VHH consisting of an anti-BMP7 and an anti-HA was constructed (Figure 1). VHH MA10 showed binding to HA in a dose dependent manner with an affinity of ~120 nM. VHH G7 was identified as a specific binder of BMP7 and a modulator of BMP7 osteogenic activity (manuscript in preparation) with an affinity of ~1 nM.

PCR was used to link the genes of the 2 VHH (Figure 2A) and introduce a linker sequence between them, as described in Material and Methods (Figure 2B). The resulting bivalent VHH is schematically illustrated in Figure 2C. Its structure was predicted by I-TASSER demonstrating that the genetic fusion did not impact the exposure of the complementary determining regions (CDR) involved in antigen binding [17-19].

G7-MA10 could be readily produced in bacteria although yield was somewhat lower compared to the individual monovalent VHH. The size of the produced monovalent and bivalent VHH had the expected molecular weight of ~16 kDa and ~30 kDa as shown by SDS-PAGE (figure 2D).

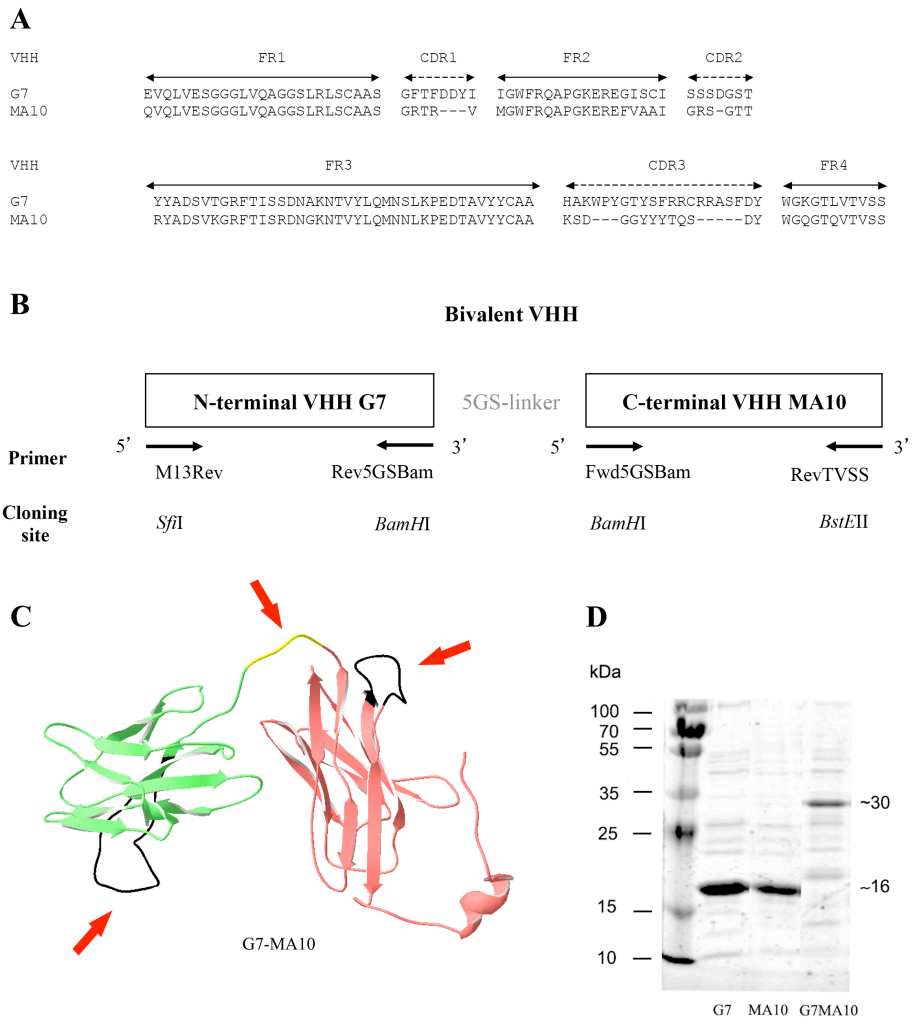

Figure 2. Construction and characterization of bivalent VHH. (A) Amino acid sequence alignment of VHH G7 and MA10. Frame works (FR) and complementary determining regions (CDR) of the VHH are indicated according to Chothia [29]. (B) The engineered bivalent VHH is schematically represented. Position of G7 at the N-terminus and MA10 at the C-terminus as well as the GS linker are indicated. (C) Predicted 3D protein model of the generated bivalent G7-MA10 where the GS linker is highlighted yellow and the CDR3 of G7 and MA10 in black. (D) Purified VHH G7, MA10 and G7-MA10 were sized-separated by a 15% SDS-PAGE and stained with Coomassie Brilliant Blue. Molecular weight markers (in kDa) are indicated at the left. Calculated molecular weight of the monovalent and bivalent are indicated at the right.

Bivalent G7-MA10 binds specifically to HA via MA10 unit

In order to determine if the bivalent VHH G7-MA10 still binds to HA only via the MA10 unit, a competitive binding assay of G7-MA10 to HA in the presence of the monovalent VHH MA10 was carried out. VHH mono- and bivalent constructs were incubated on HA

plates and a serial dilution of G7-MA10 was added while MA10 concentration remained constant (1 or 5 µg/sample) (Figure 3A). Similar to MA10 monovalent VHH, the bivalent G7-MA10 binds to HA in a dose response manner (Figure 3A). The Kd for G7-MA10 to HA was calculated by fitting the experimental data to a specific binding model. The Kd obtained, ~130 nM, is in accordance with the Kd obtained for the monovalent VHH MA10 (~120 nM). Competition between G7-MA10 and MA10 resulted in a reduction of about 50% of binding compared to binding with only G7-MA10. No difference in competition was observed between the low and high concentrations of supplemented MA10. The binding of G7-MA10 was effectively competed by MA10, which binds to HA.

Next, a competition profile of MA10 against G7-MA10 was determined. VHH mono and bivalent constructs were incubated on HA plates and a serial dilution of MA10 was added while G7-MA10 concentration remained constant (Figure 3B). The competitive binding of G7-MA10 against serial dilutions of MA10 resulted in a dose response curve. Starting at a concentration of ~3 µM and higher of MA10 a decrease in G7-MA10 signal was detected and an increased signal of MA10 was observed. No difference in competition was noticed between MA10 concentrations of 0 and ~3 µM. These results confirm that the interaction of the bivalent VHH (G7-MA10) with the biomaterial (HA) is effective through binding between the anti-HA VHH (MA10).

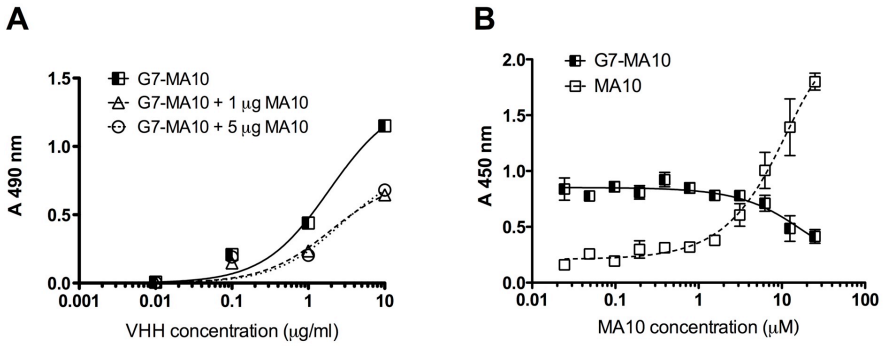

Figure 3. Competition assay of bivalent G7-MA10 with MA10 to HA determined by solid phase ELISA. (A) Bivalent G7-MA10 was added in a concentration range of 0 - 10 µg/ml to three HA plates in a well and supplemented with a constant concentration of 1 or 5 µg of the monovalent MA10. Bound G7-MA10 was detected with a mouse anti-FLAG and a donkey anti-mouse antibody coupled to HRP, whilst MA10, devoid of FLAG tag was not detectable. The amount of converted HRP (Absorbance at 490 nm; A 490 nm) is proportional to the amount of bound G7-MA10. (B) Bivalent G7-MA10 was added at a constant molarity of 1 µM to three HA plates in a well. Increasing concentration of MA10 was added to the wells. Bound G7-MA10 was detected with mouse anti-FLAG and MA10 with mouse anti-myc and a donkey anti-mouse antibody coupled to a peroxidase. The amount of converted HRP (Absorbance at 450 nm; A 450 nm) is proportional to the amount of bound VHH. Data are expressed as mean +/- SD of 3 replicates.

Bivalent G7-MA10 is biologically active

As reported in chapter 2 and 4 of this thesis, the monovalent VHH G7 has the ability to enhance BMP7 induction of ALP activity in the KS483-4C3 preosteoblastic cell line and the C2C12 mouse myoblast cell line (manuscript in preparation). ALP is an early marker of osteogenic differentiation, and it is strongly induced by BMP7. Here we determined the effect of bivalent G7-MA10 on ALP activity in combination with BMP7 in solution over a 7-day period (Figure 4). BMP7 induced ALP activity 2.5-fold at a concentration of 500 ng/ml and 2-fold at concentrations of 250 and 125 ng/ml. However, when cells were treated with BMP7 in the presence of bivalent G7-MA10 (20 µg/ml), a clearly superior induction of ALP activity was seen. This synergistic effect was not BMP7 dose-dependent. Thus, like the monovalent G7, G7-MA10 potentiates BMP7 activity.

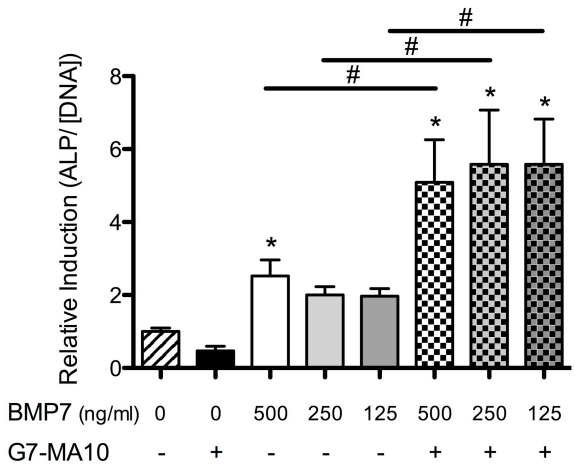

Figure 4. Biological activity of bivalent G7-MA10 in C2C12 cells. Cells were cultured in the presence of 20 µg/ml of G7-MA10 with a dose range of BMP7 (0 – 500 ng/ml). The ALP activity was normalized to the total DNA content of C2C12 cells after 7 days of culture, and expressed as relative induction with respect to control (non-treated cells). Data is expressed as mean +/- standard deviations (error bars), N=6. * indicates significance of $p < 0.05$ compared to control. # denotes significance ($p < 0.05$) between BMP7 only and the respective BMP7 / G7-MA10 condition.

Bivalent G7-MA10 has dual specificity

We demonstrated that bivalent G7-MA10 binds to HA through MA10. Now to demonstrate that G7-MA10 bivalent simultaneously binds to HA and BMP7, HA plate were saturated with G7-MA10 or blocked with BSA, and serial dilution of BMP7 was added to the HA plates. After washing, bound BMP7 was detected with biotinylated anti-BMP7 and streptavidin HRP (Figure 5). It was shown that BMP7 appears to bind non-specifically to HA in a dose-dependent manner likely through adsorption as previously described [20] in the absence of G7-MA10. There was no clear additive effect of G7-

MA10 on sequestering BMP7 at the surface of HA over adsorption, although binding at the lower BMP7 concentrations of 150 and 100 µg/ml tended to be slightly higher.

Discussion

The functionalization of biomaterials through non-covalent interactions permits to modify only the surface while the biomaterial remains unaltered. In nature, modulation of biological systems is accomplished through specific recognition and interactions of biomolecules. In this study we demonstrated an unique strategy in functionalizing biomaterials and modulating growth factors in a single step. We engineered a bivalent VHH binding to HA and BMP7. HA is a biocompatible ceramic, which is widely used in bone tissue engineering applications [21]. VHH targeting HA were previously isolated from a non-immunized llama library, which contains phages with affinity towards a large variety of epitopes by means of phage display. The selection methodology employed allowed for the identification of HA binders with good affinity (VHH MA10). The affinity of VHH observed with non-immunized libraries is often lower when compared with immunized libraries, which was also observed in this case [22].
The VHH MA10 was further engineered to have an additional unit with different specificity. In bone tissue engineering, the modulation of growth factor activity and their presentation at a specific site are primordial for faster and enhanced bone regeneration. The stabilization of growth factors, such as BMPs, can be achieved by their incorporation in biomaterials or by other biomolecules [23-25] with limitations. VHH targeting BMP7 (VHH G7), previously described elsewhere (manuscript in preparation, chapter 2 of this thesis), has been identified to further enhance BMP7 osteogenic properties. Hence, this VHH had become of great interest as a capturing agent of BMP7. The incorporation of VHH G7 to the biomaterial has been performed by the genetic fusion of the G7 unit with a GS-linker to MA10 unit. VHH G7-MA10 was obtained. Bone morphogenetic proteins are potent bone-healing compound produced at sites of bone trauma and therefore are of great interest for bone regeneration applications. The genetically engineered bivalent VHH, can be utilized as building blocks and bridging units between materials and biology. We demonstrated that the bivalent construction did not influence the binding of G7-MA10 towards HA nor did it affect the binding to BMP7. The bivalent VHH was tested in a biological assay in the presence of BMP7 where G7-MA10 enhanced BMP7 specific activity. These results are in accordance with the potentiating effect observed with the monovalent VHH G7 reported in a previous study (manuscript in preparation, chapter 2 of this thesis). An assay in which we tested the simultaneous biological activity of the bivalent VHH yielded inconsistent results. Sequestering of BMP7 on HA via G7-MA10 was obscured by the high adsorption rate of BMP7 to the HA discs. Adsorption of BMPs have previously been observed in HA [20]. Due to this technical limitation it is not possible to definitively conclude that binding of an antigen to either one of the CDRs obstructs the binding to the other CDR of the bivalent VHH. Based on modeling

experiments such an effect is not expected. Engineering of bivalent VHH have been described and demonstrated improved biological activity over monovalent VHH [26]. Alternatively, when steric hindrance may play a role it is possible to extend the linker region between the two VHH. It is expected that by increasing linker size steric hindrance can be diminished.

The construction of bivalent and multivalent VHH offers an endless combination of systems where the binding moieties can be selected according to the application. Furthermore, VHH sequences can also be varied to obtain VHH with tailored properties. In addition, VHH can also be used as a core structure for the grafting of sequences known for binding elements or with different affinities such as peptides. Several peptide sequences have been described to target HA [27, 28], these sequences could be potentially grafted in the CDR of the VHH for easy cloning and production, or covalently coupled to an unpaired cysteine genetically introduced at the C-terminus of a VHH. The functionalization of biomaterials with VHH will allow for accelerated and controlled tissue regeneration without the need of growth factors genetic modifications and reduction in growth factors bioactivity. Moreover, the versatility of the VHH allows for an endless combination of genetic modifications with potential relevance in several tissue regeneration applications.

In addition, the use of different linker sizes and cleavable linkers might be explored. Linkers with a specific amino acid sequence, which can be cleaved at different stages of inflammation or phase of tissue reconstruction, are of upmost importance to achieve a complex release pattern of bioactive compounds.

We have previously reported that VHH targeting MA10 targets to mineralized bone *in vitro* and *in vivo* (Chapter 6 of this thesis). The bivalent VHH here presented, G7-MA10 provide an opportunity to bring BMP7 binding moiety to mineralized bone where it may act as bone anabolic by sequestering locally produced BMP7 at the bone surface and may potentiate its action. Thus MA10 may be used as a targeting agent for delivery of proteins to bone. The application of bivalent VHH can be further extended to other biomaterials and growth factors and phases of tissue development. If proper targeting VHH binding to biomaterials are available, simple injections (even post implantation of scaffold) of bivalent VHH could be used to improve biofunctionalitty of the scaffold by capturing/ sequestering the adequate growth factor.

Therefore, we can further extend the use of bivalent VHH to tissue engineering in which biomaterials are already implanted.

Conclusion

With this study we demonstrated that engineering bivalent VHH could be a versatile strategy for functionalization of biomaterials with growth factors without affecting properties of the biomaterial nor permanently modifying the growth factor. Such bivalent VHH could be used to sequester locally produced growth factors at the biomaterial, thereby increasing local concentration and biological effect (chapter 2 and 3 of this thesis). Bivalent VHH could be coimplanted with the scaffold or injected post implantation of the scaffold. The targeting properties of the VHH may then result in specific accumulation of the bivalent VHH at the scaffold and thus growth factors. Thus this non-covalent strategy is very versatile and would provide a first strategy to improve scaffold function implanted in the body in a non-invasive manner.
The duality of an engineered VHH allows for the development of targeting and therapeutic solutions in a single step.

Acknowledgements

This work was supported by project P2.02 OAControl of the research program of the BioMedical Materials Institute, co-funded by the Dutch Ministry of Economic Affairs, Agriculture and Innovation. This work was supported by an unrestricted research grant of the Dutch Arthritis Association provided to MK.

References

1. Lavik, E. and R. Langer, *Tissue engineering: current state and perspectives.* Applied microbiology and biotechnology, 2004. **65**(1): p. 1-8.
2. O'Brien, F.J., *Biomaterials & scaffolds for tissue engineering.* Materials Today, 2011. **14**(3): p. 88-95.
3. Shin, H., S. Jo, and A.G. Mikos, *Biomimetic materials for tissue engineering.* Biomaterials, 2003. **24**(24): p. 4353-64.
4. Zisch, A.H., et al., *Covalently conjugated VEGF--fibrin matrices for endothelialization.* J Control Release, 2001. **72**(1-3): p. 101-13.
5. Ehrbar, M., et al., *The role of actively released fibrin-conjugated VEGF for VEGF receptor 2 gene activation and the enhancement of angiogenesis.* Biomaterials, 2008. **29**(11): p. 1720-9.
6. Drury, J.L. and D.J. Mooney, *Hydrogels for tissue engineering: scaffold design variables and applications.* Biomaterials, 2003. **24**(24): p. 4337-51.
7. Lee, K., E.A. Silva, and D.J. Mooney, *Growth factor delivery-based tissue engineering: general approaches and a review of recent developments.* Journal of the Royal Society, Interface / the Royal Society, 2011. **8**(55): p. 153-70.
8. Kuhl, P.R. and L.G. GriffithCima, *Tethered epidermal growth factor as a paradigm for growth factor-induced stimulation from the solid phase.* Nature Medicine, 1996. **2**(9): p. 1022-1027.
9. Harmsen, M.M. and H.J. De Haard, *Properties, production, and applications of camelid single-domain antibody fragments.* Appl Microbiol Biotechnol, 2007. **77**(1): p. 13-22.
10. Coppieters, K., et al., *Formatted anti-tumor necrosis factor alpha VHH proteins derived from camelids show superior potency and targeting to inflamed joints in a murine model of collagen-induced arthritis.* Arthritis and Rheumatism, 2006. **54**(6): p. 1856-1866.
11. Farajpour, Z., et al., *Identification and In Vitro Characterization of Phage-Displayed VHHs Targeting VEGF.* Journal of biomolecular screening, 2013.
12. Barradas, A.M., et al., *Osteoinductive biomaterials: current knowledge of properties, experimental models and biological mechanisms.* European cells & materials, 2011. **21**: p. 407-29; discussion 429.
13. Heise, U., J.F. Osborn, and F. Duwe, *Hydroxyapatite Ceramic as a Bone Substitute.* International Orthopaedics, 1990. **14**(3): p. 329-338.
14. Landi, E., et al., *Carbonated hydroxyapatite as bone substitute.* Journal of the European Ceramic Society, 2003. **23**(15): p. 2931-2937.
15. Saerens, D., et al., *Single domain antibodies derived from dromedary lymph node and peripheral blood lymphocytes sensing conformational variants of prostate-specific antigen.* J Biol Chem, 2004. **279**(50): p. 51965-72.
16. Roovers, R.C., et al., *High-affinity recombinant phage antibodies to the pan-carcinoma marker epithelial glycoprotein-2 for tumour targeting.* Br J Cancer, 1998. **78**(11): p. 1407-16.
17. Zhang, Y., *I-TASSER server for protein 3D structure prediction.* BMC bioinformatics, 2008. **9**: p. 40.
18. Roy, A., A. Kucukural, and Y. Zhang, *I-TASSER: a unified platform for automated protein structure and function prediction.* Nature protocols, 2010. **5**(4): p. 725-38.
19. Roy, A., J. Yang, and Y. Zhang, *COFACTOR: an accurate comparative algorithm for structure-based protein function annotation.* Nucleic acids research, 2012. **40**(Web Server issue): p. W471-7.
20. Zhou, H., et al., *Adsorption mechanism of BMP-7 on hydroxyapatite (001) surfaces.* Biochemical and biophysical research communications, 2007. **361**(1): p. 91-6.
21. Zhou, H. and J. Lee, *Nanoscale hydroxyapatite particles for bone tissue engineering.* Acta biomaterialia, 2011. **7**(7): p. 2769-81.
22. Vanlandschoot, P., et al., *Nanobodies(R): new ammunition to battle viruses.* Antiviral Res, 2011. **92**(3): p. 389-407.

23. Nguyen, T.H., et al., *A heparin-mimicking polymer conjugate stabilizes basic fibroblast growth factor.* Nature chemistry, 2013. **5**(3): p. 221-7.
24. Murali, S., et al., *Affinity-selected heparan sulfate for bone repair.* Biomaterials, 2013. **34**(22): p. 5594-605.
25. Lee, S.S., et al., *Bone regeneration with low dose BMP-2 amplified by biomimetic supramolecular nanofibers within collagen scaffolds.* Biomaterials, 2013. **34**(2): p. 452-9.
26. Hmila, I., et al., *VHH, bivalent domains and chimeric Heavy chain-only antibodies with high neutralizing efficacy for scorpion toxin AahI'.* Molecular immunology, 2008. **45**(14): p. 3847-56.
27. Segvich, S.J., H.C. Smith, and D.H. Kohn, *The adsorption of preferential binding peptides to apatite-based materials.* Biomaterials, 2009. **30**(7): p. 1287-1298.
28. Addison, W.N., et al., *Phosphorylation-dependent mineral-type specificity for apatite-binding peptide sequences.* Biomaterials, 2010. **31**(36): p. 9422-30.
29. Chothia, C., et al., *Conformations of immunoglobulin hypervariable regions.* Nature, 1989. **342**(6252): p. 877-83.

Chapter 8

Controlled release of VHH targeting DKK1 from an injectable, thermo-reversible hydrogel

Emilie Dooms Rodrigues[1], Martin Piest[2], Maarten van Dijk[2], Mohamed El Khattabi[3], Jeroen Leijten[1], Clemens van Blitterswijk[4], Theo Verrips[3], Mike de Leeuw[2], Marcel Karperien[1]

[1] Department of Developmental BioEngineering, MIRA Institute for Biomedical Technology and Technical Medicine, Faculty of Science and Technology, University of Twente, Enschede, The Netherlands;
[2] InGell Laboratories BV, Groningen, The Netherlands;
[3] QVQ BV, Utrecht, The Netherlands;
[4] Department of Tissue Regeneration, MIRA Institute for Biomedical Technology and Technical Medicine, Faculty of Science and Technology, University of Twente, Enschede, The Netherlands.

Abstract

Wingless-type (Wnt) and bone morphogenetic protein (BMP) signaling pathways have been implicated in the pathophysiology of bone and cartilage. The identification of Dickkopf-related protein 1 (DKK1) as a mediator in bone and cartilage degeneration in malignancy and arthritis, respectively has led to an urge for anti DKK1 molecules. In this study we have identified llama derived antibody fragments (VHH) capable of binding and neutralizing DKK1 activity in a dose dependent manner. We have demonstrated the anti-DKK1 VHH's potential by rescuing DKK1 inhibited osteogenesis in an in vitro osteogenic differentiation assay.
Additionally, VHH were incorporated in an injectable thermo-reversible hydrogel, which can function as a reservoir for site-specific release of active biomolecules. Together they form an injectable drug delivery system where time and space of delivery of VHH can be controlled. Such drug depot formulation could be further developed for intra-articular application to treat arthritis.

Keywords: VHH, DKK1, Signaling pathway, Antagonist, Hydrogel, Drug release

Introduction

Cartilage and bone homeostasis is regulated by a dynamic system, in which many signaling pathways are balanced. A disrupted equilibrium leads to skeletal diseases. The Wingless-type (Wnt) signaling pathways play a pivotal role in maintaining joint homeostasis [1]. It has been reported that a decrease in cartilaginous Wnt signaling results in apoptosis and subsequent joint destruction [2]. In contrast, an increase in Wnt signaling drives the chondrocytes into hypertrophic differentiation, which induces an osteoarthritis-like phenotype and leads to joint failure [3]. This process is at least partly mediated via bone morphogenetic proteins (BMPs) [3].

Wnt signaling activity is a result of the balance between the activity of agonist and antagonists. Of these, the Wnt-antagonist Dickkopf-related protein 1 (DKK1) plays a major role in joint homeostasis [4] and is a master regulator of joint remodeling [5]. Specifically, plasma and synovial fluid levels of DKK1 are decreased in osteoarthritis and elevated in rheumatoid arthritis [6, 7]. Importantly, DKK1 is a secreted molecule, which antagonizes canonical Wnt signaling by interfering with the functional interaction between Wnts and low-density lipoprotein receptor (LRPs) receptors. Interference with DKK1 activity is considered a therapeutical option for degenerative joint diseases [8, 9].

Control over DKK1 levels can be achieved by means of neutralizing antibodies. However, conventional antibodies are large and complex molecules, which dictate a number of limitations in their application [10]. In contrast, single domain antibodies (VHH) have significant advantages over conventional antibodies. VHH are small peptide antibodies with high binding affinity for a desired target, are easy to clone as they consist of a single gene and are highly soluble and stable with reduced production costs. The stability of VHH and their relative resistance to chemical manipulation without losing bioactivity renders them excellent candidates for formulation in hydrogels to achieve controlled release [10-12]. Hydrogels have been widely reported for cartilage tissue regeneration. The incorporation of VHH in such a system would render a spatiotemporal controlled drug delivery system. Injectable hydrogels are of considerable interest as drug delivery systems in joint diseases since they can be applied in the joint minimally invasively by a single intra-articular injection [13]. Temperature-responsive gelling systems are emerging hydrogels able to undergo transitional changes in response to environmental stimuli [14, 15]. Temperature can be exploited to accomplish in situ gelling. In these systems gel formulations are soluble at room temperature facilitating injection and subsequently gel at body temperature restraining the gel at the injection site [16]. Thermo-reversible hydrogels composed of block co-polymers containing poly(ethylene glycol) (PEG) are of interest as drug delivery systems as they are biocompatible and degradable, whilst drug encapsulation and release properties are tunable. In particular, such thermo reversible hydrogels are already being investigated in oncology [17]. In analogy, VHH can be easily incorporated in such systems allowing the local delivery in the joint in need of treatment by intra-articular injection.

Here we present highly effective DKK1 neutralizing VHH, which allow for dose-dependent modulation of Wnt signaling. By incorporating these VHH in thermo reversible hydrogels sustained release of VHH was obtained. The versatility of these VHH makes them excellent candidates for treating joint disorders.

Materials and methods

Llama immunization and VHH phage library construction

A VHH phage display library was generated after the immunization of 2 llamas. The immunizations were performed according to the animal welfare regulations and were approved by a local medical ethical committee. Llamas were immunized with recombinant human DKK1 (DKK1, R&D systems, #5439-DK/CF) mixed with the adjuvant Stimune (CEDI Diagnostics, Lelystad, The Netherlands) and injected intramuscularly at days 0, 14, 28 and 35. The VHH phage display library was generated as previously described [18-20]. In brief, after the immunizations total RNA was extracted from peripheral blood lymphocytes, converted into complementary DNA and cloned in a phage-display plasmid.

Selection of VHH binding DKK1

Phage display [21] was used to select phages binding to DKK1 using an immunized llama VHH phage display library. The phages were selected via the panning method by coating a MaxiSorp plate (Nunc, Thermo Scientific) with decreasing concentrations of DKK1 (5 µg, 2 µg and 0.2 µg) in phosphate buffered saline (PBS, Gibco) at 4°C overnight. After blocking with 4% Marvel (dried skimmed milk, Premier International Foods) in PBS, the wells were incubated with the phage VHH immune library (approximately 10^{10} colony forming units (cfu))for 2 hours at room temperature. After thoroughly washing, the phage VHH clones were eluted with 150 µl of 100 mM triethylamine (TEA) for 15 minutes at room temperature and immediately neutralized by the addition of 50 µl of 1M Tris-HCl, pH 7.5. DNA information of the selected phages was rescued by infection of *Escherichia coli* (*E. coli*) TG1 strain and subsequent selection on agar plates for ampicillin resistance. To obtain recombinant bacteriophages expressing the VHH as fusion proteins with the bacteriophage gene III product, transformed TG1 *E. coli* were grown to logarithmic phase and then infected with helper phage VCSM13 (Stratagene, La Jolla, CA, USA). The phage particles were precipitated with polyethylene glycol (PEG) and used in the second panning round of selection on wells coated with DKK1 as described above. Selected phages from single colonies from the second and third round of selection were sequenced (Macrogen). The VHH clones selected were G5 and H7.

VHH plasmids, production and purification

Escherichia coli strain TG1 was used for the maintenance of the plasmids, infection of phages and expression of proteins. DNA information of the individually selected and isolated VHH were subcloned into plasmid pMEK219 containing C-terminal Myc and His tags. *E. coli* TG1 was grown in Luria Broth (LB) or Yeast extract and tryptone (YT) medium containing 2% (w/v) glucose and antibiotic, ampicillin 100 ug/ml. VHH were produced from *E. Coli* TG1 by Isopropyl β-D-1-thiogalactopyranoside **(**IPTG) lac promoter induction at 37^{o}C for 4 hours under non static conditions [22, 23]. VHH proteins were produced in *E. coli* TG1 and purified from the periplasmic fraction via the C-terminal His-tag by cobalt affinity chromatography (TALON His-Tag Purification Resin, ClonTech). Purified VHH were analyzed by means of sodium dodecyl sulfate polyacrylamide gel electrophoresis (SDS-PAGE). The final VHH concentration was determined from the UV absorption at 280 nm (NanoDrop 1000 Spectrophotometer, Thermo Scientific) and the theoretical mass extinction coefficient.

VHH binding specificity

To determine the binding specificity to DKK1, the purified VHH were tested in an ELISA assay. MaxiSorb plate wells were coated overnight at 4^{o}C, with DKK1 (60 nM) in PBS. After blocking of the wells with 4% Marvel in PBS, coated wells were incubated with a concentration range of VHH (0 – 7 μM) in 2% Marvel for 2 hours. The wells were washed with PBS Tween (PBS containing 0.5% (v/v) Tween-20, PBST) and PBS. Bound VHH were detected by incubation with a mouse anti-myc antibody (myc9E10) and a donkey anti-mouse antibody coupled to peroxidase. The amount of HRP was developed by the addition of Tetramethylbenzidine (TMB, 1-Step Ultra TMB-ELISA, Thermo Scientific). The reactions were stopped by the addition of H_2SO_4 and measured at 450 nm (Micro Plate Reader).

VHH biological activity

To assess the biological activity of the VHH, KS483-4C3 mouse progenitor cells were used as a model for osteogenic differentiation [24]. Cells were cultured in α-MEM (Gibco) supplemented with 10% fetal bovine serum (FBS; Cambrex), 100 U/ml penicillin (Gibco) and 100 μg/ml streptomycin (Gibco) and were incubated at 37 ºC in humidified atmosphere and 5% CO_2. To perform differentiation assays cells were seeded at a seeding density of 10 000 cells/cm^2 (day 0). Upon reaching confluence (day 4) cells were cultured for 3 days with ascorbic acid (50 ug/ml; Sigma Aldrich) and stimulated with BMP6 (100 ng/ml; R&D Systems) in the presence or absence of DKK1 (300 ng/ml; R&D Systems) with a concentration series of VHH G5 or H7 (0 – 70 nM). At day 7, cells were washed with PBS and lysed with CDPStar lysis buffer (Roche). To evaluate alkaline phosphatase (ALP) activity, cell lysate was added to CDPStar reagent (Roche) and luminescence was measured using Vector Microplate Luminometer (Promega). The luminescence units were corrected for DNA content. DNA concentration was determined using the CyQuant Cell Proliferation Assay (Invitrogen).

VHH in gel –VHH release and Gel degradation

VHH G5 with effective binding to DKK1 and relevant biological activity was incorporated in temperature-responsive gelling system composed of acetyl-capped poly(caprolactone-lactic acid)-poly(ethylene glycol)-poly(caprolactone-lactic acid) (PCLA-PEG-PCLA) triblock copolymers [13, 15]. Two polymers with varying caproyol/lactoyl ratio. Composition A consisted of ($PEG_{1500}(CAP_{80\%}/LAC_{20\%})_{2.2}(C_2)_2$) and composition B consisted of ($PEG_{1500}(CAP_{90\%}/LAC_{10\%})_{2.2}(C_2)_2$). Both compositions were synthesized by ring-opening polymerization of caprolactane and L-lactide in toluene using PEG as initiator and tin(II) 2-ethylhexanoate as catalyst. Subsequently, triblocks were end-capped by reacting in solution with an excess of acetyl chloride [13, 16].

Gels were formulated with 22.3 wt% polymer and 0.1 wt% VHH in PBS at pH 7.4 (300 mOsm/kg). Throughout the experiment the gels were kept under static conditions at 37°C. A total volume of 600 µl of pre warmed PBS was added on top of the gels. Periodically the supernatant was rescued and substituted with new pre warmed PBS. The VHH released from the gels over time was measured from the supernatant using ELISA. Degradation/ dissolution properties of temperature-responsive gelling systems were studied in vitro in PBS buffer at pH 7.4 and 37°C over a time span of 27 days.

Statistical Analysis

Statistical analyses were performed using GraphPad Prism version 5.00 for Windows, GraphPad Software (San Diego, California). Analyses were based on one-way ANOVA and a Tukey's Post-hoc test among all samples or between samples and controls. $p< 0.05$ was considered significant.

Results

Immunization of llamas and selection of VHH targeting DKK1

To obtain VHH targeting DKK1, llamas were immunized with recombinant DKK1 protein. Following the immunizations the VHH repertoire from peripheral blood lymphocytes was cloned into a phage vector generating an immunized VHH phage library. VHH binding to DKK1 were isolated using a direct selection strategy [25]. A total of three screening rounds of selection were performed on DKK1 coated plates. Between panning rounds the enrichment of phages binding to DKK1 was achieved. From the second and third panning round 14 monoclonal VHH were successfully isolated, expressed and sequenced. The amino acid sequences of the VHH show different clones from different families (Figure 1). The size and purity of the VHH were assessed by SDS-PAGE where single bands were detected of ca. 16 kDa, which is in agreement with values found in literature [26, 27]. From the 14 clones, clones G5 and H7 were recurrent and were therefore further characterized.

VHH	FR1	CDR1	FR2	CDR2
A7	EVQLVESGGGLVQAGGSLRLSCAAS	GSIVTFNP	MGWYRQAPGNQ--RELVASI	TSGG-GA
B7	EVQLVESGGGLVQAGGSLRLACAAS	GRTFSNYR	MGWFRQAPGQE--REFVAAI	SGSGSFT
B12	EVQLVESGGGLVQPGGSLRLSCAAS	GFTFSSYA	MSWVRQAPGKG--LEWVSAI	NSGGGST
C9	EVQLVESGGGLVQPGGSLRLSCVVS	GFTISNYG	MSWVRQAPGKGPEWEWVSAI	NSGGDST
D4	EVQLVESGGGLVQAGDSLRLSCAAS	GRSISLYA	MAWFRQAAGKE--REFVAAI	NWSGGST
G5	**EVQLVESGGGLVQAGGSLRLSCAAS**	**GRALSRSP**	**MAWFRQAPGKE--REFVVHW**	**ISG--ST**
H7	**EVQLVESGGGLVQAGGSLRLSCAAS**	**G---STGA**	**MAWFRQAPGKE--RDLVASI**	**SRSGVST**

VHH	FR3	CDR3	FR4
A7	NYVDSVKGRFTISVDSAKNTVYLQMNSLKPEDTAVYYCNA	D---------IFSSSRLSWDNY	WGQGTQVTVSS
B7	YYADSVKGRSTISRDNAKNTVYLQMNSLKPEDTAVYYCGA	G------VHLGAATSYTRYD-F	WGQGTQVTVSS
B12	SYADSVKGRFTISRDNAKNTLYLQMNSLKPEDTAVYRCAK	----YYEADP----AKNEYD-Y	WGQGTQVTVSS
C9	RYADSVKGRFTISRDNAKNTLYLQMNSLKPEDAAVYFCTR	EKTAYYCSGSGCYDPRYEFD-Y	WGRGTQVTVSS
D4	RYADSVKGRFSISRDTAKNTVYLTMNSLKPEDTAVYYCAT	DSS----TTVVFYSSSNSLR-Y	WGQGTQVTVSS
G5	**YYADSVKGRFTTSRDNAENTVYLQMNSLKPEDTAVYYCAA**	**GFA---PDTPSIFTSPRTYY-Y**	**WGQGTQVTVSS**
H7	**YYADSVKVRFTISRDNAKNTVFLQMNNLKPEDTGVYYCAA**	**G--------PTFRQSRATYT-D**	**WGQGTQVTVSS**

Figure 1. Amino acid sequence alignment of VHH targeting DKK1 derived from a llama immunized library. Sequencing of the 14 isolated clones resulted in the identification of 7 unique clones. The sequence numbering is according to Chothia [31] according to whom the different framework residues (FR) and complementary-determining region (CDR) are identified. The sequences of G5 and H7 are highlighted in bold.

Selected VHH bind DKK1

VHH G5 and H7 were tested for their binding characteristics for DKK1 in a solid phase ELISA. To determine the affinity between VHH and DKK1 a titration series of VHH over a range of 0.7 nM to 7 nM was performed while DKK1 coating was kept constant at 60 nM throughout the series. When binding of VHH to DKK1 occurred a change in signal was measured (Figure 2). VHH G5 and H7 bound to DKK1 in a dose dependent manner. Both VHH display a similar binding curve. Saturation of the DKK1 coated surface is reached for VHH concentrations higher than 10 μM for both VHH. Subsequent fitting of experimental data to specific binding models yielded dissociation constants of Kd 5.9 x 10^{-8} M and Kd 1.1 x 10^{-7} M for VHH G5 and H7 respectively. The binding constants obtained from the indirect measurement via ELISA were comparable with literature [28, 29].

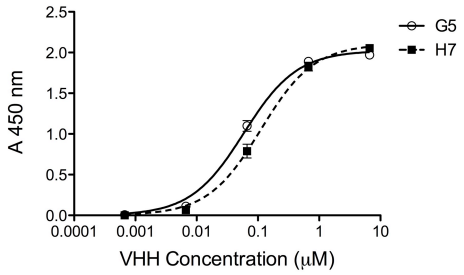

Figure 2. VHH G5 and H7 bind to DKK1. A concentration range of VHH G5 and H7 was incubated in wells coated with DKK1 (60 nM) or PBS (negative control). After several washes, bound VHH were detected with a mouse anti-VHH serum and a Donkey anti-rabbit antibody coupled to a peroxidase. The amount of converted HRP (Absorbance at 450 nm; A 450 nm) is proportional to the amount of bound VHH. Error bars represent standard deviation (N=3).

VHH neutralize DKK1

Next, we examined whether the selected VHH would modulate DKK1 biological activity. The biological activity of the selected VHH was tested *in vitro* on murine KS483-4C3 mesenchymal precursor cells induced to express Alkaline Phosphatase (ALP) after treatment with BMP6. BMP induced ALP expression is mediated via canonical Wnt-signaling [3]. Indeed co-treatment of cells with BMP6 and DKK1 effectively abrogated ALP induction (Figure 3A). This inhibition could be reversed by the addition of VHH G5 or H7 in a dose dependent manner (Figure 3B and 3C). Both VHH showed effective neutralization of DKK1 in this bioassay.

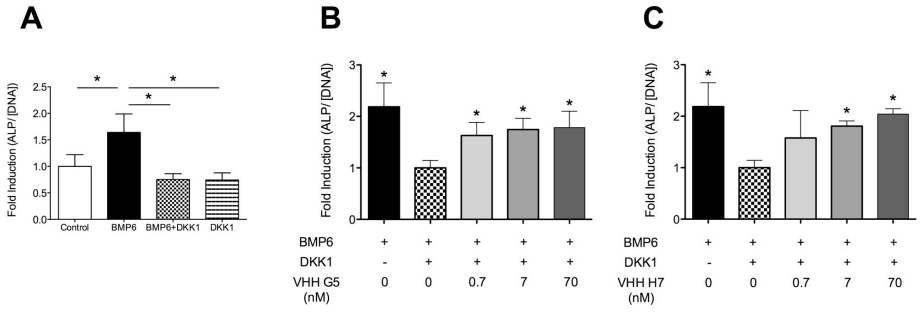

Figure 3. VHH neutralize DKK1 activity. (A) Addition of BMP6 stimulates ALP expression in KS483-4C3 cells. The co-incubation of BMP6 with DKK1 reversed the ALP expression back to basal levels. The addition of DKK1 to the standard cell culture did not show any significant difference in ALP expression when compared with control. The ALP activity is normalized by the total DNA content of KS483 cells after 7 days of culture, and expressed as fold induction relative to control. (B, C) KS483-4C3 cells were stimulated with BMP6, DKK1 and VHH G5 (B) or VHH H7 (C) in a concentration range of 0 – 70 nM. Co-incubation of VHH with DKK1 and BMP6 reversed DKK1 mediated inhibition of BMP6 induced ALP activity in a dose-dependent manner demonstrating effective neutralization of DKK1 activity by the VHH G5 and H7. ALP activity was measured and expressed as relative enzyme activity corrected for DNA, and expressed as fold induction relative to BMP6/ DKK1/ VHH (+/+/-). * $p < 0.05$. (N=3).

VHH release profiles and gel degradation

VHH G5 was incorporated in two different injectable thermo reversible gel formulations (A and B) and the *in vitro* release kinetics of VHH and gel degradation were assessed. A 22.3 wt% polymer (A or B) and 0.1 wt% VHH formulation were prepared. It was observed that polymer A formed a transparent gel, whilst polymer B formed a white gel. Both formulations were liquid solutions at room temperature and immobile gels at 37º C.

The release of VHH from gel A showed a sustained release throughout the time span of the experiment, up to 3-4 weeks (Figure 4A). The release profile of VHH from gel A appeared to be linear. A 75% release was obtained after 27 days of incubation in PBS. The release of VHH from gel B showed a significant initial burst release of about 50% during the first week of incubation in PBS followed by a slower release reaching a VHH release plateau of 75% (Figure 4B). The degradation of the triblock copolymer gels supplemented with VHH was investigated at 37º C in PBS buffer (pH 7.4). For gel A, wet gel weight remained overall constant for the five initial days of incubation, and thereafter increased, i.e. gel A swelled. The swelling phase was followed by a drop in wet weight to 60% after 27 days of incubation.

For gel B, an overall decrease in wet weight was observed throughout the experimental time span reaching 70% after 27 days of incubation.

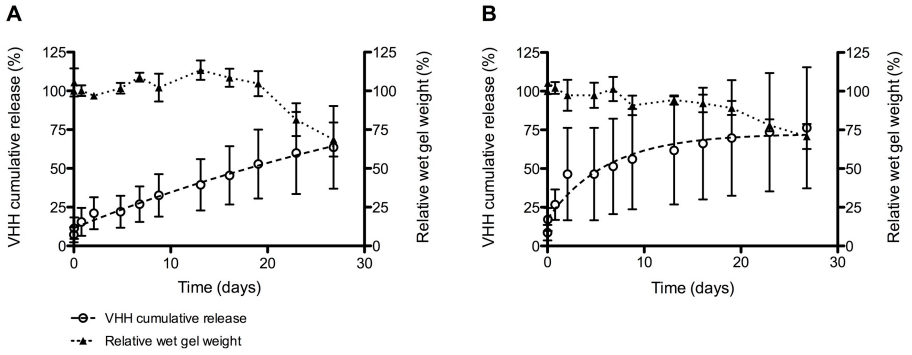

Figure 4. VHH loaded gels: VHH release and gel degradation. Percentage cumulative mass release profile of gel loaded VHH (primary y-axis) and percentage weight loss of gels during in vitro degradation (secondary y-axis) as a function of time. Gels were prepared with 22.3 wt% polymer and 0.1 wt% VHH. (A) Gel A ($PEG_{1500}(CAP_{80\%}/LAC_{20\%})_{2.2}(C_2)_2$) VHH-loaded over a time span of 27 days. (B) Gel B ($PEG_{1500}(CAP_{90\%}/LAC_{10\%})_{2.2}(C_2)_2$) VHH-loaded over a time span of 27 days. Data are expressed as mean +/- standard deviation (N=4).

Discussion

DKK1 has been described as an important molecule in the maintenance of cartilage homeostasis through its role in the regulation of the Wnt/ βcatenin-signaling pathway[4]. Anti DKK1 strategies are relevant for clinical applications since high levels of DKK1 in serum or synovial fluid are related with rheumatoid arthritis and osteolytic lesions of multiple myeloma [8, 30]. DKK1 hampers the regenerative potential of bone and/or cartilage by blocking canonical Wnt-signaling. In this manuscript we have investigated the possibility of using VHH antibodies to control DKK1 activity as a possible therapeutic strategy in degenerative joint disease.

The immunization of llamas with recombinant human DKK1 was successful leading to the selection, isolation by means of phage display and production of monoclonal VHH specifically targeting DKK1. Interestingly, the clones selected were recurrent even from different rounds of selection suggesting that these VHH sequences were generated upon immunization of llamas with DKK1.

Furthermore, we demonstrated the ability of the VHH to specifically bind to DKK1 and revealed their potential to modulate its biological activity in a dose dependent manner. In line with literature, in which BMP induced ALP activity in osteoblasts is dependent on canonical wnt signaling [3], we here demonstrated that the inhibitory role of DKK1 in this process could be blunted by addition of the VHH in a dose-dependent manner. The control over DKK1 neutralization can be further tuned by the reverse engineering of the selected VHH to improve the binding affinity even further as well as by tight control of the VHH concentration. The latter can be achieved by an adequate delivery system in the body.

In the present study we identified two VHH with DKK1 neutralizing properties. Although the binding site of the VHH to DKK1 has not been identified yet it can be hypothesized that the binding site of VHH to DKK1 does interfere with the binding of DKK1 with LRP-5 and 6 co-receptor on cell surface and prevent activation of the signaling pathways. Crystallography, proteomics and competition assays will allow clearer insight and further characterization of the VHH.

The function of VHH can be spread to several applications owed to their versatility. VHH can be engineered for incorporation in biomaterials such as hydrogels. Hydrogels have been widely reported for cartilage tissue regeneration. Here we incorporated VHH targeting DKK1 in thermo reversible gel formulations. Acetyl capped PCLA-PEG-PCLA triblock copolymers form micelles in aqueous medium [13]. At low temperatures the micelles are dispersed in an aqueous solution and can be mixed-in with drugs and homogeneously injected. The hydrophobicity and solubility of the drugs mixed-in determine if the drug resides either in the micelles or between the micelles. Upon injection, at body temperature, changes in physical interactions occur and the hydrophobic character of the amphiphilic triblock copolymers dominates leading to aggregation of the micelles, thus gel formation [13, 15]. Our strategy allows for the incorporation of anti DKK1 VHH in PCLA-PEG-PCLA thermo reversible gel to

guarantee local delivery in the knee joint and improved therapy efficacy where no super physiological concentrations would be required. The release mechanism of VHH from the thermo reversible gels A and B is diffusion controlled. VHH, mostly hydrophilic proteins, must diffuse through the micelles through tortuous pathways in order to exit the matrix. In gel A the VHH release is controlled and sustained. In contrast in gel B, an initial burst release was observed. Gel B, crystalizes leading to a decrease in gel wet weight expelling aqueous solution out of the matrix together with the VHH evidenced by shrinking of the gel which is the likely cause of the observed initial burst release. The crystallinity in gel B is due to a higher ratio of caproyl/lactoyl (CAP/LAC) [13, 15, 16]. The degradation time increases with crystallinity [15], which is in line with the results obtained. Nevertheless, experimental data should be collected until complete degradation of gels. This system allows for a delivery of VHH over a prolonged period of time (four weeks). This is particularly important for VHH due to their fast clearance from the body upon injection in the blood stream resulting in a short half life. Although sustained release over 4 weeks was achieved we do not have data indicating whether the VHH retained its bioactivity after incorporation in the gel formulations over the whole release period. Unlike growth factors, which are inherently unstable, VHH are extremely stable and resistant to mild chemical reactions [10-12]. It therefore seems likely that the VHH retained its bioactivity. More detailed follow-up studies are warranted to confirm if the bioactivity of VHH is retained.

In order to treat degenerative joint diseases, a drug depot can be injected in the synovial fluid ensuring prolonged and controlled delivery of VHH locally in the diseased joint. As Leijten reported (manuscript in preparation), high DKK1 levels were found in synovial fluid and serum from an inflamed intercarpal joint, an established horse model, leading to joint inflammation and catabolic activity in the cartilage [30]. Thermo reversible hydrogels loaded with VHH, targeting DKK1, could be tested in these horse models. The system presented here allows for a protein friendly technology and tailored release behavior.

Taken together, we here presented a strategy aimed at modulating DKK1 levels by VHH. We demonstrate the feasibility of achieving sustained release of VHH over a period of four weeks by incorporation in an injectable thermo reversible hydrogel. Upon intra-articular injection, this drug depot opens an avenue for treating degenerative joint diseases locally avoiding side effects associated with systemic application by substantially reducing the dosage of VHH required for obtaining a therapeutic effect.

Acknowledgements

This work was supported by project P2.02 OAControl of the research program of the BioMedical Materials Institute, co-funded by the Dutch Ministry of Economic Affairs, Agriculture and Innovation. This work was supported by a long term program research grant of the Dutch Arthritis Association to MK.

References

1. Kamiya, N., et al., *Wnt inhibitors Dkk1 and Sost are downstream targets of BMP signaling through the type IA receptor (BMPRIA) in osteoblasts.* Journal of bone and mineral research : the official journal of the American Society for Bone and Mineral Research, 2010. **25**(2): p. 200-10.
2. Zhu, M., et al., *Inhibition of beta-catenin signaling in articular chondrocytes results in articular cartilage destruction.* Arthritis and rheumatism, 2008. **58**(7): p. 2053-64.
3. Zhu, M., et al., *Activation of beta-catenin signaling in articular chondrocytes leads to osteoarthritis-like phenotype in adult beta-catenin conditional activation mice.* Journal of bone and mineral research : the official journal of the American Society for Bone and Mineral Research, 2009. **24**(1): p. 12-21.
4. Leijten, J.C., et al., *Gremlin 1, frizzled-related protein, and Dkk-1 are key regulators of human articular cartilage homeostasis.* Arthritis and rheumatism, 2012. **64**(10): p. 3302-12.
5. Diarra, D., et al., *Dickkopf-1 is a master regulator of joint remodeling.* Nature Medicine, 2007. **13**(2): p. 156-163.
6. Honsawek, S., et al., *Dickkopf-1 (Dkk-1) in plasma and synovial fluid is inversely correlated with radiographic severity of knee osteoarthritis patients.* BMC musculoskeletal disorders, 2010. **11**: p. 257.
7. Voorzanger-Rousselot, N., N.C. Ben-Tabassi, and P. Garnero, *Opposite relationships between circulating Dkk-1 and cartilage breakdown in patients with rheumatoid arthritis and knee osteoarthritis.* Annals of the Rheumatic Diseases, 2009. **68**(9): p. 1513-1514.
8. Gregory, C.A., et al., *How Wnt signaling affects bone repair by mesenchymal stem cells from the bone marrow.* Stem Cell Biology: Development and Plasticity, 2005. **1049**: p. 97-106.
9. Zhou, F., et al., *Dickkopf-1 is a key regulator of myeloma bone disease: Opportunities and challenges for therapeutic intervention.* Blood reviews, 2013.
10. Harmsen, M.M. and H.J. De Haard, *Properties, production, and applications of camelid single-domain antibody fragments.* Appl Microbiol Biotechnol, 2007. **77**(1): p. 13-22.
11. Dumoulin, M., et al., *Single-domain antibody fragments with high conformational stability.* Protein Science, 2002. **11**(3): p. 500-515.
12. van der Linden, R.H., et al., *Comparison of physical chemical properties of llama VHH antibody fragments and mouse monoclonal antibodies.* Biochimica et biophysica acta, 1999. **1431**(1): p. 37-46.
13. Petit, A., et al., *Modulating rheological and degradation properties of temperature-responsive gelling systems composed of blends of PCLA-PEG-PCLA triblock copolymers and their fully hexanoyl-capped derivatives.* Acta Biomaterialia, 2012. **8**(12): p. 4260-4267.
14. Vermonden, T., R. Censi, and W.E. Hennink, *Hydrogels for protein delivery.* Chemical reviews, 2012. **112**(5): p. 2853-88.
15. Petit, A., et al., *Effect of polymer composition on rheological and degradation properties of temperature-responsive gelling systems composed of acyl-capped PCLA-PEG-PCLA.* Biomacromolecules, 2013. **14**(9): p. 3172-82.
16. Sandker, M.J., et al., *In situ forming acyl-capped PCLA-PEG-PCLA triblock copolymer based hydrogels.* Biomaterials, 2013. **34**(32): p. 8002-8011.
17. Elstad, N.L. and K.D. Fowers, *OncoGel (ReGel/paclitaxel)--clinical applications for a novel paclitaxel delivery system.* Advanced drug delivery reviews, 2009. **61**(10): p. 785-94.
18. Frenken, L.G., et al., *Isolation of antigen specific llama VHH antibody fragments and their high level secretion by Saccharomyces cerevisiae.* J Biotechnol, 2000. **78**(1): p. 11-21.

19. Roovers, R.C., et al., *Efficient inhibition of EGFR signaling and of tumour growth by antagonistic anti-EFGR Nanobodies.* Cancer Immunol Immunother, 2007. **56**(3): p. 303-317.
20. Strokappe, N., et al., *Llama Antibody Fragments Recognizing Various Epitopes of the CD4bs Neutralize a Broad Range of HIV-1 Subtypes A, B and C.* Plos One, 2012. **7**(3).
21. Hoogenboom, H.R., et al., *Antibody phage display technology and its applications.* Immunotechnology, 1998. **4**(1): p. 1-20.
22. Saerens, D., et al., *Single domain antibodies derived from dromedary lymph node and peripheral blood lymphocytes sensing conformational variants of prostate-specific antigen.* J Biol Chem, 2004. **279**(50): p. 51965-72.
23. Roovers, R.C., et al., *High-affinity recombinant phage antibodies to the pan-carcinoma marker epithelial glycoprotein-2 for tumour targeting.* Br J Cancer, 1998. **78**(11): p. 1407-16.
24. van der Horst, G., et al., *Downregulation of Wnt signaling by increased expression of Dickkopf-1 and -2 is a prerequisite for late-stage osteoblast differentiation of KS483 cells.* J Bone Miner Res, 2005. **20**(10): p. 1867-77.
25. Forsman, A., et al., *Llama antibody fragments with cross-subtype human immunodeficiency virus type 1 (HIV-1)-neutralizing properties and high affinity for HIV-1 gp120.* J Virol, 2008. **82**(24): p. 12069-81.
26. Wesolowski, J., et al., *Single domain antibodies: promising experimental and therapeutic tools in infection and immunity.* Med Microbiol Immunol, 2009. **198**(3): p. 157-74.
27. de Marco, A., *Biotechnological applications of recombinant single-domain antibody fragments.* Microbial cell factories, 2011. **10**: p. 44.
28. Hulsik, D.L., et al., *A gp41 MPER-specific Llama VHH Requires a Hydrophobic CDR3 for Neutralization but not for Antigen Recognition.* Plos Pathogens, 2013. **9**(3).
29. Muyldermans, S., *Nanobodies: natural single-domain antibodies.* Annual review of biochemistry, 2013. **82**: p. 775-97.
30. Leijten, J., et al., *GREM1, FRZB and DKK1 mRNA levels correlate with osteoarthritis and are regulated by osteoarthritis-associated factors.* Arthritis research & therapy, 2013. **15**(5): p. R126.
31. Chothia, C., et al., *Conformations of immunoglobulin hypervariable regions.* Nature, 1989. **342**(6252): p. 877-83.

Chapter 9

Selection strategies for VHH targeting osteoarthritic cartilage

Emilie Dooms Rodrigues[1], Lucy Rutten[2], Mohamed El Khattabi[2], Clemens van Blitterswijk[3], Theo Verrips[2], Marcel Karperien[1]

[1] Department of Developmental BioEngineering, MIRA Institute for Biomedical Technology and Technical Medicine, Faculty of Science and Technology, University of Twente, Enschede, The Netherlands;
[2] QVQ BV, Utrecht, The Netherlands;
[3] Department of Tissue Regeneration, MIRA Institute for Biomedical Technology and Technical Medicine, Faculty of Science and Technology, University of Twente, Enschede, The Netherlands.

Abstract

Osteoarthritis (OA) is a degenerative disease of the joints. The etymology of the word has its origins in Ancient Greek: osteo- “bone”, arthro- “joint” and –itis “inflammation”. Osteoarthritis is one of the most common types of arthritis leading to chronic musculoskeletal pain and disability. The main causes of osteoarthritis are related to the wear and/or trauma of cartilage. Currently available treatments only alleviate pain symptoms. At end stage disease total joint replacement is a realistic treatment option. At present early detection of disease due to the lack of appropriate biomarkers is not possible and no treatments exist that can reverse cartilage damage in OA.
Targeting of biomarkers relevant in diseases is a strategic approach for a therapeutic treatment. In this study we explored two strategies to select single domain antibodies (VHH) that can bind to osteoarthritic or healthy cartilage. A non-immunized phage library of the llama was used for isolation of VHH with specific affinity for macroscopically looking healthy human cartilage isolated *post-mortem* or arthritic cartilage derived from an arthroplasty. Different phage display strategies were used including a cross selection on millimeter sized cartilage cubes and on cartilage cryotome sections. No proper VHH binding to cartilage was identified. In an alternative strategy a VHH was engineered by inserting in its complementary determining region 3 (CDR3) a previously identified peptide sequence targeting collagen type II. Despite successful production, this engineered VHH did not show improved binding to collagen type II.
Challenges still need to be overcome for the successful selection of VHH targeting healthy or diseased cartilage.

Keywords: Cartilage, OA, Target, VHH, Peptide, Biomarkers, Strategies

Introduction

Osteoarthritis (OA) is a degenerative disease of the joints. OA is the most common type of arthritis and causes chronic musculoskeletal pain and disability. It is a severe global medical and socio-economic problem. Cartilage has an inherent limited vasculature and capacity to heal, hence damaged cartilage, due to trauma or age related wear, gradually progresses towards OA [1]. The complete understanding of the mechanisms underlying OA is yet to be elucidated. There is an unmet need of biomarkers specific for each phase of the evolution of the disease.

The poor capacity of self-repair of cartilage defects resulted in the development of therapies, which rely on reducing pain or in case of focal cartilage defects in cell therapy like autologous chondrocyte transplantation (ACT). At end stage disease total joint replacement is an established solution [2]. ACT requires *in vitro* expansion of chondrocytes, isolated from a biopsy, which are later transplanted in the patient to fill the cartilage defect. The transplantation of the expanded chondrocytes can be done with or without the assistance of a scaffold. While this treatment has been applied successfully in many patients, its long term effect is still less clear [2]. At end stage disease total joint replacement, although rather effective, is only performed in elder patients due to the limited life span of the prosthesis and complications associated with revision surgery.

Controlled targeting of OA cartilage is a strategy, which offers a wide range of applications and treatment possibilities. Targeting of OA would allow for controlled delivery of anti-catabolic or even anabolic compounds without the use of supraphysiological doses required in systemic application thereby diminishing possible side effects. In addition, the presence of a targeting agent would allow the monitoring of the evolution of the disease.

Antibodies are the most frequently used biomolecules for targeting of epitopes in diseased tissue. However, the complexity of conventional antibodies does not allow for an easy genetic manipulation. In contrast, single domain antibodies (VHH) are a good alternative. VHH are uniquely small antibodies capable of binding specifically to an antigen, are easy to clone as they consist of a single gene, are easy to produce and are stable and soluble [3]. These characteristics make them appealing instruments for application in a targeting system.

In this study, we explored two strategies for the selection and identification of VHH that bind cartilage in general and VHH that specifically target healthy or arthritic cartilage.

Materials and Methods

Histological analysis of cartilage samples

For histological examination, healthy human cartilage isolated *post-mortem* and arthritic looking cartilage derived after an arthroplasty were embedded in cryomatrix (Cryomatrix, Shandon) and deep frozen. Ten micrometer sections were cut using a rotary

microtome (HM355S Microm International). The cryomatrix was washed by incubation in distilled water for 10 minutes. Sections were stained for glycosaminoglycans using 0.5% Alcian Blue in H_2O (pH adjusted to 1 using HCl) for 30 minutes and counterstained with 1% Nuclear Fast Red in 5% aluminum sulfate for 5 minutes, Toluidine blue (Fluka, 0.1% in deionized water) incubated for 10 minutes, Safranin O (Sigma, 0.1% in deionized water) incubated for 5 minutes and Haematoxylin incubated for 6 minutes and eosin for 2 minutes. Samples were then mounted and analyzed using optical microscopy (Nikon).

Selection of VHH targeting cartilage

VHH binders towards healthy or osteoarthritic cartilage were selected from a non-immunized llama VHH phage library (kindly provided by BAC BV). The construction of the non-immune library has been described before [4]. A two round selection was performed on millimeter cubes of cartilage or on microtome sections of cartilage. Phages (approximately 10^{12} colony forming units (cfu)), were incubated for two hours at room temperature or at 4ºC with cartilage samples. After thorough washing with phosphate buffered saline containing 0.05% Tween-20 (PBST), bound phages were (i) eluted by incubation in 100 µl of 100 mM triethylamine (TEA) for 15 minutes at room temperature and neutralized with the addition of 50 µl of 1M Tris-HCl, pH 7.5, (ii) eluted with 100 µl of trypsine (1 mg/ml) for 30 minutes at room temperature and neutralized with 50 µl of trypsine inhibitor (2 mg/ml) or (iii) directly used from the cartilage samples for infection of bacteria. DNA information of the selected phages was rescued by infection of *Escherichia coli* TG1 strain and subsequent selection on agar plates for ampicillin resistance. To obtain recombinant bacteriophages expressing the VHH as fusion proteins with the bacteriophage gene III product, transformed *E. coli* TG1 were grown to logarithmic phase and then infected with helper phage VCSM13 (Stratagene, La Jolla, CA, USA). The phage particles were precipitated with polyethylene glycol (PEG) and used in the second round of panning selection on cartilage samples as described above (Figure 1). A total of four rounds of panning were performed in cartilage samples. Polyclonal VHH were tested for binding to cartilage samples and cartilage compounds.

Production and purification of the VHH

E. coli strain TG1 was used for the maintenance of the plasmids, infection by the phages and expression of proteins. The plasmid pUR8100 contained the DNA information of the individually selected VHH as well as a Myc and His tags at the C-terminus used for detection and purification.

E. coli TG1 was grown in Luria Broth (LB) or yeast extract and tryptone (YT) medium containing 2% (w/v) glucose and ampicillin (100 µg/ml). VHH were expressed in *E. coli* TG1 after addition of 1 mM Isopropyl β-D-1-thiogalactopyranoside (IPTG). VHH were produced for 4 hours at 37ºC [5, 6]. VHH proteins were purified from the periplasmic fraction via the C-terminal His-tag by cobalt affinity chromatography (TALON His-Tag Purification Resin, ClonTech). Purified VHH were analyzed by sodium dodecyl sulfate

polyacrylamide gel electrophoresis (SDS-PAGE). The final VHH concentration was determined by UV absorption at 280 nm (NanoDrop 1000 Spectrophotometer, Thermo Scientific).

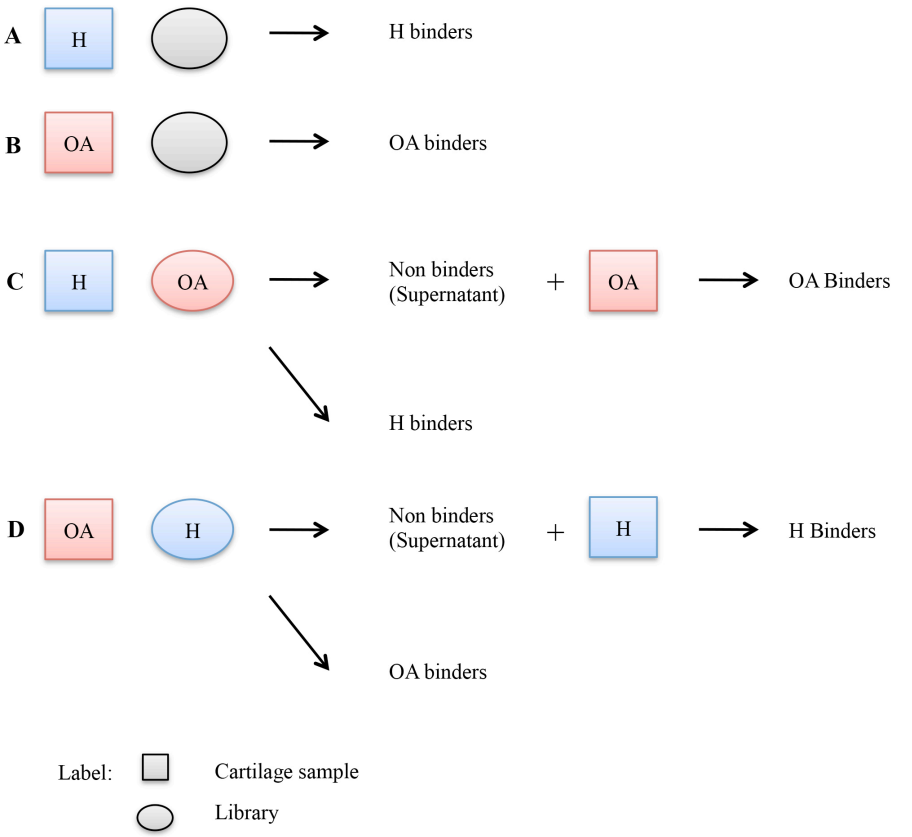

Figure 1. Schematic outline of selection procedures tried on the cartilage specimens. A and B represent a regular selection whilst C and D represent a subtractive selection. (A) Incubation of healthy cartilage with non-immunized library. (B) Incubation of OA cartilage with non-immunized library. (C) Incubation of healthy cartilage with OA binders from B. (D) Incubation of OA cartilage with H binders from A.

Binding specificity of VHH

Binding of VHH to cartilage sections was assessed by DAB Substrate (metal precipitation). Ten micrometer sections (described above) were fixed with pre-cooled acetone for 10 minutes and washed with PBS. Sections were incubated in 0.3% H_2O_2 solution in PBS at room temperature for 20 minutes to block endogenous peroxidase activity. A rabbit anti-VHH serum (K976) in 0.5% BSA in PBS was used as a primary antibody and incubated at room temperature for one hour. After washing with PBS, a

donkey anti-rabbit antibody coupled to a peroxidase was added to the sections and incubated for 30 minutes at room temperature. DAB substrate solution was added to the sections and the color was allowed to develop by incubating up to 15 minutes. Slides were rinsed with PBS, mounted analyzed using optical microscopy (Nikon).
In alternative strategy, binding specificity of the polyclonal VHH to cartilage compounds was tested in an enzyme-linked immunosorbent assay (ELISA) binding assay. 96-wells MaxiSorp (Nunc) and PolySorp (Nunc) microtiter plate wells were coated with collagen type I (Elastin Products Co, Inc), sodium hyaluronate (Lifecore Biomedical), heparin sodium (Celsus Laboratories) and collagen type X (Sigma) and blocked with 2% BSA in PBS for two hours at room temperature to achieve blocking of non specific binding sites. Subsequently, wells were incubated with a serial dilution of polyclonal VHH (ranging from 0 to 100 μg/ml) from the 4^{th} round of selection in 1% BSA in PBS for two hours at room temperature. The wells were washed with PBST and PBS. Bound VHH were detected by incubation with the mouse anti-myc antibody mAb 9E10 and a donkey anti-mouse antibody coupled to a peroxidase. The amount of HRP was developed by the addition of Tetramethylbenzidine (TMB, 1-Step Ultra TMB-ELISA, Thermo Scientific). The reactions were stopped by the addition of H_2SO_4 and measured at 450 nm (Micro Plate Reader).

Grafting peptide sequence in VHH CDR3
The peptide sequence WYRGRL targeting bovine collagen type II was grafted in the complementary determining region 3 (CDR3) of a VHH framework. The sequence has been previously identified [7]. The peptide sequence was introduced in the CDR3 of VHH C2, anti-BMP. After modeling of the predicted constructs and CDR3 interactions with I-TASSER [8-10] and SWISS MODEL [11-13] the gene was synthesized by GeneArt® (Invitrogen/LifeTechnologies). To facilitate the cloning of the fragment into the expression plasmid pMEK222 vector, unique restriction sites *Sfi*I and *Bst*EII were introduced at the 5'and 3'end of the VHH construct. Furthermore, the coding sequence of the gene was optimized for optimal expression in *E. coli*. Expression plasmid pMEK222 contains a C-terminal FLAG and His6 tag. The engineered VHH, VHH-Col2, was then produced in *E. coli*. The purified proteins were tested by means of ELISA to evaluate the binding characteristics of the new construct. In addition, the collagen peptide sequence, pep-Col2, was synthesized with a biotin for detection purposes.

VHH-Col2 binding
Binding of the purified VHH-Col2 to collagen type II was tested in an ELISA binding assay. MaxiSorp and PolySorp (Nunc) plates were coated overnight at 4^{o}C with collagen type II from human and bovine (2 mg/ml). After blocking of the wells with 4% Marvel in PBS, a concentration range of VHH (ranging from 0 to 100 μg/ml) in 2% Marvel or biotinylated peptide sequence, pep-Col2, (7 μg/ml) were incubated for one hour in the coated and blocked wells. The wells were washed with PBST and PBS. Bound VHH were detected by incubation with a mouse anti-FLAG and a donkey anti-mouse antibody

coupled to a peroxidase. Bound peptides, pep-Col2, were detected by incubation with HRP streptavidin. Collagen coating of the wells was detected by incubation of a mouse anti-human collagen type II (AbNova) and donkey anti-mouse antibody coupled to a peroxidase. The amount of HRP was developed by the addition of TMB (Ultra TMB-ELISA, Thermo Scientific). The reactions were stopped by the addition of H_2SO_4 and measured at 450 nm (Micro Plate Reader).
Alternatively, cartilage sections from bovine and human were used for detection of binding of VHH-Col2. Cartilage sections were cut using a rotary microtome as described above. The ten micrometer sections were incubated with 0.3% H_2O_2 solution in PBS at room temperature for 20 minutes to block endogenous peroxidase activity. We next incubated the sections with the engineered VHH construct, VHH-Col2, (100 μg/ml) for two hours at room temperature. After washing with PBS, a donkey anti-rabbit antibody coupled to a peroxidase was added to the sections and incubated for 30 minutes at room temperature. DAB substrate solution was added to the sections and allowed the color to develop by incubating up to 15 minutes. Slides were rinsed with PBS, mounted analyzed using optical microscopy (Nikon).

Results and discussion

A major problem of applying a targeted delivery of anti-catabolic or anabolic treatments for arthritis is the lack of specific biomarkers. Collagen type II is specific to cartilage and therefore targeting of cartilage would already allow for a more narrowed targeting therapy and limited side effects. Although cartilage is a complex tissue, there is a need to identify biomarkers specific to healthy and arthritic cartilage.
By selection of VHH specifically targeting healthy or arthritic cartilage or by combining a high affinity peptide sequence in a highly produced stable molecule with small size, it is theoretically possible to engineer a powerful tool for targeted drug delivery system.

Healthy and osteoarthritic cartilage
Biopanning of VHH phage display library from a non-immunized library was carried out on healthy human cartilage isolated *post-mortem* and arthritic looking cartilage derived after an arthroplasty.
First, the macroscopic structural differences of the cartilage samples were assessed by histological analysis (Figure 2). It was observed that the arthritic cartilage harvested from the affected area of the osteoarthritic joint from an arthroplasty revealed clear signs of degeneration and degradation (Figure 2A) when compared with healthy cartilage sample (Figure 2B). The arthritic looking cartilage showed clear signs of fibrillation and was severely damaged and expressed reduced GAGs. *Post-mortem* donors are a significant source of normal cartilage tissue. The state of the cartilage is crucial for an appropriate selection and specificity of the VHH to healthy *versus* osteoarthritic cartilage.

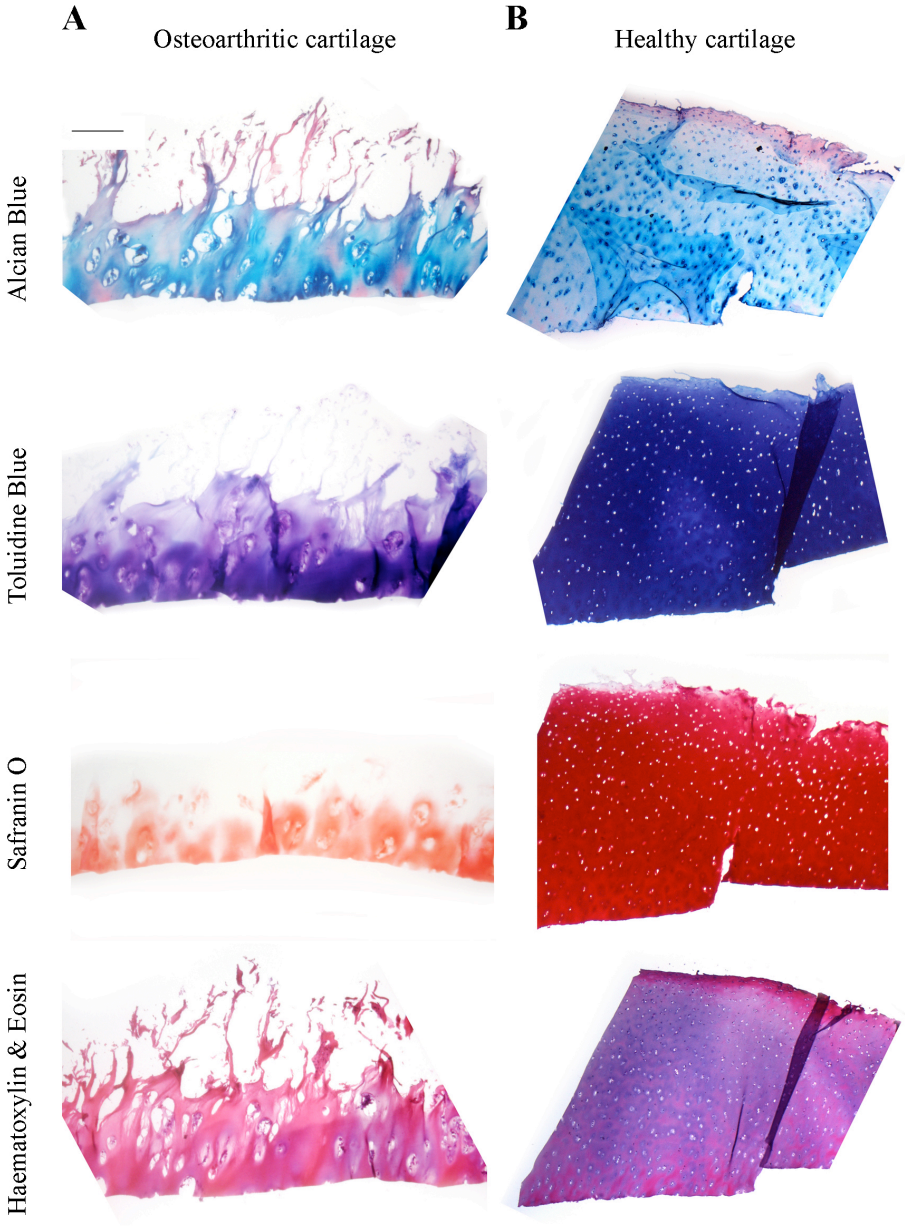

Figure 2. Histological analysis of macroscopically (A) arthritic cartilage derived after an arthroplasty and (B) healthy looking human cartilage isolated *post mortem*. Scale bar represents 0.25 mm.

Targeting OA cartilage with VHH by phage display

Non-immunized libraries were utilized for a series of biopanning steps on healthy and osteoarthritic human cartilage from different donors and donor sources. The selection of strongly-bound phages was refined by several rounds of biopanning with elution of phages in between each step. Different phage display strategies were used including a cross selection and subtractive selection where putative binders of healthy cartilage were incubated with osteoarthritic cartilage to exclude as much as possible common binders (Figure 1). The selections were performed on millimeter cartilage cubes and on cartilage cryotome sections. From the different rounds of selections the polyclonal VHH mixture was tested for binding on cartilage tissue sections by DAB Substrate staining and on isolated compounds present in cartilage by ELISA. After several attempts (different conditions and setups described in the Materials and Methods section) and despite a minimum of four rounds of selection per condition, no proper VHH were identified for binding to healthy or arthritic cartilage.

In order to obtain VHH targeting specific markers capable to distinguish between healthy and osteoarthritic cartilage, an immunized library should be constructed. Llamas might also be immunized with purified components of the extracellular matrix. Furthermore, the VHH selection could be performed with a competition elution, where the solution for elution contains peptides targeting relevant compounds in cartilage.

The challenge also remains with the screening strategy, where the targets for VHH binding should be explicitly determined and identified to differentiate healthy from arthritic cartilage.

New strategies for selection of VHH can also be envisaged based on the use of bovine cartilage either or not treated with inflammatory cytokines to induce GAG depletion and/or ECM degradation in a controlled manner and/ or the use of alternative sources of cartilage like human fetal cartilage [14].

Grafting of collagen binding peptide into CDR3 of a VHH

To overcome the fact that it was not possible to select a proper VHH binding to cartilage (healthy or arthritic) from the non-immunized library available, a new strategy was taken. VHH allow for a multitude of genetic modifications and have been used as frameworks for the exchange of antigen specificities by grafting antigen binding peptide sequences in the complementary determining region (CDR) [15]. Therefore, we here explored the grafting of a peptide sequence, targeting a relevant compound in cartilage, into the CDR3 of a VHH framework. By grafting the peptide sequence in the VHH framework we expect to achieve better presentation of the peptide sequence and preservation of the 3D peptide conformation. In addition, the presentation of the peptide sequence in the 3D context of the VHH may increase the affinity for the antigen. The peptide sequence would be incorporated in a system, VHH, with high solubility and stability and high production yields.

Others have identified peptide sequences binding to collagen type II [7]. The ligand “WYRGRL" was selected from a peptide phage display library on denuded bovine

cartilage grafts after five rounds of biopanning. The peptide sequence was shown to bind specifically to articular cartilage and when grafted on nanoparticles specifically targeted to cartilage upon intra-articular injection. Here, we tested whether grafting this collagen IIa1 binding hexapeptide WYRGRL in the CDR3 of a VHH would yield a VHH capable of binding to collagen type II. Computer based modeling was used to optimally design a strategy for introduction of the peptide in the CDR3 of the VHH using the online programs I-TASSER [8-10] and the SWISS-MODEL [11-13]. The validity of the modeling is crucial for a realistic prediction of the interactions of the amino acids within the VHH. Hence the two different models were used to compare the different structural predictions.

As backbone for grafting of the peptide we used the anti-bone morphogenetic protein (BMP) VHH called C2. This VHH was chosen for its stability and high bacterial production levels as well as minimal steric hindrance in the CDR3. To determine at which position WYRGRL would be best exposed and which residues of C2 would be best to replace with the peptide sequence, first a model was made of the anti-BMP VHH C2 (Figure 3A). We chose to replace residues 107 to 112 at the apex of the CDR3 sequence by WYRGRL. This sequence was preceded and followed by an artificially introduced glycine. In this way tyrosine 108 is preserved. The original CDR3 sequence was 101-DPDDASQYYSDWMKGYGMDY-120 and the resulting CDR3 sequence was DPDDA***G*****WYRGRL*****G***KGYGMDY, with the deviating residues underlined and in bold face. The flanking glycine residues are in italics. The whole sequence of the resulting VHH was modeled to predict the conformation of the engineered CDR3 with the collagen binding motif. In the model derived from I-TASSER, arginine R109 in the peptide made a salt bridge with the second aspartic acid (D103) in CDR3. Moreover, R111 made a salt bridge with E57. The same salt bridge was predicted in the model derived from SWISS-MODEL, where R111 made a salt bridge with E57. The side chains of these two arginines (R109 and R111) may be crucial for binding collagen type II, therefore we replaced the aspartic acid (D103) with an alanine, resulting in a new CDR3 sequence DP**A**DA***G*****WYRGRL*****G***KGYGMDY. In addition, E57 was also replaced by alanine. Once more, modeling was performed. I-TASSER yielding a model in which R109 still made a salt bridge (with D101), but R111 did not form a salt bridge anymore and was buried between CDR3 and the framework of the VHH. SWISS-MODEL provided a model in which both arginines were not involved in salt bridges at all. Since there is a high chance that in this configuration the CDR3 is highly flexible and that all residues of the grafted peptide in the final designed protein sequence are available for binding collagen type II, the gene was synthesized at GeneArt® (Invitrogen/LifeTechnologies). To facilitate the cloning of the fragment in a vector unique restriction sites *Sfi*I and *Bst*EII were introduced at the 5'and 3'end of the VHH construct. Furthermore, the coding sequence of the gene was optimized for optimal expression in *E. coli*.

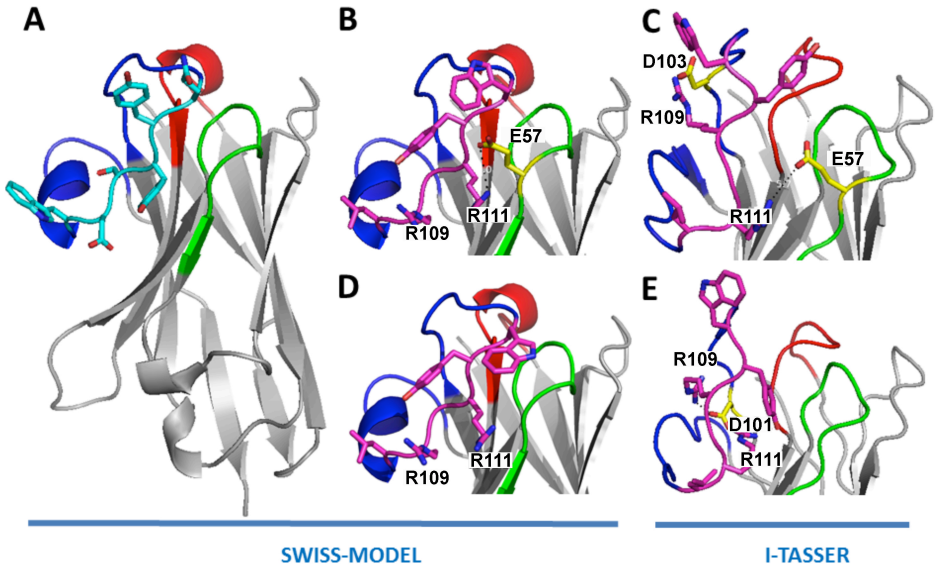

Figure 3. Modeling of grafted WYRGRL peptide on VHH C2. Schematic representations of modeled VHH. Beta-strands are depicted as arrows. Framework regions are shown in grey and CDR1 in red, CDR2 in green and CDR3 in blue, except for the regions where adaptations to the models were made, which are depicted as sticks. Residues that form salt-bridges are labeled with one-letter codes. Salt bridges are depicted as dotted lines. (A) Model of VHH C2 made with SWISS-MODEL. Residues that were chosen to be changed by the WYRGRL sequence are depicted as sticks. (B, C) 107-WYRGRL-112 grafted in C2 by replacing 107-QYYSDW-112. The model in panel (B) was made with SWISS-MODEL and the model in panel (C) with I-TASSER [8-10]. In both models R111 makes a salt-bridge with E57, which is present in CDR2. In the model from I-TASSER R109 makes a salt bridge with D103. (D, E) Similar to panels (B) and (C), with the difference that both D103 and E57 were replaced by an alanine. (D) With SWISS-MODEL the arginines do not make any salt bridge while (E) I-TASSER shows a salt bridge between R109 and D101.

The engineered VHH obtained, VHH-Col2, was produced in *E. coli*. The purified proteins were tested by means of ELISA to evaluate the binding characteristics of the new construct. The collagen peptide sequence was synthesized with a biotin for detection purposes. The VHH was assessed for binding to bovine and human cartilage sections and on bovine and human collagen type II coated plates by ELISA. Although positive detection of the collagen coating was measured, no binding of the peptide, pep-Col2 and VHH-Col2 was observed to collagen type II from bovine and human coated plates nor binding of VHH-Col2 was detected on bovine and human cartilage sections. The homology of bovine collagen type II and human collagen type II is 94% and therefore a similar binding to both tissues was expected [7]. The fact that VHH-Col2 and pep-Col2 did not bind to the coated bovine collagen type II on plates does not exclude the binding capacities of the VHH and the peptide. The collagen type II binding epitopes may not be present in the collagen utilized for coating and may not be recognized by the peptide sequence identified by others [7]. Furthermore, it can be hypothesized that the folding of the peptide in the CDR3 of the VHH resulted in loss of the original folding of the peptide

that bound to collagen type II. More detailed follow-up studies are warranted to explain the VHH configuration and binding to epitope.

It can be envisaged to graft the peptide sequence into the CDR2 of the VHH, which is smaller, and also appears to be available for binding to an epitope, or incorporate the peptide in another VHH backbone. Also, longer CDRs from different VHH backbone might be considered since their plasticity may allow the peptide for more freedom and different conformational changes. Also, longer linkers between the peptide might be considered or the use of peptide sequences in tandem repeats, bearing in mind the maximal length size of amino acids possible to insert in the CDR3 (or other) without destroying the VHH structure. Another approach would be the introduction of an unpaired cysteine at the C-terminus of the VHH and proceed to the covalent coupling of multiple peptide sequence targeting collagen type II at the C-terminus as tags at the C-terminus are known not to be hindered by VHH folding. Other binding peptides to biomolecules present in cartilage could be grafted in the different CDRs of a VHH backbone.

The successful grafting of peptides in VHH may yield VHH capable of firmly attaching to healthy cartilage and eroded cartilage surfaces. Future developments may consider hydrogels loaded with VHH and a cocktail of active compounds capable of inhibiting catabolic mechanisms and stimulate anabolic mechanisms in osteoarthritis. The engineered hydrogel will function as a reservoir for site-specific release of active compounds. The incorporated VHH or VHH engineered with peptides will ensure correct targeting of the hydrogel to the diseased cartilage. Together they will form a drug delivery system where time and space are controlled. In addition, this strategy can be further extended to complete the ACT approach and include chondrocytes and a cocktail of biomolecules for an enhanced tissue repair.

Furthermore, VHH conjugated with imaging agents can be used as *in vivo* monitoring tool for the evolution of the disease and efficacy of the treatment. The identification of biomarkers specific for arthritic cartilage would also allow for imaging and monitoring of the evolution of the disease and efficacy of the treatment by the use of VHH coupled to a dye or photosynthesizer. Such VHH may have great potential for theragnostics.

Taken together, a better understanding of the cellular and molecular process behind degenerative joint disease will allow for the development of biomarkers capable to distinguish healthy and arthritic cartilage.

Conclusion

Specific biomarkers for healthy and OA cartilage are in need for a targeted cartilage tissue regeneration strategy.
It is not excluded that the engineered VHH with a peptide sequence targeting collagen type II grafted in CDR3 does not bind to collagen type II. Follow-up studies are warranted to verify VHH binding.

Acknowledgements

Floris Lafeber and Simon Mastbergen from the Department of Rheumatology and Clinical Immunology (UMC Utrecht, The Netherlands) are gratefully acknowledged for fruitful discussions and for the supply of cartilage samples. This work was supported by project P2.02 OAControl of the research program of the BioMedical Materials Institute, co-funded by the Dutch Ministry of Economic Affairs, Agriculture and Innovation. This work is supported in part by a long term program grant of the Dutch Arthritis Association to MK.

References

1. Beris, A.E., et al., *Advances in articular cartilage repair.* Injury, 2005. **36 Suppl 4**: p. S14-23.
2. Mobasheri, A., et al., *Mesenchymal stem cells in connective tissue engineering and regenerative medicine: Applications in cartilage repair and osteoarthritis therapy.* Histology and Histopathology, 2009. **24**(3): p. 347-366.
3. Harmsen, M.M. and H.J. De Haard, *Properties, production, and applications of camelid single-domain antibody fragments.* Appl Microbiol Biotechnol, 2007. **77**(1): p. 13-22.
4. Frenken, L.G., et al., *Isolation of antigen specific llama VHH antibody fragments and their high level secretion by Saccharomyces cerevisiae.* J Biotechnol, 2000. **78**(1): p. 11-21.
5. Saerens, D., et al., *Single domain antibodies derived from dromedary lymph node and peripheral blood lymphocytes sensing conformational variants of prostate-specific antigen.* J Biol Chem, 2004. **279**(50): p. 51965-72.
6. Roovers, R.C., et al., *High-affinity recombinant phage antibodies to the pan-carcinoma marker epithelial glycoprotein-2 for tumour targeting.* Br J Cancer, 1998. **78**(11): p. 1407-16.
7. Rothenfluh, D.A., et al., *Biofunctional polymer nanoparticles for intra-articular targeting and retention in cartilage.* Nat Mater, 2008. **7**(3): p. 248-54.
8. Roy, A., J. Yang, and Y. Zhang, *COFACTOR: an accurate comparative algorithm for structure-based protein function annotation.* Nucleic acids research, 2012. **40**(Web Server issue): p. W471-7.
9. Zhang, Y., *I-TASSER server for protein 3D structure prediction.* BMC bioinformatics, 2008. **9**: p. 40.
10. Roy, A., A. Kucukural, and Y. Zhang, *I-TASSER: a unified platform for automated protein structure and function prediction.* Nature protocols, 2010. **5**(4): p. 725-38.
11. Arnold, K., et al., *The SWISS-MODEL workspace: a web-based environment for protein structure homology modelling.* Bioinformatics, 2006. **22**(2): p. 195-201.
12. Kiefer, F., et al., *The SWISS-MODEL Repository and associated resources.* Nucleic Acids Research, 2009. **37**: p. D387-D392.
13. Guex, N., M.C. Peitsch, and T. Schwede, *Automated comparative protein structure modeling with SWISS-MODEL and Swiss-PdbViewer: A historical perspective.* Electrophoresis, 2009. **30**: p. S162-S173.
14. Hughes, C., et al., *Human single-chain variable fragment that specifically targets arthritic cartilage.* Arthritis Rheum, 2010. **62**(4): p. 1007-16.
15. Saerens, D., et al., *Identification of a universal VHH framework to graft non-canonical antigen-binding loops of camel single-domain antibodies.* Journal of Molecular Biology, 2005. **352**(3): p. 597-607.

Chapter 10
Summarizing discussion

Summarizing discussion

In the present work we have investigated the possibility of using single domain antibodies, llama VHH, in tissue engineering applications. VHH were tested as modulators of molecules relevant in skeletal tissue engineering and various methods were explored for incorporating VHH in different types of biomaterials. Furthermore, VHH were also employed as carriers for imaging agents.

VHH as modulating molecules

The rational behind tissue engineering is to mimic nature [1, 2]. The trend in tissue engineering is to trigger different pathways in cells in order to manipulate cell faith for enhanced tissue formation with the ultimate goal to achieve regeneration or replacement of damaged tissue [3]. In chapter 2 we explored the possibility of selecting VHH targeting bone morphogenetic proteins relevant in skeletal tissue engineering by means of phage display [4, 5]. Immunization of llamas allowed for a successful selection of VHH with different affinities and modulating properties. VHH were found to inhibit or potentiate BMP activity. In analogy, in chapter 8 the same biopanning selection process was performed on DKK1, which is a key regulatory molecule in cartilage tissue regeneration and inhibitory VHH were found. It is important to define and specify the system where the concept of agonist and antagonist are employed. Such concepts may well be overlapped as demonstrated in chapter 3 where VHH in solution were able to inhibit BMP6 whilst the same VHH, when immobilized on a biomaterial surface, was able to potentiate BMP6 activity by concentrating BMP6 at the biomaterial – cell interface. The way of using VHH in a tissue engineering approach may determine whether it can act as an antagonist or an agonist. An antagonist in solution may turn into an agonist when coupled to a biomaterial surface. To the best of our knowledge, this is the first study to show that by changing the way of presentation of antibodies to cells, either in solution or immobilized on a solid phase revert an antagonist into an agonist.

The modulation of biomolecules is paramount to influence signaling pathways and even to interfere with the evolution of diseases [6]. In an orchestrated system, targeting of multiple growth factors is pertinent to assist the different phases of tissue reconstruction/ growth [7]. The present findings permit for widespread selection of VHH for a multitude of biomolecules relevant in tissue engineering.

VHH in biomaterials

Efforts have been made for the development of biomaterials with a constructive interaction with its surroundings upon implantation [8]. The functionalization of biomaterials with VHH is a novel strategy with endless tunable possibilities. VHH can be genetically modified in order to meet the needs for integration in biomaterials. In chapter 3 we demonstrated surface functionalization by VHH using a supramolecular approach. The tethering of VHH was performed by the introduction of a polyhistidine-tag at the C-terminus of the VHH. A combination of orthogonal supramolecular interactions of β-

cyclodextrin-adamantyl host-guest and N-nitrilotriacetic acid-histidine interactions was employed to generate reversible and homogeneous layers of VHH. These VHH remained active and captured BMP6 from the surroundings resulting in a local enrichment of the growth factor at the cell material interface. The reversible interaction between the growth factor and the antibody ensures release of the growth factor in very close vicinity to the responding cell. This approach results in very high concentrations of growth factors locally. Other immobilization strategies were tested as well. In chapter 5 we genetically introduced a cysteine in the C-terminus of the VHH for a directed coupling to a functionalized polymer surface for covalent coupling. In chapter 4 we introduced an N-linked glycosylation group in the VHH for incorporation in biomaterials. The glycosyl group can function as an anchoring agent when incorporated in biomaterial networks such as electrospun fibers or hydrogel networks. The electrospun fibers and the hydrogel properties are tunable and allow for a tailored and sustained release of VHH and therefore growth factors. In chapter 6 VHH were directly selected from a llama non-immunized library for binding to biomaterials such as hydroxyapatite. The successful isolation of VHH to non-peptide based inorganic structures opens new possibilities for biomaterial functionalization. The selection of VHH can be extrapolated to other biomaterials. Isolation of VHH, which target biomaterials, can be used for *in situ* functionalization of a scaffold even months after implantation by a simple injection in the bloodstream.

VHH allow for a diversity of functionalization strategies of biomaterials. While their directed and homogeneous immobilization on a biomaterial via non-covalent interactions is possible, the short VHH half-life might be a concern. The small VHH size (~15 kDa) can be an advantage for tissue penetration but it may become a disadvantage when used for administration leading to rapid clearance from the body/ scaffold requiring multiple injections. Such disadvantage can be, at least in part, circumvented by the use of bivalent or polyvalent VHH [9]. When covalently coupled to a biomaterial, the release of VHH is hampered by the degradation rate of the biomaterial used. This drawback might be overcome by the incorporation of cleavable linkers in the VHH that are targets for tissue secreted proteases. The immobilization strategy should be adapted to the specific needs for the tissue engineered construct.

Taken together, we demonstrated the versatility of VHH in functionalizing materials and capture growth factors with high affinities without compromising their bioactivity. These approaches allow for a biologically active concentration of growth factors at the implantation. Endogenous growth factors can possibly be captured and carried by VHH and delivered to the surroundings. The specificity of VHH and their binding constants can be employed as a variable to control the desired release profile. Despite the use of well-characterized VHH, the genetic modification features described are independent and can be associated more generally with the wider class of llama antibody fragments. These genetic modifications permit different types of immobilization strategies in different materials and more importantly do not require the genetic modification of the growth factors while still being able to present the growth factors in a directed orientation. Future

developments may incorporate multiple VHH targeting different biomolecules in biomaterials for an orchestrated tissue reconstruction.
Current alternative strategies like covalent tethering of growth factors at surfaces or incorporating growth factors in biomaterials for controlled release possess disadvantages. Direct coupling of growth factors is random and can affect their binding to the antigen [10]. Strategies we present here, either being covalent or non-covalent binding of VHH to biomaterials, allow for a homogeneous and regular coating with capacity to attract growth factors to induce cell response.

VHH as building blocks
Connections build and develop the world. VHH can be used as connecting elements between materials and growth factors. VHH can integrate materials in biological systems. The features of the VHH allow for easy genetic modifications. VHH are naturally occurring nanoparticles, which may be explored as building blocks for tissue engineering applications. In chapter 7 we presented an engineered bivalent VHH. A combination of two or more VHH can be achieved and obtain bivalent or polyvalent homospecific or heterospecific VHH. Furthermore, the linker between the VHH units can be selected according to the desired application. Metalloproteinases (MMPs) are proteases associated with normal and diseased tissue remodeling [11]. Linkers such as matrix MMPs cleavage sites can be introduced in between the biomaterial - VHH connection. This may result in the triggered release of the VHH from the biomaterial surface upon exposure to the respective MMP. Such approach has previously been used in tethering of growth factors or growth factor derived peptides to biomaterial surfaces [12-14]. These genetically and recombinantly produced growth factors are however far more complex to produce than VHH. Due to its small size, VHH can be very efficiently produced in bacteria or yeast at high levels while its inherent stability ensures very efficient refolding after denaturing of these recombinantly produced VHH. Furthermore, while the effects of genetic manipulation on bioactivity has to be tested for each growth factor individually, in this thesis and in work by others [15, 16], it has been shown that the C-terminus of the VHH is susceptible to a wide variety of modifications without compromising its bioactivity. This is most likely explained by the fact that the C-terminus is not involved in the folding and stabilization of the complementary determining regions (CDR) conformation required for antigen binding.
Complementing VHH with imaging agents would permit their use to monitor diseases and treatments. In chapter 6 VHH were selected for targeting hydroxyapatite and were conjugated to a near infrared probe. This approach allowed for the visualization of a mouse skeleton encouraging further developments for theragnostics. Bivalent and/or polyvalent VHH may contribute for improvements in treatments and local drug delivery in tissue engineering. For example, combining a VHH targeting hydroxyapatite (chapter 6 of this thesis) with a VHH synergizing with BMP7 (chapter 2 of this thesis) by genetic fusion or conjugation may result in activation of BMP signaling in all skeletal elements. Such strategy might be useful as an injectable for treating osteoporosis. In chapter 7 we

tested this strategy. The genetic fusion resulted in a bivalent VHH, which retained its affinity for hydroxyapatite and BMP7. Unfortunately we were not able to demonstrate the activity of both VHH at the same time. It is feasible that binding of one of the VHH to its antigen prevents the binding of the second antigen to the other VHH due to steric hindrance. Since antigen-antibody interactions are reversible in nature, this may not constitute a significant problem in clinical application. Whether the fusion of the two VHH affects the targeting to bone of the monovalent VHH remains to be tested. Furthermore, other fusion constructs could be made as well, for example with the VHH targeting DKK1 (chapter 8). Such bivalent VHH could be useful in preventing skeletal metastasis of multiple myeloma in bone of which the growth relies on secretion of DKK1 by the tumor cells [17]. Alternatively, the VHH targeting hydroxyapatite could be used for coating of, for example, drug loaded liposomes for systemic targeting of these drugs to the skeleton.

VHH can be used as backbone for the introduction of binding sequences either in the VHH core (substitute in CDR2 and/or CDR3) or at the C-terminus. Identified peptide sequences binding to collagen type II [18] or to apatite based materials [19] could be incorporated in the VHH sequence. In chapter 9 collagen type II binding sequence were incorporated in the CDR3 of a VHH. Although no positive binding of the grafted VHH to collagen was detected various alternatives exist for the insertion of the peptide sequence in the VHH. More detailed structure modeling is required to guarantee a compatible peptide/ VHH conformation for successful binding. It can also be envisaged the use of peptide sequences or multiple peptide repeats at the C-terminus of the VHH or at different locations (non antigen binding site of the VHH, e.g. loop 5). Although our approach was not successful, insertion of antigen binding peptides in the CDRs is a promising strategy worth of further exploration. While peptide sequences in solution are very dynamic structures continuously changing their 3-dimensional structure due to lack of sufficient internal stabilization, the framework of the VHH could ensure the preservation of the optimized binding conformation of the peptide once this is known. More research is needed to explore the possibilities and limitations for inserting peptides with affinity for a variety of antigens in the CDRs of a VHH framework.

VHH targeting 3D systems

VHH may be applied for the identification of biomarkers relevant in degenerative diseases and for monitoring diseases and treatments. In chapter 9 VHH were utilized in 3D complex systems such as cartilage tissue. An attempt to select VHH targeting arthritic cartilage was performed. The unsuccessful output may be related with the high complexity of the tissue. The use of immunized libraries or the selection against individual cartilage components may be considered. VHH could be selected for binding to biomarkers for specific tissues and engineered in hetero- bivalent or polyvalent VHH to target catabolic processes and arrest cartilage degradation.

In addition, VHH could be used as a tool to study signaling pathways. Phage display allows for the selection of VHH targeting intra or extra cellular molecules relevant in the signaling pathway.

VHH in tissue engineering

Since their discovery in 1993 [20], VHH have been included in various therapeutic applications and applied in molecular imaging [15, 21, 22]. In this thesis we have tested the potential application of VHH in tissue engineering. We here present a variety of VHH targeting different growth factors and biomaterial and have presented different approaches for their incorporation in biomaterials. We demonstrated that the versatility of VHH allow for their use in tissue engineering and in particular in the functionalization of biomaterials. VHH possess genetic and structural features that make them highly suitable for widespread application in therapy, diagnostic screening and research [23-25]. Indeed, these special molecules nicely bridge the inert world of biomaterials with the active world of biology. However, important issues still need to be addressed before testing *in vivo* efficacy of VHH. Bioactivity of VHH over extended period of time still needs to be investigated.

VHH combine the simplicity of peptide sequences with the stability of conventional antibodies.

VHH may help resolving the future challenges in tissue engineering.

References

1. Lavik, E. and R. Langer, *Tissue engineering: current state and perspectives.* Applied microbiology and biotechnology, 2004. **65**(1): p. 1-8.
2. Lutolf, M.P. and J.A. Hubbell, *Synthetic biomaterials as instructive extracellular microenvironments for morphogenesis in tissue engineering.* Nature Biotechnology, 2005. **23**(1): p. 47-55.
3. Fisher, M.B. and R.L. Mauck, *Tissue engineering and regenerative medicine: recent innovations and the transition to translation.* Tissue engineering. Part B, Reviews, 2013. **19**(1): p. 1-13.
4. Smith, G.P. and V.A. Petrenko, *Phage Display.* Chem Rev, 1997. **97**(2): p. 391-410.
5. Muyldermans, S., *Single domain camel antibodies: current status.* J Biotechnol, 2001. **74**(4): p. 277-302.
6. Zhao, J., K.A. Kim, and A. Abo, *Tipping the balance: modulating the Wnt pathway for tissue repair.* Trends Biotechnol, 2009. **27**(3): p. 131-6.
7. Suarez-Gonzalez, D., et al., *Controlled Multiple Growth Factor Delivery from Bone Tissue Engineering Scaffolds Via Designed Affinity.* Tissue engineering. Part A, 2013.
8. O'Brien, F.J., *Biomaterials & scaffolds for tissue engineering.* Materials Today, 2011. **14**(3): p. 88-95.
9. Coppieters, K., et al., *Formatted anti-tumor necrosis factor alpha VHH proteins derived from camelids show superior potency and targeting to inflamed joints in a murine model of collagen-induced arthritis.* Arthritis and Rheumatism, 2006. **54**(6): p. 1856-1866.
10. Kuhl, P.R. and L.G. GriffithCima, *Tethered epidermal growth factor as a paradigm for growth factor-induced stimulation from the solid phase.* Nature Medicine, 1996. **2**(9): p. 1022-1027.
11. Lutolf, M.P., et al., *Synthetic matrix metalloproteinase-sensitive hydrogels for the conduction of tissue regeneration: engineering cell-invasion characteristics.* Proceedings of the National Academy of Sciences of the United States of America, 2003. **100**(9): p. 5413-8.
12. Lutolf, M.P., et al., *Repair of bone defects using synthetic mimetics of collagenous extracellular matrices.* Nat Biotechnol, 2003. **21**(5): p. 513-8.
13. Rizzi, S.C., et al., *Recombinant protein-co-PEG networks as cell-adhesive and proteolytically degradable hydrogel matrixes. Part II: Biofunctional characteristics.* Biomacromolecules, 2006. **7**(11): p. 3019-3029.
14. Zisch, A.H., et al., *Cell-demanded release of VEGF from synthetic, biointeractive cell-ingrowth matrices for vascularized tissue growth.* Faseb Journal, 2003. **17**(13): p. 2260-+.
15. Kijanka, M., et al., *Rapid optical imaging of human breast tumour xenografts using anti-HER2 VHHs site-directly conjugated to IRDye 800CW for image-guided surgery.* European Journal of Nuclear Medicine and Molecular Imaging, 2013. **40**(11): p. 1718-1729.
16. Sukhanova, A., et al., *Oriented conjugates of single-domain antibodies and quantum dots: toward a new generation of ultrasmall diagnostic nanoprobes.* Nanomedicine : nanotechnology, biology, and medicine, 2012. **8**(4): p. 516-25.
17. Heath, D.J., et al., *Inhibiting Dickkopf-1 (Dkk1) removes suppression of bone formation and prevents the development of osteolytic bone disease in multiple myeloma.* J Bone Miner Res, 2009. **24**(3): p. 425-36.
18. Rothenfluh, D.A., et al., *Biofunctional polymer nanoparticles for intra-articular targeting and retention in cartilage.* Nat Mater, 2008. **7**(3): p. 248-54.
19. Segvich, S.J., H.C. Smith, and D.H. Kohn, *The adsorption of preferential binding peptides to apatite-based materials.* Biomaterials, 2009. **30**(7): p. 1287-1298.
20. Muyldermans, S., et al., *Sequence and structure of VH domain from naturally occurring camel heavy chain immunoglobulins lacking light chains.* Protein engineering, 1994. **7**(9): p. 1129-35.

21. Oliveira, S., et al., *Targeting tumors with nanobodies for cancer imaging and therapy.* Journal of controlled release : official journal of the Controlled Release Society, 2013.
22. Oliveira, S., et al., *Rapid Visualization of Human Tumor Xenografts through Optical Imaging with a Near-infrared Fluorescent Anti-Epidermal Growth Factor Receptor Nanobody.* Molecular Imaging, 2012. **11**(1): p. 33-46.
23. Wesolowski, J., et al., *Single domain antibodies: promising experimental and therapeutic tools in infection and immunity.* Med Microbiol Immunol, 2009. **198**(3): p. 157-74.
24. Harmsen, M.M. and H.J. De Haard, *Properties, production, and applications of camelid single-domain antibody fragments.* Appl Microbiol Biotechnol, 2007. **77**(1): p. 13-22.
25. Hassanzadeh-Ghassabeh, G., et al., *Nanobodies and their potential applications.* Nanomedicine, 2013. **8**(6): p. 1013-26.

Biographical sketch

Biographical sketch

Emilie Dooms Rodrigues was born on May 31st 1983, in Woluwe-Saint-Lambert, Belgium. In September 2008 she graduated as a Chemical Engineer after her studies in Chemistry and Chemical Engineering at the Instituto Superior Tecnico, Universidade Tecnica de Lisboa, Portugal. In February 2008 she worked half year at the Membrane Technology Group, University of Twente, The Netherlands, within the framework of the Erasmus program. There she worked on a project concerning cell biomaterial interactions.

In October 2008 she started her PhD research project at the Departments of Developmental BioEngineering and Tissue Regeneration, University of Twente, under the supervision of Prof. Dr. Marcel Karperien and Prof. Dr. Clemens van Blitterswijk. Her research was focused on the functionalization of biomaterials for tissue engineering and the results are presented in this thesis entitled *SINGLE DOMAIN ANTIBODIES IN TISSUE ENGINEERING*.